Genesis and Characterization of Human eNOS-Based Platelet Subpopulations. Implications for Haemostasis and Thrombosis.

by

Gabriela Maria Lesyk

A thesis submitted in partial fulfillment of the requirements for the degree of

Doctor of Philosophy

in

Pharmaceutical Sciences

Faculty of Pharmacy and Pharmaceutical Sciences
University of Alberta

ABSTRACT

Background: Myocardial infarction (MI) and ischemic stroke are responsible for nearly half of all cardiovascular deaths in Canada. Platelets play a critical role in MI and ischemic stroke by forming thrombi that occlude coronary and cerebral arteries. In spite of abundant pharmacological agents (acetylsalicylic acid, clopidogrel, prasugrel, ticagrelor, abciximab, eptibifatide) used to prevent platelet thrombus formation, the incidence of arterial thrombosis remains high. One of the reasons might be incomplete understanding of platelet biology and their function. Anucleate platelets derived from bone marrow megakaryocytes (MKs) have long been considered simple cell fragments that act as vascular system "band-aids". Hence, investigations into biochemically distinct subpopulations with differential functional roles in haemostasis and thrombosis have been limited. In 1990 Radomski et al. proposed that platelets have endothelial nitric oxide synthase (eNOS)-signalling pathway present and when activated generate nitric oxide (NO). This endogenous negative-feedback mechanism provides a balance for platelet pro-aggregatory properties by inhibiting their adhesion and aggregation. However, in recent years existence of this pathway within platelets has been questioned. To explain some discrepancies in findings, we propose that differences in platelet eNOS levels might account for a part of the divergent results. Therefore, the over-arching goal of this study was to explore if two platelet subpopulations exist based on the presence or absence of eNOS-signalling, and thereby represent functionally distinct platelet subpopulations with differential roles in adhesion and aggregation. Furthermore, inflammation that contributes to atherosclerosis and thrombosis may modulate the bone marrow microenvironment and promote formation of MKs that generate platelets with enhanced reactivity, therefore increasing risk of acute ischemic events.

In this thesis, I have addressed three hypotheses:

1) Subpopulations of eNOS-negative (eNOS^{neg}) and eNOS-positive (eNOS^{pos}) platelets exist, and due to their biochemical differences perform differential roles in haemostasis and thrombosis.

2) Subpopulations of eNOS-negative (eNOS^{neg}) and eNOS-positive (eNOS^{pos}) megakaryocytes/blasts exist and give rise to their respective eNOS-based platelet subpopulations.

3) Pro- and anti-inflammatory cytokines interferon-γ (IFN-γ) and interleukin-10 (IL-10) counter-regulate formation of eNOS-based platelet subpopulations via their effects on megakaryocyte/blast eNOS expression, and IFN-γ promotes differentiation of megakaryocytes/blasts lacking eNOS that give rise to more reactive eNOS^{neg} platelets.

Methods: Prostacyclin-washed platelets were isolated from healthy humans. Human megakaryoblastic cell line (Meg-01) was used as a surrogate of human bone marrow MKs and to generate Meg-01-derived platelets. In addition, eNOS-GFP mouse platelets and bone marrow samples were used for experiments. Production of NO was assessed by fluorescent NO indicator - DAF-FM diacetate. Detection of eNOS was performed by flow cytometry, western blot, and confocal microscopy.

Results: Our results show existence of mouse and human platelet subpopulations based on the presence (eNOS^{pos}) or absence (eNOS^{neg}) of functional intracellular eNOS and NO generation. In contrast to majority of human platelets that have eNOS and generate NO, most of mouse platelets lack eNOS and generate no or low amounts of NO. Our study also demonstrates that less abundant eNOS^{neg} platelets, due to the absence of NO generation, are more reactive and initiate aggregate formation, while eNOS^{pos} platelets limit aggregate size by generating NO. In addition,

down-regulated sGC-PKG-signalling within eNOS^{neg} platelets facilitates their refractoriness to endothelial-derived NO and increases activation of platelet fibrinogen receptor - integrin $\alpha_{IIb}\beta_3$. Consequently, eNOS^{neg} platelets more readily bind to collagen compared to more abundant eNOS^{pos} platelets that attach to collagen at later time points and form the bulk of an aggregate, ultimately limiting its size by NO generation. Similar to human platelets, the majority of Meg-01 cells are eNOS^{pos} and NO-producers. The majority of mouse platelets and mouse MKs are eNOS^{neg}. Pro-inflammatory IFN-γ in a concentration-dependent manner decreases total amount of MK eNOS, which reduces number of eNOS^{pos} Meg-01 cells and Meg-01-derived eNOS^{pos} platelets. Anti-inflammatory IL-10 in a concentration-dependent manner partially restores MK total eNOS levels and number of Meg-01-derived eNOS^{pos} platelets.

Conclusions: These findings demonstrate novel characteristics and complexity of platelets and their regulation of adhesion and aggregation. The identification of eNOS-based platelet subpopulations has potentially important consequences to human disease as impaired platelet NO-signalling has been identified in patients with coronary artery disease. Our study also provides potential insight on how chronic inflammatory states can contribute to thrombosis by promoting formation of eNOS^{neg} MKs that generate more reactive eNOS^{neg} platelets.

PREFACE

This thesis is an original work by MSc Gabriela Lesyk. A part of this thesis (Chapter 4.1 - 4.9) has been published as Aneta Radziwon-Balicka, **Gabriela Lesyk**, Valentina Back, Teresa Fong, Erica L Loredo-Calderon, Bin Dong, Haitham El-Sikhry, Ahmed A El-Sherbeni, Ayman El-Kadi, Stephen Ogg, Arno Siraki, John M Seubert, Maria Jose Santos-Martinez, Marek W Radomski, Carlos A Velazquez-Martinez, Ian R Winship, Paul Jurasz. (2017) Differential eNOS-signalling by platelet subpopulations regulates adhesion and aggregation. *Cardiovasc Res.,* 113(14):1719-1731, 2017 Dec. Doi:10.1093/cvr/cvx179. A.R.B. and I were responsible for the majority of the data collection, data analysis and manuscript composition (drafting method section). V.B., T.F., E.L.L.C., B.D., H.E.S., A.A.E.S., A.E.K., S.O., A.S., J.M.S., M.J.S.M., M.R., C.A.V.M. and I.R.W. contributed to data collection and analysis as shown in the figure legends of this chapter. P.J was the senior author and was involved with concept formation and manuscript draft composition.

A part of this thesis (Chapter 4.9 – 4.12) will be submitted for publication as **Gabriela Lesyk**, Aneta Radziwon-Balicka, Lisa Chan, Teresa Fong, and Paul Jurasz. Generation of endothelial nitric oxide synthase-negative and positive platelets via their parent megakaryocyte subpopulations: A role for interferon γ and interleukin 10. I was responsible for the majority of the data collection, data analysis and drafting method section. A.R.B., L.C. and T.F. contributed to data collection as outlined in the figure legends of this chapter. P.J who is the senior author was involved with concept formation.

The research project, of which this thesis is a part, received research ethics approval for human platelet isolation from the University of Alberta Research Ethics Board for Dr. Jurasz's lab, Project name "NOS-based platelet subpopulations", No. Pro00029836, March 8, 2012.

All animal care and experimental procedures were approved by the Animal Care and Use Committee (ACUC HS2; AUP 606) of the Faculty of Pharmacy and Pharmaceutical Sciences at the University of Alberta, and performed in accordance with Canadian Council on Animal Care guidelines, and the principles and regulations as described by Grundy (2015).

DEDICATION

To my beloved Chris

For six years of patience and constant support; and keeping me hydrated and well fed during writing this thesis.

ACKNOWLEDGEMENTS

I would like to thank my supervisor, Dr. Paul Jurasz, for taking me into his lab. I have continuously learned throughout and gained invaluable research experience. I am grateful for his time to review my abstracts, presentations and this thesis.

I would like thank the members of my committee Dr. Frances Plane and Dr. Carlos A. Velázquez-Martinez for their feedback and support throughout my program.

I am also very grateful to Dr. Andrea Holme for teaching me laser-scanning cytometry, Dr. Aja Rieger and Sabina Baghirova for helping me to learn fluorescence activated cell sorting and to troubleshoot some of the flow cytometry protocols. I would like to also mention and thank Dr. Stephen Ogg and Greg Plummer for teaching me confocal microscopy.

Last but foremost I would like to thank the amazing people I met throughout my program: Valentina Back, Natasha Govindasamy, Jan Rudzinski and Maria Yan. I really appreciate your friendship, constant support and motivation.

I would like to thank Natasha Govindasamy for her comments and suggestions regarding my thesis; I really appreciate your help.

Finally, I would like to thank my husband Chris for helping me to format this thesis.

TABLE OF CONTENTS

LIST OF FIGURES

Chapter 1

Chapter 4

Chapter 5

LIST OF TABLES

Chapter 1

Chapter 3

ABBREVIATIONS

5-HT	5-hydroxytryptamine
AA	Arachidonic acid
AC	Adenylate cyclase
ACS	Acute coronary syndromes
ADAM	A disintegrin and metalloproteinase
ADMA	Asymmetric dimethylarginine
ADP	Adenosine diphosphate
AML	Acute myeloid leukemia
AMP	Adenosine monophosphate
AMPK	Adenosine monophosphate-activated kinase
AMR	Ashwell-Morell receptor
APC	Activated protein C
AT	Antithrombin
ATP	Adenosine triphosphate
β-gal	β-galactose
BH_4	Tetrahydrobiopterin
BSA	Bovine serum albumin
Ca^{2+}	Calcium ion
CAD	Coronary artery disease
CaM	Calmodulin
CaMK II	Ca^{2+}/calmodulin-dependent protein kinase II
cAMP	Cyclic adenosine monophosphate
Cas-8	Caspase-8
Cas-9	Caspase-9
CAV-1	Caveolin-1
CCL5	Chemokine (C-C motif) ligand 5
CD	Cluster of differentiation
cGMP	Cyclic guanosine monophosphate
CHIP	Carboxyl terminus of Hsp70-interacting protein

cIMP	Cyclic inosine monophosphate
CMP	Common myeloid progenitor cell
COX-1	Cyclooxygenase 1
CVD	Cardiovascular disease
CXCL4	Chemokine (C-X-C motif) ligand 4
CXCR4	C-X-C chemokine receptor type 4
DAF-FM	4-amino-5-methylamino-2',7'-difluorofluorescein
DAG	Diacylglycerol
DEPC	Diethyl pyrocarbonate
DETA/NO	Diethylenetriamine/NO-adduct
DMEM	Dulbecco modified Eagle medium
DMS	Demarcation membrane system
DMSO	Dimethylsulfoxide
dNTP	Deoxynucleotide
DTS	Dense tubular system
DVT	Deep vein thrombosis
ECL	Enhanced chemiluminescence
ECM	Extracellular matrix
ECs	Endothelial cells
EDRF	Endothelium-derived relaxing factor
EDTA	Ethylenediaminetetraacetic
EI	Electrospray ionization
ELISA	Enzyme-linked immunosorbent assay
eNOS	Endothelial nitric oxide synthase
ERK1/2	Extracellular signal regulated kinase ½
ET	Endothelin
EV	Electronic volume
FACS	Fluorescence activated cell sorting
FAD	Flavin adenine dinucleotide
FBS	Fetal bovine serum
FC	Fluorecence concentration

FcγRIIa	Fc γ-chain receptor
FGF	Fibroblast growth factor
FGF-4	Fibroblast growth factor 4
FH	Familial hypercholesterolemia
FMN	Flavin mononucleotide
FSC	Forward light scatter
FSD	Fluorescence surface density
FVD	Fixable viability dye
G2	Glycine-2
GAS	Gamma interferon activation site
GFP	Green fluorescent protein
GM-CSF	Granulocyte-macrophage colony-stimulating factor
GP	Glycoprotein
GPCRs	G-protein coupled receptors
GPS	Grey platelet syndrome
GSNO	S-nitrosoglutathione
GTP	Guanosine triphosphate
HCII	Heparin cofactor II
HMVEC	Human cardiac microvascular endothelial cells
HMWK	High-molecular-weight kininogen
HRP	Horseradish peroxidase
HSCs	Hematopoietic stem cells
Hsp90	Heat-shock protein 90
HUVEC	Human umbilical vein endothelial cells
IAP	Integrin associated protein
ICAM-1	Intercellular adhesion molecule 1
ICAM-2	Intercellular adhesion molecule-2
IFN-γ	Interferon gamma
IFN-γR	IFN-γ receptor
IGF	Insulin-like growth factor
IgG	Immunoglobulin G

IK_{Ca}	Intermediate–conductance Ca^{2+}-activated K^+ channel
IL-1	Interleukin-1
IL-1β	Interleukin 1β
IL-3	Interleukin 3
IL-6	Interleukin 6
IL-8	Interleukin 8
IL-10	Interleukin 10
IL-10R	IL-10 receptor
IL-11	Interleukin 11
iNOS	Inducible nitric oxide synthase
IP	Prostacyclin receptor
IP3	Inositol trisphosphate
IP3R	Inositol trisphosphate receptor
IRAG	Inositol trisphosphate receptor-associated cGMP-kinase substrate
IRF-1	Interferon regulatory factor – 1
ITP	Immune thrombocytopenia
JAK2	Janus kinase 2
JAK2-STAT3	Janus kinase 2 and signal transducer and activator of transcription 3
JAM-3	Junctional adhesion molecule-3
KLF2	Krüppel-like factor 2
LC-ESI-MS	Liquid chromatography-electrospray ionization-tandem mass spectrometry
LDA	Lysophosphatidic acid
LDL	Low-density lipoproteins
LFA-1	Lymphocyte function-associated antigen-1
LIMP-1	Lysosomal integral membrane protein 1
L-NAME	N-Nitroarginine methyl ester
L-NMMA	NG-monomethyl L-arginine
LPS	Lipopolysaccharide
Mac-1	Macrophage-1 antigen
MAPK	Mitogen-activated protein kinase

M-CSF	Macrophage colony-stimulating factor
MEP	Erythroid-megakaryocyte progenitor
MI	Myocardial infarction
MK-CFU	MK colony-formation units
MKs	Megakaryocytes
MLCs	Myosin light chains
MLCK	Myosin light-chain kinase
MLCP	Myosin light-chain phosphatase
MMP-1	Matrix metalloproteinase-1
MMP-2	Matrix metalloproteinase-2
MMP-9	Matrix metalloproteinase-9
MSCs	Mesenchymal stem cells
MSD	Mechanosensory domain
MT1-MMP	Membrane-type 1 matrix metalloproteinase
NADPH	Nicotinamide adenine dinucleotide phosphate
NF-κB	Nuclear factor kappa B
NMT	N-myristoyltransferases
nNOS	Neuronal nitric oxide synthase
NO	Nitric oxide
NOHA	N-hydroxy-l-arginine
NOS	Nitric oxide synthase
NOSIP	Nitric oxide synthase-interacting protein
NOSTRIN	Nitric oxide synthase traffic inducer
NRF2	Nuclear factor-E2-related factor-2
NS	Non-significant
NTG	Nitroglycerin
$O_2^{\bullet -}$	Superoxide
OCS	Open canalicular system
ODQ	Oxadiazolo quinoxalin
$ONOO^-$	Peroxynitrite
ox-LDL	Oxidized low-density lipoproteins

PAC-1	First procaspase activating compound
PAGE	Polyacrylamide gel electrophoresis
PAH	Pulmonary arterial hypertension
PAI-1	Plasminogen activator inhibitor-1
PAI-2	Plasminogen activator inhibitor-2
PAI-3	Plasminogen activator inhibitor-3
PAR1	Protease-activated receptor 1
PAT	Palmitoyl-acyl-transferases
PBS	Phosphate buffered saline
PCI	Protein C inhibitor
PDE2	Phosphodiesterase type 2
PDE3	Phosphodiesterase type 3
PDE5	Phosphodiesterase type 5
PDEs	Phosphodiesterases
PDGF	Platelet-derived growth factor
PECAM-1	Platelet endothelial cell adhesion molecule-1
PGH_2	Prostaglandin H_2
PGI_2	Prostacyclin
PI	Propidium iodine
PI3K	Phosphatidylinositol 3-kinase
PIP_2	Phosphatidylinositol bisphosphate
PKA	Protein kinase A
PKC	Protein kinase C
PKG	Protein kinase G
PLA	Phospholipase A_2
PLC	Phospholipase C
PMCAs	Plasma membrane Ca^{2+} ATPases
PMKs	Promegakaryocytes
PPP	Platelet poor plasma
PRP	Platelet rich plasma
PS	Phosphatidylserine

PSGL-1	P-selectin glycoprotein ligand-1
PTB	Phospho tyrosine binding
PVDF	Polyvinylidene difluoride
PYK2	Proline rich tyrosine kinase 2
ROCK	Rho-associated protein kinase
ROS	Reactive oxygen species
RT-PCR	Reverse transcription polymerase chain reaction
RT-qPCR	Quantitative reverse transcription PCR
SCF	Stem cell factor
SDF1-α	Stromal cell-derived factor 1
SDS	Sodium dodecyl sulfate
sGC	Soluble guanylyl cyclase
SH2	Src homology 2
SK_{Ca}	Small-conductance Ca^{2+}-activated K^+ channel
SLE	Systemic lupus erythematosus
SMCs	Smooth muscle cells
SNAP	S-Nitroso-N-acetylpenicillamine
SNAP-23	Synaptosome associated protein 23
SNP	Sodium nitroprusside
SOCS3	Suppressor of cytokine signalling 3
SOD	Superoxide dismutase
SSC	Side scatter
STAT1	Signal transducer and activator of transcription 1
STAT3	Signal transducer and activator of transcription 3
STEMI	ST-segment-elevation myocardial infarction
T1D	Type 1 diabetes
T2DM	Type 2 diabetes mellitus
TAFI	Thrombin-activatable fibrinolysis inhibitor
TEMED	Tetramethylethylenediamine
TEMPOL	4-hydroxy-2,2,6,6-tetramethylpiperidine-N-oxyl (sod mimetic)
TF	Tissue factor

TFPI	Tissue factor pathway inhibitor
TGF-β1	Transforming growth factor-β1
TIMP-2	Tissue inhibitor of metalloproteinase-2
TIMP-4	Tissue inhibitor of metalloproteinase-4
TM	Thrombomodulin
TNF-α	Tumor necrosis factor-α
t-PA	Tissue plasminogen activator
TP	Thromboxane receptor
TPO	Thrombopoietin
TSP-1	Thrombospondin 1
TXA_2	Thromboxane A_2
u-PA	Urokinase plasminogen activator
VAMP-3	Vesicle-associated membrane proteins 3
VAMP-8	Vesicle-associated membrane proteins 8
VASP	Vasodilator-stimulated phosphoprotein
VCAM-1	Vascular cell adhesion protein 1
VDCC	Voltage-dependent calcium channel
VEGF	Vascular endothelial growth factor
VEGFR	VEGF receptor
VSMs	Vascular smooth muscles
vWF	von Willebrand factor
WT	Wild type

1. INTRODUCTION

1.1 Haemostasis and Thrombosis

1.1.1 Cardiovascular Disease

Cardiovascular disease (CVD) is now the most common cause of death worldwide accounting for 31% of all global deaths. Four out of five CVD deaths are due to myocardial infarction (MI) and stroke. Furthermore, the annual number of deaths from CVD will rise from 17.5 million in 2012 to 22.2 million by 2030 [1]. Cardiovascular disease can refer to a number of conditions that involve the heart or blood vessels; the underlying mechanisms vary depending on the disease. Cardiovascular disease is often associated with atherosclerosis - a chronic inflammatory state that is a result of gradual accumulation and oxidation of lipids in the subendothelial spaces of arteries. The rupture or occlusion of an atherosclerotic artery in the heart or brain causes MI and ischemic stroke, respectively. Blood platelets are the major cellular culprits responsible for formation of obstructive thrombi which drastically limits blood supply to the surrounding tissues and initiates the onset of MI and ischemic stroke [2].

The development of atherosclerosis varies between individuals, but usually takes more than 40 years and begins in the early teenage years [3, 4]. The primary cause of this process appears to be the retention of low-density lipoproteins (LDL) in the subendothelium and their oxidation over time. The resulting oxidized low-density lipoproteins (ox-LDL) initiate inflammation by stimulating endothelial cells (ECs) to express and secrete pro-inflammatory molecules, including growth factors, cytokines and adhesion molecules. Production of macrophage colony-stimulating factor (M-CSF) by ECs promotes the infiltration of monocytes into the vascular wall. In addition, ox-LDL inhibit the endothelial production of nitric oxide (NO) and stimulate the synthesis of prostaglandins and prostaglandin precursors which further diminishes antithrombotic properties of the endothelium [5, 6]. Early atherosclerotic lesions form when monocytes extravasate across the endothelial monolayer into the intima, where they proliferate, differentiate into macrophages and engulf ox-LDL to form foam cells. Under the microscope, the lesion now appears as a fatty streak. Damaged ECs and activated macrophages release platelet-derived growth factor (PDGF) and basic fibroblast growth factor (FGF) that respectively stimulate migration of smooth muscle cells (SMCs) from the tunica media into the

intima, and their subsequent proliferation [7, 8]. This causes the formation of a collagen-rich fibrous cap covering the fatty streak, which separates the thrombotic plaque material from the blood and prevents plaque rupture and thrombosis. Progression of the lesions to more advanced and complex plaques results from accumulation of foam cells and deposition of cholesterol crystals. In advanced plaques, foam cells remain the major culprit of the local inflammation due to secretion of pro-inflammatory mediators such as chemokines, cytokines and reactive oxygen and nitrogen species. Over time the foam cells die and release their lipid contents and tissue factor (TF), leading to the formation of a pro-thrombotic necrotic core, a key component of unstable plaques that contributes to their rupture and exposure of subendothelial matrix to the blood stream. Advanced lesions can grow large and ultimately block blood flow, but the most acute clinical complication is an artery occlusion due to the rupture or erosion of the unstable plaque, as depicted in Figure 1.1. Consequently, platelets interact with components of exposed subendothelium and adhere to collagen and other matrix proteins. This triggers platelet activation and aggregation which culminates in the formation of occlusive thrombi [9].

Blood flow dynamics appear to play a significant role in creating a favorable environment for development of atherosclerosis. Atherosclerotic plaques preferentially form in vascular regions of slow or turbulent blood flow and low wall shear stress, which occurs in medium to large vessels [10, 11]. Steady, unidirectional laminar blood flow that occurs in straight regions of blood vessels shows protection from inflammation and formation of atherosclerotic plaque. Even in the presence of essential atherosclerotic risk factors such as elevated cholesterol, smoking and hypertension [10, 11]. On the other hand, disturbed flow that occurs at curved blood vessel regions (such as branch points and bifurcations) is associated with increased risk of focal distribution of atherosclerotic lesions. In cases where a severe lesion has already formed, turbulent blood flow occurs immediately downstream to the lesion and promotes activation of plasma coagulation and deposition of fibrin, which results in the formation of a fibrin-rich tail of the thrombus [12].

Platelet function plays an essential role in arterial thrombosis occurring in CVD events such as MI and stroke. It has been suggested that different populations of platelets may play differential roles in the cascade of events in thrombus formation, depending on their activation state and surface properties. Consequently, growing body of evidence shows that overall platelet hyperreactivity or presence of subset of more reactive platelets may be associated with higher

risk of future arterial thrombosis as well as may also contribute to the pathogenesis of MI and ischemic stroke. For example, several different groups reported the presence of platelet subpopulations with different procoagulant abilities, including “COAT-platelets” that retain high levels of procoagulant-proteins on their surface. Even though the physiological function of “COAT-platelets” is not yet fully understood, it is clinically speculated that high levels of “COAT-platelets” may contribute to enhanced thrombosis during transient ischemic attack and ischemic stroke [13-18].

Additionally, platelet hyperreactive phenotype has been attributed to Type 2 diabetes mellitus (T2DM) and familial hypercholesterolemia (FH), which are considered as key risk factors for development of atherosclerosis. Interestingly, platelets from patients with T2DM and FH have increased extent of aggregation in comparison to healthy controls. In addition, these patients have a higher count of procoagulant platelets that more readily mediate thrombin generation [19-21]. The main culprit of platelet activation in the hyperlipidemic state are ox-LDL, specifically the lysophosphatidic acid (LDA) formed during oxidation of LDL that serves as the active moiety for platelet activation [22]. Platelets exposed to ox-LDL undergo immediate shape change and extend pseudopodia that enhance adhesion to ECs under flow condition [23]. Pathological activation of platelets in T2DM is associated with oxidative stress and inflammation. This leads to endothelial dysfunction and deficient production of NO which is an essential inhibitor of platelet activation [24].

In addition to their role in thrombosis, platelets interact with many mediators and effectors of atherosclerosis including the endothelium and leukocytes. Importantly, inflammation causes activation of ECs, which promotes expression of cell adhesion molecules such as P- and E-selectin, which in turn mediate leukocyte and platelet activation. Activated circulating platelets contribute to the progression of atherosclerotic lesions through deposition of chemokines on the endothelium which attract adhesion of additional leukocytes and platelets [25].

Taken together, it is generally assumed that altered haemostatic function of platelets, either by pre-activation by various components of the vessel wall or elevated numbers of activated or procoagulant platelets, have significant implications for CVDs such as MI and ischemic stroke [9]. Despite various pharmacological agents (aspirin, clopidogrel, prasugrel, ticagrelor) used to prevent platelet thrombus formation, the incidence of arterial thrombosis remains high. Surprisingly, antiplatelet therapy reduces the likelihood of suffering from an

ischemic event only by 25%. Furthermore, aspirin long-term secondary prevention of ischemic events reports only a 13% relative reduction in risk of recurrent ischemic stroke [26, 27]. Therefore, future antiplatelet therapy may require more targeted strategies directed towards subpopulations of platelet that display pro-thrombotic phenotype. Hence, understanding the biology of various platelet subpopulations is an important first step toward the goal of developing platelet subpopulation targeted drugs.

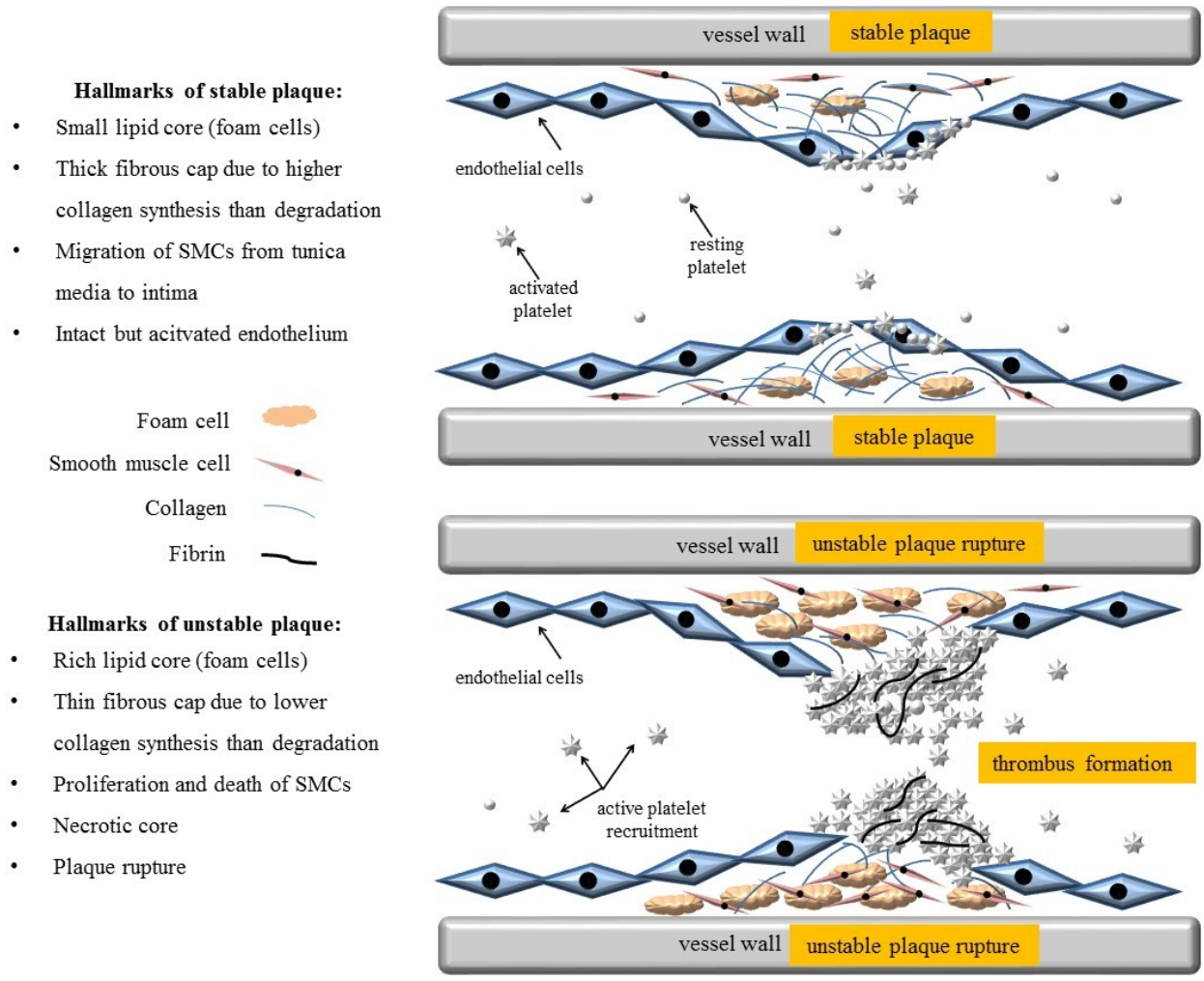

Figure 1.1. The two possible scenarios of evolution of atherosclerotic plaques

Slowly growing plaques expand gradually due to accumulation of lipid in foam cells and migration and proliferation of SMCs. These plaques tend to stabilize and are not prone to rupture. The fibrous cap on the lesion matures. In contrast, other plaques grow more rapidly as a result of more rapid lipid deposition. These have thin fibrous caps and are prone to rupture. Once a plaque ruptures, it can trigger an acute thrombosis (clot) by activating platelets and the clotting cascade. This ultimately leads to vessel obstruction and tissue ischemia.

1.1.2 Haemostasis and the Role of Platelets

Haemostasis is a process that prevents excessive haemorrhage upon damage to a vessel wall. In order to do so, vessel wall components together with circulating coagulation proteins and platelets form a plug of cells cross-linked with fibrin (Figure 1.2). Pathologically, platelets are the main cellular component in arterial thrombus, whereas venous thrombus largely consists of fibrin-trapped red blood cells. Haemostasis is often divided into two stages: primary haemostasis and secondary haemostasis (coagulation cascade). The main focus of primary haemostasis is vasoconstriction and formation of the primary platelet plug to limit further blood loss. Platelets rapidly activate and adhere to components of exposed subendothelium, and this leads to formation of platelet aggregates and a blood clot that seals off the damaged site. Injury also exposes subendothelial TF to the blood flow and plasma coagulation factors. This triggers a self-amplifying blood coagulation cascade including assembly of prothrombinase complex on the negatively charged surface of activated platelets. Coagulation cascade results in the generation of fibrin that stabilizes the blood clot. Over the next few days blood clot shrinks (clot retraction) and is degraded by the fibrinolytic system. Ultimately the site of injury is replaced by new tissue [28].

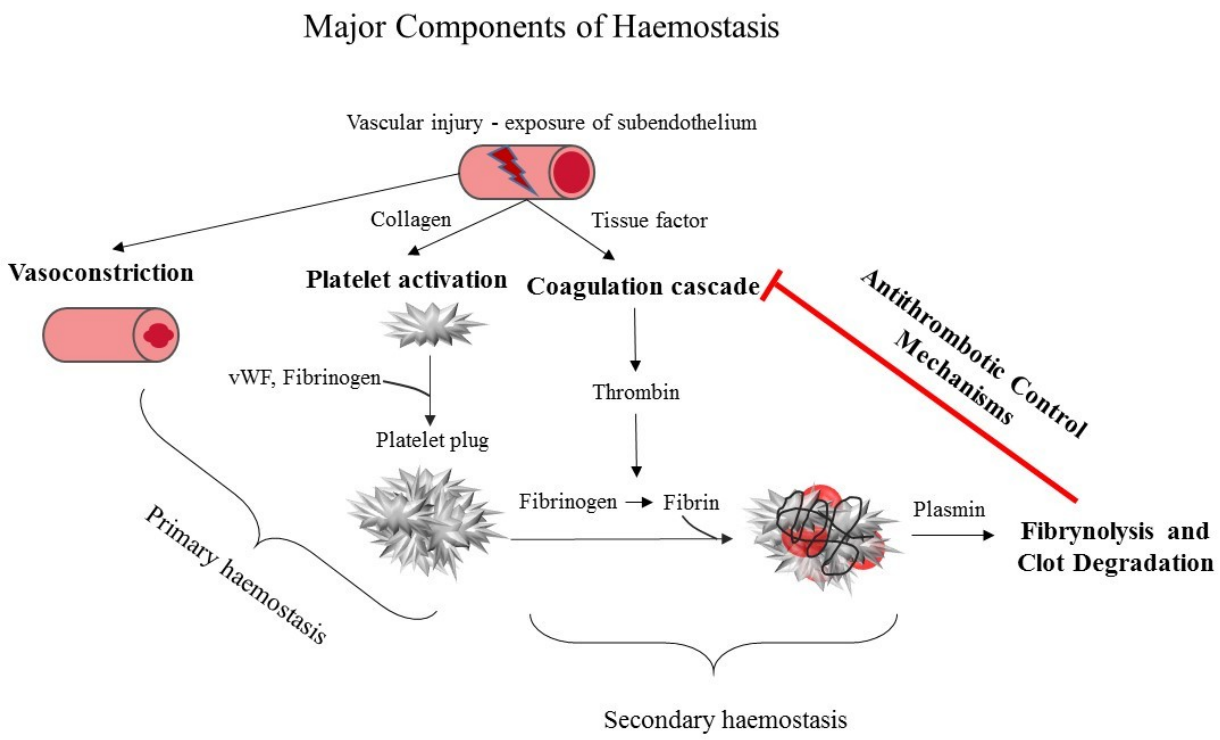

Figure 1.2. Components of haemostasis

Primary haemostasis involves vasoconstriction and platelet sequential adhesion, activation and aggregation to form a platelet plug and limit blood loss. Secondary haemostasis is related to consecutive coagulation cascade events starting with initiation of thrombin generation and its following propagation that culminates with formation of a fibrin mesh. The fibrinolytic system provides negative feedback mechanisms for the coagulation cascade and is responsible for gradual clot degradation.

1.1.3 Coagulation Cascade

Coagulation cascade is also referred to as secondary haemostasis and begins shortly after initiation of plug formation based on Furie's intravital microscopy [29]. Coagulation is governed by highly controlled pathways, including action of clotting factors that promote clot formation, and components of fibrinolytic system that limit clot propagation and aid breakdown of fibrin as the wound heals. Disruption of this delicate balance occurs whenever there is an increase in the procoagulant activity of the coagulation factors, or a decrease in the activity of the fibrinolytic system [30]. The coagulation factors are generally serine proteases produced by liver, which require calcium ions (Ca^{2+}) for binding to membrane phosphatidylserine (PS) on activated platelets. The clotting factors are represented by Roman numerals, with a lower case "a" appended to the numeral once the factor has been proteolytically converted to the active form [28].

The coagulation cascade can be described as a sequence of enzymatic reactions, in which the enzymatically active coagulation factor subsequently converts the downstream inactive coagulation factor into an active serine protease, as showed in Figure 1.3. There are two pathways of the coagulation cascade, extrinsic pathway (TF pathway) and intrinsic pathway (contact activation pathway), which converge into a common pathway. The coagulation process can be divided into three main phases: 1. generation of prothrombinase complex 2. conversion of prothrombin to thrombin and 3. conversion of fibrinogen to fibrin, which supports the platelet plug formed during primary heamostasis [31].

The extrinsic pathway is the most important for initiating the coagulation cascade and generating a "thrombin burst". It is activated when vascular injury exposes subendothelial TF on fibroblasts and smooth muscle cells, which then react with FVII found in blood. Upon reaction with TF, FVII is converted into FVIIa and both form a cell-surface complex. The TF-FVIIa complex activates both FIX and FX and in turn FIXa binds to FVIII and converts it to FVIIIa. Both complexes, the TF-FVIIa and the FIXa-FVIIIa, catalyze conversion of FX to FXa. The FXa assembles on negatively charged membrane phospholipids with its cofactor FVa (activated by thrombin) and together form FXa-FVa complex. The FXa-FVa complex (also known as prothrombinase complex) converts prothrombin to thrombin, which in turn converts fibrinogen to fibrin. Thrombin also activates FXIII, which forms covalent bonds between the fibrin monomers converting them into an insoluble meshwork - the clot. In addition, thrombin provides

a positive feedback effect ("thrombin burst") on the cascade by accelerating formation of FVIIIa, FVa and FXIa. This way the cascade is amplified to produce necessary fibrin in a short time [28, 32].

The intrinsic pathway is less significant for initiating coagulation than extrinsic pathway, but is very important for amplification of the cascade. Intrinsic pathway begins with formation of the primary complex on collagen by high-molecular-weight kininogen (HMWK), prekallikrein, and FXII. Prekallikrein is converted to kallikrein and FXII becomes activated to FXIIa by negatively charged molecules such as collagen or activated platelet phospholipids. FXIIa converts FXI into FXIa. Factor XIa activates FIX and with its co-factor FVIIIa form the tenase complex, which activates FX to FXa. At this point intrinsic pathway converges with extrinsic pathway [32, 33].

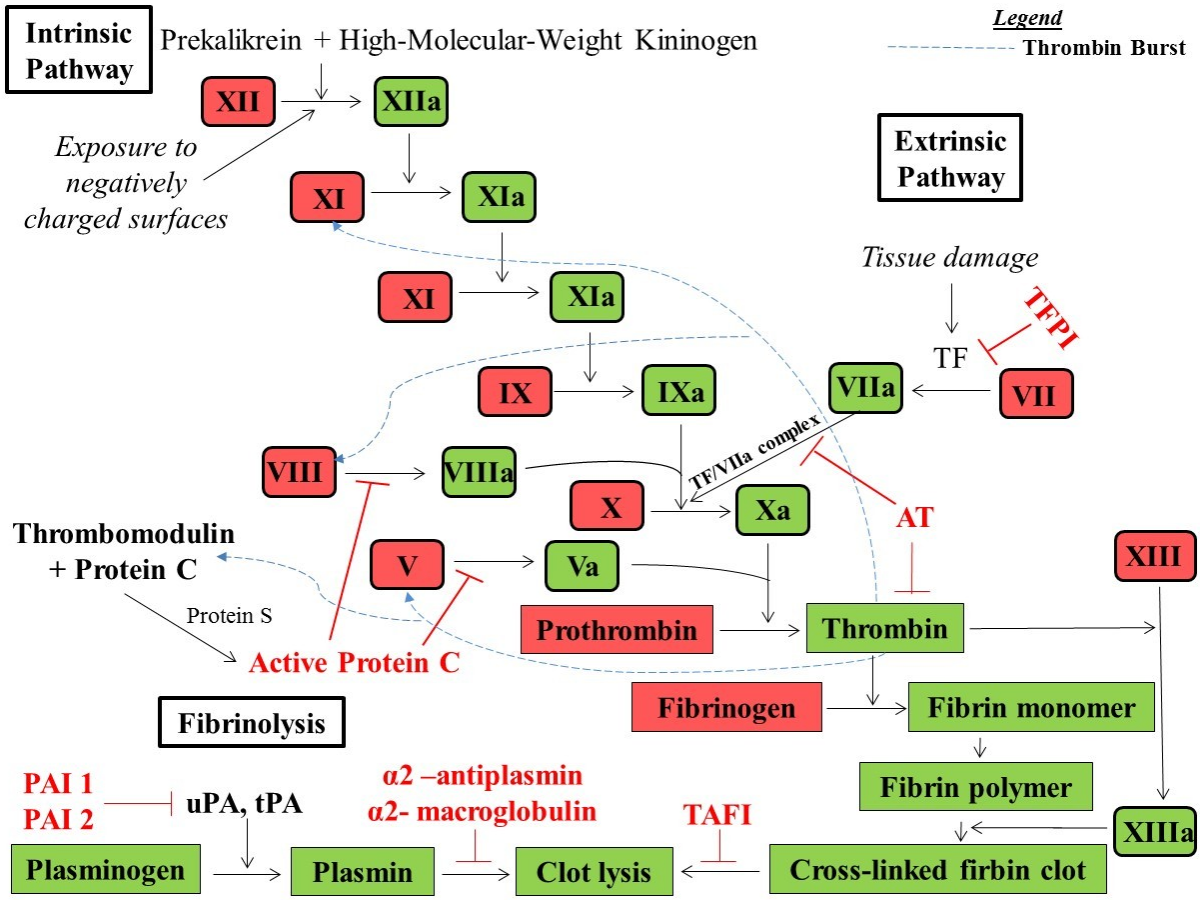

Figure 1.3. Coagulation cascade and negative regulation by the fibrinolytic system

1.1.4 Fibrinolytic System

The activation of the fibrinolytic system occurs simultaneously with the activation of the coagulation cascade. The primary task of the fibrinolytic system is to provide a counterbalance to the active coagulation cascade, thus preventing excessive blood clotting. The second task of the fibrinolytic system is to break down existing blood clots, which involves action of an enzyme called plasmin. Plasmin breaks down the fibrin clot, which leads to the formation of fibrin degradation products such as D-dimers. Plasmin is released from the liver as an inactive precursor – plasminogen. Plasminogen is converted to plasmin by the action of tissue plasminogen activator (t-PA) and urokinase plasminogen activator (u-PA), which are released from the vascular endothelium. Tissue plasminogen activator is released very slowly by the damaged endothelium and after several days the clot is broken down. Both t-PA and u-PA are irreversibly inhibited by plasminogen activator inhibitor-1 and plasminogen activator inhibitor-2 (PAI-1 and PAI-2). Plasmin activity is tightly regulated by its inhibitors alpha 2-antiplasmin and alpha 2-macroglobulin, which prevent excessive fibrinolysis. Thrombin-activatable fibrinolysis inhibitor (TAFI) also indirectly reduces plasmin activity by removing the fibrin C-terminal residues that are important for the binding and activation of plasminogen.

Healthy ECs express on their surface thrombomodulin (TM) - a glycoprotein, which binds thrombin and protects from formation of the blood clot. Interestingly, thrombin bound to TM serves as both an anticoagulant enzyme (by raising the speed of protein C activation) and a procoagulant enzyme (by activating fibrinolysis inhibitor – TAFI) [34]. Coagulation system is also kept in balance through the action of proteinase inhibitors, which under normal conditions limit the production of thrombin to prevent constant amplification of coagulation cascade and clot growth. The main inhibitors are antithrombin (AT) and protein C. The AT is a serine protease and main thrombin inhibitor, but it also binds and inhibits most of the activated coagulation factors - FIXa, FXa, FXIa, FXIIa and TF-FVIIa complex. The inhibitory activity of AT is boosted in vivo by heparin or heparin-like molecules, in particular heparan sulfate, found on the surface of ECs. Injections with heparin or heparan sulfate are used to treat and prevent deep vein thrombosis, pulmonary embolism and arterial thromboembolism [34]. The heparin cofactor II (HCII) is, similarly to AT, a thrombin inhibitor, but in contrast to AT, HCII requires far greater concentrations of heparin or heparin-like molecules for its optimal activity [34].

Another potent thrombin inhibitor - protein C - is activated when thrombin binds to TM on ECs and works by inhibiting the cofactors of the intrinsic tenase complex and the prothrombinase complex - FVIIIa and FVa respectively. Inhibition of these cofactors significantly decreases activity of their complexes and reduces thrombin generation. Activity of protein C is enhanced by protein S.

The tissue factor pathway inhibitor (TFPI) is a major extrinsic pathway inhibitor. TFPI is a polypeptide produced by ECs and present in blood at low concentrations. TFPI inhibits the TF-FVIIa complex and the TF-FVIIa-FXa complex which rapidly suppresses the initiation phase of coagulation and causes thrombin to amplify its own production. Similarly to protein C, activity of TFPI is enhanced by protein S [28]. Protein C inhibitor (PCI), also known as plasminogen activator inhibitor-3 (PAI-3), was originally identified as an inhibitor of activated protein C (APC). However, recent studies show that PCI also efficiently inhibits thrombin, FXIa, FXa and thrombin-thrombomodulin complex [34]. Alpha-1-antitrypsin and alpha-2-macroglobulin are protease inhibitors found in plasma that non-specifically inhibit any proteolytic enzymes, including activated coagulation factors.

Due to the coordinated actions of platelets, coagulation, and fibrinolysis haemostasis is a finely tuned process that maintains blood fluidity and regulates response to vessel injury. This requires the three main constituents – vessel wall, blood flow and blood components - to function properly and remain balanced. Thrombosis is a pathological extension of haemostasis, occurring when uncontrolled clot formation leads to vessel occlusion in either the arteries or veins, resulting in morbidity or even mortality (Figure 1.4).

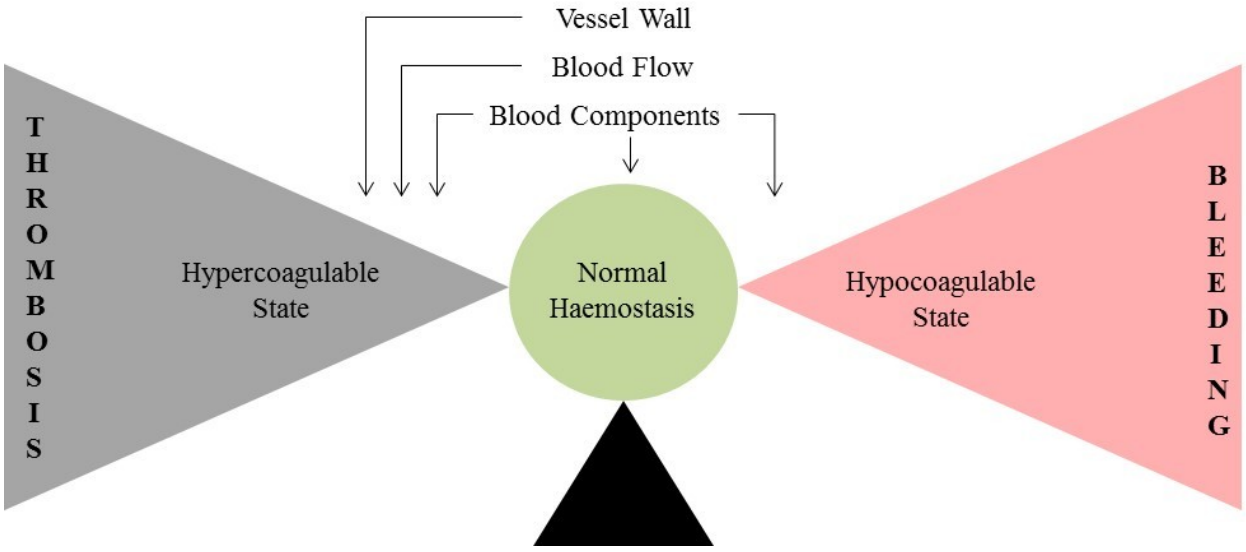

Figure 1.4. Haemostatic balance

Normal haemostasis requires balance between the three main factors: blood, blood vessel and blood flow. Imbalance between these factors may ultimately cause bleeding or thrombosis.

1.1.5 The Vessel Wall Structure and Vascular Spasm

Blood vessels facilitate transport of blood that carries oxygen and nutrients to the tissues and organs, and enable collection of waste products. Capillaries are the smallest blood vessels that consist of a monolayer of ECs adjacent to a basement membrane and nearby smooth-muscle-like cells called pericytes. Larger vessels have walls made up of three main layers and the opening inside – called lumen. The most internal layer of the vessel is tunica intima that consists of endothelial lining, basement membrane and a delicate layer of loose subendothelial connective tissue. Basement membrane and subendothelial connective tissue are made up of extracellular matrix (ECM) components such as collagen, vWF, laminin, nidogen and heparan-sulphate proteoglycan. Basement membrane ECM provides essential ligands which mediate platelet adhesion to ECs upon injury [35, 36]. Middle layer - tunica media - consists of circularly arranged elastic fibers, collagen and most importantly vascular smooth muscles (VSMs) that regulate vessel diameter through relaxation or contraction. Arteries have thicker smooth muscle layer than veins, and large arteries have additional layer of connective tissue called external elastic membrane, lying outside of the tunica media. VSMs control total peripheral resistance, primarily arterioles, and the distribution of blood flow throughout the body. Tunica externa (sometimes called adventitia) is the outermost layer of the vascular wall. It is mainly composed of connective tissue rich in collagen and fibroblasts that anchor and stabilize the blood vessel to nearby organs. Adventitia also contains autonomic nerves and in large vessels (>0.5 mm thick) network of capillaries called *vasa vasorum* ("vessels of the vessels") that provide oxygen and nutrients to the outer layers of the vessel [37-39].

Vascular spasm (vasoconstriction) is a first response to vessel injury, produced by a contraction of the VSMs. Damage to the vessel triggers sympathetic reflex through pain receptors located in the VSMs, which leads to the release of neurotransmitters (mostly norepinephrine) from sympathetic nerve endings and causes vasoconstriction. Smaller vessels have two layers of smooth muscles - inner circular and outer longitudinal, while larger vessels have only longitudinal layer. The circular muscle layer tends to constrict the flow of blood, whereas the longitudinal one draws the vessel back into the surrounding tissue. Vascular spasm is much more effective in smaller blood vessels due to contraction of the circular muscles [40].

The vascular spasm is also supported by endothelins, released from ECs in response to the vessel injury, and platelet factors secreted upon activation, such as serotonin, adenosine

diphosphate (ADP) and thromboxane A_2 (TXA_2), all of which amplify the effect of vasoconstriction. Physiological vascular spasm typically lasts few minutes. The opposite mechanism is vasodilation, which usually accompanies inflammation stage that begins as a part of physiological healing process following the injury [40].

1.1.6 The Blood Flow and Its Effect on Platelets

Blood flow is an important constituent of haemostasis because it exerts mechanical forces on the vessel wall including ECs and on the cellular components circulating in the blood including platelets. The vessel wall is continuously subjected to two main forces: circumferential stretch (perpendicular to the direction of blood flow) and fluid shear stress (parallel to the vessel wall and exerted longitudinally in the direction of blood flow). These forces are the result of pulsatile nature of blood flow and they act as regulators of cardiovascular physiology and pathophysiology [11].

Shear rate varies greatly depending on the vessel type, size and condition. In venules and large veins it is usually < 500 s^{-1}, in small arterioles < 5000 s^{-1} and in severe atherosclerotic arteries can be as high as 40 000 s^{-1} [41]. Additionally, blood hydrostatic pressure pushes platelets very close to the vessel wall because of their small size and weight. Interestingly, even in the conditions of high blood velocity platelets have a unique ability to form a stable aggregate. Shear force conditions determine which platelet adhesion receptors will be primarily engaged in response to the vessel injury. At low shear conditions (< 1000 s^{-1}) platelet adhesion (mediated by GPIbα, GPVI and $\alpha_2\beta_1$) triggers integrin $\alpha_{IIb}\beta_3$ outside in signalling causing platelet activation, but as the shear rates increase (> 1000 s^{-1}) platelets may form aggregate independent of integrin $\alpha_{IIb}\beta_3$ function referred to as "activation-independent platelet aggregation". This mechanism is mediated by binding of GPIbα not only to immobilized but also soluble vWF at high shear force conditions. Under physiological shear force platelets are unable to bind to soluble vWF (it has to be immobilized by collagen), but higher force induces conformation change (uncoils) of soluble vWF, which then binds to GPIbα on circulating platelets. This process is distinct from classical mechanism of platelet aggregation and may play a role in thrombotic occlusion of severely atherosclerotic arteries where shear conditions are considerably higher than in the normal circulation [42].

1.1.7 The Endothelium and Its Role in Regulating Vascular Tone

Until 1980's endothelium was viewed simply as the boundary between the blood in the lumen and the vessel wall. In fact, endothelium lines the lymphatic vessels and interior surface of all blood vessels from the heart to the smallest capillaries, and controls various processes such as vascular permeability, blood cell interactions with the vessel wall, the inflammatory response, and angiogenesis. Anatomically endothelium is adjacent to the VSM layer and in the arterioles both cell types even protrude through the internal elastic membrane to make direct contact (myoendothelial junctions). This proximity allows endothelium to regulate vascular tone by releasing various factors that induce VSM relaxation or contraction, which results in blood vessel dilation or constriction respectively. These factors are released in response to various stimuli that trigger mechanisms regulating vascular tone and in many instances several redundant pathways are active at the same time. The function of VSMs depends entirely on the concentration of intracellular Ca^{2+} thus when the concentration raises muscles contract and when it decreases muscles relax. All factors mentioned below or neuronal stimuli act through increase or decrease of the intracellular Ca^{2+} concentration and thus control vascular tone. VSMs remove Ca^{2+} to the extracellular space through Na^{+}/Ca^{2+} antiporter and Ca^{2+} ATPase pump [40].

VSM function is to maintain relatively constant blood flow by myogenic reflex. In situations of increased blood pressure VSMs constrict to prevent the vessel wall from overstretch and damage. The myogenic activity underlies the basal tone of small blood vessels and therefore is an important component of vascular resistance [40]. As the vessel diameter decreases, vasodilation becomes increasingly important and occurs via hyperpolarization of ECs that is transmitted to adjacent VSMs via myoendothelial junctions. This mechanism involves activation of voltage-independent small-conductance (SK_{Ca}) and intermediate–conductance (IK_{Ca}) Ca^{2+}-activated K^{+} channels on ECs. Importantly, because these channels are voltage-independent, they can operate at negative membrane potentials close to the K^{+} equilibrium potential [40, 43].

Diameter of the blood vessel is also modulated by multiple extrinsic and intrinsic factors that act either directly on the VSMs or indirectly through ECs. The extrinsic regulation is mainly exerted by neuronal sympathetic control (through α- and β-adrenergic receptors) and humoral control (through action of angiotensin II, vasopressin and atrial natriuretic peptide). The intrinsic regulation is mediated by endothelium-derived factors such as TXA_2, histamine or endothelin (ET) - the most potent constrictor [40]. On the other hand, endothelium continuously releases

molecules such as prostacyclin (PGI_2) and NO that cause vasodilation by relaxing VSMs [44-46]. In addition to its vasodilatory mechanisms endothelium-derived PGI_2 and NO also prevent circulating platelets from adhesion to intact healthy blood vessel and spontaneous activation causing thrombosis.

1.1.8 Regulation of Vascular Tone by Endothelium-Derived Nitric Oxide

Nitric oxide regulates vascular tone by inducing VSM relaxation. Low levels of NO released by ECs are essential for the maintenance of basal vascular tone. Endothelium releases NO in response to the shear stress of blood flowing through the vessel, which is the most fundamental physiologic stimulus and non-receptor-dependent mechanism [47]. In situation of elevated blood pressure, there is an increase in blood flow and vascular resistance, which exerts more shear stress on the ECs. As a compensatory mechanism, ECs generate more NO which causes vasodilatation and decreases blood flow [48]. This NO-dependent vasodilation is far greater in large diameter arteries compared to small resistance vessels.

NO produced by ECs diffuses into the VSMs where it binds to its intracellular receptor - soluble guanylyl cyclase (sGC) - and promotes formation of cyclic guanosine monophosphate (cGMP). Cyclic GMP in turn activates protein kinase G (PKG), which prevents the Ca^{2+} influx from voltage-dependent calcium channel (VDCC) and calcium release mediated by inositol trisphosphate (IP3) receptor (IP3R). When the intracellular concentration of Ca^{2+} decreases, myosin light-chain kinase (MLCK) can no longer phosphorylate myosin and relaxation of the VSMs causes vasodilation.

In addition to shear stress-induced endothelial NO production there is a number of endogenous agonists including acetylcholine, histamine, thrombin, serotonin, ADP, vascular endothelial growth factor (VEGF), bradykinin, norepinephrine and substance P that enhance NO release from the endothelium. Interestingly, some of these agonists (acetylcholine, serotonin, norepinephrine and histamine) constrict VSMs when they act directly on the muscular layer such as in the absence of endothelium [49].

1.1.9 Endothelial Phenotype and Inflammation

Endothelial cells also interact with blood cells like leukocytes and platelets via numerous receptors that facilitate thrombus formations and/or inflammatory processes. The endothelium of the blood vessels contains adhesion complexes, including tight junctions that seal off the lumen from the underlying basement membrane and interstitial matrix. Undamaged and noninflamed ECs remain in quiescent state – non-adhesive to circulating cells, including platelets and leukocytes. In addition to synthesis of PGI_2 and NO, ECs express two enzymes: CD39 and CD73, which have anti-thrombotic and anti-inflammatory properties. CD39 hydrolyzes ADP to adenosine monophosphate (AMP), which allows for ADP elimination and prevents from prothrombotic platelet activation. CD73 converts AMP to adenosine that limits thrombosis by blocking platelet activation and acting as an anti-inflammatory mediator through its receptors.

The endothelium mediates inflammatory reactions in response to injury or infection to preserve normal structure and function of the vessel wall. However, excessive or chronic inflammatory reactions can lead to severe tissue damage and contribute to the development of atherosclerosis. Atherosclerotic lesions impair the anti-thrombotic and anti-inflammatory mechanisms of ECs resulting in progression of the lesions. Activation of ECs and damage of EC surface glycocalyx are thought to be one of the first mechanisms that can induce endothelial dysfunction [50, 51].

ECs are covered luminally by glycocalyx - a negatively charged network of membrane-bound proteoglycans and glycoproteins. Glycocalyx harbors ECs adhesion molecules, such as P-selectin, E-selectin, intercellular adhesion molecule 1 (ICAM-1) and vascular cell adhesion protein 1 (VCAM-1), which primarily mediate adhesion in response to inflammation, but also are responsible for mechanotransduction in response to blood flow. Endothelial glycocalyx also regulates vascular permeability and limits access of certain molecules to the EC membrane. Recent studies suggest that glycocalyx may be involved in mechanotransduction of shear stress signals that initiate several signalling pathways, such as NO production and cytoskeletal reorganization [51]. Damage of EC glycocalyx appears to be the first detectable injury to the vascular wall during the development of atherosclerosis and is associated with increased vascular permeability and adhesiveness. High amounts of oxygen-derived free radicals mediate formation of ox-LDL, which degrades the glycocalyx layer and exposes constitutively expressed adhesion molecules that facilitate platelet-EC adhesion. Inhibition of free radicals prevents formation of

ox-LDL and limits platelet-EC adhesion. Additionally, adsorption of plasma substances onto the EC glycocalyx recovers anti-adhesive properties of endothelium [51].

Local haemodynamics significantly affect the EC phenotype which regulates ECs interactions with cellular components and response to systemic atherogenic factors [36]. In blood vessels with high laminar flow ECs align parallel to flow direction and have reduced turnover. Unidirectional flow also induces adaptations in the EC gene expression pattern in favor of anti-inflammatory and antioxidant responses [10, 11]. In contrast, ECs exposed to turbulent flow are poorly aligned and have enhanced turnover. They also have upregulated pool of pro-inflammatory genes and demonstrate elevated oxidant stress both basally and in response to stimulus [11]. The ECs localized at the blood vessel interface are constantly exposed to vascular forces, including shear stress. Shear stress has different patterns based on vessel geometry and type, ranging from unidirectional laminar flow to turbulent flow. The disturbed blood flow occurring in regions of disease-associated stenosis, arterial branch points and sharp turns can induce pro-atherogenic phenotypes in ECs. Low shear stress associated with disturbed flow causes the activation of nuclear factor kappa B (NF-κB) and expression of pro-inflammatory proteins. It also increases the production of superoxide ($O_2^{\bullet -}$) and adhesion of monocytes to ECs. The ECs localized in regions of disturbed flow have no preferred orientation and are not aligned to the direction of flow. On the other hand, normal laminar flow triggers EC physiological functions such as NO production, cytoskeleton remodeling, alignment to the direction of flow and activation of transcription factors, such as Krüppel-like factor 2 (KLF2) and nuclear factor-E2-related factor-2 (NRF2/Nrf2), which promote EC survival [52-55]. The disruption of vascular homeostasis as a result of endothelial dysfunction contributes to early and late stages of atherosclerosis [56, 57].

1.1.10 Vessel Wall Interactions in Inflammation

Under physiological conditions, cellular blood components (such as leukocytes and platelets), coagulation system and endothelium remain balanced and function in favor of each other. Development of local or systemic inflammatory state triggers complex interactions between vessel wall ECs, leukocytes and platelets. This reciprocal interplay is mediated by cell adhesion and production of soluble pro-inflammatory mediators that further propagate vascular inflammation and thrombosis.

To keep platelets in a resting state endothelium releases NO generates prostacyclin (PGI_2), and also expresses the ectonucleotidase CD39 and platelet-endothelial cell adhesion molecule-1 (PECAM-1) [58-60]. However, in certain circumstances like inflammation, human platelets adhere to endothelium which is mechanically intact but activated and procoagulant. In such instances conventional pathways that involve platelet adhesion and activation to exposed collagen and collagen-bound vWF are not applicable. Patients with chronic inflammatory diseases have high levels of plasma endotoxins and pro-inflammatory cytokines such as interferon gamma (IFN-γ), interleukin-1 (IL-1) or tumor necrosis factor-α (TNF-α), all of which contribute to ECs activation [61]. As a consequence, ECs increase the expression and/or secretion of the prothrombotic proteins (such as vWF, P-selectin and TF) and adhesion receptors (such as E-selectin, thrombospondin 1 (TSP-1), ICAM-1 and VCAM-1). P-selectin is translocated from the ECs Weibel–Palade bodies to the outer plasma membrane within minutes from inflammatory stimuli [62]. Circulating platelets upon initial contact with P-selectin start to tether and roll, and this behavior is mediated by P-selectin glycoprotein ligand-1 (PSGL-1). This initial capturing slows down platelet velocity and stimulates activation. Next, platelets weakly adhere via GPIbα to vWF that is secreted by ECs and deposited on the vessel wall; this in turn further promotes endothelial activation. There is also evidence that inflamed ECs express on their surface αvβ3 integrin and ICAM-1 bridging molecules like vWF, fibronectins and fibrinogen, which subsequently interact with platelet integrin $\alpha_{IIb}\beta_3$ and provide stable adhesion [63-65]. Another mechanism that triggers $\alpha_{IIb}\beta_3$ activation involves binding of ECs TSP-1 with platelet integrin associated protein (IAP) [66, 67]. Additionally, it has been reported that TSP-1 binding to platelet GPIbα provides firm adhesion at elevated shear rates up to 4000 s^{-1} independently of vWF [68].

Activated platelets and ECs actively secrete pro-inflammatory cytokines such as interleukin 1β (IL-1β), interleukin 8 (IL-8), CD40 L, chemokine (C-C motif) ligand 5 (CCL5) and chemokine (C-X-C motif) ligand 4 (CXCL4), which stimulate leukocyte recruitment and promote local inflammation. The leukocytes leave the bloodstream and enter subendothelium in sequential manner that can be divided into three main phases: 1) tethered leukocytes roll over the endothelial surface via E- and P-selectin, then 2) arrest and spread and 3) migrate between ECs and attach to underlying ECM components [69, 70]. Leukocyte infiltration to subendothelium further promotes local chronic inflammation and thus contributes to the development and progression of atherosclerotic lesions.

Activated platelets also directly interact with leukocyte PSGL-1 receptor via P-selectin, mobilized to platelet surface following platelet granule release [71]. The platelet-leukocyte adhesion is strengthened by additional interactions of: platelet GPIbα with macrophage-1 antigen (Mac-1), platelet intercellular adhesion molecule-2 (ICAM-2) with lymphocyte function-associated antigen-1 (LFA-1) and platelet junctional adhesion molecule-3 (JAM-3) with macrophage-1 antigen (Mac-1) [72]. Formation of platelet-leukocyte aggregates provides evidence that thrombosis and inflammation are mechanistically linked. Moreover, reciprocal interactions of endothelium, platelets and leukocytes promote vascular inflammation and chronic endothelial dysfunction associated with the progression of CVD.

1.1.11 Characteristics of Arterial and Venous Thrombosis

Thrombosis occurs in response to uncontrolled formation of obstructive blood clot inside the blood vessel, which results in tissue ischemia. Even though thrombosis can occur in both arterial and venous circulation, broadly, the pathophysiology and treatment strategies are different [73].

Venous thrombosis most often occurs in large veins of the legs (deep vein thrombosis) and in some cases can cause pulmonary embolism. Both deep vein thrombosis (DVT) and pulmonary embolism are collectively referred to as venous thromboembolism, which is the third leading cause of CVD-associated deaths, after MI and stroke [74, 75]. Importantly, both embolic MI and stroke can originate from venous thrombosis. However, cerebral venous infarctions in the course of venous thrombosis are much rarer than ischemic strokes of arterial etiology and constitute about 0.5–5% of causes of all strokes [76, 77]. Similar, coronary embolism comprises of 3% of all ACS, with most common underlying causes being valvular heart disease, cardiomyopathy and atrial fibrillation [78, 79]. Venous thrombi are referred to as red clots and their main constituents are fibrin and red blood cells.

There is no uniform pathophysiological mechanism causing venous thrombosis. However, blood stasis, plasma hypercoagulability and activation of endothelium are the three components that highly contribute to development of venous thrombosis. The triggering mechanism usually depends on harmful effects of various risk factors that promote prothrombotic environment. Some of these risk factors are: old age, obesity, alcohol consumption, smoking, malignant tumors, prolonged bed rest, pregnancy, hormonal therapy and sedentary conditions. In addition, hypercoagulable state is also associated with some genetic mutations: specific conditions such as antiphospholipid syndrome or metabolic syndromes like diabetes and hypercholesterolemia [76, 80, 81]. DVT begins at the venous valves, which are prone to blood stasis. This in turn leads to local hypoxia, which activates ECs and increases hematocrit causing hypercoagulable microenvironment. Furthermore, under normal conditions ECs do not express procoagulant TF, except when they are exposed to proinflammatory cytokines or hypoxia [81, 82].

On the other hand, arterial thrombosis is the prevalent cause of MI and about 80% of strokes [83]. The most common pathophysiology of arterial thrombosis causing MI and ischemic stroke is related to atherosclerotic plaque rupture, which leads to formation of thrombus that

occludes an artery and stops the blood flow. The rupture of the plaque exposes the subendothelium, which triggers platelet-mediated thrombus formation. The arterial thrombus forms via a series of sequential steps in which platelets adhere to subendothelium, and then they become fully activated and recruit additional platelets to the growing aggregate. The damage to the vessel wall also leads to release of TF from atherosclerotic plaque and VSMs. Upon contact with flowing blood, TF activates the clotting cascade causing generation of thrombin. The thrombin burst facilitates fibrin formation, which additionally stabilizes the platelet aggregates. Arterial thrombi formed on atherosclerotic lesions have white color, because platelets remain their main constituent. Separate type of ischemic stroke is cardioembolic-stroke that is caused by blockage of cerebral artery by thrombotic material traveling from the heart most commonly after MI or due to atrial fibrillation [84].

Because of different pathophysiology and mechanisms involved in thrombus formation, the arterial thrombosis requires different pharmacological treatment than the venous thrombosis. In general, the arterial thrombosis is treated with the drugs that target platelets, while the venous thrombosis is treated with drugs that target components of the coagulation cascade [39].

1.2 Platelet Biology

1.2.1 Platelet Discovery and Role

First observations of blood platelets date back to the late 1800's, when several physicians described interesting phenomena related to blood and blood cellular components, which were called at the time blood-corpuscles [85-89]. Italian physician Dr. Giulio Bizzozero was the first who elucidated function of platelets in the blood clotting. While studying histological and histopathological samples under the microscope, he noticed small cell elements clumped together at the sites of vessel damage [90]. He also described the morphological changes of platelets after exposure to "foreign surfaces", followed by the formation of aggregates and subsequent "white thrombi" [91].

Blood platelets are a key cellular component of haemostasis. These small (2-4μm) anucleate cell fragments have crisp discoid shape when unstimulated, but upon activation they become spherical and extend filopodia. Human platelets originate from bone marrow megakaryocytes (MKs) and have a life span of 7–10 days, whereas mice platelets survive in circulation only for 4–5 days [92, 93]. Approximately $^{2}/_{3}$ of all available platelets circulate in blood at physiological concentration of 150,000-450,000 per μl and the remaining $^{1}/_{3}$ is sequestered to the spleen as a reserve. To maintain steady-state physiological platelet count, the human body produces and removes 10^{11} platelets daily [94, 95].

Historically platelets were thought to be cellular debris but in fact they are a key cellular component of haemostasis, responsible for the physiological formation of a platelet plug (also called an aggregate or thrombus) in response to vascular injury. Multiple studies also demonstrated that platelets are indispensable for processes such as wound healing, angiogenesis, inflammation, innate immunity and cancer metastasis. These multiple processes are mediated by abundant surface receptors anchored in platelet plasma membrane that respond to various molecules and finely regulate signal-dependent platelet activation and granule release [96].

1.2.2 Platelet Plasma Membrane and Other Membrane Systems

The exterior surface of circulating and resting platelets contains a layer of glycoproteins and glycolipids known as the glycocalyx. The net negative charge of the glycocalyx provides a repulsive force which protects circulating platelets from spontaneous activation when they interact with other platelets, blood cells and ECs in the blood vessel. In addition, this negative charge allows for the capture of plasma proteins and subsequent endocytosis into platelet granules [97-99]. Glycocalyx also regulates platelet lifespan via changes in sialic acid composition of platelet glycoproteins, mainly GPIb [100].

Platelet plasma membrane is selectively permeable, and the membrane bilayer provides phospholipids that support platelet activation and plasma coagulation. While the neutral phospholipids phosphatidylcholine and sphingomyelin are located in the outer plasma layer, the negatively charged or polar phospholipids phosphatidylinositol, phosphatidylethanolamine and PS predominate in the inner, cytoplasmic layer. The phosphatidylcholine and phosphatidylinositol serve as substrates for production of arachidonic acid (AA), which is enzymatically converted into eicosanoids – prostaglandin H_2 (PGH_2) and thromboxane A_2 (TXA_2) - during platelet activation. Furthermore, negatively charged PS and phosphatidylinositol are actively kept in the cytoplasmic layer by ATP-dependent enzymes called flipases to maintain non-procoagulant state of the platelet membrane. However, upon platelet activation ATP-dependent flippases and scramblases expose the phospholipids on the platelet surface. Exposed phospholipid - PS together with Ca^{2+} aid assembly of tenase complex and prothrombinase complex, which triggers platelet-surface based coagulation reactions [101]. The hydrophobic internal layer also contains dynamic, cholesterol and sphingolipid-rich microdomains called lipid rafts, most notably caveolae, that play important roles in signalling and intracellular trafficking in platelets [102, 103].

Submembrane layer consists of actin and myosin microfilaments that enable platelet movement and shape change. Platelet cytoplasm is composed of randomly dispersed organelles such as ribosomes, lysosomes, mitochondria, alpha (α) granules and dense (δ) granules. Moreover, cytoplasm contains a large amount of glycogen as a source of energy, Golgi apparatus and complex membranous systems called an open canalicular system (OCS) and dense tubular system (DTS) [104, 105]. OCS and DTS intertwine but are not interconnected and in contrast to the OCS, the DTS does not associate with the plasma membrane [104, 106].

The OCS is formed by unique invaginations of inner plasma membrane that create tunneling network of surface-connected channels that span the platelet interior [107]. The main function of platelet OCS is to increase the surface of intake and release of granule contents to the platelet exterior. Because platelets have very little capacity for protein synthesis, they take up through OCS a number of plasma proteins including fibrinogen and tissue factor (TF) that are later redistributed to platelet organelles (e.g. α- and δ-granules). OCS also remains an internal membrane reservoir that may facilitate filopodia formation and spreading following platelet adhesion. Lastly, the OCS may function as an internal storage site for cell adhesion glycoproteins such as GPIIb/IIIa, GPIb/XI/V complex and GPVI, which primarily localize on the external plasma membrane. When platelets activate these receptors evaginate and increase pool of platelet surface receptors [108].

The DTS (or demarcation membrane system) derives from MK smooth endoplasmic reticulum and is localized in the platelet submembrane region in the vicinity of microtubules. DTS forms closed-channel network of elongated and irregular flattened cisternae and tubules. The DTS serves as storage of 30% of total platelet Ca^{2+} content and a variety of metabolic enzymes involved in platelet activation, such as phospholipase A_2 (PLA), cyclooxygenase 1 (COX-1) and TXA_2 synthase that catalyzes the conversion of PGH_2 to TXA_2 [109, 110]. The storage of Ca^{2+} is controlled by ATPase pumps located on DTS membranes and coupled to plasma membrane Ca^{2+} ATPases (PMCAs). The Ca^{2+} ATPases are controlled by the cytosolic cyclic adenosine monophosphate (cAMP) level, which keeps calcium stored in the DTS. Decrease in cytosolic cAMP favors the liberation of Ca^{2+} from the DTS into cytosol, which initiates platelet activation. Moreover, release of Ca^{2+} from intracellular stores is also critical for platelet granule movements and secretion [111].

Taken together, platelet plasma membrane and inner membrane systems - OCS and DTS - play a vital role not only in selective transport and trafficking of molecules, storage and/or synthesis of various factors and ions, but also in activation of platelets and coagulation cascade.

1.2.3 Platelet Cytoskeleton

The discoid shape of the resting platelet is supported by a well-defined and highly specialized cytoskeleton that withstands shear and other forces in the circulation. On the other hand, platelet cytoskeleton is very dynamic because it has to remodel rapidly upon activation, which allows to respond quickly to vascular damage and helps platelets to change shape and form aggregates during hemostasis. Spectrin, actin and tubulin are the three major proteins that structure platelet cytoskeleton. Spectrin strands assemble with actin filaments and both form meshwork that underlies the plasma membrane. Some portion of actin filaments is not attached to spectrin and forms actin cytoplasmic network. Network of actin filaments also interacts with the cytoplasmic tails of GPIbα, which mediates platelets adhesion and capture at high shear [112]. Spectrin also associates with membrane phospholipids which provides further anchor of the cytoskeleton to the plasma membrane [113]. Spectrin-actin meshwork and actin cytoplasmic network are important for the maintenance of membrane stability and integrity. Moreover, MK actin-spectrin-dependent cortical forces balance microtubule forces, which determine platelet size during formation from MKs [114].

Another important feature of platelet cytoskeleton is peripheral microtubule coil which maintains the disc shape of resting platelets and is directly involved in the shape change and internal reorganization triggered by platelet activation. The microtubules are hollow tubes made of polymerized α-β tubulin dimers and are decorated with proteins that modulate polymer stability [115, 116]. Kinesin and cytoplasmic dynein are the major microtubule motors and MK cytoplasmic dynein drives elongation of MK proplatelets [117].

Platelets change their shape upon activatory stimulus, which triggers events that involve a rearrangement of the cytoskeletal proteins. Normally, platelets as disc-shaped cells change into spheres with filopodia and ultimately spread at the site of injury. This is associated with disassembly of a microtubule ring, which results in an intermediate spherical shape and extension of membrane tethers and/or filopodia due to actin polymerization. Biochemical process that initiates shape change is induced by phosphorylation of the regulatory myosin light chain, which facilitates association of myosin with actin filaments and thereby activates platelet contractile machinery. Fully activated platelets spread out and retract filopodia, taking the shape that resembles “fried egg”. Increasing wall shear rate enhances platelet shape change dynamics [118].

1.2.4 Platelet Secretory Organelles

Human platelets have three major secretory organelles: α-granules, δ-granules and lysosomes that next to OCS are another important delivery system. Platelet adhesion via surface receptors initiates signalling that promotes degranulation and release of organelles content to platelet surface and extracellular space. Following platelet activation, α- and δ-granules fuse with the OCS or plasma membrane and release their cargo in the process of exocytosis. The fusion with OCS is mediated by granule surface proteins - vesicle-associated membrane proteins 3 and 8 (VAMP-3 and -8)(family of SNARE proteins), which interact with syntaxins 2 or 4 and synaptosome associated protein 23 (SNAP-23) on the OCS membrane, linking tightly and forming an exocytic complex [119]. This liberates a great number of molecular mediators such as: coagulation factors, chemokines, adhesion molecules, immunologic molecules, regulators of growth and angiogenesis, adenosine triphosphate (ATP), ADP, Ca^{2+}, enzymes, neurotransmitters and sugars.

The most abundant and heterogenous are α-granules. Under electron microscope α-granules have round to oval shape, size of 200-500 nm and are present in number of 40-80 per platelet [120]. As an important secretory organelles α-granules store the majority of platelet factors associated with haemostasis, but also proteins involved in inflammation, wound healing, mitogenic growth factors and a broad range of chemokines (list of major α-granule content in a table listed below). Proteomic study identified 284 proteins in a sample of fractioned α-granules [121]. The membrane of α-granules also contributes to the pool of platelet adhesion-mediating receptors (GPIb/XI/V complex, GPVI, GPIIb/IIIa, PECAM-1 and CD9), which upon platelet degranulation are exposed on the platelet surface. Interestingly, P-selectin is exclusively expressed on α- and δ-granules and often used as a marker of granule secretion [106].

The other platelet granules are small (~150 nm) δ-granules, which also have round to oval shape and are present in number of 3–8 per platelet. Platelet δ-granules store high levels of Ca^{2+} (60-70% of total platelet Ca^{2+} content), ADP, ATP and serotonin. Similarly to α-granules, δ-granules also express some of the glycoproteins (GPIb, GPIIb/IIIa) that mediate platelet adhesion when present on the surface upon secretion [122]. Granule secretion upon platelet activation results in release of platelet agonist-ADP that potentiates recruitment of nearby platelets to the growing aggregate. Release of serotonin causes local vasoconstriction and acts as weak platelet agonist on serotonin $5HT_2$ receptors which helps limit blood loss [123].

Platelet lysosomes have a similar size (~200 to ~250 nm) and morphology as α-granules; therefore, their identification is aided by cytochemical staining directed towards lysosomal enzymes such as acid phosphatase. Lysosome interior is highly acidic (pH of 4.5 to 5.0) due to the presence of hydrolytic enzymes that upon release degrade extracellular matrix (ECM), which facilitates tissue remodeling. Similar to α- and δ-granules, platelet lysosomes release their content upon platelet activation but it requires greater stimulation. Expression of lysosomal integral membrane protein 1 (LIMP-1) on the platelet surface is used as a marker of significant platelet activation [123].

1.2.5 Platelet Mitochondria

Platelets are highly reactive circulating blood cells but contain relatively small number of simple mitochondria. It was once thought that platelet mitochondria act only as ATP providers to meet energy demands of resting and activated platelets. Platelets activated by various agonists undergo dynamic morphological and biochemical changes which require large amounts of energy, therefore to sustain ATP production platelets oxidize the essential energetic substrates such as glucose, glutamine and fatty acids [124]. Under physiological conditions, oxidative phosphorylation is the primary source of ATP, but in hypoxia, platelets switch to glycolysis [125-127]. Interestingly, emerging new mechanisms of platelet mitochondria implicate their function in platelet apoptosis and enhancing of platelet activation. During activation platelet mitochondria generate high levels of reactive oxygen species (ROS) which have been reported to play a role in high-level PS exposure which potentiates initial activatory signals [128]. In addition, platelet mitochondria contribute to Ca^{2+} homeostasis by providing additional pool of Ca^{2+} upon strong activation, which allows for high-level of PS exposure. Importantly, this mechanism is enhanced in subpopulation of procoagulant platelets [129]. Lastly, mitochondria also participate in regulation of platelet lifespan by programmed cell death via intrinsic apoptotic pathway.

1.2.6 Platelet Clearance Mechanisms

Hundreds of billions of platelets are cleared daily from the circulation by efficient and highly regulated mechanisms. Platelets reaching their lifespan are destroyed mainly in the liver and spleen, but in some pathological conditions also by the immune system. Senescent platelets are removed from the circulation by two major pathways that involve mitochondrial (intrinsic) apoptotic signalling and platelet desialylation.

Similar to many nucleated cells, platelet intrinsic apoptosis depends on the balance between pro-apoptotic and anti-apoptotic proteins. Anti-apoptotic Bcl-2 family proteins restrain the pro-apoptotic Bak and Bax proteins. Human platelets express several anti-apoptotic Bcl-2 proteins (Bcl2, Bcl-$_{XL}$, Bcl-w, Mcl1, and Bcl2A1) but it is BCL-$_{XL}$ that predominantly suppresses the pro-apoptotic Bak and Bax. In aging platelets the level of anti-apoptotic Bcl-$_{XL}$ protein decreases over time due to the degradation, which ultimately triggers the cell death. Furthermore genetic removal or pharmacological inactivation of Bcl-$_{XL}$ reduces platelet half-life and causes thrombocytopenia in a dose-dependent manner. And vice versa platelets from Bak-deficient mice have longer life span than from wild type (WT) mice [130, 131].

This intrinsic apoptotic mechanism also mediates platelet death in response to non-receptor-mediated stress signals such as intracellular injury or exposure to chemotherapeutic agents, which activate the BH3-only proteins (Bid, Bim, Bad, and Bik). The BH3-only proteins overwhelm pro-survival activity and directly activate Bax and Bak proteins, which transmit the death signal leading to mitochondrial membrane damage and release of cytochrome *c* into the cytosol. This triggers formation of the apoptosome and activation of caspase-9 (Cas-9) that initiates the apoptotic caspase cascade to execute cellular demolition. Lastly, the PS exposure targets apoptotic platelets for phagocytosis [131, 132].

According to more recent data, platelet apoptosis can be induced by the extrinsic signalling via death receptor-mediated response causing activation of caspase-8 (Cas-8) and its downstream pathways. However, limited and contradictory data do not support so far its unquestionable presence and role in regulating platelet lifespan [132-134].

Recent studies have also brought attention to the role of desialylation of senescent platelets in mediating their clearance. Over platelet lifespan, the surface glycoproteins, most notably GPIbα, lose the terminal sialic acid residues in their glycans by action of glycoside hydrolase enzyme, causing increased exposure of penultimate β-galactose (β-gal). The exposed

β-gal on the platelet surface can be recognized by the Ashwell-Morell receptor (AMR) on the surface of hepatocytes and/or liver macrophages (Kupffer cells), which facilitate the clearance of the platelet from circulation [135, 136]. The removal of senescent platelets through the AMR receptor also stimulates hepatocyte TPO mRNA production via janus kinase 2 and signal transducer and activator of transcription 3 (JAK2-STAT3) signalling which provides positive feedback loop for a normal steady state platelet production [100, 135].

It is unknown whether platelet desialylation in vivo triggers the intrinsic apoptotic machinery or maybe the Bcl-2 family proteins modify platelet surface sialic acid content. Whether both mechanisms interact with each other or operate independently remains to be established.

There are also multiple mechanisms that involve shedding or of platelet glycoprotein GPIbα that contribute to accelerated platelet clearance. In platelets, the GPIbα mechanosensory domain (MSD) is continuously cleaved by ADAM metallopeptidase domain 17 (ADAM17). This mechanism not only affects circulating platelets but also resting platelets stored for transfusion, which limits their shelf life [137-139]. In physiological shear flow conditions the shedding occurs when MSD is unfolded, but in high or turbulent shear flow conditions GPIbα spontaneously binds to soluble vWF, which unfolds MSD and further exposes the ADAM17 cleavage site. Under normal shear flow, soluble vWF does not spontaneously associate with the GPIbα. This enhanced mechanism of GPIbα cleavage leads to platelet desialylation and accelerated clearance [140]. Interestingly, an antibiotic ristocetin was pulled from clinical use because it caused thrombocytopenia and clotting by inducing spontaneous association of soluble vWF to GPIbα [141].

In pathological conditions such as immune thrombocytopenia (ITP) auto-antibodies induce platelet desialylation of surface glycoproteins (primarily GPIIb/IIIa and GPIbα), leading to Fc-dependent clearance via macrophages and cytotoxic T lymphocytes [142-145].

1.2.7 Platelet Activation and Aggregation

Platelets are primarily responsible for limiting blood loss upon vascular injury by formation of the platelet plug or aggregate. This involves coordinated series of events divided into three major phases: initiation, extension and stabilization, each of which is supported by signalling events within the platelet (Figure 1.5-1.6). All above phases greatly rely on platelet receptors that activate transduction pathways signalling to maintain platelet haemostatic function.

Initiation Phase - Platelet Adhesion

Under steady state conditions, platelets circulate with other cellular blood components in an environment surrounded by a continuous monolayer of ECs. They move freely but are quiescent. Mechanical trauma, chronic inflammation and certain diseases can cause damage to the vessel wall, which exposes vascular extracellular matrix (ECM) to the flowing blood. Some components of ECM such as vWF, collagen, laminin, TSP-1, fibronectin and vitronectin act as ligands for platelet surface receptors and upon contact mediate platelet adhesion, as summarized in Table 1.1.

Initial contact and adhesion to ECM is mediated by vWF and platelet GPIb/IX/V complex. This receptor interaction mediates platelet rolling on the subendothelium until they firmly adhere or return to the circulation. Platelets only bind to vWF that is immobilized by subendothelial collagen and GPIb/IX/V complex does not bind soluble vWF under physiological conditions. The GPIb/IX/V complex is made up of four subunits: GPIbα, GPIbβ, GPIX and GPV, but only GPIbα binds vWF, while GPIbβ and GPIX anchor the complex in platelet membrane. The interaction between vWF and GPIbα is rapid but reversible and insufficient for stable adhesion. Furthermore, this initial interaction via GPIbα significantly decelerates platelets and allows engaging collagen receptors, which facilitate strong adhesion. Collagen receptors GPVI and GPIa/IIa (or integrin $\alpha_2\beta_1$) complex are less abundant than GPIb/IX/V complex, thus have slower on-rates for collagen comparing to very fast on-rates of GPIb/IX/V complex for vWF - which is especially important under high shear rates (> 1000 s^{-1}) such as in microcirculation [146]. However, under high shear rates subendothelial vWF interacts with both the GPIb/IX/V receptor complex and platelet GPIIb/IIIa complex (or integrin $\alpha_{IIb}\beta_3$), known as platelet fibrinogen receptor [147]. Platelet binding to subendothelial collagen via GPVI and GPIa/IIa complex reinforces initial adhesion and triggers platelet activation [148]. GPVI

mediated "inside-out" signalling is a major platelet activator although weak signals from GPIb/IX/V also contribute to activation. Other platelet integrins such as $\alpha_5\beta_1$, $\alpha_6\beta_1$, $\alpha_v\beta_3$ bind to their respective ligands and therefore further supporting platelet adhesion to subendothelium.

Summarizing, the initiation phase creates a platelet monolayer which serves as foundation for growing aggregate. GPVI mediated "inside-out" signalling promotes granule secretion which stimulates additional pro-aggregatory pathways and recruitment of other platelets to the growing aggregate. In parallel, tissue factor (TF) triggers local thrombin generation and coagulation cascade, which also contributes to platelet activation.

Extension Phase - Platelet Activation

Activation begins seconds after platelet initial adhesion which triggers weak signals from GPIb-IX-V that are soon reinforced by potent signals from collagen receptors, mainly GPVI signalling. Signal transduction mediated by GPVI and GPIb/IX/V leads to activation of phospholipase C (PLC) and generation of the second messengers inositol triphosphate (IP_3) and diacylglycerol (DAG), which are responsible for mobilization of intracellular Ca^{2+} and activation of protein kinase C (PKC) respectively. Activation of these multiple pathways mediates platelet spreading (cytoskeletal rearrangement - shape change and organelle centralization), platelet granule secretion at the site of vascular injury and secondary activation of platelet integrins. Activated platelet integrins link ECM with platelet cytoskeleton by focal adhesions. This mechanism is enhanced by generation of IP_3 which activates Rap1 downstream mechanism which in turn stimulates focal adhesion proteins - talin and kindlin - to bind to cytoplasmic tail of platelet integrins β-subunit [149]. This changes integrin conformation (most importantly β_3 subunit of integrin $\alpha_{IIb}\beta_3$) from low-affinity to high-affinity state for ligand binding and hence further promotes activation and integrin clustering [150].

Stabilization Phase - Platelet Aggregation

Platelets degranulation leads to release/generation of soluble agonists such as ATP, ADP, TXA_2, fibrinogen, matrix metalloproteinase-2 (MMP-2), serotonin and thrombin. These agonists act on platelet G-protein coupled receptors (GPCRs) and generate "inside-out" signalling that induces full platelet activation and recruitment of nearby platelets to the forming aggregate (Table 1.2). Stabilization phase begins with conformational activation of integrin $\alpha_{IIb}\beta_3$, which facilitates binding of soluble fibrinogen. Adjacent platelets are bound to each other via fibrinogen bridges, which stabilize the aggregates. Integrin $\alpha_{IIb}\beta_3$ preferentially binds to

fibrinogen, however other molecules such as vWF, fibronectin, TSP-1 and vitronectin also bind to $\alpha_{IIb}\beta_3$ but with lower affinity [151].

Moreover, platelet activation exposes inner membrane PS outward, which results in negative net charge of the platelet surface. This provides a "procoagulant" surface for assembly of tenase and prothrombinase complexes, leading to massive thrombin generation on the platelet surface. Consequently thrombin cleaves fibrinogen to form rigid fibrin mesh that additionally supports the blood clot. Over the next few days platelets pull on the fibrin threads via their integrin $\alpha_{IIb}\beta_3$ causing clot retraction (clot shrinking), which slowly brings the damaged vessel edges together [150].

Receptor	Family	Ligands
GPIb-IX-V complex consists of four subunits: GPIbα, GPIbβ, GPV and GPIX	Leucine-rich repeat family	vWF, TSP-1, P-selectin, thrombin, FXII, FXII
GPVI	Ig superfamily	Collagen, laminin
$\alpha_{IIb}\beta_3$ (GPIIb/IIIa)	Integrin	Fibrinogen, fibrin, vWF, TSP-1, fibronectin, vitronectin
$\alpha_2\beta_1$ (GPIa/IIa)	Integrin	Collagen
$\alpha_5\beta_1$	Integrin	Fibronectin
$\alpha_6\beta_1$	Integrin	Laminin
$\alpha_v\beta_3$	Integrin	Vitronectin, fibrinogen, vWF

Table 1.1. Platelet major integrin receptors and their ligands

Receptor	Family	Ligands
$P2Y_1$ and $P2Y_{12}$	G protein-coupled receptors	ADP
$P2X_1$	Ion channel	ATP
TPα	G protein-coupled receptors	Thromboxane
Serotonin receptor	G protein-coupled receptors	Serotonin (5-HT)
PAR1 (high affinity) and PAR4 (low affinity)	G protein-coupled receptors	Thrombin

Table 1.2. Platelet major G protein-coupled receptors and $P2X_1$ ion channel, and their ligands

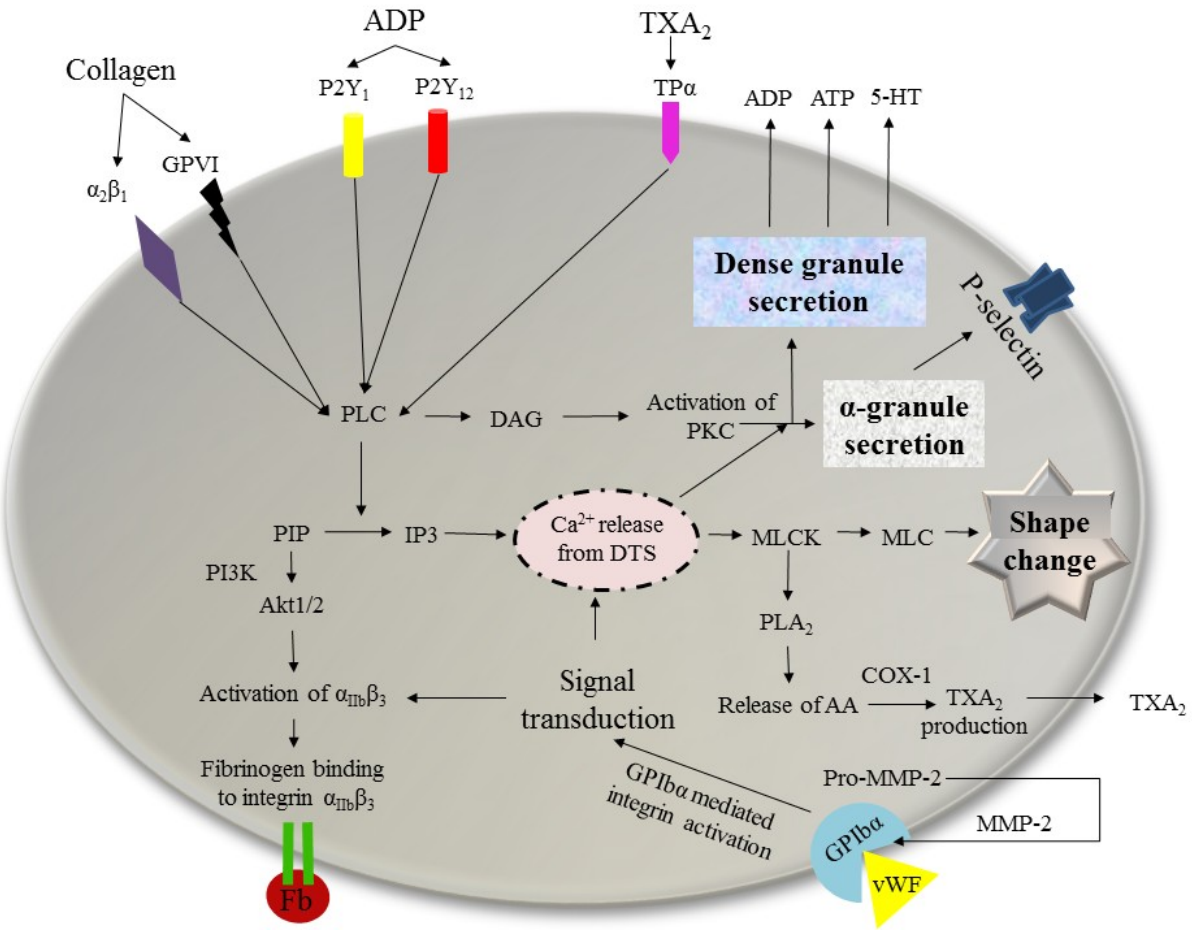

Figure 1.5. Platelet signalling pathways and mechanisms activated in response to injury

These mechanisms involve platelet integrin GPIbα signal transduction that causes platelet initial activation and triggers release of platelets endogenous soluble agonist (ADP, ATP and 5-HT). These soluble agonists mediate platelet further activation, generation of TXA_2 and shape change. The initial activation via GPIbα is reinforced by GPVI signalling upon collagen biding causing platelet strong activation. These overlapping mechanisms activate platelet fibrinogen receptor $\alpha_{IIb}\beta_3$ which facilitates formation of bridges between adjacent platelets to stabilize the aggregate.

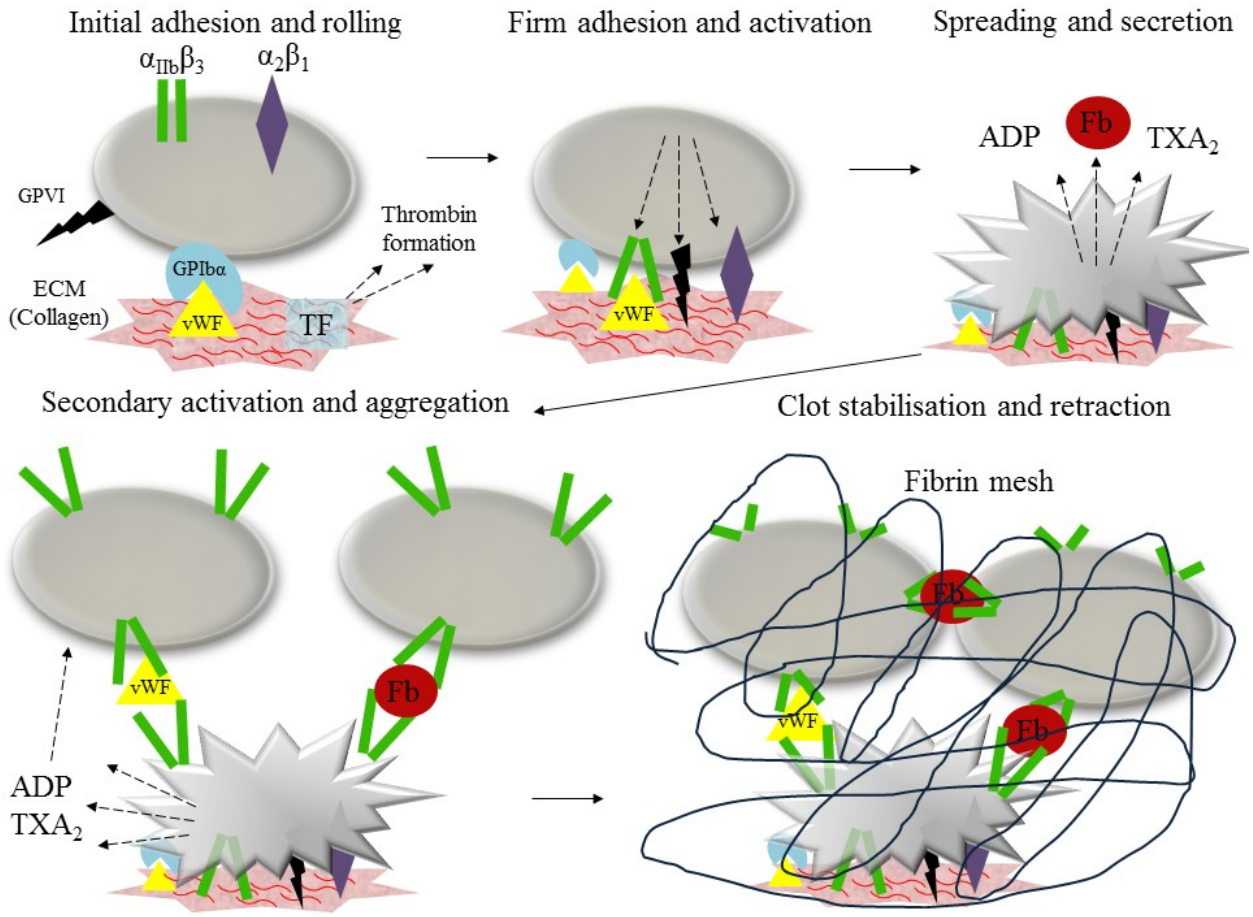

Figure 1.6. Steps of platelet adhesion, activation and thrombus formation

The vessel wall damage exposes subendothelial ECM which triggers initial tethering of platelets via GPIbα-vWF interaction. Rolling platelets undergo stable adhesion through GPIa/IIa-collagen receptor and $\alpha_{IIb}\beta_3$-vWF interaction. At this stage both integrins become activated mainly through inside-out signaling triggered by GPVI engagement to collagen. Platelet activation and integrin engagement cause platelet shape change and spreading as well as secretion of prothrombotic agents (ADP, TXA_2 and fibrinogen). This process recruits additional platelets and stabilizes the growing thrombus. Highly activated platelets within this thrombus provide a 'procoagulant' surface leading to massive thrombin generation, which further reinforces platelet activation but also generates a rigid fibrin mesh and leads to clot retraction, which is based on $\alpha_{IIb}\beta_3$-fibrin interaction.

1.2.8 Positive and Negative Regulation of Platelet Function

Platelet haemostatic function is regulated by complex highly controlled pathways that keep circulating platelets in a quiescent state, and mechanisms which initiate platelets activation upon vessel damage. Molecules that regulate platelet haemostatic balance include platelet inhibitors (NO, PGI_2, MMP-9, TIMP-4) and activators (ADP, TXA_2, MMP-2, MMP-1) (Figure 1.7-1.8).

Following damage to the vascular endothelium, endogenous inhibitory signals are overcome and activatory signals mediated by adhesion receptors initiate platelet activation. Activation leads to release of platelet matrix metalloproteinase-2 (MMP-2) and matrix metalloproteinase-1 (MMP-1), secretion of ADP from δ-granules and generation of TXA_2 from the phospholipids. The MMP-2, MMP-1, ADP and TXA_2 act as positive-feedback mediators, which promote platelet aggregation and recruit other platelets into a primary haemostatic plug.

Negative regulation of platelet function is essential to prevent uncontrolled thrombosis. The NO and PGI_2 provide negative feedback mechanisms for platelet adhesion and aggregation and also act as potent vasodilators in cardiovascular system. Endothelial cells synthesize and basally release NO and PGI_2 to maintain antithrombotic environment in the blood vessels. In addtion, platelets also generate NO upon activation [152-154]. Other anti-aggregatory molecules like tissue inhibitor of metalloproteinase-4 (TIMP-4) and matrix metalloproteinase-9 (MMP-9) are also released upon platelet activation and provide counterbalance to platelet positive feedback mechanisms [155-158].

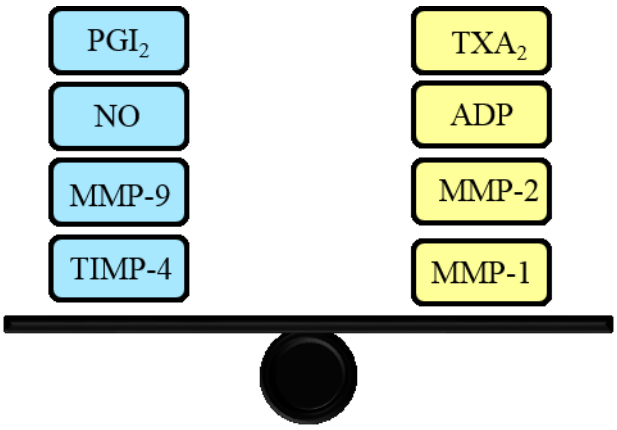

Figure 1.7. Common platelet inhibitors and activators

Balance between platelet anti- and pro-aggregatory mechanisms regulates their haemostatic function.

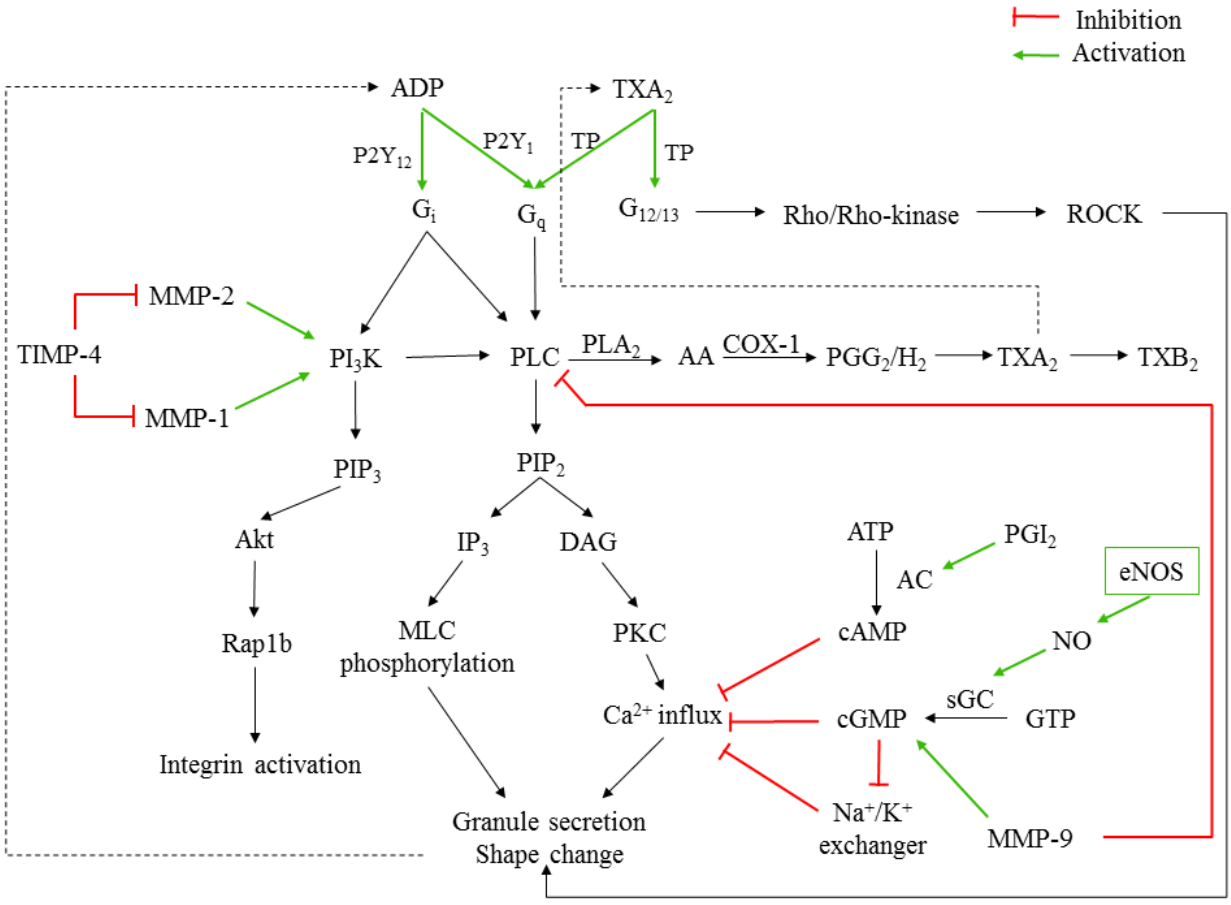

Figure 1.8. Mechanisms and effects of common platelet activators and inhibitors

1.2.9 Platelet Positive Feedback Mechanisms

Pro-Aggregatory Role of Matrix Metalloproteinase-2 and Matrix Metalloproteinase-1

MMP-2 belongs to a family of zinc- and calcium-dependent proteolytic enzymes that that are involved in the degradation of the ECM, specifically type IV collagen, gelatin, elastin, fibronectin and laminin-1. In addition, MMP-2 is also known to cleave proteins and non-matrix substrates that interact with cell surface receptors. Within resting platelets the latent form of MMP-2 called pro-MMP-2 is present in cytosol, but during activation it translocates from the cytosol to the platelet membrane and extracellular space via platelet surface-connected OCS [159]. However, at the early stages of aggregation, MMP-2 remains in close association with the platelet plasma membrane [159, 160]. Upon platelet stimulation released pro-MMP-2 forms a trimolecular complex with cell surface membrane-type 1 matrix metalloproteinase (MT1-MMP) and tissue inhibitor of metalloproteinase-2 (TIMP-2) which leads to activation of pro-MMP-2. Active MMP-2 briefly interacts with platelet surface integrins $\alpha_{IIb}\beta_3$ and GPIbα, which primes their activation before binding to their respective ligands. Presence of the ligands such as fibrinogen and vWF during aggregation triggers gradual dissociation of integrin-bound MMP-2 [161-163]. Active MMP-2 is unable by itself to induce aggregation at physiologically relevant concentrations but it facilitates platelet aggregation triggered by agonists such as ADP, collagen and thrombin. Furthermore, it has been suggested that active MMP-2 amplifies the platelet aggregation response to several agonists by potentiating the phosphatidylinositol 3-kinase (PI3K) activation, causing integrin activation and mobilization of intracellular Ca^{2+} [164]. Another proposed pathway in which active MMP-2 enhances platelet activation is related to cleavage of protease-activated receptor 1 (PAR1) at noncanonical extracellular site. This triggers PAR1-biased signalling, which is unable to induce aggregation but primes platelets to full activation by other agonists [165]. There is also evidence that active MMP-2 mediates hydrolytic activation of talin, which is a final step for activation of integrin $\alpha_{IIb}\beta_3$. The conformational change of integrin $\alpha_{IIb}\beta_3$ induced by activation via talin, enables high-affinity binding of fibrinogen and vWF - which are responsible for formation of platelet aggregates [166]. Lastly, atherosclerotic plaques contain high levels of pro-MMP-2 which, upon plaque rupture, comes into contact with blood and surface of circulating platelets. Contact with platelets activates pro-MMP-2 and provides positive feedback mechanism for platelet aggregation in atherosclerosis. In contrast, loss of MMP-2 in platelets reduces arterial thrombosis in vivo [167, 168].

In addition to MMP-2, resting platelets also constitutively express significant amounts of pro-MMP-1, which is released and activated upon thrombin stimulation. MMP-1 similar to MMP-2 enhances platelet aggregation upon stimulation with agonist. Activation of MMP-1 triggers phosphorylation of intracellular proteins, which results in the redistribution of β_3-integrins to areas of cellular contact (integrin clustering) and primes platelets for aggregation [169].

Pro-Aggregatory Role of Adenosine Diphosphate

ADP was the first identified platelet agonist and despite being weak agonist, it is essential for platelet secondary aggregation. Platelets store ADP at high concentrations in δ-granules and release it in response to the platelet activation. ADP induces platelet shape change, potentiates granule secretion and stimulates generation of TXA_2. These mechanisms activate and recruit nearby platelets to the injury site. ADP mediates platelet aggregation through GPCRs that include purinergic receptors: $P2Y_1$ and $P2Y_{12}$ [170]. Binding of ADP to $G\alpha_q$-coupled $P2Y_1$ receptors induces activation of PLC which hydrolyzes the phospholipid phosphatidylinositol bisphosphate (PIP_2) into the "secondary messengers" IP_3 and DAG [171]. IP_3 stimulates release of Ca^{2+} from intracellular stores and DAG facilitates PKC translocation from the cytosol to the plasma membrane and its activation. PKC phosphorylates the myosin light chains (MLCs) which then interact with the platelet actin network to traffic granules and induce platelet shape change. The $P2Y_{12}$ receptor stimulation results in $G\alpha_i$-mediated inhibition of stimulated adenylate cyclase (AC) and decrease of cAMP levels, which promotes platelet aggregation. Furthermore, $P2Y_{12}$ receptor mediates activation of PI3K and downstream Akt phosphorylation and Rap1b activation. All these events cause granule secretion, TXA_2 generation, $\alpha_{IIb}\beta_3$ activation and enhance aggregation [172, 173]. Although ADP does not act as agonist on platelet $P2X_1$ receptors, it stimulates ATP release from δ-granules, which in turn activates $P2X_1$ receptors. Activation of $P2X_1$ receptors generates significant increase of intracellular Ca^{2+} leading to amplification of other pro-aggregatory signalling and functional pathways in platelets [174]. Furthermore, simultaneous signalling through $P2Y_1$, $P2Y_{12}$ and $P2X_1$ is sufficient for fibrinogen receptor $\alpha_{IIb}\beta_3$ activation. Interestingly, platelet responses to low and intermediate concentrations of platelet agonists - thrombin and TXA_2 - are reduced in the absence of ADP receptors. This emphasizes the importance of ADP as a positive-feedback mediator for sustained platelet activation [173].

Pro-Aggregatory Role of Thromboxane A_2

Both TXA_2 and PGI_2 belong to family of eicosanoids but play opposing roles in platelet function. While TXA_2 is a platelet agonist, PGI_2 inhibits platelet activation. In cardiovascular system TXA_2 acts also as a vasoconstrictor and a potent hypertensive agent. Platelets synthesize TXA_2 *de novo* upon activation when PLA liberates arachidonic acid (AA) from the platelet plasma membrane. AA is sequentially oxygenized by cycloxygenase 1 (COX-1) and TXA_2 synthase to obtain TXA_2. The platelet TXA_2 receptor (TP) couples to $G\alpha_q$ and $G\alpha_{12/}G_{13}$ proteins [175-177]. Similarly to ADP, $G\alpha_q$-coupled TP receptor mediates activation of PLC and its downstream signalling molecules - IP_3, DAG and PKC. Addtionally to $G\alpha_q$, TXA_2 binds to $G\alpha_{12/}G_{13}$-coupled TP receptor, which activates Rho/Rho-kinase signalling, causing phosphorylation of MLCs and Ca^{2+}-independent shape change [178].

1.2.10 Platelet Negative Feedback Mechanisms

Anti-Aggregatory Role of Tissue Inhibitor of Metalloproteinase-4

In circulating quiescent platelets TIMP-4 likely forms a complex with pro-MMP-2 in the platelet cytosol, as the two proteins co-localize by electron microscopy. Upon platelet activation it is proposed that pro-MMP-2 (72 kDa) dissociates from the complex and translocates to the platelet surface where it is converted to active MMP-2 (64 kDa). At the same time TIMP-4 is released from platelets, where it may bind to active MT1-MMP found on the platelet membrane limiting MT1-MMP-dependent pro-MMP-2 activation. As a result, pro-MMP-2 is not activated and cannot contribute to activation of integrin $\alpha_{IIb}\beta_3$ and GPIbα - therefore TIMP-4 in some extent suppresses platelet activation [159, 179, 180].

Anti-Aggregatory Role of Matrix Metalloproteinase-9

Platelets express both mRNA and protein of MMP-9 to provide counterbalance to MMP-2 pro-aggregatory activity. A number of studies localized MMP-9 in plasma membrane, α-granules, open canalicular system and within the cytosol both in resting and activated platelets [157, 181-183]. However, some studies question whether platelets in fact express MMP-9 and speculate that leukocyte contamination could contribute to previous false positive results [184]. In addition, it was recently reported that activated platelets bind plasma-derived MMP-9, suggesting that platelet MMP-9 could be in fact plasma derived [185].

According to Fernandez-Patron and colleagues resting platelets release small quantities of pro-MMP-9 and maximal release is observed during partial platelet activation [181]. Following release from platelets, MMP-9 is likely activated by proteases such as plasmin, elastase and tissue kallikrein [186-188]. Active MMP-9 provides a negative feedback mechanism for platelet aggregation induced by a variety of agonists including collagen, thrombin and ADP. MMP-9 inhibits activation of PLC and its downstream effects involving hydrolysis of PIP_2, PKC activation and TXA_2 formation. Therefore MMP-9 acts by lowering the intracellular Ca^{2+} mobilization induced by platelet agonists. In addition, activated MMP-9 also stimulates the formation of cGMP, that subsequently inhibits the Na^+/H^+ exchanger. This leads to reduced intracellular Ca^{2+} mobilization, which ultimately inhibits platelet aggregation [157, 158]. Summarizing, MMP-9 is a negative feedback regulator during platelet activation and release of MMP-9 in the area of thrombus formation weakens the recruitment of other platelets [189].

Anti-Aggregatory Role of Prostacyclin

PGI_2 is the most potent inhibitor of platelet function. PGI_2 derives from AA, which is metabolized to PGH_2 by COX enzymes and converted into PGI_2 by action of the PGI_2 synthase. ECs produce and release PGI_2 to circulation where it binds to platelet PGI_2 surface receptor (IP), which belongs to family of GPCRs associated with $G\alpha_s$-subunit. The PGI_2 binding to IP receptor initiates activation of membrane-associated AC and synthesis of cAMP from ATP [46, 190]. An increase in cAMP cellular concentration activates cAMP-gated channels and protein kinase A (PKA). PKA phosphorylates various substrates, which inhibit multiple aspects of platelet function including Ca^{2+} mobilization, actin dynamics, integrin activation and granule secretion. Mass spectrometry-based proteomic studies suggest that the platelet inhibitory mechanism of PGI_2 mediated by PKA involves phosphorylation of more than 100 potential substrates [191]. PKA reduces intracellular Ca^{2+} by phosphorylation of IP_3-receptor (IP_3R)-associated protein (IRAG). Consequently, decrease of intracellular Ca^{2+} reduces the activity of MLCK and the Ca^{2+}-dependent small GTPase Rap1b and Rap1GAP2, which inhibits dynamics of platelet cytoskeleton modification. In addition, PKA also directly phosphorylates and decreases MLCK activity, preventing cytoskeletal rearrangement and shape change [192]. PKA also phosphorylates RhoA and thus disables its relocalization from cytosol to the membrane, causing inactivation of RhoA kinase (ROCK) signalling. In turn, inhibition of RhoA/ROCK promotes MLC phosphatase activity, which prevents phosphorylation of MLC and thus inhibits platelet shape change [193]. Moreover, recent studies provide evidence that cAMP-PKA signalling can also switch off activated RhoA in addition to blocking its activation even under conditions of high shear stress. This shows that PGI_2 downstream effects could potentially reverse platelet activation in vivo which would explain platelet ability to function effectively in a high shear environment [194]. Other targets of PKA mediated phosphorylation include VASP protein and integrin GPIbα, which inhibits activation of platelet integrins and platelet adhesion, respectively [195-197].

Overall, PGI_2 by stimulating cAMP-PKA pathway blocks several steps of cytosolic Ca^{2+} elevation and controls a multitude of cytoskeleton-associated proteins that are directly involved in platelet contractile activity and granule secretion. Through these mechanisms, PGI_2 inhibits platelet activation and causes disaggregation of existing platelet aggregates.

Anti-Aggregatory Role of Nitric Oxide

Next to PGI_2, NO mediated signalling is one of the most important among anti-aggregatory pathways in platelets. NO is electrically neutral diatomic gas and free radical that is more soluble in hydrophobic environments than in water, hence it can easily diffuse across cell membranes (Figure 1.9). It acts primarily in local environments due to relatively short half-life of ~5–30 s and thus level of free NO in plasma is fairly low at approximately 3 nM. Additionally, NO forms more stable adducts by being incorporated into organic compounds such as S-nitrosothiols and S-nitroso-proteins such as S-nitroso-albumin, which may be the biggest reservoir of NO in the human plasma [198].

Under physiological conditions NO is synthesized and released in the CV system mainly by ECs to regulate vascular tone and to inhibit platelet function. Most of NO released to the blood stream rapidly auto-oxidizes to yield nitrite ion (NO_2^-), which interacts with hemoglobin to yield relatively stable nitrate ion (NO_3^-) [199]. Only a fraction of NO generated by ECs manages to diffuse across membranes of blood cells to induce its biological effects. Hence, it is advantageous for platelets, which are free of hemoglobin, to synthesize its own NO for a more localized response. In addition, NO short half-life limits its biological availability but, platelets travel very close to the endothelium (due to their small size and weight platelets are pushed to the periphery by larger in size and weight white and red blood cells) and interact with NO before it gets scavenged or decays. Importantly, human platelets express endothelial nitric oxide synthase (eNOS) and generate their own NO, although there are some controversies whether that is true or not, which will be discussed below in a great detail [200, 201].

NO is a platelet antagonist which acts in paracrine (when derived from ECs) and autocrine (when synthesized by platelet eNOS) manner. Human platelets express intracellular NO receptor sGC, specifically the $\alpha_1\beta_1$ isoform. After entering the platelet, NO binds to the heme moiety of sGC and activates the enzyme by inducing a conformational change that displaces iron out of the planar porphyrin ring configuration. This causes 200-fold increase of sGC catalytic rate in conversion of guanosine triphosphate (GTP) to cGMP [202, 203]. High cellular concentration of cGMP activates protein kinase G (PKG) which phosphorylates various substrates, including three major molecules that, when phosphorylated, provide inhibitory mechanism of platelet activation. The phosphorylation of VASP at S239 by PKG mediates first mechanism of NO/cGMP-induced platelet inhibition [204]. Phosphorylation of VASP facilitates its binding to the platelet cytoskeleton and inhibits GPIIb/IIIa activation which prevents platelet

adhesion and aggregation. Importantly, this is the most widely recognized mechanism by which NO mediates its platelet inhibitory effects (Figure 1.10) [197]. Second mechanism involves PKG phosphorylation of IRAG at S677, which suppresses IP_3R mediated release of intracellular Ca^{2+}, granule secretion and GPIIb/IIIa activation [205, 206]. The C-terminus of TP receptor is the third major PKG substrate and its phosphorylation disrupts receptor G-protein coupling and inhibits platelet aggregation [207]. NO-mediated activation of PKG inhibits almost all agonist-induced events, including the increase of intracellular Ca^{2+} levels, integrin activation, granule secretion and cytoskeletal reorganization.

Furthermore, NO may inhibit platelet function in a non-cGMP manner, involving protein nitration of tyrosine residues and S-nitrosylation of cysteine [208, 209]. However, this cGMP-independent mechanism likely does not contribute significantly to NO-induced inhibition of platelet adhesion and aggregation. Highly selective inhibitor of the sGC – oxadiazolo quinoxalin (ODQ) - almost entirely reverses inhibitory effect of exogenous NO donor S-Nitroso-N-acetylpenicillamine (SNAP) on human platelets. The remaining inhibitory effect of SNAP on platelets is very modest but still requires a high concentration of NO in a short amount of time, which would be hard to achieve under normal conditions [210]. In addition, mice deficient in β_1 subunit of sGC show lack of NO platelet inhibitory activity. Addition of exogenous NO has no inhibitory effect on collagen stimulated platelet aggregation in these mice compared to WT, which confirms that sGC-cGMP-dependent pathway predominates in NO-induced platelet inhibition [211].

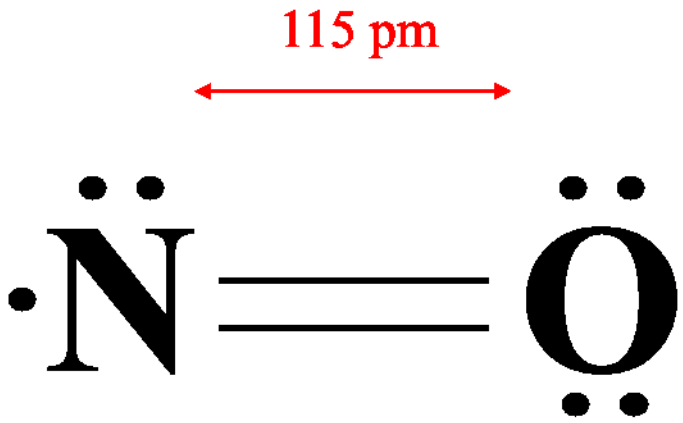

Figure 1.9. Molecule of NO

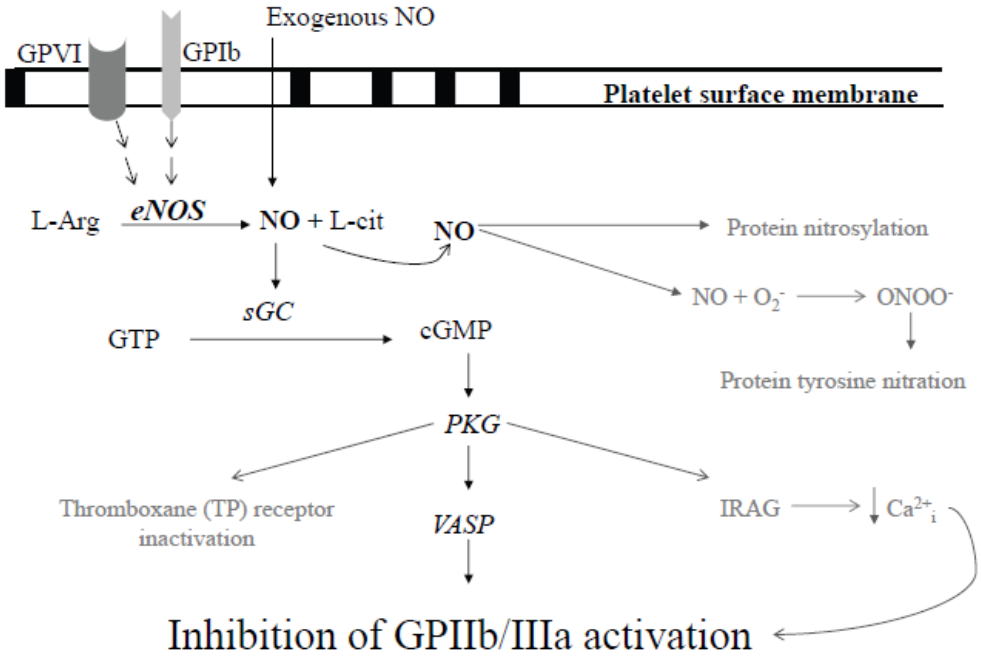

Figure 1.10. Overview of platelet NO signalling

1.2.11 Platelet Phosphodiesterases

Phosphodiesterases (PDEs) are intracellular enzymes that catalyze the hydrolysis of the second-messengers cAMP and cGMP to the inactive metabolites AMP and GMP. Platelet cGMP is primarily hydrolyzed by cGMP-specific phosphodiesterase type 5 (PDE5) [212]. Some cGMP binds to allosteric sites on PDE5 and preserves its activated state for more than an hour and during that time cGMP is protected from breakdown. In addition, phosphorylation of PDE5 by PKG has been shown to increase the affinity of PDE5 allosteric sites for cGMP, suggesting the potential for regulation of a reservoir of cGMP bound to this protein. Interestingly, cGMP also increases platelet cAMP levels by inhibiting phosphodiesterase type 3 (PDE3), which preferentially hydrolyzes cAMP. This mechanism inhibits platelet activation [213, 214]. Additionally, it is thought that high levels of NO elicit high cGMP accumulation that activates platelet less abundant phosphodiesterase 2 (PDE2) and reduces cAMP. cGMP stimulates conformational change of platelet PDE2, which increases enzyme activity to hydrolyze both cAMP and cGMP [215-217].

The PDE5 inhibitors (e.g. sildenafil) are a group of drugs used to treat erectile dysfunction and some are also used as therapy for pulmonary arterial hypertension (PAH). The PDE5 inhibitors have similar structure to cGMP and act as competitive substrates for PDE5 which slows down cGMP hydrolysis and enhances the vasodilatory effects of NO [218].

1.3 Endothelial Nitric Oxide Synthase and Generation of Nitric Oxide

1.3.1 Studies of Endothelium-Derived Relaxing Factor and the Discovery of Nitric Oxide in Platelets

In October of 1998 three scientists: Robert Furchgott, Louis Ignarro and Ferid Murad received the Nobel Prize in Physiology and Medicine for significant contribution in discoveries of NO as a key molecule in the cardiovascular system.

However, studies of NO effects on cardiovascular system date back to the 1960s when Hampton et al. reported the inhibition of platelet function by nitroglycerin (NTG) [219]. In 1970s Dr. Ferid Murad's group proposed that NTG and other nitro-vasodilators act simply by liberating NO (e.g. sodium nitroprusside - SNP) or by reduction of nitrates to NO (e.g. NTG). They also observed that NO increases sGC activity followed by formation of cGMP which causes SMCs relaxation [220, 221]. Similar experiments with nitro-vasodilator drugs performed on human platelets also found increased sGC activity and formation of cGMP, which caused inhibition of platelet aggregation in response to ADP [222, 223].

In 1980 Dr. Robert F. Furchgott and John V. Zawadzki reported for the first time that the presence of endothelial lining is mandatory to observe relaxation of rabbit aorta in response to acetylcholine [45]. Authors concluded that the vasodilation of the vessel is caused by unknown calcium-dependent factor localized in the endothelium, which they named endothelium-derived relaxing factor (EDRF). The vasodilatory mechanism of EDRF was proposed few years later by Dr. Ferid Murad's and Dr. Louis Ignarro's groups. They indicated that EDRF acts on sGC in the vascular SMCs and causes its relaxation in cGMP-dependent manner which leads to vasodilation of the vessel [224-227]. This intriguing observation prompted intensive studies attempting to identify the chemical nature of EDRF. In July 1987 during the meeting "Mechanism of Vasodilatation" in Rochester (MN) Dr. Robert F. Furchgott and Dr. Louis J. Ignarro independently announced that EDRF and NO are the same or very similar molecules [228, 229]. Their proposal was supported by experiments showing that superoxide dismutase (SOD) protects EDRF from rapid inactivation by scavenging $O_2^{\bullet-}$ and that haemoglobin selectively inhibits vasodilatory mechanism of EDRF. They also presented that inorganic nitrite (NO_2^-) solutions cause relaxation of rabbit aorta as a consequence of its reduction to NO [226, 227]. The proposal was very surprising, since it was unprecedented for NO to be generated in mammals, and even

more so to be synthesized for a specific biological purpose. When Dr. Salvador Moncada's group published their results concluding that NO released by the ECs could account for the biological activity of EDRF, it became apparent that the elusive EDRF was in fact NO [230]. The same group also identified that NO is enzymatically generated from amino acid L-arginine by enzyme called nitric oxide synthase (NOS) [231]. This discovery was aided by access to new L-arginine analogue - NG-monomethyl L-arginine (L-NMMA), which inhibits NOS mediated NO production by competing for a binding site with L-arginine [232, 233]. Interestingly, human body produces L-arginine analogue - asymmetric dimethylarginine (ADMA), which is an endogenous inhibitor of NOS [234].

In 1987 it was evident that the generation of NO not only takes place in the vascular wall, but is rather a widespread mechanism with important biological significance. Hibbs et al. and Iyengar et al. showed that NO is involved in the responses of macrophages such as respiratory burst [235, 236]. Another group reported that NO synthesis occurs in the brain through NO-cGMP pathway in response to activation by neurotransmitters in different neurons [237]. These diverse studies raised the question whether NO production observed in different tissues and parts of the body is associated with different subtypes of NO-producing enzymes. The answer was found few years later when neuronal-isoform of NOS (nNOS or NOS I) enzyme was isolated and subsequently cloned from rat's brain [238, 239]. Another identified isoform was inducible NOS (iNOS or NOS II) found in macrophages [240, 241]. The last isoform that was purified and cloned was endothelial NOS (eNOS or NOS III) [242, 243]. Names "endothelial" and "neuronal" may imply that NOS isoforms are only found in endothelium or neurons, however all isoforms are found in various tissues or even cell types.

First studies describing effects of endothelium-derived NO on platelet aggregation emerged several years after the discovery of endothelium-derived relaxing factor (EDRF) by Dr. Robert F. Furchgott in 1980 [45]. In 1986 group from Japan described for the first time that EDRF, known today as NO, inhibits aggregation of rabbit platelets [244]. A year later group of Dr. Salvador Moncada published results presenting inhibitory effect of NO on human platelet aggregation. Both groups used thoracic aorta from rabbits as a source of endothelial NO, however Moncada group used human platelets instead of rabbit's for aggregation experiments. To verify that if the inhibitory effect on platelet aggregation is mediated by NO and not other vessel-derived factor, Moncada's group performed control experiments with authentic NO and

NO derived from cultured porcine aortic ECs stimulated with bradykinin [153]. Dr. Moncada group also demonstrated that platelet adhesion to collagen and ECM is inhibited in the presence of bovine EC monolayers stimulated with bradykinin, which suggests that NO liberated from ECs inhibits platelet adhesion to collagen and ECM [245]. Until 1990 all studies in platelet NO field regarded mechanisms of EDRF on platelet aggregation and there were no reports whether human platelets can generate NO and respond to it in an autocrine manner. However, in 1990 Radomski et al. published manuscript "An L-arginine/nitric oxide pathway present in human platelets regulates aggregation", showing for the first time presence of NO-cGMP signalling pathway endogenous to human platelets. They demonstrated that addition of amino acid - L-arginine as substrate for NO production by NOS enzymes, stimulates the sGC and increases levels of cGMP which ultimately inhibits platelet aggregation. Moreover, this anti-aggregatory effect of NO was abrogated by NOS inhibitors [200]. The same group further verified their initial discovery by utilizing porphyrinic microsensor placed in suspension of human washed platelets. They induced platelet aggregation by adding a potent platelet agonist – collagen, and via porphyrinic microsensor directly measured concentration of platelet released NO. The results showed that single platelet in absence of additional L-arginine produces maximum of $10.5 \pm 2.4 \times 10^{-18}$ mol of NO [154]. Different group showed production of NO by human platelets using spin trapping/EPR spectroscopy experiments. Addition of NOS inhibitor L-NMMA suppressed NO production detected as decreased formation of spin adducts within nitroso spin traps [246]. Another study gave insight into signal transduction mechanism by which NO-cGMP pathway inhibits platelet activation. They proposed that NO-cGMP pathway decreases intracellular Ca^{2+} levels by interfering with PLC activation, which inhibits PKC mediated phosphorylation and prevents serotonin secretion from δ-granule [247]. Soon after, Ca^{2+}-dependent isoform of NOS was purified from cytosolic fractions of human platelets [248]. In 1995 Sase et al., using reverse transcription polymerase chain reaction (RT-PCR) followed by sequencing, provided first evidence that platelets express eNOS mRNA which was later corroborated by other independent groups [201, 249, 250]. Only one group has reported the presence of iNOS in human platelets based on experiments with pro-inflammatory cytokines such as tumor necrosis factor-alpha (TNF-α) and interferon-gamma (IFN-γ). Both cytokines increased platelet NO production in Ca^{2+}-independent manner, which was attributed to iNOS. Additional follow up study by this group showed also iNOS protein and mRNA expression in human platelets [250, 251]. However,

authors do not speculate about the origin of iNOS protein and mRNA expression in anucleate platelets. Moreover, other groups did not corroborate this observation. There are also no reports whether human platelets express nNOS [249, 250]. Attempts to confirms eNOS expression in human platelets by immunoprecipitation (IP) followed by mass spectrometry (MS) analysis were unsuccessful [252]. Studies by Freedman et al. demonstrated that platelet-derived NO acts in a paracrine fashion to inhibit the recruitment of platelets into aggregates [253]. In a follow up study they also showed that WT mice transfused with platelets collected from mice lacking eNOS gene (eNOS $^{-/-}$) had significantly decreased bleeding times even in conditions of sustained endothelial NO production, which proves importance of endogenous platelet NOS activity in haemostatic reactions [254]. Recent studies by Cozzi et al. also corroborate previous findings by visualizing NO production within an individual human platelet perfused over collagen at high shear rates. For these experiments platelets were loaded with a cell permeable regent 4-amino-5-methylamino-2',7'-difluorofluorescein diacetate (DAF-FM diacetate) that is weakly fluorescent until reaction with NO, which results in formation of fluorescent benzotriazole. They demonstrated that collagen-induced platelet NO production and Ca^{2+}elevation depend on shear rate: the higher shear the more NO is being generated by an individual platelet. Interestingly, in their experiments NO production is preceded by an increase of intracellular Ca^{2+}, which is mechanistically similar to what is seen in SMCs and ECs [255-257].

Taken together, over the last 30 years different studies provided evidence that human platelets respond to both endothelium-derived NO and endogenously generated NO via eNOS and possibly iNOS in pro-inflammatory setting or environment.

1.3.2 Controversies Regarding Expression of Endothelial Nitric Oxide Synthase in Human Platelets and Their Ability to Generate Nitric Oxide

While it is generally accepted that endothelial-derived NO regulates platelet function, the expression of platelet NOS/eNOS and the ability to generate endogenous NO has been widely debated in recent years. There is a significant amount of evidence showing presence of eNOS-signalling within human platelets and thus their ability to generate their own NO, but few studies failed to demonstrate its existence.

First aspect of discrepancies is related to pharmacological and transgenic animal studies claiming that platelet-derived NO and cGMP stimulate platelet aggregation. The authors propose that stimulation with low thrombin concentrations promotes rather than inhibits aggregation in a NO-cGMP-dependent manner, suggesting a biphasic effect of NO on platelet function [258]. These observations are supported by studies on platelets from eNOS-deficient (heterozygous) mice ($eNOS^{+/-}$), which also present biphasic response upon stimulation with platelet agonists, where low concentrations of thrombin and collagen diminish platelet secretion and aggregation, as well as reduce ability to form occlusive arterial thrombus in an in vivo thrombosis model. Worth mentioning is the fact that authors of this study never measured NO production and their results were never replicated by others [259]. Different studies complicated this aspect even further, showing that lack of platelet eNOS ($eNOS^{-/-}$) has minor consequences for platelet function and arterial thrombus formation in vivo [260, 261]. Mentioned studies differ in both experimental conditions and animal models, which can partly explain the nature of the discrepancies. However, it is difficult for both expert and non-expert readers to draw any conclusions as to the role of platelet NO. Therefore more systematic approach is required for future studies including different mice models and various methods of platelet eNOS-cGC-cGMP pathway detection.

Another aspect of scientific dispute is related to the difficulties of detecting platelet eNOS by western blot and to the fact that activation of cGMP-signalling may be NO-independent and mediated by activation of Src kinase and tyrosine phosphorylation of the sGC β_1-subunit. The same authors also suggest that platelet NO originates from leukocyte-contaminated preparations [262]. Others also report that protein S-nitrosylation in response to exogenous NO may act as a potentially important cGMP-independent signalling which inhibits platelet function [209]. Finally, some studies question the relevance of platelet-derived NO to

haemostasis and thrombosis arguing, that endothelial-derived NO is far more important [260, 263].

Taken together, some of the potential pitfalls can be attributed to several methodological diffrences, such as lack of extraction of eNOS from platelet caveolae [262], using different agonists, inhibitors and concentrations [200, 259], omitting the use of L-arginine in eNOS functional studies [258, 260], not taking into account differences between human and mouse platelets or differences between various mouse strains and age of animals used for experiments [260, 262], and finally performing eNOS functional studies in the presence of Ca^{2+} chelators [260, 263].

1.3.3 Mechanism of Nitric Oxide Generation by Nitric Oxide Synthases

Mammals generate NO via three isoforms of the NO-synthase: nNOS, iNOS and eNOS, along with several splice variants. NOS enzymes share approximately 50%–60% sequence identity and each isoform is encoded by genes located on different chromosomes, as summarized in Table 1.3.

The NOS isoforms share many chemical and enzymatic properties but catalytic and regulatory properties vary between them. Importantly, NOS enzymes require binding of multiple substrates and cofactors to efficiently synthesize NO. In addition, eNOS and nNOS are constitutively expressed and Ca^{2+} dependent, which means that in order to become active they require an increase in intracellular Ca^{2+} with half maximal activity between 200 – 400 nM of Ca^{2+} intracellular concentration. On the other hand, iNOS - an inducible isoform, has a different molecular structure of calmodulin binding site, which results from lack of autoinhibitory loops around that region, so the enzyme is active even at basal levels of intracellular Ca^{2+} (below 40 nM). This allows for irreversible binding of Ca^{2+}/CaM complex to iNOS protein which supports continuous NO production. Importantly, addition of Ca^{2+} chelators completely inhibits iNOS activity. The autoinhibitory loops present within the eNOS reductase domain constrain its activity, which results in slower heme reduction and less efficient NO synthesis compared to iNOS [264, 265].

All three NOS isoforms are a homodimers made up of two identical monomers with C-terminal reductase domain and N-terminal oxidase domain, as depicted in Figure 1.11. NOS enzyme monomers have to dimerize to produce NO, which is supported by the heme and a central zinc thiolate (ZnS_4) cluster as well as by tetrahydrobiopterin (BH_4) which additionally stabilizes formed dimer. The reductase domain accepts electrons from nicotinamide adenine dinucleotide phosphate (NADPH) and transfers them over through flavins - flavin adenine dinucleotide (FAD) and flavin mononucleotide (FMN) - to the oxidase domain of the other monomer. These electrons reduce the heme-iron to the ferrous state so it can bind oxygen that is later incorporated into L-arginine to generate NO and L-citrulline [266]. The reductase and oxidase domains are loosely connected by flexible hinges that, when extended, prevent the flow of electrons between the two domains. When calmodulin (CaM) binds to its active site, hinges change their conformations and bring the domains into close active state. In eNOS and nNOS, affinity of Ca^{2+}/CaM complex for its binding site on enzyme increases only upon elevation of

intracellular Ca^{2+}, which occurs only transiently in response to receptor or physical stimulations. In contrast, iNOS binds Ca^{2+}/CaM complex with high affinity even at the resting concentration of intracellular Ca^{2+} and its activity is regulated by transcriptional induction but not by transient elevation of intracellular Ca^{2+} [265].

NO production via NOS is quite complex enzymatic reaction but very efficient under normal conditions. NOS enzymes catalyze the oxidation of L-arginine to NO and L-citrulline in a two-step reaction, with NADPH and molecular oxygen O_2 serving as cosubstrates. In the first step of NO synthesis, an electron reduces ferric to ferrous heme which binds O_2. Subsequently, O_2 hydroxylates terminal guanidino nitrogen of L-arginine in the substrate-binding pocket to generate an enzyme-bound intermediate molecule N-hydroxy-l-arginine (NOHA). In the second step, NOHA is further oxidized to generate NO and L-citrulline [267]. The NOS enzymes use 1.0 mol of L-arginine, 2.0 moles of O_2 and 1.5 moles of NADPH to form 1.0 mole of NO, 1.0 mole of L-citrulline and 2.0 moles of H_2O (Figure 1.12). NOS are the only enzymes known to require simultaneously five bound cofactors/prosthetic groups for their physiological catalytic activity: FAD, FMN, heme, BH_4 and Ca^{2+}-calmodulin (Ca^{2+}/CaM) complex [268]. Moreover, disruption of this highly coordinated reaction can lead to reduction of NO synthesis in instances such as subthreshold concentrations of the substrate – L-arginine and cofactors [269, 270]. In addition, the ZnS_4 cluster and the BH_4 are susceptible to oxidation by free radicals which leads to disruption of the central Zn^{2+}, oxidation of the thiol groups and BH_4 to BH_2 [271, 272]. As a result NOS dimers dissociate into monomers and become uncoupled. In situation of cofactors deficiency or NOS uncoupling, electrons that normally flow from the reductase domain to the oxygenase domain are diverted to molecular oxygen rather than to L-arginine, which results in production of $O_2^{\bullet-}$ rather than NO [273]. In addition, reaction of NO with $O_2^{\bullet-}$ leads to formation of peroxynitrite ($ONOO^-$) which is a powerful oxidant, implicated in deleterious effects in conditions such as hypercholesterolemia, diabetes and coronary artery disease [274]. In addition, NOS enzymes no longer support sufficient production of NO under hypoxia (oxygen deficiency) and in conditions associated with increased formation of asymmetric dimethylarginine (ADMA). ADMA is the most abundant endogenous NOS inhibitor in human plasma and it acts by competing with L-arginine for the binding site. ADMA is formed in the body by action of methyltransferase enzymes that methylate arginine residues within proteins. Importantly, it has been also established that high plasma concentration of ADMA is an

independent risk factor for endothelial dysfunction, progression of atherosclerosis and cardiovascular death [275, 276].

Characteristic	Neuronal NOS (NOSI)	Inducible NOS (NOSII)	Endothelial NOS (NOSIII)
Human chromosomal location and number of exons	12q24.22 29 exons	17q11.2 26 exons	7q36.1 26 exons
Molecular mass and number of amino acids of monomer	161 kD 1433 aa	131 kD 1153 aa	133 kD 1203 aa
Calcium dependence	Ca^{2+} dependent	Ca^{2+} independent	Ca^{2+} dependent
Expression	Constitutive, short pulsative synthesis of NO Moderate NO production (nM to μM)	Inducible, constant synthesis of NO High NO production (μM)	Constitutive, short pulsative synthesis of NO Low NO production (pM to nM)
Tissue localization	Central and peripheral nervous system (e.g. perivascular nitrergic nerves of skeletal and smooth muscles and corpus cavernosum), mucous cells of pulmonary epithelium and cells of macula densa in the kidney	Macrophages, Kuppfer cells, Meg-01 cells, induced expression in various cell types in response to inflammatory mediators such as cytokines	Endothelial cells, platelets, megakaryocytes, Meg-01 cells, erythrocytes, cardiomyocytes, skeletal muscles, hepatocytes, hippocampus
Cellular localization	Cytosol and cell membrane (caveolin-3), sarcolemma, sarcoplasmic reticulum (cardiomyocytes)	Cytosol and phagosomes of macrophages and mainly in cytosol when expressed in other cell types such as Meg-01 cells	In platelets and ECs mostly in the membrane (caveolin -1) and in ECs also in cytosol and Golgi apparatus, in cytosol of Meg-01 cells, in sarcoplasm , in nucleus and mitochondria (cardiomyocytes)
Function	Cell communication regulating neuronal excitability and firing, release of neurotransmitters such as acetylcholine, histamine and serotonin, central regulation of blood pressure, synaptic plasticity in memory and learning processes, decreasing the tone of various types of smooth muscle including blood vessels	Physiological: host defense mechanisms/inflammation Pathological: inflammatory neurodegeneration, septic shock	Vasodilation, inhibition of platelet activation and aggregation, platelt release via MK-apoptotosis, inhibition of leukocyte adhesion to the vascular endothelium, modulation of myocardial relaxation, long-term potentiation of neurons
Regulation by various interactions and modifications	Unique PDZ/GLGF motif found within N-terminal interacts with dystrophin and syntrophin. Interactions with other proteins: Ca^{2+}/CaM, caveolin-3, Hsp90 Phosphorylation	Intracts with Ca^{2+}/CaM. Transcriptional regulation including DNA methylation. There is no evidence that iNOS associates with cell membrane scaffolding proteins. N-terminus of iNOS associates with NOS-associated protein 110 kDa blocking the formation of NOS2-NOS2 dimers	Interaction with proteins: Ca^{2+}/CaM, caveolin-1, Hsp90, NOSTRIN, NOSIP Acylation:palmitoylation and myristoylation Phosphorylation DNA methylation

Table 1.3. Comparison of human NOS enzymes characteristics

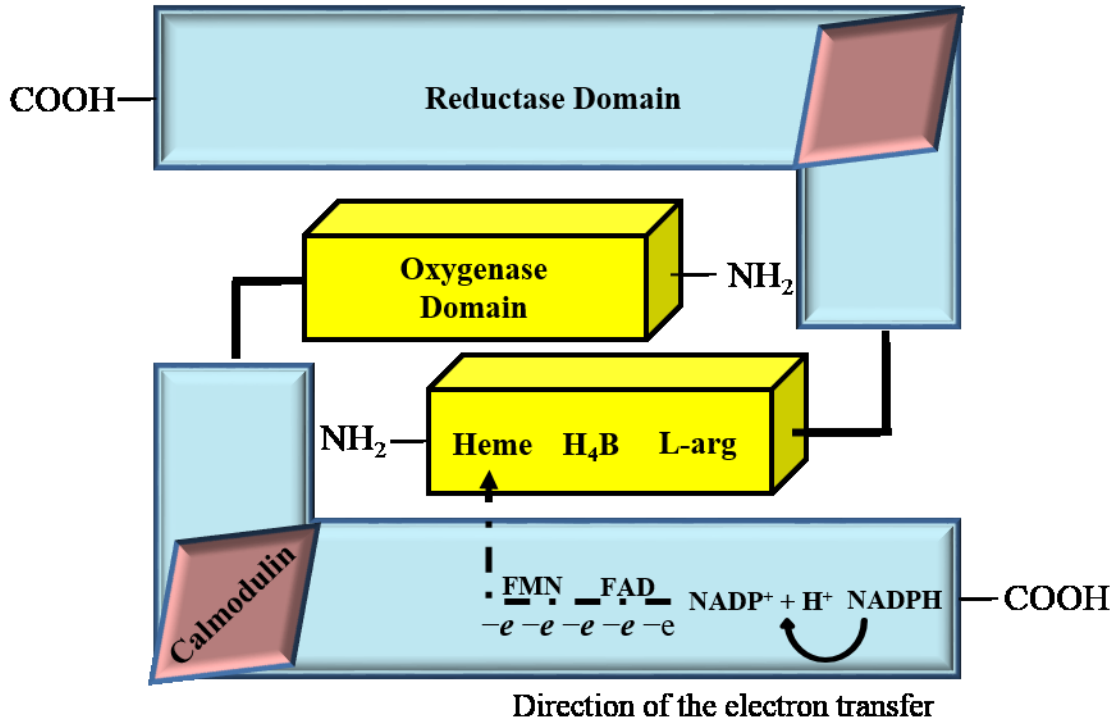

Figure 1.11. Overview of NOS homodimeric structure, cofactors and catalyzed reaction

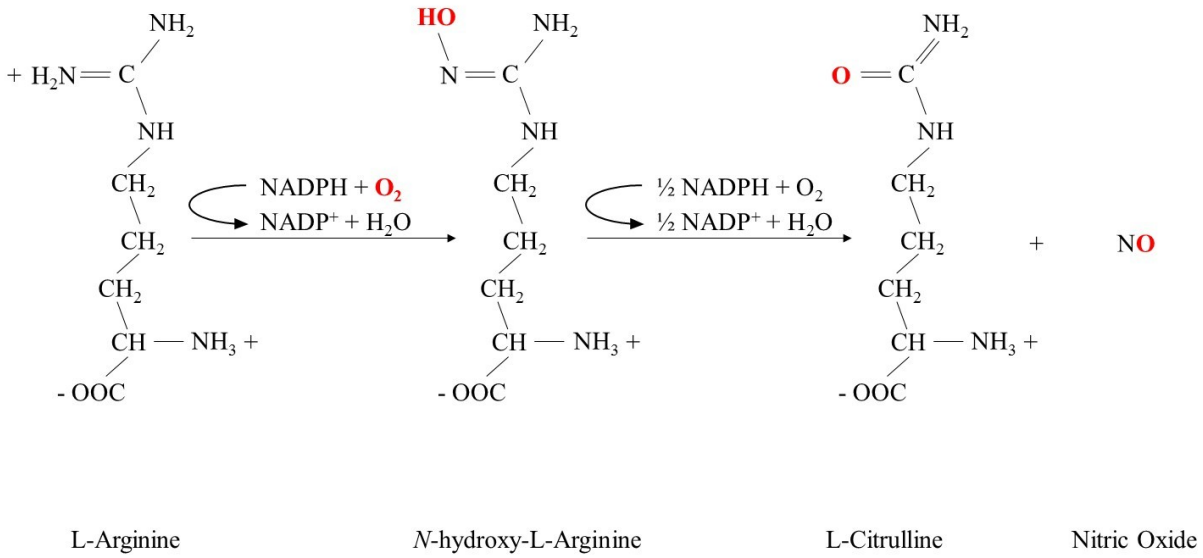

Figure 1.12. Reaction of NO production from L-arginine by NOS enzymes

1.3.4 Inducible Nitric Oxide Synthase - Role and Implications for Cardiovascular Disease

The iNOS protein was first discovered in activated macrophages, but has since been identified in many activated immune cells and other nucleated cell types [277]. While some claimed that normal human platelets may express iNOS protein but not mRNA [249], others were able to identify iNOS mRNA but not protein in porcine platelets [278]. *In vitro* studies by Chen and Mehta identified iNOS mRNA expression and activity in human platelets only when stimulated with IFN-γ, TNF-α and lipopolysaccharide (LPS) [250, 251]. Expression of iNOS protein was also reported in platelets from patients with type 1 diabetes (T1D) [279]. While there are inconsistencies in regard to iNOS mRNA expression under normal conditions, the data suggest that anucleate platelets could potentially synthesize iNOS protein in inflammatory conditions if they had had iNOS mRNA present. However, another study failed to identify iNOS activity and protein in platelets from patients with coronary atherosclerosis [280]. Furthermore, some authors question presence of iNOS in human platelets, as they speculate that leukocyte contamination of platelet preparations may contribute to detection of iNOS mRNA and/or protein in human platelets [281]. Therefore at present, there is no consensus whether human platelets express iNOS mRNA and/or protein under physiological conditions. Moreover, anucleate platelets cannot simply induce expression of iNOS mRNA in response to the inflammatory stimulus. In contrast, several studies showed that MKs from healthy individuals and patients with CAD express both iNOS protein and mRNA. In addition, iNOS was also identified in megakaryoblastic cell line - Meg-01 but in most cases they were stimulated with pro-inflammatory cytokines [249, 280, 282, 283]. During inflammation, in addition to eNOS, ECs start to express iNOS, which in long term can induce vascular dysfunction by depleting BH_4 which is necessary for NOS enzyme coupling. Enzymatic production of NO by iNOS is far greater than by eNOS and nNOS. Local release of large amount of NO metabolites has been linked to vascular hyperreactivity due to the production of cell-damaging oxidative products, such as $ONOO^-$. $ONOO^-$ may enhance platelet adhesion and aggregation, promotes lipid peroxidation, causes vasoconstriction and raises blood pressure [284, 285].

In immune cells iNOS is primarily localized in phagosomes and when expressed in other cell types it is mainly found in the cytosol. The expression of iNOS is believed to be a part of the nonspecific host defense mechanism. The primary function of iNOS is to mediate cell death in response to the pathogens by generating NO at toxic levels. Thus, iNOS produces high

concentrations of NO over short periods. However exacerbated or prolonged systemic overproduction of NO may account for the clinical manifestations of acute or chronic inflammatory conditions respectively [286]. In septic shock uncontrolled production of NO by iNOS can even cause the hypotension and cardiodepression.

The levels of iNOS are low in healthy individuals but pro-inflammatory factors such as IFN-γ significantly augment iNOS levels not only in immune cells, but also in any cell type that expresses cytokine specific surface receptor. Once bound to the cell surface receptor, cytokines transduce their downstream signals through different pathways including JAK-STAT and p38/ mitogen-activated protein kinase (MAPK). These pathways in turn mediate activation of transcription factors like nuclear factor-κB (NF-κB), transducer and activator of transcription 1 (STAT1), interferon regulatory factor – 1 (IRF-1), STAT3 and thus stimulate nuclear iNOS promoter and iNOS mRNA transcription [287]. In contrast, anti-inflammatory cytokines like IL-10 can suppress iNOS induction by multiple inhibitory mechanisms which will be discussed later [287-290].

1.3.5 Endothelial Nitric Oxide Synthase - Role and Implications for Cardiovascular Disease

In the cardiovascular system eNOS is highly expressed in ECs but is also reported to be found in cardiomyocytes, blood platelets and platelet parent cells - MKs [200, 201, 249, 250, 277, 282]. Furthermore, under basal conditions, eNOS mRNA is extremely stable (average 24 to 48 hours), however, it destabilizes in the presence of hypoxia, ox-LDL and pro-inflammatory cytokines [291-293]. NO produced by eNOS plays an important role in the blood vessel homeostasis causing vasodilation, enhancing vascular permeability, inhibiting platelet aggregation, inhibiting VSMs proliferation and inhibiting oxidation of LDL. NO derived from endothelium also inhibits vascular inflammation by suppressing EC expression and activity of adhesion molecules and chemokines which prevents adhesion of monocytes and leukocytes on endothelium.

Hence, NO is an important endogenous anti-atherosclerotic molecule and its deficiency may result in endothelial dysfunction attributed by impaired vasodilator response or a paradoxical constrictor response to endothelium-dependent agents, such as acetylcholine [294, 295]. Endothelial dysfunction is thought to precede an active atherosclerotic disease and is a good predictive of future cardiovascular events [296, 297]. In addition, ECs overlying advanced atherosclerotic plaques present decreased expression of eNOS mRNA and increased expression of ET mRNA [298, 299].

Impairment of eNOS function in endothelium and platelets has serious clinical implications including atherosclerosis and hypertension, which can result in MI and stroke. Hence, there are a number of pharmaceutical agents acting in the sGC-cGMP pathway used as therapeutic options for patients with CVD. The NO-donating agents such as organic nitrates are group of drugs used clinically in CV medicine since the 19th century to treat angina, MI and hypertensive crisis [300, 301]. In the coronary circulation, they dilate the coronary arteries and arterioles even when endogenous production of NO is impaired by coronary artery disease. Nitrates preferentially dilate the coronary arteries and arterioles greater than 100 μm and relieve angina symptoms by relaxing the epicardial vessels, which facilitates flow of blood to endocardial vessels. This improves circulation in the collaterals and relieves myocardial ischaemia by improving the regional myocardial blood flow. Nitrates reduce the preload and the workload on the heart by increasing the venous capacitance and pooling of blood in the peripheral veins and thereby a reduction in venous return and in ventricular volume. As a result,

there is less mechanical stress on the myocardial wall and the myocardial oxygen demand is reduced. In addition, the fall in the aortic systolic pressure reduces the myocardial oxygen demand [301-303].

All organic nitrates undergo serial enzymatic denitration, releasing NO. The most well known NO-donating agents are sodium nitroprusside (SNP) and nitroglycerin (NTG) also known as glyceryl trinitrate (GTN). NTG has pharmacokinetics that is not well understood. It rapidly disappears from the blood, with a half-life of only a few minutes, largely by extrahepatic mechanisms that convert the parent molecule to longer acting dinitrates and mononitrates. Of the many different nitrate preparations, sublingual nitroglycerin remains the "gold standard" for acute anginal attacks [304]. Other nitrates include isosorbide dinitrate, isosorbide 5-mononitrate and pentaerythritoltetranitrate. Isosorbide dinitrate is converted in the liver to active mononitrates that have half-lives of about 4 to 6 hours. The mononitrates do not undergo any hepatic metabolism and are 100% bioavailable with a half-life of 4 to 6 hours [305]. In circulation these drugs release NO which activates sGC-cGMP pathway causing vessel dilation and limiting platelet adhesion and aggregation. The effects of NTG on platelet aggregation are controversial. Most *in vitro* and *in vivo* investigations suggest that NTG suppresses platelet aggregation only at suprapharmacological concentrations [306-309]. Importantly, some patients with endothelial dysfunction exhibit attenuated responses to exogenous vasodilators like NTG and SNP. Reduced vasodilator response to NO-donating drugs within the coronary circulation is associated with poor long-term outcomes [310, 311]. A proposed mechanism of nitrate tolerance may be prolonged nitrate therapy causing enhanced formation of $ONOO^-$ and other free radicals, which in turn impairs eNOS activity [312, 313]. Clinical studies have shown that deficient platelet NO production predicts acute coronary syndromes (ACS) and correlates negatively with increasing numbers of coronary risk factors [314, 315]. Moreover, platelet refractoriness to NTG and SNP was observed in patients with ACS, primary hypertension and insulin resistance [316-318]. Platelet refractoriness to NO-donors has been shown as an independent predictor of increased CV morbidity and mortality in patients with high-risk ACS. Moreover, the same patients had ~6-fold increased risk of death during long-term follow-up [316]. Other reports show that platelets from patients with severe coronary atherosclerosis and those at risk of CVD have low eNOS mRNA expression and enzyme activity, which is associated with higher cardiovascular mortality [319-321]. It was postulated that chronic inflammation, which often accompanies CVDs,

promotes platelet pre-activation causing their reduced sensitivity to NO. Patients with ACS were found to have altered platelet sGC-cGMP signaling pathway that could explain their unresponsiveness to NO-donors [322]. The onset of NO resistance observed in patients with CVD has been attributed to partial inactivation of sGC which suppresses cGMP generation and/or scavenging of NO by increased concentrations of $O_2^{\bullet -}$ [322-325]. Therefore, oxidation or loss of the heme moiety of sGC results in enzyme insensitivity to NO [326].

1.3.6 Regulation of Endothelial Nitric Oxide Synthase Function

eNOS expression and activity are highly controlled by multiple interconnected mechanisms of regulation present at the transcriptional, posttranscriptional and posttranslational levels. The eNOS transcriptional and posttranscriptional regulation involves binding of various transcription factors to the NOS3 promoter, DNA methylation, and alteration of eNOS mRNA processing and stability [327]. The eNOS initial transcript is also modified by posttranslational mechanisms that include fatty acid acylation, protein-protein interactions and various types of phosphorylation.

Regulation of Endothelial Nitric Oxide Synthase Function by DNA Methylation

The DNA methylation is a natural epigenetic mechanism, which negatively regulates gene expression including the eNOS gene. Enzymes - methyltransferases add methyl groups at the 5-position of cytosine within the DNA CpG dinucleotide which fixes the gene in the "off" position [328]. Human eNOS gene consists of 26 exons spanning approximately 21 (kb) of genomic DNA on chromosome 7q35–36 [292, 329]. The eNOS promoter region does not contain TATA box and is G-C rich. In addition it also exhibits multiple potential *cis*-regulatory DNA sequences, including a CCAT box, Sp1 sites and GATA motifs, CACCC boxes, AP-1 and AP-2 sites, a p53 binding region, NF-1 elements, acute phase reactant regulatory elements, sterol regulatory elements and shear stress response elements. DNA methylation of promoters is often accompanied by histone modifications that render the chromatin effectively inaccessible to transcription factors [330, 331].

Genomic sequencing showed that differential methylation of various eNOS DNA promoter regions predetermines cell-specific eNOS expression. Consequently, cells that are considered eNOS nonexpressors in fact have eNOS DNA but mRNA transcription is repressed by the methylation of the eNOS DNA. For example, in normal ECs the eNOS promoter regions remains unmethylated resulting in expression of high levels of eNOS mRNA and fully functional eNOS protein. Whereas in cells that are considered eNOS-nonexpressors including VSMs, eNOS DNA is present but the promoter regions are densely methylated. Therefore eNOS mRNA and protein are not detected in these cells under normal conditions. Addition of DNA methyltransferase inhibitor such as 5-azacytidine causes demethylation of eNOS promoters and induces mRNA expression in normally nonexpressing cell types like VSMs [327, 332].

Alterations in DNA methylation patterns are involved in atherogenesis and include age-related global hypomethylation [333].

Regulation of Endothelial Nitric Oxide Synthase Function by Protein-Protein Interactions

In human platelets eNOS is localized in the membrane caveolae, while in ECs is primarily localized in the membrane caveolae and in smaller part in Golgi apparatus and cytosol [334]. Interestingly, endothelial eNOS activity is 7-fold greater in the membrane fraction than in the cytosol [335, 336]. Therefore, correct subcellular trafficking and localization to the membrane caveolae is necessary for proper eNOS function. Displacement of the enzyme to the cytosol or Golgi impairs agonist-stimulated eNOS activation and optimal NO release from cells. Associated with atherosclerosis accumulation of ox-LDL in subendothelium depletes EC membrane caveola cholesterol which results in eNOS displacement and impairs its enzymatic activity. This pathological mechanism may play a role in the early atherosclerosis [337].

Activity of eNOS protein is tightly controlled by mechanisms that involve post-translational lipid modifications, phosphorylation on multiple residues and regulated protein-protein interactions. eNOS enzymatic activity is mediated by positive allosteric regulation (e.g. $Ca^{2+/}$CaM complex or heat shock protein 90 binding) but also negative allosteric regulation (e.g caveolin-1 binding). Mechanistically, binding of calmodulin and hsp90 to eNOS can displace caveolin-1 and cause its activation [338].

CaM is a Ca^{2+}-binding protein that is vital for activity of eNOS and nNOS proteins [277, 339]. eNOS binding site for $Ca^{2+/}$CaM complex is localized between the N-terminal oxygenase and C-terminal reductase domains of eNOS (amino acid (aa) 493–512). Recently eNOS region between aa 594–613 in the reductase domain has been suggested as additional calmodulin binding site that may also regulate its enzymatic activity. Binding of $Ca^{2+/}$CaM complex to eNOS displaces adjacent autoinhibitory loops and “unlocks” NADPH-dependent electron flux from the reductase to the oxygenase domain and ultimately to the heme moiety for production of NO [340]. Furthermore, eNOS activity is proportional to the elevation of intracellular Ca^{2+} which promotes the binding of $Ca^{2+/}$CaM complex [45].

A second eNOS-interacting protein is a 21 kDa caveolin-1 (CAV-1) which contrary to CaM is a negative regulator of eNOS activity and NO production. CAV-1 is a major structural protein of – caveolae - flask-shaped 60–80-nm in diameter plasma membrane invaginations. Caveolae are rich in proteins as well as lipids such as cholesterol and sphingolipids. Caveolae

also contain a myristic and palmitic fatty acids that can form covalent bonds with cellular proteins. The binding site for CAV-1 within eNOS lies between amino acids 310 and 570 which masks eNOS CaM binding domain and prevents binding of Ca^{2+}/CaM complex and electron flux to the eNOS heme, thereby maintains eNOS inactive state [335]. Interestingly, synthetic peptides flanking this region can potently and reversibly inhibit eNOS activity by interfering with binding of the Ca^{2+}/CaM complex to eNOS [341]. Also over-expression of CAV-1 reduces basal eNOS activity [342]. Elevation of intracellular Ca^{2+} levels or exposure of EC to shear stress causes CAV-1 to become displaced and this allows the Ca^{2+}/CaM complex to associate with eNOS CaM binding domain. Subsequently eNOS is de-palmitoylated and translocated from membrane caveolae to the cell cytosol [343, 344]. The major functions of caveolae are related with ion transport, endocytosis, transcytosis, signal transduction, stretch sensing in SMCs and in ECs serve as mechanosensors [345, 346]. ECs caveolae are involved in flow sensation by tight connection to integrins and the focal-adhesion machinery [346]. Acute shear stress results in increased levels of CAV-1 and eNOS in ECs plasma membrane due to redistribution from the Golgi complex. Subsequently, integrin mechanotransduction and eNOS shear stress-induced activation promotes caveolin-1 phosphorylation and actin reorganization. This mechanism facilitates remodeling of blood vessels in response to changes in a blood flow [347].

eNOS also interacts with the 90kDa heat-shock protein 90 (Hsp90) which is a molecular chaperone that can modulate protein folding and activity. Hsp90 is physically associated with eNOS N-terminal oxygenase domain (aa 310–323) in resting ECs and upon activation causes dissociation of eNOS from the caveolae. The allosteric activation of eNOS via Hsp90 facilitates the dissociation of CAV-1 and unmasks eNOS CaM binding domain [338]. This allows for Ca^{2+}/CaM complex association with CaM domain causing increase in eNOS activity which is abrogated by the Hsp90 inhibitor – geldanamycin [348, 349]. Additionally, Hsp90 brings eNOS and sGC together thereby reduces the diffusion distance of NO and facilitates the efficient production of cGMP [350]. Hsp90 is modulated by physical interaction with its co-chaperones such as carboxyl terminus of Hsp70-interacting protein (CHIP). CHIP is involved in the ubiquitination and degradation of Hsp90 client proteins but it does not degrade eNOS. Instead CHIP interacts with eNOS and displaces it from the Golgi apparatus to the cytosol. Furthermore, CHIP knockout mice have higher expression of eNOS in the Golgi apparatus and cell membrane which contributes to greater eNOS activity [351]. On the other hand both of eNOS-associated

proteins nitric oxide synthase-interacting protein (NOSIP) and the nitric oxide synthase traffic inducer (NOSTRIN) promote the intracellular redistribution of eNOS from membrane caveolae to cytosol. NOSTRIN and NOSIP decrease eNOS activity and NO release by displacing eNOS from the optimal signalling localization close to the cellular membrane [351-354].

Regulation of Endothelial Nitric Oxide Synthase Function by Acylation

eNOS is unique among the NOS isoforms because is dually acylated by myristate and palmitate. Furthermore, association of eNOS with CAV-1 is independent of the state of eNOS acylation [355]. Redistribution of eNOS to Golgi promotes eNOS palmitoylation, however myristoylation is mandatory for the membrane association of eNOS and for subsequent palmitoylation [356]. Co-translational lipid modification of eNOS includes attachment of myristic acid to eNOS N-terminal glycine-2 (G2) on cytoplasmic ribosomes by N-myristoyltransferases (NMT) and posttranslational palmitoylation at the Golgi apparatus by palmitoyl-acyl-transferases (PAT) on cysteines-15 and 26 (C15, C26) [357-359]. The myristoyl group anchors eNOS to membranes via hydrophobic interactions with membrane lipids. Palmitoylation of eNOS provides additional hydrophobic interactions that stabilize the weak membrane association created by myristoylation alone. Moreover, membrane association requires myristoylation but not palmitoylation [359]. However, both myristoylation and palmitoylation target eNOS localization to membrane caveolae which provides a close proximity to GPCRs, ion channels regulating calcium entry, kinases and arginine transporters, all of which support optimal synthesis of NO. Mutagenesis of the myristoylation, which prevents both myristoylation and palmitoylation, blocks eNOS association with cell membrane and causes partial redistribution of enzyme to the cell cytosol [360, 361]. Similarly stimulation with platelet agonists induces depalmitoylation of eNOS and partial redistribution of enzyme to the cell cytosol [329].

Regulation of Endothelial Nitric Oxide Synthase Function by Serine and Threonine Phosphorylation

Human eNOS can be regulated by multiple phosphorylation sites at tyrosine (Y), serine (S), and threonine (T) residues. There are seven primary sites of eNOS phosphorylation which include Y81, S114, T495, S615, S633, Y657 and S1177. It is thought that phosphorylation of eNOS residues changes its allosteric conformation which in most cases removes the steric hindrance caused by non-catalytic inserts and permits better fidelity of electron flux from the

reductase domain to the oxygenase domain. This enhances eNOS enzymatic activity and NO generation. Phosphorylation of human eNOS at S1177 in the C-terminal reductase domain appears to be the most important of the regulatory eNOS phosphorylation sites and most, if not all, of the diverse stimuli that induce eNOS activation are observed to cause phosphorylation of this site. Factors such as bradykinin, VEGF, estrogen, histamine, insulin-like growth factor (IGF) and shear stress stimulate the activation of eNOS via S1177 phosphorylation by the protein kinase Akt [362]. Additionally, other protein kinases are implicated in the regulation of eNOS S1177 phosphorylation including protein kinase A (PKA), protein kinase G (PKG) adenosine monophosphate-activated kinase (AMPK) and Ca^{2+}/calmodulin-dependent protein kinase II (CaMK II) [363-366]. Phosphorylation of eNOS at S1177 increases electron flux in the reductase domain and enhances sensitivity to Ca^{2+}/CaM complex. This Ca^{2+}-independent mechanism allows eNOS to remain active and produce NO even at basal or low levels of intracellular Ca^{2+}. Importantly localization of eNOS in the membrane caveolae is essential for phosphorylation at S1177 in response to agonist and lack of myristoylation greatly diminishes eNOS activity which is fully restored by targeting of eNOS to the membrane [367].

The role of S615 phosphorylation located in the CaM autoinhibitory sequence within the FMN binding domain is still not fully understood. It is catalyzed by AKT and PKA and it appears to sensitize eNOS for binding of Ca^{2+}/CaM complex, which results in displacement of the autoinhibitory loop but does not enhance NO generation alone. It has been proposed that phosphorylation of S615 does not directly regulate NO production but instead it modulates phosphorylation at other sites and promotes protein-protein interactions [368, 369].

Phosphorylation of S633 is under control of PKA, AMPK and extracellular signal regulated kinase 1/2 (ERK1/2). It is located in the CaM autoinhibitory sequence of eNOS within the FMN binding domain and provides a positive regulatory site. Phosphorylation of S633 occurs in response to the same stimuli that cause phosphorylation of S1177. Phosphorylation of Ser 633 happens slower than that of S1177 which helps to sustain NO synthesis after the initial NO burst caused by activation at S1177 [370]. Thus phosphorylation of Ser 633 appears to play a role in chronic regulation of eNOS in response to mechanical and humoral stimuli [368].

It is noteworthy that phosphorylation of eNOS sites S615, S633 and S1177 localized in autoinhibitory regions of the reductase domain causes displacement of autoinhibitory domains and enhances the Ca^{2+} sensitivity and overall activity of eNOS. Experimental deletion of these

autoinhibitory regions makes eNOS insensitive to changes in Ca^{2+} levels similarity to Ca^{2+} - independent iNOS protein that lack these autoinhibitory regions [340].

Contrary to phosphorylation sites that positively regulate eNOS activity, phosphorylation of T495 represents the major negative regulatory site of eNOS. Phosphorylation of T495 interferes with the binding of Ca^{2+}/CaM complex to eNOS due to effect of repulsive steric or charge effects. The eNOS phosphorylation at T495 is mediated mainly by PCK, AMPK and Rho kinases [365]. Interestingly, stimulation with agonists of NO synthesis such as bradykinin and VEGF induces dephosphorylation of eNOS T495.

Also phosphorylation of eNOS S114 in the oxygenase domain maintains its inactive state. Experiments with inhibitors of PKC and AMPK showed that both kinases are responsible for S114 phosphorylation. Stimulation of ECs with potent eNOS activator - VEGF promotes dephosphorylation of eNOS at S114 which is coordinated with phosphorylation of eNOS at S1177**;** as a result this augments NO production [371]. In addition, phosphorylation at S114 also promotes eNOS association with its negative regulators - CAV-1 and Pin1 [372, 373]

Regulation of Endothelial Nitric Oxide Synthase Function by Tyrosine Phosphorylation

Mechanisms of eNOS tyrosine (Y) phosphorylation have not been investigated as extensively as those of eNOS serine/ threonine phosphorylation. It still remains unresolved whether tyrosine phosphorylation is involved in modulating enzyme activity or rather in providing binding sites for proteins with a Src homology 2 (SH2) or a phospho tyrosine binding (PTB) domain**.** Phosphorylation at Y81 promotes basal eNOS activity via Src kinase mechanism in response to H_2O_2 and agonist (mainly VEGF and bradykinin) stimulation [374, 375]. On the other hand stimulation with insulin, angiotensin II or fluid shear stress causes proline rich tyrosine kinase 2 (PYK2) mediated phosphorylation of Y657. The Y657 phosphorylation attenuates eNOS enzyme activity, probably in order to attenuate the deleterious effects of maintained high NO output such as in situations of elevated redox stress [376]. This mechanism may play a role in cardiovascular diseases associated with endothelial dysfunction and increased activity of the renin-angiotensin system [377].

1.4 Megakaryocyte Biology

1.4.1 Megakaryocytes and Megakaryopoiesis

Dr. James Homer Wright was the first scientist who demonstrated that platelets arise from bone marrow MKs. He studied blood and bone marrow samples under microscope using various staining methods and described his observations in an article from 1906 "A Rapid Method for the Differential Staining of Blood Films and Malarial Parasites" [378]. Wright also correctly associated reduced platelet blood concentration with bleeding and performed first semi-quantitative platelet count using the microscope. These findings were published in 1906 titled "The Origin and Nature of the Blood Plates" [379]. His article published in 1910 "The Histogenesis of the Blood Platelets" includes a number of great quality watercolor drawings (made with the aid of a camera lucida) showing MK protruding into bone marrow sinusoid and releasing platelets [380]. Wright's pioneering studies at the beginning of XX century made significant progress in understanding the origin of blood platelets and introduced bone marrow MKs as a new interesting object of research.

Approximately 100 billion new platelets are produced daily from bone marrow MKs to support physiological platelet count. The process of platelet generation from MKs is called thrombopoiesis. Mature MKs are large (50-100 μm) and rare myeloid cells accounting for less than 1% of all bone marrow cells and their numbers are modulated by factors like thrombopoietin (TPO), chemokines or ligands expressed on some of the bone marrow components that interact with MK surface receptors [381].

MKs arise from pluripotent hematopoietic stem cells (HSCs) in process called megakaryopoiesis. Pluripotent HSCs reside mainly in the osteoblastic niche of the bone marrow where they either self-renew or produce progenitors which commit to a specific cellular linage that ultimately gives rise to mature blood cells. MK-committed progenitor cell differentiates down the megakaryocyte lineage (Figure 1.13). During embryonic and fetal development megakaryopoiesis occurs within the yolk sac, fetal liver, and spleen because the marrow cavities are not fully formed. In adult humans MK differentiation, maturation and platelet release take place primarily in the bone marrow. However, some MKs migrate to vessels in the lungs, where they become trapped in pulmonary microvessels because of their size and release platelets into the pulmonary circulation. Furthermore, it has been suggested that haematopoietic progenitors

can also migrate from the bone marrow to the lungs and differentiate into platelet-releasing MKs [382-384]. Little is known about the factors responsible for the homing of these cells into and out of the lungs.

Megakaryopoiesis can be divided into two main phases: differentiation and maturation. The differentiation is associated with formation of increasingly restricted lineage that culminates in the formation of MK precursors. It starts with commitment of pluripotent HSC, in response to various stimuli such as TPO, to develop common myeloid progenitor cell (CMP) from which develops erythroid-megakaryocyte progenitor (MEP). These cells then give rise to more differentiated progenitors, like megakaryocyte precursor cells that proliferate producing a pool of promegakaryocytes (PMKs). MK differentiation form HSC is also accompanied by gradual decrease of CD34 antigen expression. MK differentiation is predominantly driven by TPO signalling through the myeloproliferative leukemia protein (c-mpl) receptor, expressed on the HSC through entire megakaryocyte lineage including platelets, and is supported by additional growth factors such as interleukin-3 (IL-3), stem cell factor (SCF), interleukin -6 (IL-6) and interleukin -11 (IL-11).

During maturation phase which usually lasts few days MKs do not proliferate anymore. Instead mononuclear megakaryocyte precursors exit diploid state to differentiate and undergo multiple rounds of endomitosis (shortened mitosis caused by a block in late anaphase B), a process that amplifies the DNA up to 64N without cell division. Most cells fall within three ploidy classes (8N, 16N, and 32N), and the 16N is the most dominant [385]. The mechanism of endocytosis in MKs is only partially understood. MKs in response to TPO upregulate cell cycle proteins – cyclins: D1, D3 and E1 which mediate multiple rounds of endomitosis by promoting MKs to reenter G1/S –phase, yet it is still unknown how MK abrogate anaphase and skip cytokinesis [386-388]. Such high DNA content in MKs allows for fast and efficient protein synthesis, which is especially important for anucleate platelets. At this stage MKs contain large number of ribosomes to facilitate the production of platelet-specific protein. Before reaching the ability to release platelets, megakaryocytes undergo a pronounced cytoplasmic maturation for platelet biogenesis by expanding their cytoplasmic content of cytoskeletal proteins and platelet-specific granules. Certain proteins that are later found on the platelet surface such as vWF and fibrinogen receptors are synthesized and sent to the megakaryocyte surface. Other factors like vWF are packaged into MK secretory granules and are later found in platelet α-granules. Finally,

some other molecules such as fibrinogen are absorbed by MKs from plasma through endocytosis and/or pinocytosis and selectively placed in platelet-specific granules (17, 18). MK maturation also involves assembly of future platelet mitochondria, δ-granules and α-granules both derived from MK Golgi apparatus. MKs also develop a highly tortuous invaginated demarcation membrane system (DMS) which serves as a membrane reservoir for the formation of proplatelets, the precursors of platelets [384, 389-391]. Expression of surface adhesion molecules such GPIIb/IIIa, GPIb-IX-V or GPVI is another indicator of MK maturation (Figure 1.13). For instance GPIIb/IIIa is expressed in MK lineage from progenitors to platelets and as the cell matures the abundance of this receptor increases. In contrast the GPIb-IX-V is being expressed later than GPIIb/IIIa so this difference can be used as a tool to differentiate more mature MKs [392, 393]. Fully differentiated MK complete maturation having all elements and machinery required for the major task of platelet biogenesis. MK maturation is also associated with their migration from the osteoblastic niche to the vascular niche of the bone marrow. MK migration to vascular niche highly depends on activity of multiple factors and chemokines released by bone marrow stroma. Mature MKs localize close to the subendothelial layer of the bone marrow sinusoids and complete their maturation which culminates in platelet release. Single mature MK releases into the bone marrow sinusoids around 1000–3000 platelets that form at the end of long (>100 μm) cytoplasmic structures called proplatelets [394, 395]. Interestingly, it has been shown that 2N mature MK will give rise to 1-2 platelets, while a 16N MK will give rise to ~2000 platelets; this emphasizes the importance of endomitosis in platelet production [396, 397]. Prior to proplatelet formation MKs concentrate microtubules in the cell cortex and at the same time one pole of the MK spontaneously develops pseudopodia. Initially pseudopodia are large and blunt but as they extend further away from the cell they become thinner, branch out repeatedly and form 10-20 proplatelets that serve as the assembly lines for platelets [398]. Proplatelet extension is facilitated by β1-tubulin that lines the shafts of proplatelets and cytoplasmic dynein motor proteins that provide the mechanical force for microtubules. The branching reaction is driven by F-actin and is inhibited by drugs that disrupt actin filaments. Platelets assembly also requires transport of platelet intracellular organelle into the platelet buds that form at the end of proplatelets. Platelet cargo delivery from the MK body is carried out by microtubule tracks in the shafts, and when platelets fully assemble they are released from the ends of proplatelets [398]. When whole MK is converted into proplatelets its nucleus is extruded and phagocytosed by

macrophages. The time required for MKs to complete endomitosis, mature, and release platelets is ~5 days in humans and 2–3 days in mice [399].

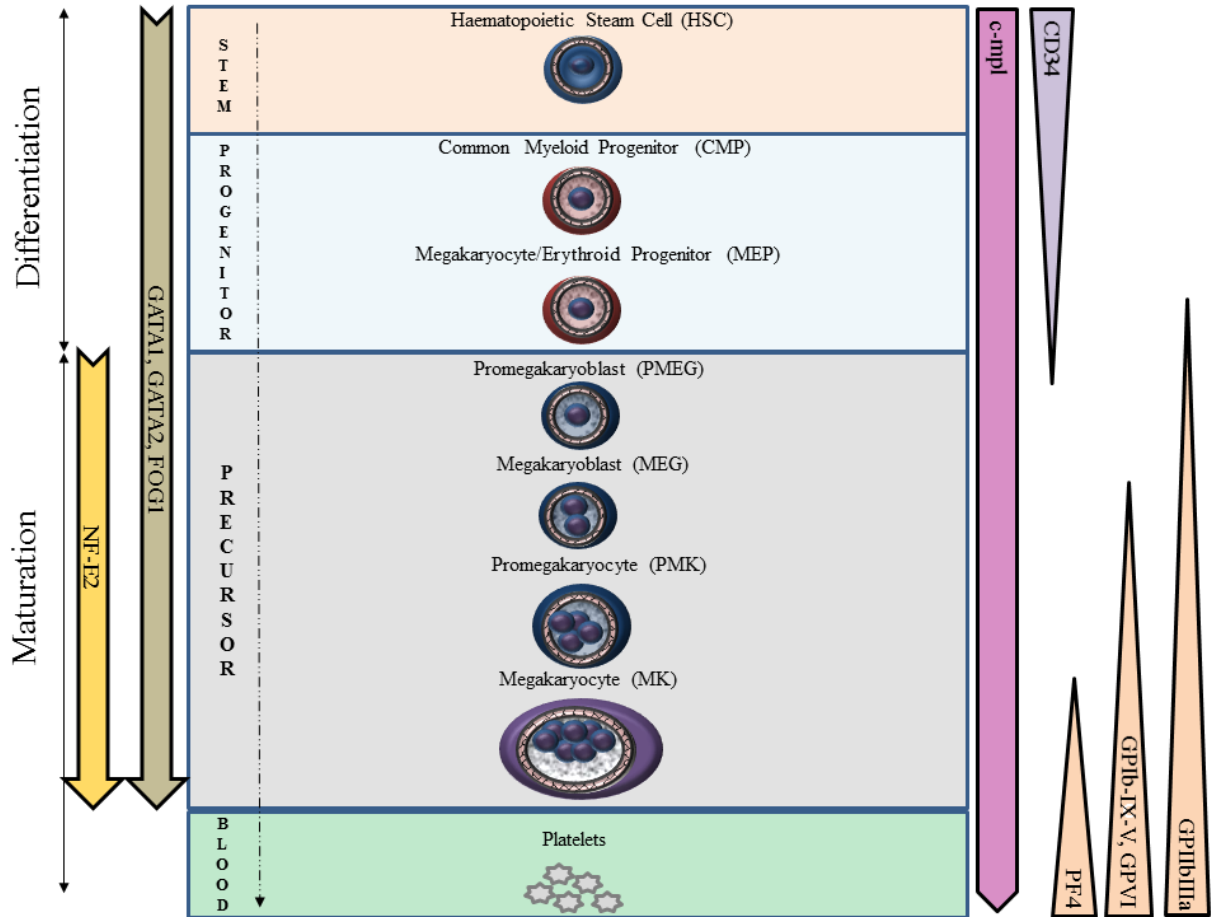

Figure 1.13. Overview of megakaryopoiesis

Megakaryocytes derive from the HSC which proliferate and differentiate under the influence of TPO and multiple transcription factors. In addition, MK differentiation and maturation is also associated with expression or repression of certain surface antigens/markers.

1.4.2 Genomic Regulation of Megakaryopoiesis

Megakaryopoiesis begins with determination of the lineage fate and commitment of MEPs toward the MK-lineage. This phase of megakaryopoiesis is highly regulated by transcriptional and epigenetic mechanisms. These mechanisms promote expression of genes required for differentiation of MK precursors and suppress genes that assist development of other cell types. The genetic regulation of megakaryopoiesis is also complemented by effects of synchronized TPO signal transduction through its receptor - c-mpl [400].

GATA1 and NF-E2 are key transcription factors regulating megakaryopoiesis (Figure 1.13). While NF-E2 modulates the later stage of MKs development, transcription factor - GATA1 controls multiple stages of megakaryopoiesis. At the early stage of haematopoesis GATA1 promotes MEPs differentiation down the MK-lineage and *in vitro* studies show that enforced expression of GATA1 in multipotential precursors induces their commitment to MK-lineage [401]. Conversely, global loss of GATA1 causes early embryonic death as a result of severe thrombocytopenia and anemia [402]. In addition GATA1 regulates polyploidization by driving expression of the gene coding phase G_1 cell cycle regulator - cyclin D1. Consequently, MKs from GATA1 deficient mice are smaller, contain less platelet-specific granules and their DMS is underdeveloped or disorganized, suggesting that maturation of these MKs is arrested. In effect these mice have 15% of a normal platelet count [403, 404]. Moreover, GATA1 activity is regulated by nuclear protein - friend of GATA1 (FOG1) and missense mutations of GATA1 prevent interaction with FOG1. This results in severe thrombocytopenia but FOG1 interaction with GATA2 partially compensates loss of GATA1. Interestingly, FOG1 knockout animals lack the MK-lineage, which demonstrates that FOG1 acts as a critical cofactor for GATA1 and GATA2 in MEP commitment toward MK-lineage [405, 406]. Other transcription factor FLI1 acts in concert with GATA1-FOG1 and ETS1 to promote expression of several MK-specific and platelet-specific receptors like c-mpl, GPIIb and GPIX [407].

On the other hand, NF-E2 transcription factor controls the later stage of MK development and regulates transcription of genes essential for MK maturation and platelet biogenesis. However, complete loss of NF-E2 is detrimental and causes hemorrhage and death of transgenic mice shortly after birth due to complete loss of circulating platelets. Mice that are partially deficient in NF-E2 (NF-$E2^{+/-}$) produce larger and less granular MKs, have underdeveloped DMS and ultimately fail to generate proplatelets *in vitro*. This phenotype is associated with the late

block in MK maturation, which emphasizes NF-E2 control of genes involved in cytoplasmic maturation and platelet formation. Genetic studies identified β1-tubulin encoding gene as the potential downstream target of NF-E2 [408, 409]. The β1-tubulin is restricted to the MK-lineage where it appears late in differentiation and localizes to microtubule shafts and coils within proplatelets. Importantly, β1-tubulin is essential for the MK cytoskeletal rearrangement and platelet formation [410-412]. Murine megakaryoblastic cell line (L8057) deficient in NF-E2 has almost entirely suppressed expression of β1-tubulin mRNA and protein, and restoration of NF-E2 activity rescues the expression of β1-tubulin [412]. Additionally, congenital macrothrombocytopenia is the condition where mutation of the β1-tubulin gene results in synthesis of mutant protein prone to aggregation, which impairs microtubule assembly and leads to release of large platelets [411]. Some studies also propose other downstream targets of NF-E2 including TXA_2 synthase and proteins that regulate inside-out signalling via $\alpha_{IIb}\beta_3$ integrin [413-415].

1.4.3 Regulation of Megakaryopoiesis by the Microenvironment of Bone Marrow Niche

Bone marrow is a semi-solid tissue localized in the bone cavity that is responsible for the production of the new blood cells. It is composed of a complex network of sinusoids surrounded by haematopoietic cells supported by a tridimensional mesh of ECM. Bone marrow provides soluble factors, forces and cell-mediated interactions necessary to maintain the haematopoietic potential of HSCs that reside there. This dynamic and unique microenvironment called bone marrow niche supports all stages of megakaryopoiesis (Figure 1.14). Anatomically there are two main areas in the bone marrow niche, osteoblastic niche which is an outer region that encompasses osteocytes and bone matrix and vascular niche the inner region of the bone marrow that contains sinusoids [416]. Osteoblastic niche supports the microenvironment for HSCs quiescence, self-renewal or production of haematopoietic progenitors but prevents them from terminal differentiation. On the other hand, the vascular niche consists of mesenchymal stem cells (MSCs) and sinusoidal ECs, which by secreting various cytokines support haematopoietic progenitor commitment toward specific lineages like MK-lineage. The released cytokines also promote differentiation of committed progenitors down the MK-lineage, MK maturation and platelet production [417]. When HSCs proliferate, the newly formed progenitors migrate from the osteoblastic niche, where environmental cues encourage expansion, but suppress terminal maturation, to vascular niche in the center of the bone marrow cavity. During migration, haematopoietic progenitors differentiate down the MK-lineage due to activity of TPO, which is additionally reinforced by various cytokines including IL-3, SCF, IL-6 and IL-11 (Figure 1.14).

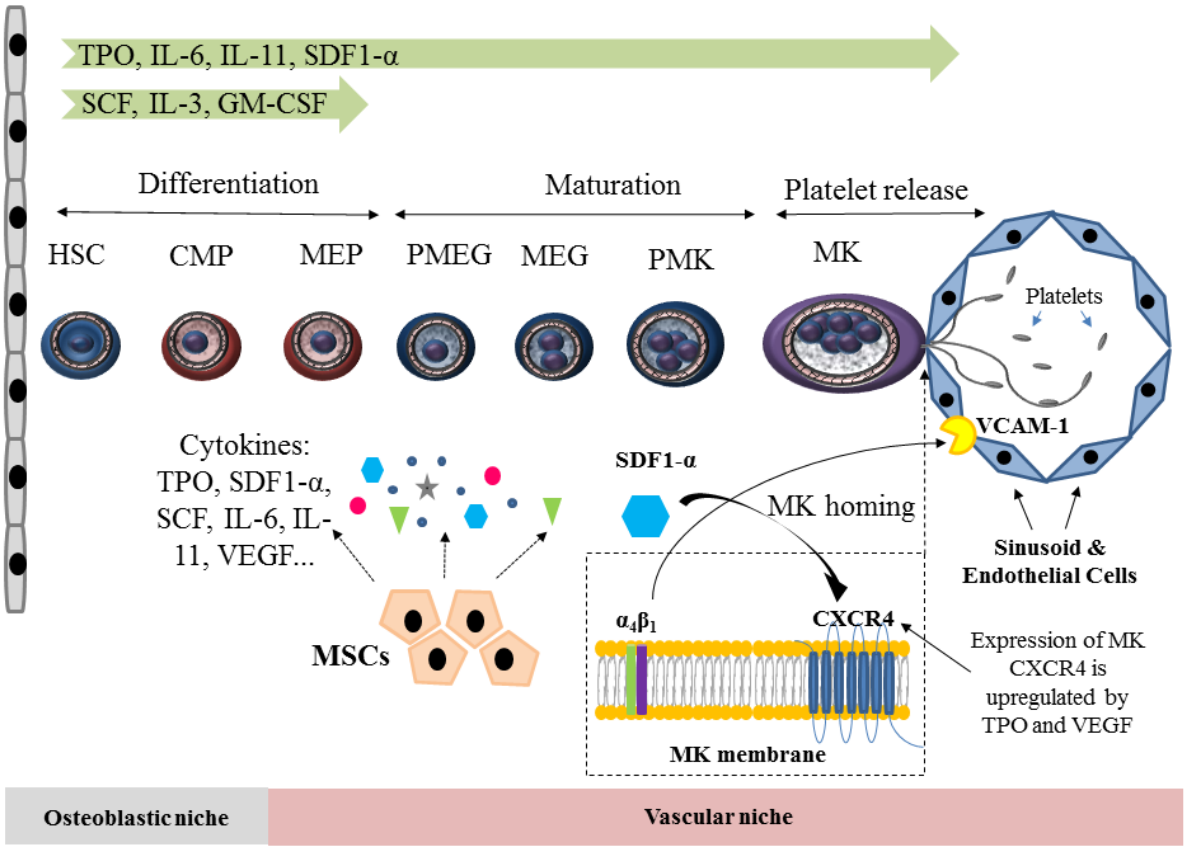

Figure 1.14. Overview of megakaryopoiesis in bone marrow niche

Figure depicts the development of mature MKs from HSCs. This process is mediated by specific bone marrow microenvironment and constituents of osteoblastic and vascular niche. The cytokines generated by bone marrow MSCs and sinusoidal ECs regulate all stages of MK development including migration toward sinusoid and release of platelets.

1.4.4 Role of Thrombopoietin in Megakaryopoiesis

TPO is the key physiological regulator of steady-state megakaryopoiesis and the most potent in vivo stimulus of platelet production of all known cytokines. TPO is a glycoprotein hormone primarily produced in the liver; however, it is also detectable in kidneys and bone marrow mesenchymal stem cells (MSCs) [418]. Physiological concentration of TPO in humans ranges from 7 to 99 pg/ml and can increase up to 1500 pg/ml in hypoproliferative thrombocytopenia patients [419].

TPO acts on myeloproliferative leukemia receptor (c-mpl) expressed on HSCs, haematopoietic progenitors, entire MK-lineage and platelets [420, 421]. However HSCs, MKs and platelets present the highest surface expression of c-mpl receptor. Binding of TPO to c-mpl receptor promotes proliferation and differentiation of HSCs into haematopoietic progenitor cells committed to the MK-lineage (Figure 1.15). During MK development, TPO stimulates the cytoplasmic reorganization and formation of demarcation membranes, promotes endomitosis and expression of characteristic cell surface glycoproteins - GPIIb/IIIa and GPIb-IX-V. Due to these TPO-mediated effects MK become mature and generate platelets [422]. Therefore TPO deficient mice have reduced numbers of progenitor MEP cells as well as reduced MK ploidy [423-426]. Conversely, MK isolated from mouse fetal liver and incubated with TPO for 4–5 days become mature and polyploid, and fully competent to generate and release large numbers of platelets. While mouse embryonic stem cells incubated with TPO require 10–12 days to mature into megakaryocytes [427].

TPO mediates these diverse functions through several pathways that are activated upon binding to c-mpl receptor (Figure 1.16). Association of TPO with extracellular portion of c-mpl receptor brings the cytoplasmic tails of the receptor close together. This leads to autophosphorylation and activation of janus kinase 2 (JAK2) (associated with the cytoplasmic portion of the c-mpl receptor). Activated JAK2 phosphorylates T_{112} residue on c-mpl receptor which serves as a docking for STATs and adapter proteins (SHC or SHP2) [428-430]. Recruitment of STATs (mainly STAT 3 and STAT5) and adapter proteins activates signalling via STATs, PI3K and the Ras/mitogen-activated protein kinase (Ras/MAPK). Once active, these pathways mediate cell survival, proliferation and maturation. For example, STAT5 promotes expression of the antiapoptotic Bcl-$_{XL}$ and PI3K inhibits expression of the cell-cycle inhibitor p27 and stimulates expression of the phase G_1 regulator - cyclin D_1 [431-435]. Lastly, TPO

stimulates miR-150 expression which in turn reduces mRNA levels of important erythropoiesis inducer - c-Myb. This mechanism shifts the MEP fate decision toward MK-lineage [436, 437].

In healthy humans steady production of platelets is sustained by the hepatic Ashwell–Morell receptor which provides a positive feedback mechanism promoting hepatic TPO mRNA expression ultimately leading to production of new MK that generate platelets [100]. Additionally, MKs and platelets also regulate TPO bioavailability through their c-mpl receptors that act as a sink by binding, internalizing and degrading the excess of circulating TPO (Figure 1.15). This depletes free-circulating TPO, which slows down the production of new MK and generation of platelets [438, 439]. Consequently, transgenic mice lacking c-mpl receptor have high plasma levels of TPO [439]. Action of this feedback mechanism is especially appreciated in situation of thrombocytopenia. Low platelet number increases TPO plasma concentration, which stimulates production of the MKs and platelet generation to balance out thrombocytopenia. Genetic loss of either the c-mpl or TPO gene in mice leads to severe thrombocytopenia, with ~85% reduction in MK and platelet number [426, 440, 441]

Taken together, TPO to some degree regulates all stages of MK development, from HSC proliferation through MK cytoplasmic maturation and platelet release [151]. TPO is essential for early stage of megakaryopoiesis but is dispensable for MK maturation and platelet production. However, TPO synergizes with other cytokines present in the bone marrow milieu throughout entire megakaryopoiesis, which becomes very important during later stage of MK development [442, 443].

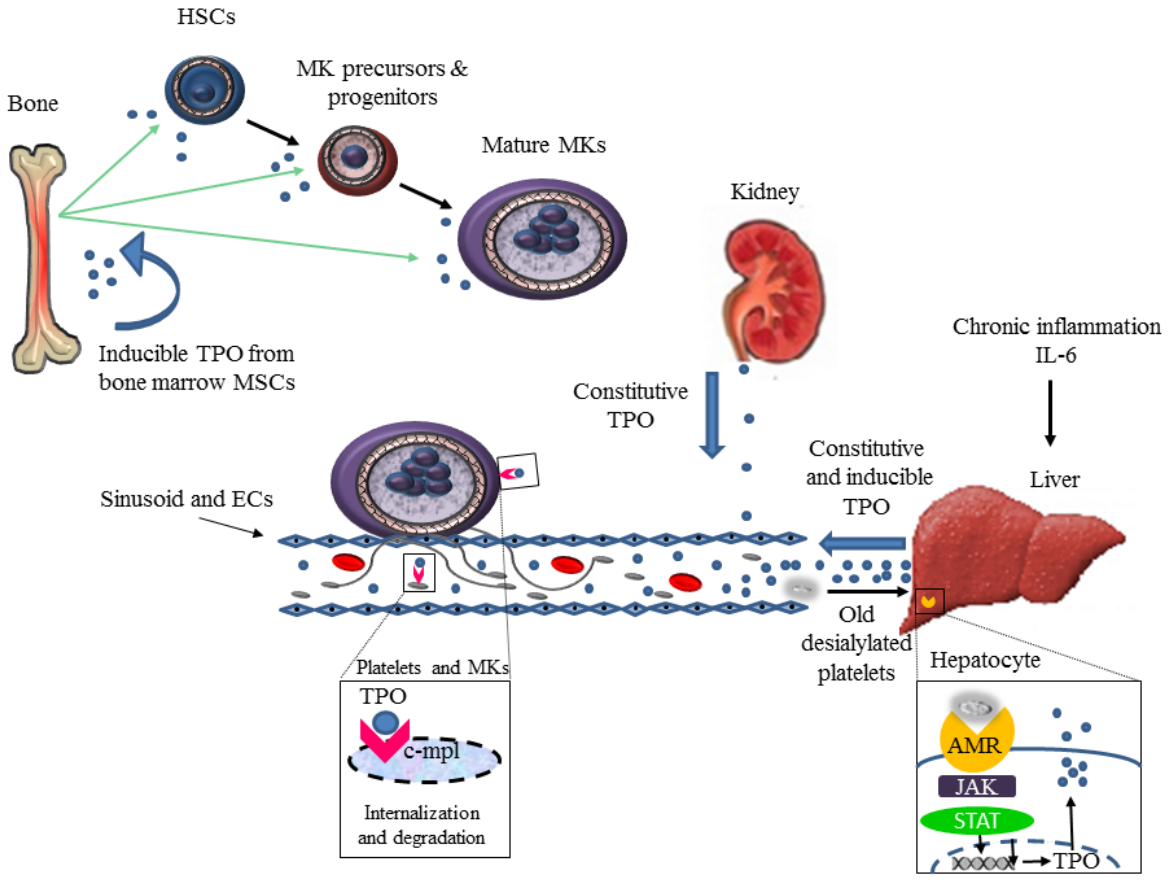

Figure 1.15. Mechanisms of TPO production and regulation

TPO production occurs predominately in the liver parenchymal cells and in lesser extent in MSCs and in proximal tubule cells of the kidney. Excess of free plasma TPO is internalized and degraded mainly by platelets and MKs. The TPO production is constitutive (no change in TPO mRNA levels), however binding of old desialylated platelets to Ashwell–Morell receptor stimulates TPO mRNA expression. During chronic inflammation IL-6 stimulates hepatic TPO mRNA production which may cause thrombocytosis.

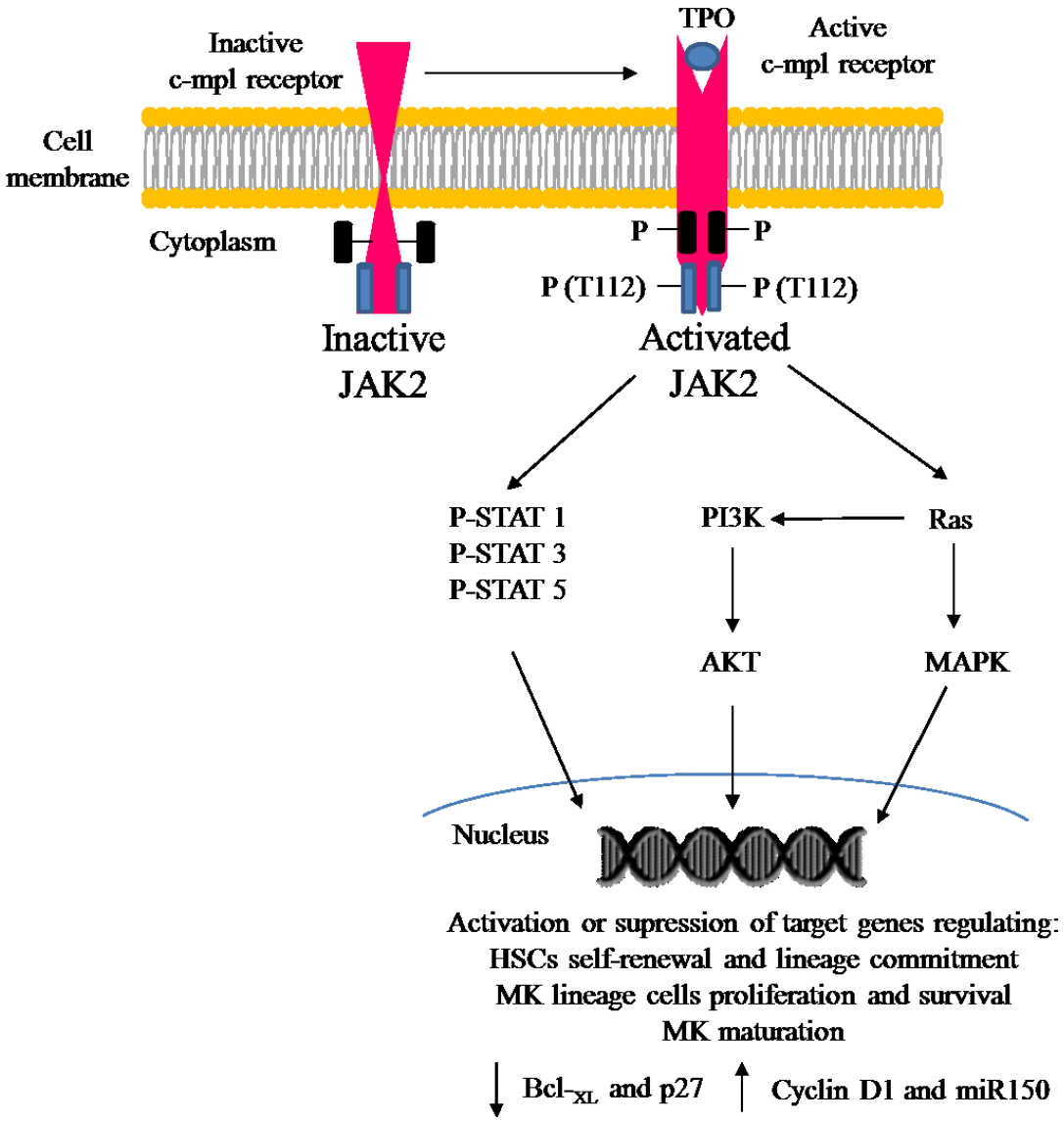

Figure 1.16. Mechanisms of TPO signalling

TPO binds to its receptor c-mpl causing homodimerization of c-mpl. This leads to activation of multiple downstream signalling pathways mediated by the receptor-associated tyrosine kinase – JAK2. Activation of these pathways supports the HSCs self-renewal and lineage commitment. TPO enhances MK progenitor proliferation, survival and differentiation, and stimulates MK maturation.

1.4.5 Role of Cytokines in Megakaryopoiesis

MK development is not exclusively regulated by TPO but also supported by several cytokines such as SCF, IL-3, IL-6, IL-11, granulocyte-macrophage colony-stimulating factor (GM-CSF), chemokine - stromal cell-derived factor 1 (SDF1-α), and growth factors such as VEGF and fibroblast growth factor 4 (FGF-4) (Figure 1.14). These cytokines and growth factors are actively secreted by several components of the vascular niche including MSCs and sinusoidal ECs [444]. *In vitro* studies demonstrated that MSCs and sinusoidal ECs are able to maintain haemopoietic progenitors and support MK differentiation in absence of exogenous cytokines [437].

In the early stage of MK development, bone marrow cytokines (especially SCF, IL-3 and GM-CSF) act as colony-stimulating factors and support the growth of immature MK progenitors. However, IL-3 and GM-CSF alone do not contribute to basal platelet levels in the absence of TPO signalling and even more so G-CSF in later-stage of MK development suppresses MK maturation [422, 445]. IL-6 and IL-11 augment actions of IL-3 and SCF but alone have little or no effect on proliferation of immature MK progenitors. However, IL-6 and IL-11 can induce MK growth and polyploidization during maturation [417, 446].

MKs migrate to sinusoids toward higher gradient of chemokine - stromal cell-derived factor 1 (SDF1-α), which is the natural ligand for C-X-C chemokine receptor type 4 (CXCR4). This MK progenitor migration from osteoblastic niche to vascular niche in response to cytokine chemoattraction is sometimes called “MK homing” (Figure 1.14). Multiple studies show that SDF1-α is a major cytokine/chemokine responsible for “MK homing”. Furthermore, SDF1-α acts synergistically with TPO to upregulate the MK chemokine receptor CXCR4, which increases MK migration toward sinusoid. Up-regulation of CXCR4 expression is also a hallmark of MK maturation [447]. Furthermore, single nucleotide polymorphism of SDF1-α is closely correlated with idiopathic thrombocytopenia [448-450]. MK maturation is also enhanced by VEGF via activation of VEGF receptor (VEGFR). This also up-regulates expression of MK CXCR4 and enhances redistribution of Mk to the vascular niche. When MKs migrate to vascular niche and localize close to sinusoid they interact with sinusoidal ECs via VCAM-1 and MK surface integrin $\alpha_4\beta_1$. MK adhesion to the sinusoid is additionally promoted by fibroblast growth factor 4 (FGF-4), which upregulates VCAM-1 expression on sinusoidal ECs [451]. At this stage mature MKs extend proplatelets that protrude through the endothelial layer and release platelets

directly into the marrow intravascular sinusoidal space. *In vitro* experiments showed that MKs cultured with MSCs increase formation of proplatelets even in the absence of exogenous cytokines, which emphasizes the role of MSC-derived cytokines in the final stage of megakaryopoiesis [437, 445].

Mature unstimulated MKs constitutively expressed genes for IL-1β, IL-6, GM-CSF and TNF-α, which are all detected at the protein level except TNF-α [452]. Moreover MKs are the main producer of bone marrow transforming growth factor-β1 (TGF-β1) which maintains HSC quiescence under homeostatic conditions and provides negative-feedback mechanism for megakaryopoiesis in addition to GM-CSF [437, 453].

Inflammation is associated with increased production and release of pro-inflammatory cytokines including some of the cytokines that physiologically regulate megakaryopoiesis like IL-6. Pro-inflammatory TNF-α stimulates fibroblasts and macrophages to produce and release high amounts of IL-6, which circulates to the liver and enhances synthesis of hepatic TPO mRNA by activating JAK1-STAT3 pathway. Increase of circulating TPO in response to inflammation promotes megakaryopoiesis and provides the mechanism responsible for increased platelet count in the blood of patients with chronic inflammatory disease [435, 454-456]. However, in addition to IL-6 there are other pro-inflammatory cytokines involved in enhanced megakaryopoiesis during inflammation.

1.4.6 Megakaryopoiesis in Inflammation – Implications for Cardiovascular Disease

Under normal conditions multiple cytokines (TPO, IL-3, IL-6, IL-10 etc.) present at the physiological plasma concentrations (very low or undetectable) regulate important cellular responses such as proliferation and differentiation including megakaryopoiesis. In response to inflammatory stimuli levels of both pro-inflammatory and anti-inflammatory cytokines increase that for the most part are the elements of normal host defense mechanism. However, uncontrolled acute inflammation may become chronic, contributing to a variety of chronic inflammatory diseases like atherosclerosis. Increased plasma levels of pro-inflammatory cytokines, including IFN-γ, during inflammation have been widely recognized as the contributing factors to thrombocytosis that often accompanies chronic inflammatory diseases [457-459]. Chronic inflammation modifies bone marrow milieu in a manner, which stimulates megakaryopoiesis and platelet generation. This is why thrombosis often complicates chronic inflammatory disorders like atherosclerosis [460-462]. Moreover, increased platelet blood count and platelet activity, even in absence of symptomatic inflammation, were associated with increased risk of CVD. One prospective study demonstrated that "apparently" healthy men with higher platelet blood count and activity had significantly higher coronary heart disease mortality at 13.5 years of follow up [463]. Similar observation was made by a population-based cohort study which found that high platelet count is associated with future cardiovascular disease [461]. However, more importantly platelets form patients with CVD have enhanced activity and thus show greater extent of aggregation in response to agonists comparing to healthy humans [309, 323, 464-468].

Taken together, there is a very strong link between inflammation and thrombocytosis and the new mechanisms of inflammation-induced megakaryopoiesis are being identified. Hoverer, less is known how inflammation affects the expression of MK proteins during megakaryopoiesis and whether this results in generation of platelets with changed pro-thrombotic phenotype(s).

1.5 Interferon Gamma and Interleukin 10 - Two Cytokines with Opposing Immunomodulatory Effects

1.5.1 Role of Pro-Inflammatory Interferon Gamma and Anti-Inflammatory Interleukin 10 - Implications for Cardiovascular Disease

IFN-γ and IL-10 represent two cytokines with opposing immunomodulatory responses. While IFN-γ promotes inflammation, IL-10 provides a counterbalance by suppressing pro-inflammatory activity of multiple cytokines including IFN-γ [469]. IFN-γ and IL-10 induce their effects through widely expressed receptors in various tissues and cells, and cell activation or inflammation further increase expression and *de novo* synthesis of these receptors [470].

IFN-γ is a soluble cytokine, which is synthesized and secreted by T lymphocytes, and macrophages as an important factor for macrophage activation involved in both innate and adaptive immunity [471]. In addition to the key role in host defense, IFN-γ overproduction has been associated with the pathogenesis of chronic inflammatory diseases like atherosclerosis. Therefore it is not surprising that patients with CVD have higher plasma levels of IFN-γ (in ACS mean 300 pg/ml) than healthy humans in which IFN-γ plasma level is usually below limit of detection (< 8 pg/ml). [472, 473]. In septic shock human IFN-γ plasma concentrations may reach up to 10 ng/ml [474, 475]. Pro-atherogenic effects of IFN-γ contribute to all stages of atherosclerosis development; at the early stage IFN-γ promotes expression of adhesion molecules on ECs and enhances proliferation of VSMCs, and at the later stage accelerates apoptosis of macrophages localized at the atherosclerotic plaque [476]. Mononuclear cells from patients with coronary heart disease have higher level of IFN–γ protein and mRNA than healthy controls, which positively correlates with increased concentration of serum triglycerides [477].

On the other hand, IL-10 is a cytokine with potent anti-inflammatory properties that plays a key role in limiting host immune response to pathogens. This prevents damage to the host and maintains normal tissue homeostasis. Under physiological conditions, IL-10 is primarily synthesized by T_H2 lymphocytes to suppress cytokine production by T_H1 lymphocytes. However, in response to inflammatory stimuli IL-10 is synthesized by almost all types of leukocytes including monocytes, macrophages, dendritic cells, T_H0 lymphocytes and B-lymphocytes. Following release, IL-10 inhibits T-lymphocyte activation, limits proliferation of monocytes and

attenuates production of multiple pro-inflammatory cytokines. It is well established that IL-10 counterbalances effects of pro-inflammatory cytokines including IFN-γ [478, 479].

Anti-inflammatory IL-10 mediates mechanisms that protect from atherosclerosis such as by deactivating of macrophages and T-lymphocytes – the main culprits of atherosclerotic inflammation. Deactivation of macrophages and T-lymphocytes enhances collagen deposition on atherosclerotic lesion which improves stability of the atherosclerotic plaque [480]. Conversely, IL-10 deficiency has been linked with susceptibility of developing atherosclerosis, thus IL-10 appears to be crucial as a protective factor against inflammation [480]. Deficiency of IL-10 enhances proteolytic and procoagulant activity of advanced atherosclerotic lesions. Patients with CVD, including ACS, similarly to healthy humans have either very low or undetectable levels (< 3.9 pg/mL) of IL-10 plasma concentration whereas high plasma levels of IL-10 are found in sepsis [472, 473, 481].

1.5.2 Effects of Interferon Gamma and Interleukin 10 on Megakaryopoiesis

IFN-γ stimulates megakaryopoiesis and thrombopoiesis both in mice and humans [482-485]. However, IFN-γ stimulatory effect on megakaryopoiesis is unique because it inhibits proliferation of other haematopoietic progenitor cells by causing G_1 phase arrest and apoptosis [483, 486, 487]. IFN-γ in absence of TPO enhances colony formation of the MK lineage and promotes MK endomitosis, which correlates with increased production of platelets in vivo. However, IFN-γ stimulatory effects on MK colony formation are weaker than those induced by TPO [488, 489]. In addition, IFN-γ alone induces MK growth and differentiation attributed by expression of surface receptors: GPIIb/IIIa and GPIb-IX-V, and accompanied by increase in MK size and DNA ploidy [490, 491]. This indicates that IFN-y stimulates not only the proliferation of MK progenitors but also the maturation of MK precursors [489]. Furthermore, IFN-γ stimulates megakaryopoiesis synergistically with other cytokines like SCF and IL-3 [457, 485, 489, 492].

During normal MK development, transcription factor GATA1 mediates activation of STAT1, which promotes the early stage of megakaryocyte development and differentiation. During various inflammatory states, IFN-γ activates this pathway enhancing MK proliferation, maturation and platelet release. IFN-γ binds to IFN-γ receptor (IFN-γR) on MK progenitors and activates JAK-mediated phosphorylation of transcriptional factor STAT1 bound to IFN-γR. Phosphorylated STAT1 leaves the IFN-γR and translocates into the nucleus, where it binds to the gamma interferon activation site (GAS) element of the IRF-1. In turn IRF-1 binds to promoters of IFN-γ-target genes and induces transcription of cyclins: D1, D2, E1 and transcription factor - NF-E2. Thus IFN-γ-induced JAK-STAT1 pathway stimulates MK polyploidization by enhancing expression of cyclins. While increased expression of NF-E2 stimulates megakaryocyte maturation and platelet biogenesis - particularly granule and proplatelet formation [489, 491, 493]. This IFN-γ-induced mechanism shows that inflammatory disorders may predispose affected individuals to thrombosis.

In contrast to IFN-γ, IL-10 has a positive effect on overall haematopoesis and it stimulates self-renewal of HSCs [494]. In addition, it has been shown that IL-10 enhances proliferation of haematopoietic progenitors suppressed by the increased production of IFN-γ [495]. However, the effects of IL-10 on megakaryopoiesis somewhat unclear, mainly due to limited evidence and few inconclusive reports. One *in vitro* study demonstrated that IL-10 alone

does not stimulate MK colony-formation units (MK-CFU) but does so in combination with other cytokines [496]. Another study has shown that IL-10 has negative effect on the proliferation of cultured bone marrow cells collected from patients with acute myeloid leukemia (AML) likely through suppression of an endogenous cytokines [497]. However, a different study showed that subcutaneous injections with very high doses of IL-10 (8 μg/kg per day) induced thrombocytopenia in healthy adult volunteers. Furthermore, bone marrow aspirates from individuals receiving the IL-10 showed decreased number of CFU-MKs which was not observed in any of placebo-treated subjects [498]. Another study on healthy adult volunteers also demonstrated transient decline in platelet count following IL-10 subcutaneous injections. In addition, blood samples from IL-10 treated volunteers showed suppressed synthesis of pro-inflammatory IL-1β and TNF-α upon stimulation with lipopolysaccharide (LPS) [499]. This corroborates results of *in vitro* studies that also demonstrated suppressing effects of IL-10 towards multiple pro-inflammatory cytokines [478, 479]. Lastly, patients with immune thrombocytopenic purpura (ITP) have increased levels of plasma IL-10 with suggests the role of this cytokine in immunotolerance [500]. Although there are no direct studies demonstrating effect of IL-10 on megakaryopoiesis, the observed decrease of platelet production in response to IL-10 can be an indicator of MK function and if so this would imply that IL-10 attenuates MK platelet production.

1.5.3 Effects of Interferon Gamma and Interleukin 10 on Endothelial Nitric Oxide Synthase and Inducible Nitric Oxide Synthase Expression

In addition to regulating megakaryopoiesis, pro-inflammatory cytokines have been reported to downregulate the expression and activity of eNOS while enhancing iNOS expression in various cells including ECs, Meg-01 cells and human bone marrow MKs [249, 282, 293, 319, 501, 502]. Expression of eNOS was shown in both human megakaryoblastic cell line Meg-01 and normal human bone marrow MKs. While small subset of normal human bone marrow MKs was reported to express iNOS, the Meg-01 cells required stimulation with pro-inflammatory cytokines (IL-1β and/or TNF-α) in order to induce iNOS expression [249, 280, 282, 283]. Consequently, the increase of iNOS expression resulted in time-dependent decrease of eNOS activity in the Meg-01 cells [282] . Importantly, MKs collected form patients with coronary atherosclerosis express significantly greater amount of iNOS than eNOS, which is the opposite to MKs from healthy controls. In addition, MKs from patients with severe coronary atherosclerosis have enhanced iNOS activity, whereas MKs form patients with normal coronary arteries show significantly higher eNOS activity. Interestingly, platelets isolated from the same patients with severe coronary atherosclerosis showed eNOS activity similarly to platelets form patients with normal coronary arteries. However iNOS activity was not observed in platelets from either group [280]. One of the reasons why MK iNOS is not passed onto the platelets is that it may function exclusively to regulate MK megakaryopoiesis. NO has been shown to regulate the growth of many cell types, including haematopoietic cells and MKs. Studies on normal human bone marrow cells demonstrate that high μM concentrations of exogenous NO-donors (SNP, SNAP) suppress human haematopoiesis *in vitro*, however low to moderate μM concentrations of these NO-donors selectively inhibit formation of the bone marrow erythroid but not the myeloid lineage [503, 504]. In addition, exogenous NO-donor - diethylenetriamine/NO-adduct (DETA/NO) at concentration of 125 μM also suppresses TPO-stimulated proliferation of MK haematopoietic progenitors and markedly decreases viability of these cells. Furthermore, stimulation with exogenous NO-donors (DETA/NO and SNP) inhibits growth and induces apoptosis of the mature bone marrow MKs stimulated with TPO. Addition of pro-inflammatory cytokines (IL-1β, TNF-α, IFN-γ) also stimulates MK endogenous NO production by upregulation or induction of iNOS expression that also inhibits their growth [283, 505]. Another study also found that both exogenous (NO-donor - S-nitrosoglutathione – GSNO) and

endogenous sources (stimulation with multiple pro-inflammatory cytokines) of NO can induce apoptosis in megakaryoblastic cell line - Meg-01 [283]. Furthermore, their follow up study demonstrated that exogenous NO (NO-donor – GSNO) alone significantly facilitates platelet release by Meg-01 cell and used in combination with TPO shows synergistic effect [506]. Therefore, it is possible to speculate that MK NOS-isoforms regulate MK apoptosis by generating NO which also stimulates platelet production by these MKs. Experiments with pro-inflammatory cytokines suggest that this mechanism could be enhanced by chronic inflammatory states contributing to thrombocytosis.

Currently there are no studies indicating the effects of pro-inflammatory IFN-γ and anti-inflammatory IL-10 on eNOS and iNOS expression in MKs. However, in ECs, which derive from the same common precursor cell as MKs and thus share many developmental regulators, IL-10 induces while IFN-γ suppresses eNOS expression [470, 507-509]. In ECs pro-inflammatory cytokines attenuate eNOS catalytic activity which is accompanied by decrease of eNOS mRNA due to loss of mRNA stability. The inhibition of eNOS activity in these cells occurs in pool of the enzyme associated with membrane fraction but not cytosolic fraction [502]. Decrease of eNOS transcript in ECs caused by IFN-γ is usually followed by upregulation of iNOS expression in these cells which involves activation of p38 MAPK pathway and its downstream target transcription factor - nuclear factor-κB (NF-κB) [510]. However, there might be other mechanisms involved such as one present in macrophages where IFN-γ induces iNOS expression via activation of JAK-STAT1 pathway. This causes IRF-1 binding to iNOS gene promoter region which stimulates iNOS transcription [511, 512].

On the other hand, IL-10 counteracts the effects of IFN-γ by inhibiting induction of iNOS and enhancing eNOS expression and activity in ECs and other cell types [288, 469, 470, 513]. In ECs IL-10 was showed to promote eNOS expression by binding to IL-10 receptor (IL-10R), which activates JAK-STAT3 pathway. Phosphorylated STAT3 translocates to the nucleus and interacts with its binding site within human eNOS gene promoter [470, 514]. In monocytes for example IL-10 suppresses IFN-induced tyrosine phosphorylation of STAT1 and thus prevents STAT1-assebley to its specific promoter motifs on IFN-γ-inducible genes [515, 516]. This mechanism of IL-10 is mediated by upregulation of suppressor of cytokine signalling 3 (SOCS3) gene which is a negative regulator of cytokine signalling. The members of the SOCS family bind

to phosphorylated JAKs causing their inactivation (this inhibits phosphorylation of STAT1) and degradation through the proteasome pathway [517].

1.6 Platelet and Megakaryocyte Heterogeneity

1.6.1 General Overview

Nowadays due to numerous studies, it is widely recognized that circulating blood platelets are heterogeneous in size, density, ultrastructure, biochemical composition, transcriptome and reactivity [16, 18, 129, 518-522]. Therefore it has become more apparent that some of these differences may reflect the heterogeneity of their parent cells – MKs [521, 523, 524]. Especially that platelets are anucleate and contain no DNA and only residual mRNA, thus they inherit most of the proteins from MKs [524]. However, it has been suggested that platelet heterogeneity and divergent RNA profiles also result from their ability to take up the RNA from vascular cells [525]. Recent papers describe that certain compositions (profiles) of mRNA and miRNA correlate with platelet phenotype which influence platelet functions including atherosclerosis and thrombosis [526, 527]. These miRNAs can repress the expression of their target genes and thus regulate platelet reactivity. For example, miR-96 regulates vesicle-associated membrane protein 8 (VAMP8) mRNA expression level and VAMP8 protein is an important SNARE protein involved in platelet degranulation. Subjects with higher VAMP8 expression tend to have hyperreactive platelets [528]. One of the most abundant miRNAs in platelets are miR-223 and miR-126, and both appear to be involved in regulating platelet reactivity. Specifically, miR-223 has ability to bind to the 3′UTR of human $P2Y_{12}$ receptor mRNA. This suggests that miR-223 could regulate $P2Y_{12}$ receptor levels and thereby platelet reactivity [529, 530]. Moreover, Shi and colleagues reported reduced levels of platelet miR-223 in association with high platelet reactivity, despite treatment with clopidogrel [531]. In addition, platelets can modulate EC apoptosis by releasing miR-223 and platelet miR-223 can be upregulated by stimulation with thrombopoietin [532]. Platelets stimulated with agonist also release miR-126, which is considered a biomarker of platelet activation, diminished in presence of aspirin [533]. Although the role of miR-126 in human platelets remains unknown, higher plasma or serum levels of miR-126 are associated with an increased risk of MI [534, 535].

In the light of recent finding, it is suggestive that differences associated with platelet phenotype may predetermine their roles in regulation of haemostatic plug or thrombus formation, where some platelets have more pro-thrombotic/reactive phenotype [18, 536-538]. Consequently, conditions associated with chronic inflammation can modify bone marrow microenvironment

and thus affect MK development by promoting certain characteristics that are later passed onto platelets [539]. Hoverer, there is no available studies demonstrating that distinct MKs (in the bone marrow) also yield different types of platelets. However, it has been shown that megakaryopoiesis in the inflammatory setting alters MK phenotype and induces thrombocytosis. More recently, a growing body of evidence demonstrates that various conditions including inflammation can contribute to generation of platelets that are changed to have a pro-thrombotic phenotype [482, 483, 539, 540].

1.6.2 Intrinsic and Microenvironmental Factors that Affect Platelet Heterogeneity

It was initially thought that platelet heterogeneity is limited to differences in size and density, which was assumed to correspond with platelet age, so that young platelets are large and light, and old platelets are small and dense [541, 542]. This theory was rejected as more reports showed that platelets neither change their size nor density as they age in the circulation [543]. Another study speculated that light and small platelets arise from MKs with higher ploidy (32N) and that bigger and denser platelets derive from MKs with lower ploidy (16N) [544]. There was also a contradicting report claiming that in fact higher ploidy MKs produce larger and more heterogenous (denser) platelets [545].

Megakaryocytes differ considerably from each other in terms of levels of cytoplasmic and membrane proteins. Flow cytometry experiments on MKs derived from single clone of forward-programmed human pluripotent stem cells show 100-fold difference in expression levels of common platelet receptors such as glycoprotein GPIbα, GPVI and integrin $\alpha_{IIb}\beta_3$ [523]. It has been also demonstrated that modification of the microenvironment around MKs like during chronic inflammation affects platelet transcriptome. Incubation of immortalized megakaryoblastic cell line - Meg-01s with IFN-α caused significant increase in the expression of CD69. Similarly, platelets isolated from patients with systemic lupus erythematosis (SLE) display increased expression of CD69 and other IFN-regulated protein, which is associated with increased procoagulant activity and platelet-monocyte interactions in SLE patients [540]. Importantly, changes in platelet transcriptome precede some of the CV events and can predict the risk of future cardiovascular events. Profiling studies of platelet mRNA isolated from patients with ST-segment-elevation myocardial infarction (STEMI) and CAD contained 54 differentially expressed transcripts. They also established that elevation of one transcript product - myeloid-related protein-14 precedes STEMI and can predict future CV events [546]. Recent, genome editing validation with super-enhancers transcription factor interactions found in MKs 423 non-coding variants associated with platelet count and traits. Few variants were linked to changes in platelet activation, as shown by multiparameter tests of platelet function. Next approach should be identifying modifications of the super-enhancer sites in patients with haemostatic or thrombotic disorders [547]. These findings suggested that the MK genomic regulation is dynamic and determines platelet transcriptome with functional consequences of clinical importance.

Sorting and loading of MK organelles, proteins or mRNA to single platelet is not fully understood. It appears to be a controlled mechanism so that single platelet receives pre-sorted and well defined content from the parent cell - MK. Cecchetti et al. have showed that MKs differentially sort mRNAs for MMPs and TIMPs into platelets but the mechanism remains unknown. Therefore changes in genetic code and other factors that affect quality or quantity of MK mRNA could affect platelet phenotype and their function [183, 526, 527]. Grey platelet syndrome (GPS) is a bleeding disorder characterized by thrombocytopenia and large platelets that lack α-granules as a result of NBEAL2 gene mutation in MK. The faulty gene deregulates the biogenesis of MK α-granules which was found to provide protection from arterial thrombosis and thromboinflammatory stroke [548, 549]. Furthermore, RNA sequencing showed that NBEAL2 gene mutation affected expression of over a hundred transcripts in platelets from GPS patients compared to platelets from unaffected individuals. This underlines the importance of MK intrinsic mechanisms in regulation of platelet phenotype [549].

Platelet haemostatic function greatly depends on a number and variety of surface receptors, and normal human platelets show considerable variation in expression levels of these receptors including $\alpha_{IIb}\beta_3$, GPIbα or GPVI. Consequently, stimulation with respective platelet agonists causes differential activation of these receptors [550-552]. Also certain conditions that are often associated with chronic inflammation can alter the expression levels of platelet surface receptors. As an example, pro-inflammatory IFN-γ was shown to increase expression of collagen GPVI associated Fc γ-chain receptor (FcγRIIa) on MK precursors and high expression of FcγRIIa on platelets is associated with enhanced platelet reactivity in response to varies immune stimuli [539, 553]. Different study showed that GPVI-FcγRIIa can also serve as signalling receptor for fibrin, thereby providing another link between coagulation and platelet activation [554]. In addition, synergistic effect of thrombin and collagen on activation of thrombin and GPVI-FcγRIIa receptors results in platelet population expressing high levels of procoagulant proteins, also known as “COAT” platelets [15, 555]. A number of studies also reported platelet differential exposure of P-selectin, which is a sign of α-granule release and classical marker of platelet activation [128, 552]. Because PS exposure facilitates the generation of thrombin by allowing assembly of the prothrombinase complex on the platelet surface, platelets with enhanced PS exposure are considered to have a procoagulant phenotype [17, 522, 556].

Importantly, this observation laid the groundwork into studies of different subsets of platelets and their role in haemostatic reactions.

1.6.3 Platelet Heterogeneity and Its Role in Haemostatic Reactions

The most studied aspect of platelet heterogeneity is platelet differential procoagulant activity and function. Activated platelets via exposure of PS provide negative charge for the assembly of the tenase and prothrombinase complexes required for localized and efficient generation of thrombin, and conversion of soluble fibrinogen into insoluble fibrin. This stabilizes the platelet plug into a firm clot that prevents bleeding and promotes healing. According to multiple studies not all platelets become procoagulant even after strong activation. The literature describes two different platelet phenotypes, procoagulant platelets which enhance coagulation at the wound site by exposing PS and binding tense and prothrombinase complexes, and second phenotype of aggregating platelets which supports aggregation and clot retraction via activation of integrin $\alpha_{IIb}\beta_3$. In addition, procoagulant platelets also show prolonged and elevated intracellular Ca^{2+} response to agonists, which is essential for strong activation [522, 556].

Dale et al. have identified a population of "COAT" platelets, which have enhanced surface immobilization of procoagulant α-granule proteins such as FV, TSP-1, fibrinogen, fibronectin and vWF. According to the study "COAT" platelets require simultaneous stimulation with 2 agonists - thrombin and collagen to become active. Formation of the coat occurs after PS exposure, most likely as a consequence of the assembly of platelet secretion products and plasma factors on the platelet outer membrane [15, 551]. Another distinct feature of pro-coagulant platelets is a synchronised membrane ballooning stimulated by local thrombin generation. Mechanism of membrane ballooning mediates shedding of platelet microvesicles which further amplifies local coagulation and platelet recruitment [557]. Because thrombin generation is the central event in coagulation, coated-platelets are considered to be pro-thrombotic. Importantly high levels of "COAT" platelets not only positively correlate with transient ischemic attack and stroke, but also improve prediction of stroke and transient ischemic attack in asymptomatic atherosclerotic patients [537, 538]. On the other hand, patients with spontaneous intracerebral hemorrhage have lower levels of "COAT" platelets shortly after the hemorrhagic event compared with normal controls, and these levels inversely correlate with the size of the bleed. Furthermore, lower "COAT platelet levels are also associated with increased mortality after spontaneous intracerebral hemorrhage [558-560]. Similar model of two functionally distinct platelet populations was described by Patel et al. where "vanguard" platelets more readily spread

out on collagen and “follower” platelets attach to the “vanguards” via highly-activated integrin $\alpha_{IIb}\beta_3$ [561].

Summarizing, CVDs remain the largest single contributor to mortality and morbidity globally. The pro-thrombotic platelet phenotype in haemostatic reaction may underscore this statistic. Therefore, pro-thrombotic/highly reactive platelets could serve as a potential pharmacological target or biomarker, in the management of thrombotic CVD. Furthermore, presence of platelet subpopulations, with distinct phenotypes and functions, where one is highly pro-thrombotic can be a reason for the high incidence of arterial thrombosis in light of good pharmacological inhibitors. Therefore, we need to better understand platelet biology in order to design better prevention strategies that will target the pro-thrombotic or hyperreactive platelets.

2. HYPOTHESES AND OBJECTIVES

2.1 Rationale

Despite abundant pharmacological agents used to prevent platelet thrombus formation, the incidence of arterial thrombosis remains high, especially among patients with antiplatelet therapy used as a secondary prevention of ischemic events such as MI and stroke [27, 562, 563]. Moreover current therapies used to treat arterial thrombosis strongly limit the activity of platelets which impairs their haemostatic function and increases the risk of bleeding in patients [564]. Given the limitations in prevention and treatment of ischemic events, there is a need for identification of novel anti-platelet therapies for a better prophylaxis and treatment of thrombosis. Modern anti-platelet therapeutic paradigm should be centered on preserving platelet haemostatic function while effectively targeting platelet responses and/or platelet subpopulations that are responsible for thrombosis. In order to achieve this we have to better understand platelet biology, especially as they have long been considered a small cell fragments acting simply as vascular system "*band-aids*". Another advantage of studying platelet biology is associated with potential identification of platelets or platelet subpopulation that has highly pro-thrombotic/reactive phenotype and function. These platelets could not only serve as a potential novel drug-target but also as an effective prognostic biomarker of adverse CV events.

As discussed in previous sections NO acts as a negative feedback mechanism, limiting platelet aggregation, and the inhibitory role of endothelium-derived NO on platelet function is widely accepted and well understood [245, 565]. However the existence and importance of platelet eNOS, and thus the ability of platelets to generate their own NO has been questioned by some authors [262, 263]. Importantly, impaired platelet NO production has been documented in patients with symptomatic ischemia, chronic heart failure and various risk factors for CVD, and has been shown to predict ACS. In addition, platelet hyperreactive response to agonists observed among these patients is considered as an important contributor of thrombosis [315, 467, 566].

In this study, the overarching question is whether platelet subpopulations exist based on the presence and absence of eNOS, and if so, whether these two subpopulations have differential roles in haemostatic/thrombotic reactions. Furthermore, we also aim to understand if

inflammation that contributes to atherothrombosis attenuates platelet eNOS (as it has been shown in ECs) and thus is responsible for enhanced thrombogenicity of these platelets [567, 568].

2.2 Hypotheses

1) *Platelet subpopulations exist based on the presence ($eNOS^{pos}$) and absence ($eNOS^{neg}$) of eNOS-signalling pathway and this may contribute to their differential roles in haemostasis and thrombosis.*
2) *Subpopulations of $eNOS^{neg}$ and $eNOS^{pos}$ megakaryocytes/blasts exist and give rise to their respective eNOS-based platelet subpopulations.*
3) *Pro- and anti-inflammatory cytokines IFN-γ and IL-10 counter-regulate formation of eNOS-based platelet subpopulations via their effects on megakaryocyte/blast eNOS expression, and IFN-γ promotes differentiation of megakaryocytes/blasts lacking eNOS that give rise to more reactive $eNOS^{neg}$ platelets.*

2.3 Objectives of the Study

1) *To determine presence and/or absence of eNOS-signaling pathway within human and mouse platelets.*
2) *To determine biochemical differences between $eNOS^{neg}$ and $eNOS^{pos}$ platelet subpopulations*
3) *To determine the roles of $eNOS^{neg}$ and $eNOS^{pos}$ platelet subpopulations in adhesion and aggregation reactions.*
4) *To determine presence and/or absence of eNOS-signaling pathway within human and mouse megakaryocytes/blasts.*
5) *To determine whether pro-inflammatory cytokine IFN-γ impairs megakaryocyte/blast eNOS expression and promotes formation of $eNOS^{neg}$ megakaryocytes/blasts.*
6) *To determine whether anti-inflammatory cytokine IL-10 counter-regulates IFN-γ inhibitory effect on megakaryocytes/blasts eNOS expression.*
7) *To determine if IFN-γ and IL-10 modulate generation of $eNOS^{neg}$ and $eNOS^{pos}$ platelets from their respective parent $eNOS^{neg}$ and $eNOS^{pos}$ megakaryocytes/blasts.*

3. MATERIALS AND METHODS

3.1 Reagents

Reagents for whole blood and platelet isolation such as trisodium citrate, sodium chloride (NaCl), prostacyclin (PGI_2) and Tyrode's salt solution were obtained from Sigma (St. Louis, MO, USA). Tyrode's buffer is an isotonic solution pH adjusted to 7.4 containing $CaCl_2$, $MgCl_6$, KCl, $NaHCO_3$, NaCl, NaH_2PO_4, and D-glucose. Type I fibrillar collagen for aggregation studies was purchased from Chrono-Log (Havertown, PA, USA).

Primary cardiac-derived human microvascular endothelial cells (HMVEC) were purchased from Lonza (Walkersville, MD, USA). Human umbilical vein endothelial cells (HUVEC) and megakaryoblastic cell line (Meg-01) were purchased from ATCC (Manassas, VA, USA). Cell basal medium EBM-2 supplemented with hydrocortisone and growth factors (EGM-2 MV SingleQuots): human fibroblastic growth factor-b, vascular endothelial growth factor (VEGF), R3-insulin-like growth factor-1, ascorbic acid, human epidermal growth factor, GA-1000 and 5% fetal bovine serum (FBS) required for growth of HMVEC and HUVEC was purchased from Lonza (Walkersville, MD, USA).

RPMI-1640 medium (30-2001) containing 2 mM L-glutamine, 10 mM HEPES, 1 mM sodium pyruvate, 4.5 mg/ml glucose and 1.5 mg/ml sodium bicarbonate required for growth of Meg-01 cells was purchased from ATCC (Manassas, VA, USA). The RPMI-1640 Medium was additionally supplemented with fetal bovine serum (FBS) and antibiotic (penicillin 0.06 mg/ml and streptomycin 0.01 mg/ml) obtained from Sigma (St. Louis, MO, USA). Complete RPMI-1640 medium contained 10% FBS and 1% antibiotic, whereas serum starved medium was defined as medium supplemented with 2% FBS. For detachment of cellular monolayers from tissue culture flasks, sterile Trypsin-Ethylenediaminetetraacetic acid (Trypsin-EDTA) solution was purchased from Sigma-Aldrich (St. Louis, MO, USA). Components of phosphate buffered saline (PBS) such as KCl, NaCl, KH2PO4, Na2HPO4 and dimethylsulfoxide (DMSO) for cryopreservation were purchased from Sigma-Aldrich (St. Louis, MO, USA).

Antibodies and fluorescent dyes used in flow cytometry, confocal microscopy and immunoblot:

- Fluorescent nitric oxide indicator 4-Amino-5-methylamino-2',7'-difluorofluorescein (DAF-FM)-diacetate was obtained from ThermoFisher Scientific (Rockford, IL, USA) and 2-[4,5-Bis[(6-(2-ethoxy-2-oxoethoxy-2-methylquinolin-8-ylamino)methyl]-6hydoxy-3-oxo-3H-xanthen-9-yl] benzoic acid FL2E fluorescent nitric oxide sensor (CuFL2E probe) was obtained from STREM (Newburyport, MA, USA). For flow cytometry, confocal microscopy or immunoblot following antibodies were used:
- Primary mouse monoclonal anti-eNOS antibodies detecting C-(clone M221) and N-(clone 6H2) terminal regions and respective mouse monoclonal IgG isotype control antibodies (IgG1κ; clone 15-6E10A7) were purchased from Abcam (Cambridge, MA, USA) along with primary monoclonal mouse anti-sGC alpha 1 subunit antibodies (IgG1κ; clone GC10), rabbit anti-COX-1 antibodies (IgG1κ; clone EPR5866) and primary polyclonal rabbit anti-PKG (cGKI) (ab90502), rabbit anti-VASP (ab26650), and rabbit anti-iNOS antibodies (ab3523).
- Primary horseradish peroxidase (HRP)-conjugated mouse monoclonal anti-β-actin antibodies (IgG1κ; clone AC15) and secondary HRP-conjugated goat antibodies detecting mouse IgG and HRP-conjugated goat antibodies detecting rabbit IgG were purchased from Sigma-Aldrich (St. Louis, MO, USA).
- Secondary Alexa Fluor 488-conjugated goat antibody $F(ab')_2$ fragments detecting mouse IgG, R-phycoerythrin-conjugated goat $F(ab')_2$ anti-mouse IgG, PerCP-conjugated anti-rabbit IgG, R-phycoerythrin-conjugated anti-rabbit IgG, and rabbit and goat IgG whole molecule (ChromPure) were purchased from Jackson ImmunoResearch Laboratories,Inc. (West Grove, PA, USA).
- The marker for human platelets (detecting GPIbα) frequently used in flow cytometry and confocal microscopy experiments, anti-CD42b-PE antibody (clone HIP1), was obtained from BD Biosciences (Mississauga, ON, Canada) along with respective mouse monoclonal IgG–PE isotype control antibodies (IgG1κ; clone MOPC-21).
- Primary antibody detecting platelet activated GPIIbIIIa - PAC-1 was obtained from BD Biosciences (Mississauga, ON, Canada).
- The marker for mouse platelets and MKs (detecting GPIIb) used in flow cytometry experiments, anti-CD41-PerCP/Cy5.5 antibodies (clone MWReg30), was purchased from BioLegend (San Diego, CA, USA) along with respective rat monoclonal IgG - PerCP/Cy5.5 isotype control antibodies (IgG1κ; clone RTK2071).

- The marker for HMVEC (detecting PECAM-1) used in flow cytometry experiments, anti-CD31 - PerCP/Cyanine 5.5 antibodies (clone WM59) was purchased from BioLegend (San Diego, CA, USA) along with respective mouse monoclonal IgG - PerCP/Cy5.5 isotype control antibodies (IgG1κ; clone MOPC-21).
- Phalloidin (binds F-actin) conjugated to Alexa Fluor 568 used to visualize platelet, HMVEC and Meg-01 cells cytoskeleton was purchased from ThermoFisher Scientific (Rockford, IL, USA).
- Fixable Viability Dye (FVD-green) was purchased from ThermoFisher Scientific (Rockford, IL, USA).

Other reagents used in flow cytometry and confocal microscopy:

- Pierce 16% formaldehyde methanol-free, normal goat serum 5 ml, and antifade mountant reagents: ProLong Diamond and ProLong Gold to cure confocal microscopy samples were obtained from ThermoFisher Scientific (Rockford, IL, USA).
- Fc Receptor Saturating Reagent was obtained from Southern Biotech (Birmingham, AL, USA).
- 1 μm fluorescent yellow-green and 0.5 μm fluorescent orange polystyrene latex beads were obtained from Sigma-Aldrich (St. Louis, MO, USA).
- Size standard 5 μm and 3.8 μm Spherotech beads were obtained from Beckman Coulter (Mississauga, ON, Canada).

ELSA kit to detect cGMP (sensitivity: 3.06 pmol/ml) was purchased from R&D Systems (Minneapolis, MN, USA).

Prior western blot and gelatin zymography total protein concentration within samples was determined by colorimetric DC Protein Assay (reagents: A, B, and S) purchased from Bio-Rad (Hercules, CA, USA). Bovine serum albumin (BSA) purchased from Sigma-Aldrich (St. Louis, MO, USA) was used as a protein standard. All reagents for western blot and gelatin zymography analysis such as, glycerol, sucrose, protease inhibitors, ammonium per sulfate, glycine, sodium dodecyl sulfate (SDS), bromophenol blue, Tris-base, Tris-hydrochloride (HCl), ammonium per sulfate, tetramethylethylenediamine (TEMED), coomassie blue, NaN3, and Tween 20, were supplied by Sigma (St. Louis, MO, USA). 30% acrylamide/Bis solution was purchased from Bio-Rad (Hercules, CA, USA), and 2-mercaptoethanol, b-mercaptoethanol, as well as, Triton X-

100 were purchased from ThermoFisher Scientific (Waltham, MA, USA). Protein molecular weight marker (Precision Plus Protein Dual Color Standards) and 0.45 μm polyvinylidene difluoride (PVDF) transfer membrane was purchased from Bio-Rad (Hercules, CA, USA).

Pharmacological reagents such as 5-azacytydine, L-NAME, L-arginine, SOD, TEMPO, IL-10, IFN-γ were obtained from Sigma-Aldrich (St. Louis, MO, USA).

Prior to RNA isolation bench top and pipettes were cleaned with RNase AWAY Decontamination Reagent ThermoFisher Scientific (Waltham, MA, USA). Cellular RNA was isolated using RNeasy Mini Kit from Qiagen (Redwood City, CA, USA). Genomic DNA was removed from RNA samples by Deoxyribonuclease I Amplification Grade Kit purchased from ThermoFisher Scientific (Waltham, MA, USA) and RT-PCR reactions were performed using Sensiscript RT Kit obtained from Qiagen (Redwood City, CA, USA) supplemented with RNase inhibitor SUPERase-In and Oligo(dT) 18 Primer purchased from ThermoFisher Scientific (Waltham, MA, USA).

3.2 Cell Culture

3.2.1 HUVEC and HMVEC

Human umbilical vein endothelial cells (HUVEC) and primary human cardiac microvascular endothelial cells (HMVEC) were cultured in EBM-2 basal medium supplemented with EGM-2 MV SingleQuots containing necessary growth factors, vitamins and other components required for the cell growth (specified in Section 3.1). Cells were grown in a humidified cell incubator supplied with 5% CO_2 at 37°C. Fresh medium was exchanged every second day, and cells were passaged once approximately 80% confluent. To detach cells from flasks, Trypsin-EDTA was added to the flasks and left for 5 minutes in the cell incubator. Trypsin-EDTA was neutralized with triple volume of EGM-2 MV medium. Collected cells were pelleted by centrifugation (130g for 7 minutes at 18°C) in an Eppendorf 5810R centrifuge (Eppendorf, Hamburg, Germany), and re-suspended in appropriate volume of EGM-2 MV medium or PBS buffer for further experiments. Cells from passages 4-7 were used in experiments.

3.2.2 Meg-01 Cells

The immortalized human megakaryoblastic cell line (Meg-01) was derived in 1983 at the Nagoya University School of Medicine, Nagoya, Japan from bone marrow cells taken from a patient with blast crisis of Philadelphia chromosome-positive chronic myelogenous leukemia [569]. Meg-01 cells are primarily distributed across 3 ploidy classes 2n, 4n and 8n, and the higher ploidy the more mature are the cells [570]. In addition, Meg-01 cells spontaneously release platelet-sized particles that express platelet-specific glycoprotein IIbIIIa (GPIIbIIIa) [506, 571]. Meg-01 cells were cultured in complete RPMI-1640 medium in humidified cell incubator supplied with 5% CO_2 at 37°C, and the medium was changed 2 to 3 times per week (population doubling time 36-48 hours) when cells reached 80% confluence. Under the usual culture conditions, approximately half of the cells extended pseudopodia and adhered to the culture flask. Meg-01 cells were passaged twice a week by decanting non-adherent cells into a sterile centrifuge tube, to detach adherent cells Trypsin-EDTA was added to the flasks and left for 5 minutes in the cell incubator. Trypsin-EDTA was neutralized with triple volume of complete RPMI-1640 medium and the cells were pelleted by centrifugation (130g for 7 minutes at 18°C) in an Eppendorf 5180R centrifuge (Eppendorf, Hamburg, Germany). Subsequently, cells were split for subcultivation (ratio of 1:2 to 1:3) and re-suspended in appropriate volume of the complete RPMI-1640 medium. For experiments cells were re-suspended and cultured in serum-starved RPMI-1640 medium or washed with PBS buffer and collected for further processing. Cells from passages 9-18 were used in experiments.

3.3 Collection of Human Blood and Platelet Isolation

Following informed consent blood was obtained from healthy volunteers (22-35 years of age) who had not taken any drugs known to affect platelet function for 2 weeks prior to the study. Blood was collected via venous puncture of the arm with butterfly needle (21G) attached to 50 ml syringe (to avoid turbulent blood flow such as caused by vacuum collection tubes), and 36 ml of blood was collected into a 50 ml tube, with 4 ml previously prepared trisodium citrate inside (12 μM, 9:1 ratio), and isolated according to the protocol previously established by Radomski and Moncada [572]. Kept on ice 0.06 μg/ml prostacyclin (PGI_2) (stock solution: 1 mg PGI_2 of dissolved in 1M Tris buffer adjusted to pH of 9.0) was added to prevent platelet activation during centrifugation. Whole blood was than centrifuged in an Eppendorf 5810R centrifuge (Eppendorf, Hamburg, Germany) at 250g for 20 minutes (acceleration/brake - 7/0) to separate haematocrit from the platelet rich plasma (PRP). PRP was then transferred into a separate tube, to which 0.3 μg/ml PGI_2 was added, and then centrifuged at 900g for 10 minutes (acceleration/brake - 7/0). The resultant supernatant (platelet poor plasma - PPP) was removed and discarded, and the platelet pellet that formed at the bottom of the tube was washed without resuspension 3x with 1 ml of Tyrode's buffer. The platelets were then re-suspended, and counted using a haemocytometer (Assistant Sondheim, Germany) and diluted with Tyrode's buffer to a final physiological concentration of $2.5x10^8$ platelets/ml. For platelet functional studies isolated platelets were left on a bench top for 1-hour resting period to allow PGI_2 inhibitory effect on platelet function to wear off.

3.4 Animal Care and Use

Approval for the current study was obtained from the University of Alberta Animal Care and Use Committee. Both genders of wild type (WT) C56BL/6 mice and eNOS knockout mice ($eNOS^{-/-}$) were obtained from The Jackson Laboratory (Jax) (Bar Harbor, ME, USA). The eNOS knockout mice ($eNOS^{-/-}$) were created by Dr. Oliver Smithies (University of North Carolina at Chapel Hill) by genetic disruption of the calmodulin binding site of the protein and introducing a premature stop codon into the eNOS gene transcripts [573]. Breeding pairs of eNOS-GFP transgenic mice (C57BL/6) were provided by Dr. Robert Krams (Imperial College, London, UK) and have been described by van Harpen et al [574]. The eNOS-GFP mice express mouse eNOS as well as functional human eNOS gene fused to green fluorescent protein (GFP) which allows for detection/visualization of eNOS-GFP in the cells and tissues that normally express eNOS. The mice were regenerated by initially mating homozygous male eNOS-GFP transgenic with WT female C57BL/6 mice (Jax). WT mice were used as controls and were obtained from nontransgenic littermates.

All mice were housed in an enriched environment maintained on a 12/12 h light–dark cycle at ~23°C with fresh tap water and standard chow available *ad libitum*. Both male and female mice at age of 14-16 weeks (18-28 g) were used for experiments. Mice were anesthetized using isoflurane (1.5-2.0% with oxygen at medical grade with flow set to 500 ml/min) to obtain surgical plane which was assessed by lack of toe pinch reflex on the front and hind limbs. Animals were placed on a 37°C water-heating pad to maintain body temperature. Cardiac puncture procedure was performed to obtain blood samples as described in Section 3.6.1. Next, mice were euthanized by inhalation of isoflurane (5.0% with oxygen flow set to 1000 ml/min) followed by cervical dislocation. Following euthanasia femur and tibia bones were collected to isolate mouse bone marrow, as described in Section 3.6.4, for further experiments. Gastrocnemius muscle tissue from homozygous eNOS-GFP mice was dissected from both hind limbs of each mouse and flash frozen in liquid nitrogen to validate presence of eNOS-GFP fluorescence via confocal microscopy (Section 3.6.7).

All procedures and protocols were approved by the University of Alberta Health Sciences Welfare Committee and were performed in adherence to the guidelines set by the Canadian Council of Animal Care.

3.5 Methods for Studies of Human eNOS-Based Platelet Subpopulations

3.5.1 Confocal Microscopy – Detection of Platelet eNOS

Human platelets

Platelets were fixed for 20 min in 4% formaldehyde in Tyrode's buffer, washed (3x) with Wash Buffer (0.3% BSA in a PBS buffer with 0.05% Tween 20) and cytospinned onto 0.1% poly-lysine-coated coverslips. Next, coverslips with platelets on top were placed in small petri dishes and permeabilized with Tyrode's buffer containing 0.1% Triton X-100 for 10 min at room temperature. Specimens were blocked in a Blocking Buffer (5.0% goat serum in PBS buffer with 0.05% Tween 20) for 2 hours at room temperature. Blocking Buffer was discarded and coverslips were placed in a Wash Buffer for incubation with primary anti-eNOS (clone M221, 1.25 μg/ml) or isotype control IgG1 (1.25 μg/ml) antibodies for 2 hours at room temperature. Following incubation coverslips were washed (3x) with Wash Buffer and incubated with secondary antibodies Alexa Fluor 488-conjugated goat $F(ab')_2$ fragments anti-mouse IgG (15 μg/ml) for 1 hour, and then washed (3x) with Wash Buffer. Subsequently, eNOS-stained coverslips were incubated with anti-CD42b-PE antibody (1:100) or in some experiments Alexa Fluor 568 Phalloidin (1:40) to detect F-actin. Coverslips were washed once again (3x) with Wash Buffer. Preparations were mounted in ProLong Gold antifade solution and analyzed at room temperature on a Leica TCS SP5 microscope with a Leica inverted DMI 6000 B microscope base equipped with a 100x/1.4 NA oil objective (Leica, Wetzlar, Germany). Electronic shutters and image acquisition were under the control of Leica LAF AS software (Leica, Wetzlar, Germany). Fluorescence was excited with the argon ion (488 nm) and helium-neon (543 nm) lasers. Finally, images were equally adjusted for contrast and brightness.

HMVEC (positive control)

HMVEC (seeding density: 5,000 cells/cm²) were cultured as described in Section 3.2.1 for 3 days on sterile glass coverslips in 6-well tissue culture plates. Subsequently, coverslips with cells were placed in small petri dishes and fixed with 4% paraformaldehyde in Tyrode's buffer for 20 minutes. Paraformaldehyde was discarded and coverslips were washed (3x) with Wash Buffer (PBS buffer, 0.3% BSA and 0.05% Tween 20) for 5 minutes with gentle agitation. Cells were permeabilized (to aid intracellular staining) with 0.1% Triton X-100 for 10 minutes at room temperature and washed (3x) with Wash Buffer for 5 minutes with gentle agitation. Next,

coverslips were blocked in a Blocking Buffer (5% goat serum in PBS buffer and 0.05% Tween 20) for 2 hours at room temperature. Blocking Buffer was discarded and inverted coverslips were placed onto a parafilm with 500 µl droplet of Wash Buffer with either mouse monoclonal eNOS M221 clone (1.25 µg/ml), eNOS 6H2 clone (5 µg/ml) or respective (1.25 µg/ml and 5 µg/ml) mouse monoclonal IgG isotype control antibodies. Coverslips were incubated with primary antibodies for 1 hour at room temperature and washed (3x) for 5 minutes with Wash Buffer with gentle agitation. Secondary antibodies Alexa Fluor 488-conjugated goat $F(ab')_2$ fragments detecting mouse IgG (15 µg/ml) were added to Wash Bufferr and pipetted to form a 500 µl droplet on a parafilm, inverted coverslip was placed on top of the droplet and incubated for 1 hour in the dark at room temperature. Next, coverslips were washed (3x) with Wash Buffer for 5 minutes with gentle agitation. Next, Alexa Fluor 568 Phalloidin (1:40) was added to Wash Buffer and pipetted onto a parafilm to create a droplet. Inverted coverslip was placed on top of the droplet and incubated for 30 minutes in the dark at room temperature. Coverslips were washed (3x) with Wash Buffer and mounted onto microscope slides with transparent nail polish. Preparations were mounted in 5 µl of ProLong Diamond antifade solution and slides were left for 24 hours at 4°C (protected from light with foil). Next microscope slides with coverslips on top were sealed with nail polish and imaged when dry. An Olympus IX-81 (Olympus America Inc., Melville, NY, U.S.A.) microscope base with Yokagawa CSU10 (Yokogawa Electric Corporation, Tokyo, Japan) spinning disk confocal scan-head equipped with digital camera Hamamatsu EMCCD (C9100-13) (Hamamatsu, Photonics K.K., Hamamatsu City, Japan) was used to image HMVEC. Images were captured using magnification of 600x (60x/1.42 NA oil objective) and lasers used were for Alexa 488 – 491nm laser and for Alexa 568 – 561nm laser. Images were acquired using Perkin Elmer Volocity software (Perkin Elmer Inc., Waltham, MA, USA).

3.5.2 Western Blot – Detection of Platelet eNOS

Protein assay

The standard curve was prepared using the BSA standard. The stock solution of BSA (2.0 mg/ml) was serially diluted in double distilled water (ddH_2O) to create a standard curve. In brief, 3 ml of working reagents A' was prepared by adding 60 µl of reagent S into 3 ml of reagent A. The assay was set up in 96 well plate in duplicates and 5 µl of test sample or 5 µl of standard curve sample, 25 µl of reagent A', and 200 µl of reagent B. The 96 well plate was left in the dark for 15 minutes and then absorbance was read. The protein concentration in each sample was calculated based on BSA standard curve values.

Sample preparation

Immediately after platelet isolation as descriebd in Section 3.3, 1 ml of platelet suspension ($2.5x10^8$ platelets/ml) was transferred to an eppendorf and centrifuged at 900g for 10 minutes. Supernatant was discarded and platelet pellet was resuspended in homogenizing buffer (RIPA buffer, 10% protease inhibitors, 1.0% SDS and 1 µM cyclodextrin). Next, lysed platelets were sonicated three times for 5 seconds with Misonix Ultrasonic Liquid Processor (Misonix Inc., Farmingdale, NY, USA) at 30% output and centrifuged at 8 000g for 3 minutes at room temperature. The resultant supernatant was then assayed for protein content as described above. Immunoblot analysis was performed under reducing/denaturing conditions. Briefly, 100 µg protein aliquots were denatured by boiling (5 minutes) and 5 µl of loading buffer (containing reducing agent – 8% SDS, denaturing agent – 16% β-mercaptoethanol, glycerol, 4x Tris-HCl/SDS pH 6.8, ddH_2O, bromophenol blue) was added to make a final sample volume of 25 µl. Primary HMVEC cells from one T25 flask (grown and collected as described in Section 3.2.1) were used as a positive control. HMVEC pellet was processed for western blot in the same manner as platelet samples.

Electrophoresis and transfer

Platelet samples (100 µg of total protein) were loaded in wells of 8% dodecyl sulfate–polyacrylamide electrophoresis (SDS–PAGE) gel. As a molecular weight reference, 15 µl of Precision Plus Protein Ladder was loaded adjacent to the samples. Gel electrophoresis was performed using a Bio-Rad Powerpac HC system set at 150 volts. After run (~1 hour 15 minutes), protein was transferred from the gel on to a 0.45µm PVDF membrane using a semi-dry

method Trans-Blot SD (Biorad, Hercules, CA, USA) at 25 volts for 30 minutes at room temperature.

Detection

After protein transfer, PVDF membranes were cut at the 75kDa molecular weight marks. The top membrane (>75kDa) was blocked in 5% skim milk in Tris-buffered saline with 0.1% Tween 20 (TTBS) for one hour at room temperature followed by overnight incubation at 4°C with anti-eNOS M221 and anti-eNOS 6H2 (1:1000 each). After incubation with primary antibodies each membrane was washed four times for 5 minutes in TTBS, and then probed for one hour at room temperature with anti-mouse IgG conjugated to horseradish peroxidase (1:2000). The lower membrane (<75kDa) was blocked in 5% skim milk in TTBS at 4°C overnight, followed by a 30-minute incubation with a monoclonal β-actin antibody conjugated to horse radish peroxidase (1:40 000 dilution). This was followed by a final four washes with TTBS for all membranes, and developed using an ECL kit. Chemiluminescence was detected using an enhanced chemiluminescence (ECL) prime western blotting detection reagent (GE Healthcare, Chicago, IL, USA), and imaged using a VersaDoc Imaging System (Bio-Rad, Hercules, CA, USA). Band densitometry was measured using Quantity One software. The eNOS band densitometry (133kDa) was normalized to the respective β-actin (42kDa) bands. Data was then normalized and expressed as % of HMVEC control.

3.5.3 Flow Cytometry – General eNOS Staining Protocol

Cells (platelets, Meg-01 cells or HMVEC) were fixed in 4% paraformaldehyde in Tyrode's buffer for 20 minutes at room temperature and centrifuged at 900g for 10 minutes to pellet cells. Paraformaldehyde solution was removed and discarded, and cells were washed (3x) and resuspended in a Wash Buffer (0.3% BSA in a PBS buffer with 0.05% Tween 20). Samples were then permeabilized (to aid intracellular staining) using 0.1% Triton X-100 in PBS buffer for 10 minutes at room temperature on a sample rotator, and centrifuged at 900g for 10 minutes to pellet cells. Triton X-100 solution was discarded, cells were washed (3x), centrifuged (900g for 10 minutes) and resuspended in Wash Buffer. Next, samples were blocked with Blocking Buffer (5.0% goat serum in PBS buffer with 0.05% Tween 20) (to prevent non-specific antibody binding) for 2 hours at room temperature on a sample rotator. After incubation time samples were centrifuged at 900g for 10 minutes, Blocking Buffer was discarded and cells were resuspended in a Wash Buffer. To identify $eNOS^{pos}$ and $eNOS^{neg}$ subpopulations two-color intracellular flow cytometry was performed. Platelet samples were incubated with primary antibodies: mouse anti-eNOS clone M221 or concentration-matched isotype control IgG1 (1.25 μg/ml) for 1 hour at room temperature on a sample rotator. In some control experiments the mouse anti-eNOS clone 6H2 (5 μg/ml) was utilized. The samples were washed with Wash Buffer (3x) and incubated with secondary antibodies Alexa Fluor 488-conjugated goat $F(ab')_2$ fragments anti-mouse IgG (15 μg/ml) for 1 hour in the dark at room temperature on a sample rotator. Finally, cells were washed (3x) and resuspended in a PBS buffer.

Extra step only for platelet eNOS staining

Anti-CD42b-PE antibody (1:100) was added to the sample and incubated for 15 minutes on sample rotator and then diluted to a final volume of 1 ml with PBS buffer before flow cytometry analysis.

Extra step only for HMVEC eNOS staining

Anti-CD31-PerCP/Cyanine 5.5 (1:500) was added to the sample and incubated for 15 minutes on a sample rotator and then diluted to a final volume of 1 ml with PBS buffer before flow cytometry analysis.

Flow cytometry was carried out with a Quanta SC flow cytometer (Beckman Coulter, Mississauga, ON, Canada). FSD (fluorescence surface density) and FC measurements were made and 10 000 platelet-specific events were analysed for each experiment. Unlike a traditional flow

cytometer, which determines size based on forward light scatter (FS), the Quanta SC which we utilize uses the 'Coulter principle' (measures change in electrical resistance produced by cells suspended in electrolyte) to determine event volume. Quanta SC software then calculates an event's fluorescence concentration or fluorescence surface density based on event volume. Compensation was performed using Cell Lab Quanta analysis software to account for spectral overlap.

3.5.4 Flow Cytometry – Detection of Platelet sGC-PKG-VASP Pathway and COX-1

To investigate the sGC-PKG-VASP pathway and COX-1 levels in eNOS^{pos} and eNOS^{neg} platelet subpopulations three-color flow cytometry was performed. Intracellular staining for platelet eNOS was carried out as described in Section 3.5.3. Subsequently, for sGC, PKG, VASP or COX-1 determination, eNOS-stained platelets were then incubated with either of primary antibodies (anti-sGC 10 μg/ml, anti-PKGI 10 μg/ml, anti-VASP 2 μg/ml or anti-COX-1 1.5 μg/ml) or corresponding concentration-matched isotype/IgG controls overnight at 4 °C. Next, the platelets were washed with PBS buffer (3x). Following, samples were incubated in the dark with PE-conjugated or PerCP-conjugated secondary antibodies (1:100) for the detection of sGC, VASP, or PKG, respectively. Platelets were then washed with PBS and incubated with anti-CD42b-PE antibody (for PKG samples) or anti-CD41a-PE-Cy7 (for sGC, VASP and COX-1 samples) for 15 minutes and then diluted to a final volume of 1 ml with PBS before analysis by flow cytometry. Flow cytometry was carried out with a Quanta SC flow cytometer. FSD and FC measurements were made and 10,000 platelet-specific events were analyzed for each experiment. Compensation was performed using Cell Lab Quanta analysis software to account for spectral overlap.

3.5.5 Flow Cytometry – Measurement of Activated Integrin $\alpha_{IIb}\beta_3$

In order to investigate the integrin $\alpha_{IIb}\beta_3$ activation by $eNOS^{pos}$ and $eNOS^{neg}$ platelet subpopulations, platelets were stimulated with collagen (3 μg/ml) and aggregation was allowed to proceed to 50% light transmittance. At this point platelet samples were fixed, permeabilized, and incubated with anti-eNOS (M221 clone) antibodies (1.25 μg/ml) and secondary antibodies Alexa Fluor 488-conjugated goat $F(ab')_2$ fragments anti-mouse IgG (15 μg/ml) as described in Section 3.5.3. Subsequently, samples were incubated with primary PAC-1 antibody (2.5 μg/ml) for 15 minutes and washed (3x) with PBS buffer and incubated with secondary PE-Cy7 conjugated anti-mouse IgM antibody (2 μg/ml) (clone R6-60.2) for 15 minutes in the dark. Next, the platelet samples were washed (3x) with PBS buffer and then diluted to a final volume of 1 ml before analysis by a Quanta SC MPL flow cytometer. 100,000 platelet-specific events were analyzed.

3.5.6 Flow Cytometry and Fluorescence Microscopy –DAF-FM Diacetate Staining – Detection of Platelet NO Production

DAF-FM diacetate (4-amino-5-methylamino-2'-7'-difluorofluorescein diacetate) is a fluorescent dye often used to detect/quantify low concentrations of NO. The dye is very weakly fluorescent, until it reacts with NO to form a benzotriazole with an almost 160 fold increase in fluorescence. Fluorescence excitation and emission maxima are 495 and 515 nm, respectively [575]. A 5 mM stock solution of DAF-FM diacetate (1 mg packaging) was made by dissolving in 400 μl of high quality anhydrous DMSO.

Isolation of PGI_2-washed human platelets described above in Section 3.3 was performed as usual until obtaining PRP and then DAF-FM diacetate (10 μM) was added to the PRP, and incubated for 30 minutes at 37°C in the dark. Subsequently, DAF-FM-loaded platelets were prepared according to platelet isolation protocol that follows after obtaining PRP (Section 3.3). Briefly, 0.3 μg/ml PGI_2 was added and DAF-FM-stained PRP was centrifuged at 900g for 10 minutes, PPP was removed and the platelet pellet was gently washed (3x) with 1 ml of Tyrode's buffer. Platelet suspension was adjusted with Tyrode's buffer to the final physiological concentration of $2.5x10^8$ platelets/ml. Isolated DAF-FM-stained platelets were left in the dark at room temperature for 1-hour resting period in which the PGI_2 inhibitory effect on platelets was allowed to wear off. Next, DAF-FM-stained resting platelets were preincubated with L-arginine (100 μM) for 15 minutes and NO production was visualized by brightfield fluorescence microscopy or detected via flow cytometry. For flow cytometry analysis 20,000 events per sample were collected and platelet NO-production was measured as DAF-FM fluorescence concentration in FL1 channel set to log scale. During analysis we identified two distinct overlapping fluorescence peaks within DAF-FM histogram corresponding to low/non NO-producing and NO-producing subpopulations of platelets. Gate for low/non NO-producing subpopulation was set based on platelet unstained control sample.

Brightfield fluorescence microscopy images were captured using total magnification of 630x (63x/1.4 NA oil objective) on the Widefield Leica inverted DMI6000 (Leica Microsystems, Concord, ON, Canada) equipped in argon ion laser (488 nm).

3.5.7 Flow Cytometry – Evaluation of DAF-FM Sensitivity – Detecting Changes of NO Production by Stimulated HMVEC

To determine if DAF-FM may detect changes in NO production by maximally stimulated ECs, HMVEC were cultured under standard conditions in EGM-2 MV medium as described in Section 3.2.1. Flasks with adherent HMVEC cells were washed (2x) with 2 ml of PBS buffer. Next, cells were incubated (37°C) with 5 ml of PBS buffer for a brief (30 minutes) serum starvation. Next, DAF-FM diacetate (5 μM) was added to the cells and incubated for another 20 minutes in the dark. Residual DAF-FM diacetate that did not diffuse into the cells was washed out (2x) with 2 ml of PBS buffer. Subsequently Tyrode's buffer (2 ml) was added to each flask along with L-arginine (100 μM) and either L-NAME (100 μM) or $VEGF_{165}$ (10 ng/ml) (R&D Systems). Flasks were placed in an incubator (37°C) for 10 minutes. To detach cells, Trypsin-EDTA was added to the flasks and left for 5 minutes in the cell incubator (37°C). Trypsin-EDTA was neutralized with triple volume of EGM-2 MV medium. Collected cells were pelleted by centrifugation (130g for 7 minutes at 18°C), washed (1x) with cold PBS buffer and resuspended in Tyrode's buffer to measure NO production by flow cytometry. 10,000 events were analyzed.

3.5.8 Light Transmission Aggregometry

Platelet activation and aggregation was measured by Chrono-log Dual Channel Lumi-Aggregator (Model 560, Chrono-Log, Harveston, PA, USA). Optical aggregometer is a fixed wavelength spectrophotometer with a sample chambers designed so that a beam of infra-red light shines through two cuvettes, one test cuvette (containing the sample) and one blank cuvette (the reference). In this assay, platelets suspended in Tyrode's buffer are aliquoted into a transparent test cuvette containing a magnetic stir bar. Homogenously dispersed platelet suspension, which is turbid, is stirred in a test cuvette maintained at 37°C. Platelet suspension is arbitrarily considered to be 0% light transmission or 0% aggregation and blank cuvette (filled with Tyrode's buffer) is considered to be 100% light transmission or 100% aggregation. The difference in light transmission outputs from the photodiodes is transferred to recording instrument. When the agonist is added, the platelets will form increasingly larger aggregates and the platelet suspension will begin to clear, allowing more light to pass through the test cuvette. This increase in light transmittance is directly proportional to the amount of aggregation over the specified time and digitized into a computer using Aggro-Link software (Chrono-Log, Harveston, PA, USA).

3.5.9 Light Transmission Aggregometry – Pharmacological Characterization of Platelet-Derived NO

In experiments with pharmacological characterization of platelet-derived NO we utilized PGI_2-washed human platelets ($2.5x10^8$ platelets/ml) (prepared as described in Section 3.3). Pharmacological agents such as the NOS inhibitor (L-NAME 100 μM), NOS enzyme substrate for NO production (L-arginine 100 μM) or vehicle control (Tyrode's buffer) were added to transparent cuvettes with platelet aliquots (0.5-1 ml) at time 0 of the experiment. Next, cuvettes were placed in the aggregometer chamber (37°C) with the magnetic stir bar rotating at 900 revolutions per minute (rpm). Platelet aggregation was initiated with addition of collagen (3 μg/ml) following 2-minute equilibration period and the reaction was monitored by Aggro-Link software for further 3-4 minutes. Platelet aggregation was reported as percent maximal aggregation.

3.5.10 Light Transmission Aggregometry Followed by Flow Cytometry – Pharmacological Evaluation of DAF-FM Specificity for NO

In experiments testing DAF-FM diacetate specificity for NO, aliquots of DAF-FM-stained platelet (staining protocol described in Section 3.5.6) were pipetted into transparent cuvettes and pre-incubated with L-arginine (100 μM) and either L-NAME (100 μM), SOD (100 U/mL) or TEMPOL (100 μM) for 2 minutes in aggregometer chamber (37°C). Platelet aggregation was initiated by collagen (5 μg/ml) and monitored by Aggro-Link software for another 3-4 minutes. Following aggregation, DAF-FM-stained platelet samples were incubated with anti-CD42b-PE antibody (1:100) for 10 minutes in the dark and then diluted to a final volume of 1 ml with saline before analysis with a Beckman Coulter Quanta SC flow cytometer with Cell Lab Quanta analysis software. During flow cytometry data acquisition 10,000 platelet-specific events were collected and analysis was performed following compensation to account for fluorophore spectral overlap.

3.5.11 Light Transmission Aggregometry Followed by Flow Cytometry – Detection of Platelet NO Production by CuFL2E Fluorescent Probe

The ability of human platelets to generate NO was also evaluated using non-DAF-FM copper-based NO specific fluorescent probe 2-[4,5-bis[(6-(2-ethoxy-2-oxoethoxy-2-methylquinolin-8-ylamino)methyl]-6hydoxy-3-oxo-3H-xanthen-9-yl] benzoic acid FL2A (CuFL2E). The platelet CuFL2E (20 μM) staining was carried out as described above for DAF-FM-stained platelets (Section 3.5.6). CuFL2E-stained platelets were then pre-incubated with L-arginine (100 μM) and L-NAME (100 μM) or SOD (100U/ml) for 2 minutes at 37°C in the aggregometer. Platelet aggregation was initiated by collagen (5 μg/ml) and monitored by Aggro-Link software for a further 4 minutes. Following aggregation, CuFL2E-stained platelet samples (10 μl) were diluted to a final volume of 1 ml with saline before analysis on a Becton Dickinson Aria III BSL-2FACSor Beckman Coulter Quanta SC flow cytometer. During flow cytometry data acquisition 10,000 events were collected and analyzed where the mean fluorescence of CuFL2E (FL1 channel) was determined. The results were expressed as CuFL2E mean fluorescence following subtraction of the mean autofluorescence of unstained platelet samples.

3.5.12 Platelet Fluorescence Activated Cell Sorting (FACS)

In order to separate NO-producing from non-NO-producing platelets fluorescence activated cell sorting (FACS) was performed on platelets isolated according to protocol described in Section 3.3 and stained with DAF-FM diacetate as described in Section 3.5.6. DAF-FM-stained platelets were resuspended at $1.5x10^7$/ml in Tyrode's buffer with L-arginine (100 μM). FACS was performed on a Becton Dickinson Aria III BSL-2 sorter (Franklin Lakes, NJ, United States) using 100 micron nozzle and 1.0 FSC ND filter. DAF-FM fluorescence was excited with the 488 nm laser and detected on FL1 channel set to log scale. To discriminate between NO-producing and non-NO-producing platelets, sorting regions were established to encompass the top and bottom 20% fluorescence of DAF-FM-stained platelets, respectively. Platelet sorting was carried out at a rate of 10 000 - 15 000 events/second for 3 – 3.5 hours typically resulting in yields of approximately $3.0x10^7$ of each NO-producing and non-NO-producing platelets in 70 – 100 ml of PBS buffer.

For further experimentation, platelets were isolated by the addition of PBS buffer with 3% BSA at a ratio of 1:9 of sorted platelets in PBS buffer. Subsequently, PGI_2 (0.067 μg/ml) was added to the sorted platelets to prevent platelet activation, and the platelets were centrifuged at 900g for 20 minutes at room temperature. Following centrifugation, the buffer was removed and the pelleted platelets were resuspended in 1 ml of fresh PBS buffer with 0.3% BSA and centrifuged for a further 10 minutes at 900 g. The resulting platelets were resuspended in 30 μl of Tyrode's buffer, counted, and further diluted to a concentration of $2.5x10^8$/ml typically yielding 40 – 50 μl of both NO-producing and non-NO-producing platelets at this concentration. Platelets were subsequently either fixed in 4% paraformaldehyde in Tyrode's buffer for eNOS intracellular flow cytometry or in other experiments allowed to rest for a further 30 minutes before platelet aggregometry.

3.5.13 Aggregometry and Microscopic Evaluation of Aggregates Formed by DAF-FM^{neg} and DAF-FM^{pos} Platelets Obtained via FACS

DAF-FM-negative and DAF-FM-positive FACS-sorted platelets (30 µl of $2.5x10^8$ platelets/ml) (protocol of platelet FACS sorting is described in Section 3.5.12) were incubated at 37°C with stirring (900 rpm) for 2 minutes in an aggregometer. Collagen (1 µg/ml) was added and aggregation allowed to proceed for a further 4 minutes. Subsequently, aggregated platelets were fixed (5 minutes) with 4% paraformaldehyde in Tyrode's buffer. Samples (10 µl) were mounted onto microscope slide and imaged using an Olympus CKX41 phase-contrast microscope (Olympus America Inc., Melville, NY) equipped with an Infinity 1 digital camera. Photomicrographs were captured at the top, bottom, right, left, and center of each slide. The platelet aggregate areas in each field of view were measured using ImageJ software, and the results were expressed as the mean platelet aggregate area.

3.5.14 ELISA – Measurement of cGMP Synthesis by DAF-FM^{neg} and DAF-FM^{pos} Platelet Samples Obtained via FACS

A cGMP ELISA kit was obtained R&D Systems. FACS-sorted DAF-FM-negative and DAF-FM-positive platelets (100 µl) (protocol of platelet FACS sorting is described in Section 3.5.12) were incubated in an aggregometer at 37^{o}C under stirring conditions (900 rpm) in the presence of L-arginine (100 µM) and sildenafil (10 µM) and stimulated with collagen (10 µg/ml) for 10 minutes. Subsequently, platelets were separated from their releasates by centrifugation (1000g for 10 minutes) and the releasates were stored at -80°C before further analysis. Subsequently, platelets were lysed in 100 µl of Cell Lysis Buffer (provided by manufacturer) and the cGMP ELISA was carried out according to manufacturer's instructions. Data was normalized and expressed as % of DAF-FM-positive FACS-sorted platelets.

3.5.15 Mass Spectrometry – Detection of DAF-FM Metabolite Following Reaction with NO

Human PGI_2-washed platelets (protocol in Section 3.3) were isolated and stained with DAF-FM diacetate as described in Section 3.5.6. Subsequently platelet sample was incubated with L-arginine (100 μM) at 37^{o}C for 6 minutes. Platelet aliquots (200 μl) were transferred to 2 ml tubes with 0.1 M acetic acid solution (15 μl), stirred for 3 seconds, and then ethyl acetate (1000 μl) was added. The samples were stirred for 15 seconds and then frozen by keeping the mixture in a dry ice bath for 5 minutes. The samples were then centrifuged (14,000 rpm) at 4^{o}C for 10 minutes to separate the organic layer from which an 800 μl aliquot of the solvent was taken and transferred to glass vial to evaporate the solvent under vacuum (rotavapor) and a nitrogen atmosphere. The residues were reconstituted by adding 200 μl of acetonitrile. Aliquots of the solution were injected into the mass spectrometer for analysis by electrospray ionization (EI). The spectrometric analyses were carried out using a Waters Micro Mass ZQ-4000 single quadruple mass spectrometer (ESI-MS), recording the corresponding fragmentation patterns in both positive (EI+) and negative (EI-) ionization modes. The DAF-FM signal ($C_{21}H_{14}F_2N_2O_5$; *m/z* =413.1) was detected in positive ionization mode [ES+], and the final metabolic product benzotriazole derivate ($C_{21}H_{10}F_2N_3O_5$) was detected as the corresponding triple anion of form (*m/z*= 421.1**)** in negative ionization mode [ES-].

3.5.16 Mass Spectrometry – Measurement of Platelet TXA_2 Stable Metabolite – TXB_2

FACS-sorted DAF-FM-negative and DAF-FM-positive platelets (100 µl) (protocol of platelet FACS sorting is described in Section 3.5.12) were preincubated in an aggregometer at 37°C under stirring conditions (900 rpm) in the presence of L-arginine (100 µM). Next, platelet samples were stimulated with collagen (10 µg/ml) and allowed to aggregate for 4 minutes. Subsequently, platelets were separated from their releasates by centrifugation (1000g for 10 minutes) and the releasates were stored at -80^{o}C for further LC-ESI-MS analysis. The stable metabolite of TXA_2, TXB_2, was analyzed in 50 µl of platelet releasate using LC-ESI-MS (Waters Micromass ZQ 4000 spectrometer). An equivolume (50 µl) of absolute ethanol containing 0.5 µg/ml of TXB_2-D4, as the internal standard, and 50 µg/ml of butylated hydroxytoluene was added to each sample; thereafter, the samples were evaporated to dryness and reconstituted with 25 µl acetonitrile. The mass spectrometer was run in negative ionization mode with single ion monitoring: m/z= 369 for TXB_2 and m/z = 373 for TXB_2-D4. The nebulizer gas was acquired from an in house high purity nitrogen source. The temperature of the source was set at 150°C, and the capillary and cone voltage were 3.51 kV and 25 V, respectively. An isocratic separation was performed on a reverse phase C18 column (Alltima HP, 150 × 2.1 mm) at 35°C using acetonitrile/water/acetic acid (40/60/0.01, v/v/v) as mobile phase. The concentrations were calculated based on peak area and the linear ranges of the calibration curve were from 0.001 µg/ml to 10 µg/ml. The results were subsequently normalized to platelet count and expressed as ng of $TXB_2/10^8$ platelets.

3.5.17 Aggregometry Followed by Gelatin Zymography – Detection of Platelet Pro-MMP-2

Gelatin zymography, which is 1000x more sensitive than immunoblot was used to measure platelet secreted pro-MMP-2 [576]. Gelatin zymography was performed on platelet releasates obtained during aggregometry of collagen-(3 μg/ml)-stimulated platelets. Platelet releasates were obtained at 1 minute prior to the addition of collagen, at shape change, at 50% and maximal light transmittance as measured by an aggregometer with Aggro-Link software as described above in Section 3.5.8. Next, platelet samples were centrifuged (1000 g for 10 minutes) and the releasates were collected and stored at -80^{o}C until further analysis. Subsequently, gelatin zymography was performed as described previously [577]. Briefly, zymography was performed using 8% SDS–PAGE electrophoresis with copolymerized gelatin (2 mg/ml). After electrophoresis, gels were washed (3x) for 20 minutes in 2% Triton X-100. Next, gels were washed (2x) for 20 min in developing buffer (50 mM Tris– HCl pH 7.6, 150 mM NaCl, 5 mM CaCl2, and 0.05% NaN3) and then incubated in developing buffer at 37^{o}C overnight to allow for enzyme activity to degrade gelatin substrate. Next, to image the degraded portions of gelatin, the gels were stained with 0.05% Coomassie Brilliant Blue and then destained in a 4% ethanol and 8% acetic acid solution. Gels were imaged using a VersaDoc Imaging System (Bio-Rad, Hercules, CA, USA) and Quantity One software was used to analyze densitometry of degraded bands of gelatin. Gelatinolytic activity was detected as transparent bands against a blue background of Coomassie-stained gelatin. Pro-MMP-2 (72kDa) activity was identified by comparison with standards from conditioned medium of HT-1080 human fibrosarcoma cells (pro-MMP-2) and recombinant human MMP-2 [578].

3.5.18 Gelatin Zymography – Detection of Pro-MMP-2 Levels in DAF-FM^{neg} and DAF-FM^{pos} Platelet Samples Obtained via FACS

Gelatin zymography was performed on *DAF-FM^{neg} and DAF-FM^{pos}* platelets separated by FACS as described in Section 3.5.12. During aggregometry (method principle described in Section 3.5.8) *DAF-FM^{neg}* and *DAF-FM^{pos}* platelets were stimulated with collagen (1 µg/ml) and allowed to aggregate for 4 minutes. Following centrifugation to obtain platelet pellets subsequent sample preparation was performed on ice. Next, pellets were lysed with SDS-free homogenizing buffer (50 mM Tris HCL/base, 3.1 mM sucrose and 10% protease inhibitors). Homogenized lysates were sonicated for five seconds with Misonix Ultrasonic Liquid Processor (Misonix Inc., Farmingdale, NY, USA), left to rest for 20 seconds on ice (to avoid overheating and thus preserve activity of MMP-2) and sonicated for another five seconds. Loading buffer (without denaturing agents – β-mercaptoethanol) (5 µl) was added to each sample to make a final sample volume of 25 µl. The entire sample volume was loaded onto 8% SDS–PAGE electrophoresis with copolymerized gelatin (2 mg/ml). Precision Plus Protein Ladder was loaded as a molecular weight reference (15 µl) adjacent to samples. Gel electrophoresis was performed using Bio-Rad PowerPac HC (Bio-Rad, Hercules, CA, USA) at 150 volts on ice.

According to previously described protocol, after run completion the gel was cut at the 50kDa mark, using the molecular weight marker as a reference [578]. The portion >50kDa was washed three times for 20 minutes in 2% Triton-X-100 (Thermofisher Scientific, Rockford, IL, USA) followed by two 20 minute washes in zymography buffer (2M Tris-HCl, NaCl, $CaCl_2 \times 2H_2O$, NaN_3). The gel was incubated in fresh zymography buffer at 37°C overnight to allow for enzyme activity to degrade gelatin substrate. To image degraded portions of gelatin, the gel was stained with Coomassie Blue for two hours followed by de-staining using 4% methanol + 8% acetic acid solution. Gels were imaged using a VersaDoc Imaging System (Bio-rad, Hercules, CA, USA), and QuantityOne software was used to analyze densitometry of degraded bands of gelatin.

The gel section <50kDa mark was transferred on to a 0.45 µm thick polyvinylidine difluoride (PVDF) (Bio-Rad, Hercules, CA, USA) membrane using a semi-dry transfer method (Trans-Blot SD, 25 volts, 30 minutes). After transfer, the PVDF membrane was blocked overnight in 5% skim milk in Tris-buffered saline with 0.1% Tween 20 (TTBS), and then probed with a monoclonal β-actin antibody conjugated with horseradish peroxidase (1:40 000) for 30

minutes followed by four wash cycles in TTBS. Chemiluminescence was detected using an enhanced chemiluminescence (ECL) prime western blotting detection reagent (GE Healthcare, Chicago, IL, USA), and imaged using a VersaDoc Imaging System. Band densitometry was analyzed using Quantity One software. Band densitometry from the upper portion gel (zymogram >50kDa) was normalized to the respective β-actin bands from the lower portion of gel (<50kDa). Data was then normalized and expressed as % of DAF-FM^{neg} platelets.

3.5.19 Video Confocal Microscopy to Study Platelet Adhesion and Aggregation Reactions

In order to assess adhesion by NO-producing and low/non-NO-producing platelets confocal microscopy was performed. DAF-FM loaded platelets ($1.5x10^8$ platelets/ml) (staining protocol – Section 3.5.6) pre-incubated with L-arginine (100 μM) were added to collagen-coated (type I fibrillar collagen – 10 μg/ml) coverslips in a Chamlide TC-A Live Cell Chamber mounted on a Wave FX Olympus IX-81 microscope. The chamber was incubated at 37°C and fluorescent yellow-green beads (1:1,000,000) were added to the cover slips to aid in focusing prior to addition of platelets. Images were captured every 10 seconds with a Hamamatsu EMCCD (C9100-13) camera for approximately 15 minutes. Platelets with peak fluorescence above 1000 units were classified as NO-producers, while platelets with peak fluorescence below 1000 units were classified as low/non-NO producers.

In addition, platelets were allowed to aggregate for a further 45 minutes, post adhesion experiment coverslips containing collagen adhered and aggregated platelets were fixed for 20 minutes in 4% paraformaldehyde in Tyrode's buffer to examine the 3-dimensional aggregate architecture. Coverslips were then permeabilized with 0.1% Triton X-100, washed, blocked and incubated with anti-eNOS antibodies according to protocol in Section 3.5.1. All steps up to this point were carried out in room light to bleach residual DAF-FM fluorescence. Subsequently, coverslips were incubated in the dark with Alexa Fluor 488-conjugated goat $F(ab')_2$ fragments detecting mouse IgG (15 μg/ml) as described above along with Alexa Fluor 568 Phalloidin (1:40) to image F-actin. Z-stack images were captured every 0.3 μm on a Leica TCS SP5 microscope. Fluorescence was excited with argon ion (488 nm) and helium-neon (543 nm) lasers.

3.5.20 Platelet Flow Chamber Assay

In order to assess the functional role of eNOS^{neg} and eNOS^{pos} platelets under flow conditions experiments were carried out with the Spinning Disc Confocal Microscope WaveFX (Olympus IX-81 motorized microscope base) equipped with a BIOPTECHS FCS2 flow chamber assembly and pump. Flow chamber coverslips were incubated 10 µg/ml type I fibrillar collagen and 10 µl of diluted 1 µm fluorescent yellow-green beads (1:1,000,000) was added to aid in focusing. The experiment was performed at 37^{o}C and DAF-FM-loaded human platelets (1.5x10^{8} platelets/ml) in Tyrode's were pumped through the chamber at a flow rate of 50 µl/min for 10 min. Images were captured every 10 seconds with a Hamamatsu EMCCD (C9100-13) camera and non-adhered platelets which passed through the flow chamber were collected for further analysis of eNOS$^{neg/pos}$ subtype by intracellular flow cytometry.

3.6 Methods for Studies of Mouse eNOS-Based Platelet and Megakaryocyte Subpopulations

3.6.1 Collection of Mouse Blood and Isolation of Platelet Rich Plasma (PRP)

The mouse was placed under terminal anesthesia by inhalation of isoflurane (2.0% with oxygen at medical grade with flow set to 500 ml/min) to obtain surgical plane, which was assessed by lack of toe pinch reflex on the front and hind limbs. The blood sample was collected via cardiac puncture into 3 ml syringe with a needle (25G). Approximately 0.5-1.0 ml of blood was obtained per one mouse. Blood collected into a syringe was immediately transferred to an eppendorf with 3.15% trisodium citrate (1:9), and then PGI_2 (1.0 μg/ml) was added to prevent platelet spontaneous activation during centrifugation. Mouse blood samples were centrifuged at 300*g* for 5 minutes at room temperature. This resulted in pelleting larger cellular elements such as red blood cells and leukocytes. The upper layer of platelet-rich plasma (PRP) was collected (~250-500 μl per mouse) and transferred to clean eppendorf for further experiment. Remaining pellet with mouse leukocytes and red blood cells was discarded.

3.6.2 Flow Cytometry – Detection of Mouse eNOS-Based Platelet Subpopulations

For this experiment we used eNOS-GFP mice (hemizygous and homozygous) and control WT (C57BL/6) mice. Mouse PRR was isolated as described in Section 3.6.1. Freshly isolated aliquots of PRP (150 µl each) were incubated in dark for 30 minutes at room temperature with rat anti-mouse CD41-PerCP/Cy5.5 conjugated antibody (5 µl) or rat PerCP/Cy5.5 IgG1 isotype control (5 µl). After incubation, PBS buffer with 0.3% BSA was added (850 µl) and platelet samples were centrifuged at 300g for 5 minutes. Next, supernatant was discarded (~900 µl) and cells were resuspended in 400 µl of PBS buffer with 0.3% BSA. Prior flow cytometry samples were strained through a 70 µM cell strainers to remove cell clumps. Flow cytometry was performed using Quanta SC flow cytometer (Beckman Coulter, Mississauga, ON, Canada).

During flow cytometry data acquisition 20,000 events per sample were collected and mouse eNOS^{pos} (GFP^{pos}) platelets (CD41 positive events detected in FL3 channel set to log scale) were identified based on GFP fluorescence (detected in FL1 channel set to linear scale). Percent of double positive cells was reported as eNOS^{pos} (GFP^{pos}) platelets following subtraction of FL1 auto-fluorescence of platelets from WT mice.

3.6.3 Flow Cytometry – DAF-FM Diacetate Staining – Detection of NO Production in Mouse Platelets

To study NO production within mouse platelets we utilized platelets from WT (C57BL/6) mice as GFP fluorescence of eNOS-GFP mouse platelets would interfere with DAF-FM staining (both are detected in FL1 channel). In addition eNOS-GFP mice overexpress eNOS (they express both mouse and human eNOS) and thus have increased NO production which would confound the results [574]. Therefore we isolated PRP from blood of WT (C57BL/6) and control eNOS knockout ($eNOS^{-/-}$) mice as described above in Section 3.6.1. DAF-FM diacetate (10 μM) was added to mouse PRP (~250-500 μl per mouse) and incubated for 30 minutes at 37°C in the dark. Next, 0.5 μg/ml PGI_2 was added to the PRP (with DAF-FM loaded platelets) and samples were centrifuged at 300*g* for 5 minutes at room temperature. PPP was removed and the platelet pellet was gently washed (3x) with 1 ml of Tyrode's buffer to remove residual DAF-FM diacetate that did not diffuse into the platelets. Mouse platelets were resuspended in 200 μl of PBS with 0.3% BSA and samples were incubated in dark for 30 minutes at room temperature with rat anti-mouse CD41-PerCP/Cy5.5 conjugated antibody (5 μl) or rat PerCP/Cy5.5 IgG1 isotype control (5 μl). After incubation, Tyrode's buffer was added (850 μl) and platelet samples were centrifuged at 300g for 5 minutes. Next, supernatant was discarded (~900 μl) and cells were resuspended in 400 μl of Tyrode's buffer and left in the dark for 1 hour at room temperature to allow PGI_2 inhibitory effect on platelets to wear off. Next, DAF-FM stained resting platelets were preincubated with L-arginine (100 μM) for 15 minutes. Prior flow cytometry samples were strained through a 70 μM cell strainers to remove cell clumps.

During flow cytometry data acquisition 20,000 events per sample were collected and mouse NO-producing platelets (CD41-positive events detected in FL3 channel set to log scale) were identified based on DAF-FM fluorescence (detected in FL1 channel set to log scale). Percent of double positive cells was reported as NO-producing platelets following subtraction of auto-fluorescence (and DAF-FM background staining as it is weakly fluorescent in unbound form) of control eNOS knockout ($eNOS^{-/-}$) mouse platelets.

3.6.4 Isolation of Mouse Bone Marrow

Following blood collection by cardiac puncture, eNOS-GFP mice (hemizygous and homozygous) and control WT (C57BL/6) mice were euthanized via cervical dislocation and placed in a supine position with all limbs fixed. Small incision was made to the right of midline in the lower abdomen, just above the hip. Next, the incision was extended down the leg and past the ankle joint. After carefully cutting away the connective tissue and muscles mouse femoral and tibia bones were collected and submerged in a CATCH buffer (1x Hanks' Balanced Salt Solution, 0.38% sodium citrate, 1 mM adenosine, 2 mM theophylline, and 5% heat-inactivated FBS). Remaining muscle or connective tissue fragments attached to the femoral and tibia bones were removed by scalpel, forceps, scissors and Kimwipes. The bone marrow was flushed out of tibia and femur bones with a syringe (30G needle) filled with CATCH buffer. This resulted in approximately 1000 μl of bone marrow suspension in CATCH buffer. Bone marrow samples were placed in an eppendorfs and centrifuged at 300g in a microcentrifuge for 5 minutes. Following centrifugation, supernatant was discarded and the bone marrow pellet was washed 2x with PBS buffer with 0.3% BSA (1 ml) and centrifuged at 300g in a microcentrifuge for 5 minutes. Next, bone marrow samples were resuspended either in RPMI medium supplemented with 10% FBS or PBS buffer with 0.3% BSA and used for further experiments.

3.6.5 Flow Cytometry – Detection of Mouse eNOS-Based Megakaryocyte Subpopulations

Flow cytometry was performed using Quanta SC flow cytometer (Beckman Coulter, Mississauga, ON, Canada). Fresh aliquots of the bone marrow (~1000 µl suspension in CATCH buffer) isolated and processed accrording to the protocol in Section 3.6.4 were incubated in the dark for 30 minutes at room temperature with rat anti-mouse CD41-PerCP/Cy5.5 conjugated antibody (5 µl) or rat PerCP/Cy5.5 IgG1 isotype control (5 µl). After incubation with antibodies PBS buffer with 0.3% BSA (800 µl) was added and samples were centrifuged at 300g for 5 minutes, supernatant was discarded (~900 µl) and cells were resuspended in 200 µl with PBS buffer with 0.3% BSA. Prior flow cytometry samples were strained through a 70 µM cell strainers to remove cell clumps. During flow cytometry data aquition 10,000 CD41-positive events per sample were collected and mouse $eNOS^{pos}$ (GFP^{pos}) MKs (CD41-positive events detected in FL3 channel set to log scale) were identified based on GFP fluorescence (detected in FL1 channel set to log scale). Percent of double positive cells was reported as $eNOS^{pos}$ (GFP^{pos}) MKs following subtraction of FL1 auto-fluorescence of MKs from WT mice.

3.6.6 Flow Cytometry of Mouse Bone Marrow Samples Treated with DNA Methyltransferase Inhibitor – 5-Azacytidine

Bone marrow samples from eNOS-GFP homozygous mice were isolated according to protocol described in Section 3.6.4. Next, bone marrow samples were resuspended in 200 µl of RPMI medium with 10% FBS and grown in 24 well plate. Subsequently, mouse bone marrow samples were treated with DNA methylase inhibitor - 5-azacytidine (5 µM) on day: 0, 2, 4 and 6. Medium was replaced every 2nd day prior to treatment with - 5-azacytidine (5 µM). On day 7, cells were non-adherent cells were collected directly to the 15 ml tube and adherent cells were trypsinsed and pooled with non-adherent cells. Following centrifugation at (300g for 5 minutes), cells were resuspended in 1 ml of PBS with 0.3% of BSA. Samples were centrifuged again (300g for 5 minutes) and resuspended in 200 µl of PBS with 0.3% of BSA. Samples were stained with rat anti-mouse CD41-PerCP/Cy5.5 conjugated antibody (5 µl) or rat PerCP/Cy5.5 IgG1 isotype control (5 µl) for 45 minutes at room temperature and processed as described above in Section 3.6.5. Briefly, after incubation with abtibodies samples were washed, pelleted and resuspended in a fresh buffer (PBS with 0.3% of BSA). Prior to flow cytometry samples were strained through a 70 µM cell strainers to remove cell clumps. During flow cytometry aqusition 10,000 CD41-positive events per sample were collected and mouse eNOS^{pos} (GFP^{pos}) MKs (CD41-positive events detected in FL3 channel set to log scale) were identified based on GFP fluorescence (detected in FL1 channel set to log scale). Percent of double positive cells was reported as eNOS^{pos} (GFP^{pos}) MKs.

3.6.7 Confocal Microscopy of Mouse Gastrocnemius Muscle Tissue - Confirmation of Human eNOS-GFP Expression in eNOS-GFP Transgenic Mice

Prior to collection of the mouse femur and tibia bones gastrocnemius muscle tissue was dissected and flash frozen in liquid nitrogen to confirm eNOS-GFP fluorescence within eNOS-GFP transgenic mice via confocal microscopy. Tissue samples were cryoembedded in optimal cutting temperature compound and cryosectioned on to slides for microscopy (histology performed on a service by fee basis by HistoCore at University of Alberta). To image eNOS-GFP, slides were mounted using ProLong Diamond antifade solution and coverslipped. Images were acquired on Olympus IX-81 (Olympus America Inc., Melville, NY, U.S.A.) microscope base with Yokagawa CSU10 (Yokogawa Electric Corporation, Tokyo, Japan) spinning disk confocal scan-head equipped with digital camera Hamamatsu EMCCD (C9100-13) (Hamamatsu, Photonics K.K., Hamamatsu City, Japan). Images were captured using magnification of 200x (20x/0.75 NA dry objective) and argon ion laser (488 nm). Images were acquired using Perkin Elmer Volocity software (Perkin Elmer Inc., Waltham, MA, USA).

3.7 Methods for Studies of eNOS-Based Megakaryoblast Subpopulations using Human Megakaryoblastic Cell Line - Meg-01

3.7.1 Confocal Microscopy - Detection of eNOS-Based Meg-01 Cell Subpopulations

Meg-01 cells were collected according to the protocol provided in Section 3.2.2 and stained as described in Section 3.5.3. Following eNOS staining additional F-actin staining was performed to visualize cytoskeleton of Meg-01 cells. Alexa Fluor 568 Phalloidin (1:40) was added to Meg-01 cell suspension in a Wash Buffer (0.3% BSA in a PBS buffer with 0.05% Tween 20) and incubated for 30 minutes in the dark at room temperature. Cells were washed (3x) with Wash Buffer, centrifuged at 900g for 10 minutes and cytospinned onto 0.1% poly-lysine-coated coverslips. Preparations were mounted in ProLong Diamond antifade solution and analyzed at room temperature on a Leica TCS SP5 microscope with a Leica inverted DMI 6000 B microscope base equipped with 60x/1.2 NA water objective (Leica Microsystems, Concord, ON, Canada). Electronic shutters and image acquisition were under the control of Leica LAF AS software. Fluorescence was excited with the argon ion (488 nm) and helium-neon (543 nm) lasers. Finally, images were equally adjusted for contrast and brightness.

3.7.2 Flow Cytometry - Detection of eNOS-Based Meg-01 Cell Subpopulations

In this study Meg-01 cells (passages 10-15) were used in two separate sets of experiments: 1) where samples were stained with anti-eNOS 6H2 clone antibodies and 2) where samples where stained with anti-eNOS M221 clone antibodies.

In the first set of experiments following collection as described in Section 3.2.2 Meg-01 cells were resuspended in 1 ml of PBS buffer and stained with 1 µl of Fixable Viability Dye eFluor 520 (FVD) (Thermofisher Scientific, Cat no. 65-0867-14), mixed and incubated for 30 minutes in the dark at room temperature. Next, cells were washed (2x) with PBS buffer and centrifuged at 200g for 5 minutes and processed as described in Section 3.5.3. Briefly, following fixation with 4% paraformaldehyde and permeabilization with Triton X-100, samples were incubated on a rotator for 1 h with primary anti-eNOS 6H2 clone antibodies (5 µg/ml) and following 3 washing steps cells were resuspended in Wash Buffer (0.3% BSA in a PBS buffer with 0.05% Tween 20). Next, Meg-01 cells samples were incubated with secondary PE-conjugated anti-mouse IgG antibodies for 2 hours at room temperature on a rotator. Following incubation, samples were washed (3x) with Wash Buffer, resuspended in 500 µl of PBS buffer and analyzed by flow cytometry. Twenty thousand events per sample were collected and eNOS fluorescence was detected in FL2 channel set to log scale. FVD fluorescence was measured in FL1 channel set to log scale. During analysis viable Meg-01 cells were identified as a population of cells with no FVD fluorescence. Gating based on viable Meg-01 cells we identified two peaks within eNOS fluorescence histogram (FL2 channel) corresponding to $eNOS^{neg}$ and $eNOS^{pos}$ subpopulations of Meg-01 cells. Gate for $eNOS^{neg}$ subpopulation was set based on unstained control sample of Meg-01 cells. Background staining for eNOS was assessed by IgG isotype control (5 µg/ml).

In the second set of experiments following collection as described in Section 3.2.2 Meg-01 cell samples were processed according to the protocol described in Section 3.5.3 using for eNOS detection - primary anti-eNOS M221 clone antibodies (1.25 µg/ml) and secondary Alexa Fluor 488-conjugated goat $F(ab')_2$ fragments anti-mouse IgG (15 µg/ml). Prior to flow cytometry cells were resuspended in 500 µl of PBS buffer. During flow cytometry data acquisition 20,000 events per sample were collected and eNOS fluorescence was detected in FL1 channel set to log scale. During analysis we identified two peaks within eNOS fluorescence histogram (FL1 channel) corresponding to $eNOS^{neg}$ and $eNOS^{pos}$ subpopulations of Meg-01 cells. Gate for

eNOS^{neg} subpopulation was set based on unstained control sample of Meg-01 cells. Background staining for eNOS was assessed by IgG isotype control (1.25 μg/ml).

3.7.3 Flow Cytometry - Detection of NO Production by Human Meg-01 Cells

Following Me-01 cell collection as described in Section 3.2.2 Meg-01 cells were washed (2x) in PBS buffer. Next, DAF-FM diacetate (10 μM) was added to the cell suspension in PBS and incubated for 30 minutes at 37°C in the dark. Subsequently, DAF-FM-loaded cells were washed (2x) with PBS buffer, to remove residual DAF-FM diacetate that did not diffuse into the cells, and centrifuged (130g for 7 minutes at 18°C) to pellet the cells. Next, DAF-FM-stained Meg-01 cells were resuspended in Tyrode's buffer with L-arginine (100 μM) and preincubated for 15 minutes in the dark at room temperature. During flow cytometry data acquisition 20,000 events per sample were collected and the NO-production of Meg-01 cells was detected as DAF-FM fluorescence in FL1 channel set to log scale. During analysis we identified two peaks within DAF-FM fluorescence histogram (FL1 channel) corresponding to low/non NO-producing and NO-producing subpopulations of Meg-01 cells. Gate for low/non NO-producing subpopulation was set based on unstained control sample of Meg-01 cells.

3.7.4 Flow Cytometry – Evaluation of Ploidy, Size and Granularity of Human Meg-01 Cells

Meg-01 cells (passages 14-18 used for this experiment) were cultured and collected for experiments according to protocol described in Section 3.2.2 and eNOS staining was performed as described in Section 3.5.3. Briefly, Me-01 cells samples were fixed with 4% paraformaldehyde and permeabilized with 0.1% Triton X-100. Next, Meg-01 samples were incubated for 1 hour with primary anti-eNOS M221 clone antibodies (1.25 µg/ml) followed by 2-hour incubation with secondary Alexa Fluor 488-conjugated goat $F(ab')_2$ fragments anti-mouse IgG (15 µg/ml) in the dark at room temperature. Next, samples were washed (3x) with a Wash Buffer (0.3% BSA in a PBS buffer with 0.05% Tween 20), centrifuged (130g for 7 minutes) and incubated for 15 minutes with anti-human CD42b-PE antibody (1:100) in the dark at room temperature. Samples were washed (1x) with a Wash Buffer and resuspended in a PBS buffer (500 µl). To digest RNA and thus ensure that propidium iodine (PI) will only stain DNA RNase A treatment was performed. Meg-01 cells were incubated (30 minutes) with RNase A (50 µg/ml) (Sigma-Aldrich, Cat no. R4875-100MG) at 37°C and subsequently washed (1x) with a Wash Buffer. Following centrifugation (130g for 7 minutes) samples were resuspended in a PBS buffer (500 µl) with PI (10 µg/ml) and incubated in the dark for 15 min at room temperature. Following PI staining samples were analyzed using a Cell Lab Quanta SC MPL Flow Cytometer (Beckman Coulter INC., Fullerton, CA, USA). During flow cytometry data acquisition 20,000 of CD42b-positive events were collected for each sample. Meg-01 cells with different ploidy (2n, 4n, and 8n) were identified based on the PI fluorescence (DNA content), detected in FL3 channel (set to log scale). Next, for each ploidy class percentage of $eNOS^{neg}$ and $eNOS^{pos}$ Meg-01 cells were reported (eNOS fluorescence was measured in FL1 channel set to log scale). In addition, size of $eNOS^{neg}$ and $eNOS^{pos}$ Meg-01 cells was reported as value of mean electronic volume (EV, arbitrary units of volume) and granularity as value of mean side scatter (SS, arbitrary units of scattered light intensity).

3.7.5 Treatment of Meg-01 Cells with Interferon Gamma and Interleukin 10

After thawing, Meg-01 cells (passages 9-14) were (2x) subcultivated and then passaged into T25 flasks with 5 ml of basal RPMI medium supplemented with 2% FBS (Sigma-Aldrich, St. Louis, MO, USA) and 1% Penicillin-Streptomycin (Pen-Strep 10,000 U/mL each) (Thermofisher Scientific, Rockford, IL, USA). Cells were serum-starved (2% FBS) overnight and treated on the following day with increasing concentrations of pro-inflammatory cytokine IFN-γ (0.1-100 ng/ml). In some experiments Meg-01 cells were treated simultaneously with IFN-γ (10 ng/ml) and increasing concentrations of anti-inflammatory cytokine IL-10 (0.1-100 ng/ml). Following treatment cells were cultured for 48 hours and collected by decanting non-adherent cells and trypsinizing adherent cells into a sterile 50 ml tube. Cell samples were pelleted by centrifugation (130g for 7 min at 18°C) and supernatant was discarded. Subsequently, cell pellets were washed (1x) with 1 ml of sterile PBS buffer, transferred into 1.5 ml eppendorf tube and centrifuged at 1000g for 5 minutes. The resultant cell pellet was used for further experiments and processed accordingly.

3.7.6 Flow Cytometry - Viability of Meg-01 Cells Following Interferon Gamma and Interleukin 10 Treatment

Meg-01 treated with cytokines (IFN-γ and IL-10) were cultured in T25 flasks and collected as described above in Section 3.8.5. Cell pellets were resuspended in 1 ml of PBS buffer with 1 µl of Fixable Viability Dye eFluor 520 (FVD) (Thermofisher Scientific, Cat no. 65-0867-14) and briefly vortexed. Samples were incubated for 30 minutes at 4°C in the dark and washed twice with PBS buffer. Finally, cells were resuspended in 500 µl of PBS buffer and analyzed using a Cell Lab Quanta SC MPL Flow Cytometer (Beckman Coulter INC., Fullerton, CA, USA). During flow cytometry data acquisition 10,000 events per sample were collected and FVD fluorescence was measured in FL1 channel. Unstained Meg-01 cell sample was used to establish gate for FVD-negative population. Viable Meg-01 cells were identified on a dot plot (FL1/SS) as FVD-negative population in FL1 channel and reported as % of viable Meg-01 cells.

3.7.7 Flow Cytometry – Detection of eNOS-Based Meg-01 Cell Subpopulations Following Treatment with Increasing Concentrations of Interferon Gamma

Meg-01 cells (passages 9-13 used for this experiment) treated with increasing concentrations of IFN-γ (0.1-100 ng/ml) were cultured and collected for experiments according to protocol described in Section 3.8.5. Next, Meg-01 cell samples were stained according to the protocol described in Section 3.5.3 using for eNOS detection - primary anti-eNOS M221 clone antibodies (1.25 μg/ml) and secondary Alexa Fluor 488-conjugated goat $F(ab')_2$ fragments anti-mouse IgG (15 μg/ml). Prior to flow cytometry cells were resuspended in 500 μl of PBS buffer. 20,000 events per sample were collected and eNOS fluorescence was detected in FL1 channel set to log scale. During analysis we identified two peaks within eNOS fluorescence histogram (FL1 channel) corresponding to $eNOS^{neg}$ and $eNOS^{pos}$ subpopulations of Meg-01 cells. Gate for $eNOS^{neg}$ subpopulation was set based on unstained control sample of Meg-01 cells. Background staining for eNOS was assessed by IgG isotype control (1.25 μg/ml).

3.7.8 Isolation of RNA and DNase I Treatment – General Protocol

Preparation of the workspace

Designated area in the lab was used for RNA isolation, DNase I treatment, RT-PCR, PCR, qPCR and sample preparation for DNA sequencing experiments. Prior to each experiment bench-top and all pipets were decontaminated with RNase AWAY Decontamination Reagent (ThermoFisher Scientific, Cat No. 10328011). For all RT-PCR, PCR and qPCR experiments pipet tips containing hydrophobic filters were used to minimize the risk of cross contamination. All eppendorf tubes used for RNA isolation, DNase I treatment, RT-PCR, PCR and qPCR were PCR grade (DNase and RNase free).

RNA isolation

Meg-01 cells (passages: 10-15) and HUVEC cells (passages: 4-7) used as a positive control, were cultured according to protocols in Section 3.2.1 and Section 3.2.2. Collected cell pellets were washed (2x) with PBS buffer and centrifuged at 1,000g for 5 minutes to remove residues of phenol red (from cell culture media). Total RNA was isolated from Meg-01 and HUVEC cells using RNeasy Mini Kit (Qiagen, Cat No. 74104) according to the manufacturer's protocol. Briefly, cell pellets were lysed with 700 µl of RLT buffer by vortexing for 1 minute. Next, 700 µl of 70% ethanol was added to the homogenate and mixed by thorough pipetting. Subsequently, RNeasy spin column were placed in a 2 ml collection tube and 700 µl of sample was transferred onto a column and spun down at 10,000g for 15 seconds, and flow-through was discarded. This step was repeated with another 700 µl of remaining sample. To wash a spin column membrane 700 µl of RW1 buffer was added and spun down at 10,000g for 15 seconds, and flow-through was discarded. To again wash a spin column membrane 500 µl of RPE buffer was added and spun down at 10,000g for 15 seconds, and flow-through was discarded. This step was repeated except the samples were spun down at 10,000g for 2 minutes to ensure that no ethanol is carried over during RNA elution. RNeasy spin column were placed in a new 2 ml collection tube and spun down at 17,000g for 1 minute. RNeasy spin column was placed in a new 1.5 ml eppendorf tube and 50 µl of RNase-free water was added directly to the spin column membrane, and spun down at 10,000g for 1 min to elute the RNA. RNA samples were stored at -80°C until ready to use. Concentration and purity of the RNA was measured via spectrophotometer NanoDrop ND 8000 (Thermofisher Scientific, Rockford, IL, USA). RNA samples with 260/280 ratio of 1.9-2.0 were qualified as pure and used for experiments.

DNase I treatment

Next, to eliminate genomic DNA contamination prior to RT-PCR, Deoxyribonuclease I Amplification Grade (ThermoFisher Scientific, Cat No. 18068-015) treatment was performed, following the manufacturer's protocol. Briefly, to 0.2 ml eppendorf tube 1 µg of RNA, 1 µl of 10x reaction buffer with $MgCl_2$ and 1 µl of DNase I were added and topped up to 10 µl with diethyl pyrocarbonate (DEPC)-treated water. Samples were incubated in Bio-Rad Thermal Cycler S1000 (Bio-Rad, Hercules, USA) at 37°C for 30 minutes, next to inactivate DNase I 1 µl of 50 mM EDTA was added and samples were incubated again at 65°C for 10 min. Following DNase I treatment, RNA samples were kept on ice and used for reverse transcription.

3.7.9 Reverse-Transcription – General Protocol

All steps of sample preparation for RT-PCR were performed on ice to avoid premature cDNA synthesis and minimize the risk of RNA degradation. For all RT-PCR reactions, High-Capacity cDNA Reverse Transcription Kit (ThermoFisher Scientific, Cat No. 4368814) was used. All reagents were thawed on ice and subsequently RT-PCR master mix was prepared based on the total sample number plus 10% to account for a reagent loss during pipetting. First RNase inhibitor SUPERase-In 20 U/µl (ThermoFisher Scientific, Cat No. AM2696) was diluted to a final concentration of 10 U/µl in ice-cold 1x Buffer RT. Next, RT-PCR master mix components were added to 1.5 ml eppendorf. Volumes given are per one sample:

1. 2 µl of 10x Buffer RT, final conc. 1x
2. 0.8 µl of dNTP Mix (100 mM), final conc. 4 mM
3. 2 µl of 10x Random Primers , final conc. 1x
4. 1 µl RNase inhibitor SUPERase-In™ 10 U/µl, final conc. (not provided with a kit), final conc. 10 units per reaction
5. 1 µl MultiScribe Reverse Transcriptase
6. Variable volume of PCR-grade water (calculated based on the volume of 1µg of RNA, so that the final reaction volume is 20 µl)

Ready master mix was vortexed for 5 seconds and briefly centrifuged to collect residual liquid from the walls of the tube. RT-PCR master mix was divided into single reaction eppendorf tubes (0.2 ml) and 1 µg of RNA was added. No template control (NTC) and no reverse transcriptase control (NRT) were included, using RNase-free water in place of RNA. Ready samples were vortexed for 5 seconds and briefly centrifuged to collect residual liquid from the walls of the tube. Samples were incubated in a Bio-Rad Thermal Cycler S1000 (Bio-Rad, Hercules, USA) set to program Step 1: 25°C for 10 minutes, Step 2: 37°C for 120 minutes, Step 3: 85°C for 5 minutes and Step 4: 4°C for ∞. Following RT-PCR samples were stored at -20°C until ready to use.

3.7.10 Agarose Gel Electrophoresis Followed by Sanger Sequencing - Confirmation of eNOS Expression in Meg-01 Cells

Agarose gel electrophoresis

Meg-01 cells (passages: 10-15) and HUVEC cells (passages: 4-7) used as a positive control, were cultured according to protocols in Section 3.2.1 and Section 3.2.2. Collected cell pellets were washed (2x) with PBS buffer and centrifuged at 1,000g for 5 minutes to remove residues of phenol red (from cell culture media). Total RNA was isolated from Meg-01 cells and HUVEC cells according to protocol described in Section 3.8.8. Next, RT-PCR was performed as described in Section 3.8.9. Following RT-PCR, agarose gel (2%) was prepared by addition of 1 g of agarose to 50 ml of TBE buffer (89mM Tris-base, 89mM boric acid, 2mM EDTA, ddH_20). Mixture was boiled until agarose was fully dissolved and left to cool down for about 5-10 minutes at room temperature before adding 4 µl of SYBR Safe DNA Gel Stain (ThermoFisher Scientific, Cat No. S33102). Next, agarose gel was poured into a mold and left for 45 min to solidify. Completely solidified agarose gel was fully submerged in TBE buffer. Next, 5 µl of DNA ladder GeneRuler 100-1000 bp (ThermoFisher Scientific, Cat No. SM0243) was added to the first well and 2 µl of cDNA (obtained from 100 ng of RNA) from samples and appropriate controls were added to the following wells. Agarose Gel Electrophoresis was run at 100V for 40 min and imaged via UV light exposure for 0.5 second and analyzed using Versa Doc 5000MP (Bio-Rad, Hercules, CA, USA). The Meg-01 eNOS cDNA was identified as 241 bp cDNA band, matching eNOS cDNA band of positive control HUVEC sample. Data was then normalized and expressed as % of HUVEC control.

Sanger sequencing

Next, the eNOS cDNA bands (241 bp) of Meg-01 cells and HUVEC were excised from agarose gel under UV lamp using clean, sharp scalpel. Next, QIAquick Gel Extraction Kit (Qiagen, Cat No.28704) was used to extract cDNA from the agarose gel slices. Each sample consisted of 5 agarose gel slices from 5 separate cDNA bands:

1. Meg-01 cells – 1.2 g (3.6 ml of QG buffer was added)
2. HUVEC cells – 2.0 g (6.0 ml of QG buffer was added)

To 15 ml tube 300 µl of QG buffer per each 100 mg of agarose gel slices was added and incubated at 50°C for 15 minutes in a heating block, until all gels slices dissolved into yellow mixture, indicating appropriate pH of ≤ 7.5 for efficient DNA adsorption onto the spin column

membrane. Next, 300 µl of isopropanol (100%) was added to the mixture and vortexed for 10 seconds. Subsequently, QIAquick spin column was placed into 2 ml collection tube and 750 µl of the mixture was added to the column and spun down at 17,000g for 1 min and the flow-through was discarded; the centrifugation step was repeated with another 750 µl of the mixture that remained in the 15 ml tube. Next, 500 µl of QG buffer was added to the QIAquick spin column and spun down at 17,000g for 1 minute and flow-through was discarded. As a next step, 750 µl of PE buffer was added to wash QIAquick spin column and left for 5 minutes (recommended for a better residual salt removal from the cDNA template), and spun down at 17,000g for 1 minute, flow-through was discarded. QIAquick spin column was spun down in a new 2 ml collection tube at 17,000g for 1 minute, to remove residual wash buffer. QIAquick spin column was placed into clean 1.5 ml eppendorf tube. DNA was eluted from QIAquick column membrane with 50 µl of DNase & RNase free water and spun down at 17,000 g for 1 minute.
Concentration and purity of cDNA in samples was measured via spectrophotometer NanoDrop ND 8000 (Thermofisher Scientific, Rockford, IL, USA). To eppendorf tube 15 ng/µl of DNA template and 0.25 µM of primer was added and topped up with DNase & RNase free water (Qiagen, Cat No. 129112) to 10 µl of final reaction volume. Following four samples were sent for Sanger DNA sequencing in Molecular Biology Service Unit (University of Alberta):
Sample 1: HUVEC cells conc. Total of 150 ng cDNA (15 ng/µl) + 0.25 µM of forward primer
Sample 2: HUVEC cells conc. Total of 150 ng cDNA (15 ng/µl) + 0.25 µM of reverse primer
Sample 3: Meg-01 cells conc. Total of 150 ng cDNA (15 ng/µl) + 0.25 µM of forward primer
Sample 4: Meg-01 cells conc. Total of 150 ng cDNA (15 ng/µl) + 0.25 µM of reverse primer

Sequencing was performed on Applied Biosystems 3730 DNA Analyzer (Thermofisher Scientific, Rockford, IL, USA) and the results were analyzed in Applied Biosystems Sequence Scanner Software v2.0. The DNA sequencing showed two eNOS matching DNA nucleotide sequences both on positive (1^{st}-165 and 2^{nd} - 150 nucleotide long) and negative (1^{st}-164 and 2^{nd} - 72 nucleotide long) DNA strands.

3.7.11 Quantitative Polymerase Chain Reaction – Evaluation of eNOS and iNOS mRNA Levels in Meg-01 Cells Following Treatment with Interferon Gamma and Interleukin 10

RNA was isolated (protocol - Section 3.8.8) from Meg-01 cells following experiment with IFN-γ and IL-10 described in Section 3.8.6. Next, RT-PCR reaction was performed to acquire cDNA from 1 µg of RNA in total volume of 20 µl (Section 3.8.9). Next, 2 µl of cDNA (corresponding to ~100 ng of RNA) was used per one reaction well. All qPCR experiments were performed using SYBR green dye method. Reactions were performed in a total volume of 15 µl per well. Next, qPCR master mix components were added to 1.5 ml eppendorf. Volumes given are per one well:

1. 10 µl of KAPA SYBR FAST qPCR Master Mix (2x), final conc. 1x
2. 0.4 µl of forward primer (10 µM), final conc. 200 nM
3. 0.4 µl of reverse primer (10 µM), final conc. 200 nM
4. 2.2 µl of PCR-grade water

First, the total volume of 12 µl of qPCR master mix was added to all wells and then 2 µl of cDNA was added to each well. Cycling conditions for human iNOS, human eNOS and human GAPDH detection:

- ✓ HOLD: 95°C for 3 minutes
- ✓ 40 CYCLES:
- Denature: 95°C for 30 seconds
- Anneal: 61°C for 30 seconds
- Extend: 72°C for 30 seconds
- ✓ MELT CURVE

Primers used for qPCR (SYBR green dye)			
Gene/Species	Primer sequence	Product size (bp)	Manufacturer
iNOS/human	F 5'-ACAACAAATTCAGGTACGCTGTG-3' R 5'-TCTGATCAATGTCATGAGCAAAGG-3'	84	Integrated DNA Technologies
eNOS/human	F 5'-GTCCTGCAGACCGTGCAGC-3' R 5'-GGCTGTTGGTGTCTGAGCCG-3'	241	Integrated DNA Technologies
GAPDH/human	F 5'-GAGAAGGCTGGGGCTCATTT-3' R 5'-AGTGATGGCATGGACTGTGG-3'	231	Integrated DNA Technologies

Table 3.1. Primers used for qPCR

Levels of iNOS and eNOS mRNA were analyzed using relative quantification method ΔCt (ΔCt=Ct $_{(gene)}$ - Ct $_{(GAPDH)}$ and ΔΔCt=ΔCt $_{(experimental)}$ - Ct $_{(control)}$. GAPDH was used as a reference gene. Untreated sample was used as a control in calculation of ΔΔCt. Fold change is expressed as $2^{\wedge -\Delta\Delta Ct}$.

3.7.12 Flow Cytometry – Detection of eNOS-Based Platelet Subpopulations Derived from Meg-01 Cells Treated with Interferon Gamma and Interleukin 10.

Meg-01 cells (passages 14-18) were cultured in T25 flasks with 5 ml of RPMI full medium for 8 days at 37°C in a humidified atmosphere of 5% CO_2. To stimulate platelet production, Meg-01 cells were treated with 100 ng/ml of human TPO (Sigma-Aldrich, Cat no. SRP3178-10UG) every 48 hours. Concomitantly, Meg-01 cells were treated every 48 hours with pro-inflammatory cytokine IFN-γ (10 ng/ml) and anti-inflammatory cytokine IL-10 (0.1-100 ng/ml). Non-adherent Meg-01 cells and released platelets were collected to 50 ml tube and additionally flasks were washed twice with the full RPMI medium to thoroughly collect all remaining platelets. Cells were spun down (200 g for 10 min at room temp. 22°C) and the platelet-rich supernatant was collected and transferred to a new 50 ml tube and spun down again (1800 g for 20 minutes at room temp. 22°C). The supernatant was discarded and pellet containing platelets was washed once with a Wash Buffer (0.3% BSA in a PBS buffer with 0.05% Tween 20) and spun down after each wash at 10,000g for 5 minutes. Next, Meg-01 released platelets were fixed in 4 % paraformaldehyde for 20 minutes and washed (2x) with a Wash Buffer and centrifuged at 10,000g for 5 minutes. Meg-01 released platelets were permeabilized in PBS + 0.1% Triton X-100 + 0.5% BSA for 10 minutes (room temp. 22°C) on a sample rotator. Samples were centrifuged at 10,000 g for 5 minutes and washed (2x) with Wash Buffer. Next, samples were blocked in PBS + 5.0 % BSA for 2 hours (room temp. 22°C) on a sample rotator. After blocking step, 10 µl (1.25 µg) of primary mouse anti-eNOS M221 antibodies was added to samples and incubated overnight at 4°C on a sample rotator. Samples were washed tree times with Wash Buffer and spun down at 10,000 g for 5 minutes after each wash. Next, 5 µl (5.0 µg/ml) of secondary anti-mouse $F(ab')_2$ fragment antibodies Alexa 488 were added and samples were incubated at room temperature for 2 hours on a rotator. After addition of secondary antibodies, samples were protected from longer light exposure. Samples were washed (3x) with Wash Buffer and spun down at 10,000g for 5 minutes after each wash. Next, 10 µl (1:100) of anti-human CD42b-PE antibody was added and incubated for 15 minutes at room temperature; samples were washed (2x) with Wash Buffer and spun down at 10,000g for 5 minutes after each wash. Samples were resuspended in 500 µl of the Wash Buffer and analyzed using a Cell Lab Quanta SC MPL Flow Cytometer (Beckman Coulter INC., Fullerton, CA,

USA). During flow cytometry acquisition 20,000 CD42b-positive events were collected for each sample and analyzed following compensation to account for fluorophore spectral overlap.

3.7.13 Western Blot – Detection of iNOS Protein Levels in Meg-01 Cells Treated with Interferon Gamma and Interleukin 10

Sample preparation

Following the 48-hour treatment with cytokines (10 ng/ml IFN-γ and 0.1-100 ng/ml IL-10) as described in Section 3.7.5 Meg-01 cell pellets were stored in -80°C. Samples (Meg-01 cell pellets) were thawed on ice and resuspended in homogenizing buffer (RIPA buffer, 10% protease inhibitors, 1.0% SDS and 1 μM cyclodextrin). Next, lysed platelets were sonicated three times for 5 seconds with Misonix Ultrasonic Liquid Processor (Misonix Inc., Farmingdale, NY, USA) at 30% output and centrifuged at 8 000g for 3 minutes at room temperature. The resultant supernatant was then assayed for protein content as described in Section 3.5.2. White blood cells (WBC) were used as a positive control. Immunoblot analysis was performed under reducing/denaturing conditions. Briefly, 50 μg protein aliquots were denatured by boiling (5 minutes) and 5 μl of loading buffer (containing reducing agent – 8% SDS, denaturing agent – 16% β-mercaptoethanol, glycerol, 4x Tris-HCl/SDS pH 6.8, ddH_2O, bromophenol blue) was added to make a final sample volume of 25μl. Meg-01 samples (100 μg of total protein) were loaded into lanes on 8% dodecyl sulfate–polyacrylamide electrophoresis (SDS–PAGE) gel. Electrophoresis and protein transfer on PVDF membrane (0.45μm) was performed according to the protocol in Section 3.5.2.

Detection

After protein transfer, PVDF membranes were cut at the 75kDa molecular weight marks. The top membrane (>75kDa) was blocked in 5% BSA in Tris-buffered saline with 0.1% Tween 20 (TTBS) for one hour at room temperature followed by overnight incubation at 4°C with 1:100 (20 μg) of rabbit polyclonal anti-iNOS antibody (Abcam, Cat No. ab15323). After incubation with primary antibodies, membrane was washed 4x times for 5 minutes in TTBS, and then probed for one hour at room temperature with 1:2000 anti-rabbit IgG conjugated to horseradish peroxidase (60 μg). The lower membrane (<75kDa) was blocked in 5% skim milk in TTBS at 4°C overnight, followed by a 30-minute incubation with a monoclonal β-actin antibody conjugated to horse radish peroxidase (1:40 000 dilution). This was followed by a final 4x washes with TTBS for all membranes, and developed using an ECL kit. Chemiluminescence was detected using an enhanced chemiluminescence (ECL) prime western blotting detection reagent (GE Healthcare, Chicago, IL, USA), and imaged using a VersaDoc Imaging System (Bio-Rad,

Hercules, CA, USA). Band densitometry was measured using Quantity One software. The iNOS band densitometry (~131kDa) was normalized to the respective β-actin (42kDa) bands.

3.8 Statistics

Statistical analysis was performed using Graphpad Prism 5.0. Results were expressed as mean + standard error of the mean. Comparison between two groups were performed using two-tailed t-test. Comparison of variance between multiple groups was performed using one-way analysis of variance (ANOVA) with Tukey's multiple comparison test or Dunnett's multiple comparison test. Comparison between more than one variable was performed using two-way ANOVA. P value less than 0.05 was accepted as statistically significant.

4. RESULTS

4.1 Human Platelets Express Smaller Amounts of eNOS than Human Endothelial Cells

A number of studies have demonstrated that human platelets express eNOS and generate NO as an endogenous negative-feedback mechanism [154, 200, 201, 246, 247, 249, 250, 252, 253, 257]. However, in recent years several reports have questioned presence of eNOS in human platelets and their ability to generate NO [260, 262, 263, 579]. To explain some of these discrepancies we first decided to use confocal microscopy to visualize eNOS expression in human platelets. As a positive control for eNOS intracellular staining we used human cardiac microvascular endothelial cells (HMVEC), which are known to constitutively express high levels of eNOS. Utilizing confocal microscopy and two anti-eNOS antibodies (anti-eNOS M221 clone biding within C-terminal and anti-eNOS 6H2 clone binding within N-terminal of eNOS protein) we were able to visualize eNOS both in HMVEC and human platelets. In HMVEC eNOS was highly abundant within the cytoplasm and plasma membrane (Figure 4.1, Panel A). On the other hand, human platelets had relatively low abundance of eNOS which was primarily localized in the plasma membrane. Importantly, we also identified few human platelets that lacked eNOS protein while majority had eNOS protein present (Figure 4.1, Panel B).

We also performed western blot experiments to compare the total amount of eNOS protein between HMVEC and human platelets, as demonstrated in Figure 4.2, Panel A. Densitometric analysis of immunoblots showed that platelets had significantly smaller amount of total eNOS protein when compared to HMVEC (100 ± 0.00% HMVEC control vs. 19.97 ± 1.73%), as summarized in Figure 4.2, Panel B.

A

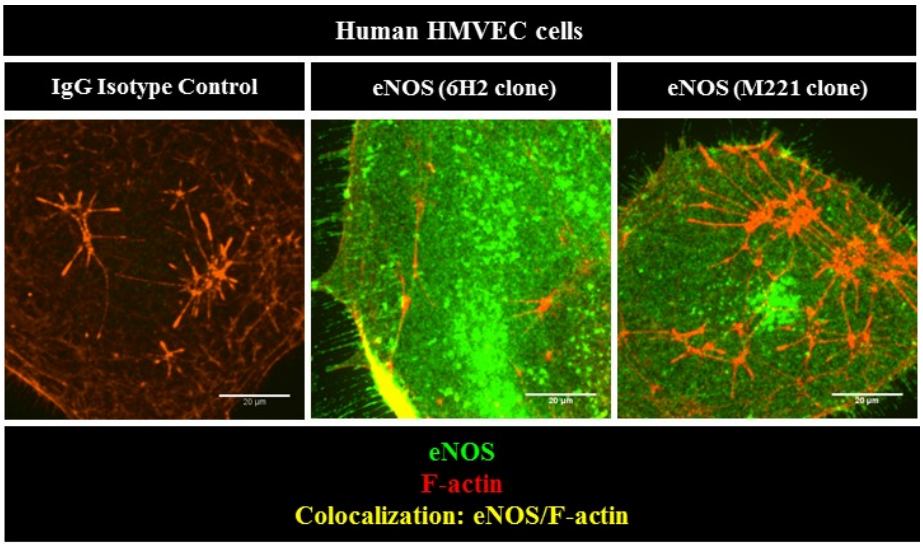

B

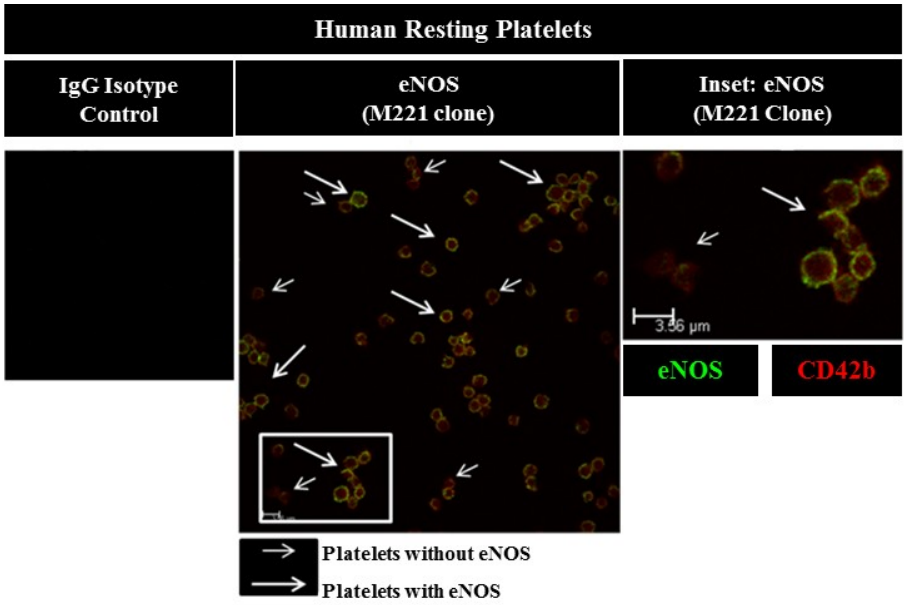

Figure 4.1. Confocal microscopy of eNOS protein within adherent human HMVEC and resting human platelets

(A) Confocal microscopy of eNOS within HMVEC. Scale bars = 20 µm. $N = 3$. Images were taken with Olympus IX-81 spinning disk confocal microscope using 60x/1.4 NA oil objective. **(B)** Confocal microscopy of platelets with eNOS (small arrows) and platelets without eNOS (large arrows). Scale bars = 3.56 µm. $N = 3$. Leica TCS SP5, 100x/1.4 NA oil objective. (Confocal microscopy of human platelets was performed by Dr. Radziwon-Balicka).

A

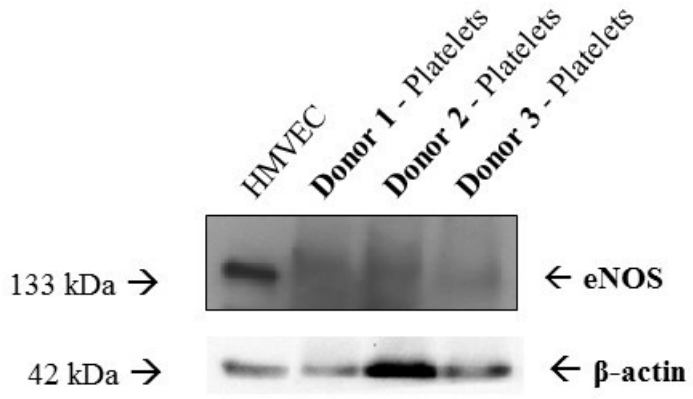

B

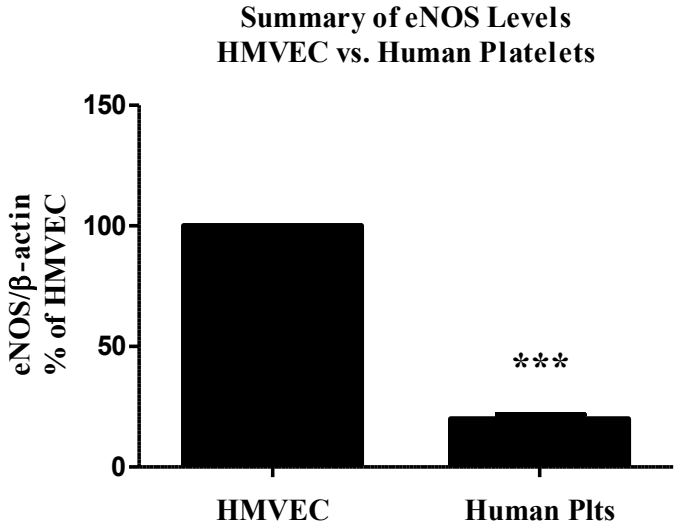

Figure 4.2. Comparison of total eNOS protein levels between HMVEC and human platelets **(A)** Representative immunoblot of eNOS in HMVEC and human platelets. **(B)** Summary bar graph of total eNOS protein expression by HMVEC and human platelets (Plts). Statistics: paired, two-tailed Student's *t*-tests. $N = 3$. ***$P < 000.5$.

4.2 Identification of eNOS-Based Platelet Subpopulations

After identifying low level of eNOS protein in human platelets using two techniques - confocal microscopy and western blot, we decided to further investigate the cause of inconsistent reports about presence or absence of eNOS protein in human platelets. Since our confocal microscopy revealed that some platelets lacked eNOS, we decided to use high-throughput method that allows for identification of cellular subpopulations. First we developed a sensitive intracellular flow cytometry protocol to measure eNOS protein in permeabilized human platelets. Next, we performed two-color flow cytometry where we measured eNOS expression based on cell-specific surface marker. As a cell specific marker for human platelets we used anti-CD42b (detecting GPIbα) antibody and measured eNOS expression based CD42-positive cells to exclude from analysis any potential contamination with EC or leukocyte microparticles. As a positive control for eNOS detection we also utilized HMVEC within our flow cytometry protocol. We used anti-CD31 (detecting PECAM-1) antibody to confirm the identity of our cultured ECs.

Based on CD42b-positive cells (Figure 4.3, Panel A), we analyzed eNOS presence in human platelets. Using this protocol we identified the presence of distinct eNOS-negative ($eNOS^{neg}$) and eNOS-positive ($eNOS^{pos}$) platelet subpopulations. We denoted the platelets found within the lower histogram peak as eNOS-negative ($eNOS^{neg}$) as they overlapped with unstained control, and platelets found within the larger histogram peak as eNOS-positive ($eNOS^{pos}$) (Figure 4.3, Panel B). We further determined eNOS fluorescence surface density (FSD) (Figure 4.3, Panel C). Since confocal microscopy showed that platelet eNOS is localized in plasma membrane, we decided to use FSD parameter instead mean fluorescence intensity. This allowed us to account for platelet size and exclude possibility that low/absent eNOS fluorescence resulted simply from smaller platelets. Moreover, the histograms for eNOS content demonstrated bimodal distribution (Figure 4.3, Panel C). In young healthy adults (22-35 yrs) the $eNOS^{neg}$ subpopulation accounted for 19.4 ± 3.2% of total platelets and $eNOS^{pos}$ subpopulation accounted for 80.6 ± 3.3% of total platelets, as summarized in Figure 4.3, Panel D. Non-specific background signal of eNOS and CD42b staining was controlled with respective IgG isotype controls.

To further confirm that the detection of eNOS-negative platelet subpopulation was not an artefact of our intracellular flow cytometry protocol, we performed flow cytometry to detect

eNOS within HMVEC. Using our protocol we identified that nearly all HMVEC expressed eNOS, which we denoted as eNOS-positive ($eNOS^{pos}$). The HMVEC histogram for eNOS content demonstrated unimodal distribution as there was no distinct eNOS-negative population of HMVEC (Figure 4.3, Panel F). The $eNOS^{pos}$ HMVEC accounted for 99.15 ± 0.18% of total HMVEC as summarized in Figure 4.3, Panel G. Non-specific background signal of eNOS and CD31 staining was assessed by respective IgG isotype controls.

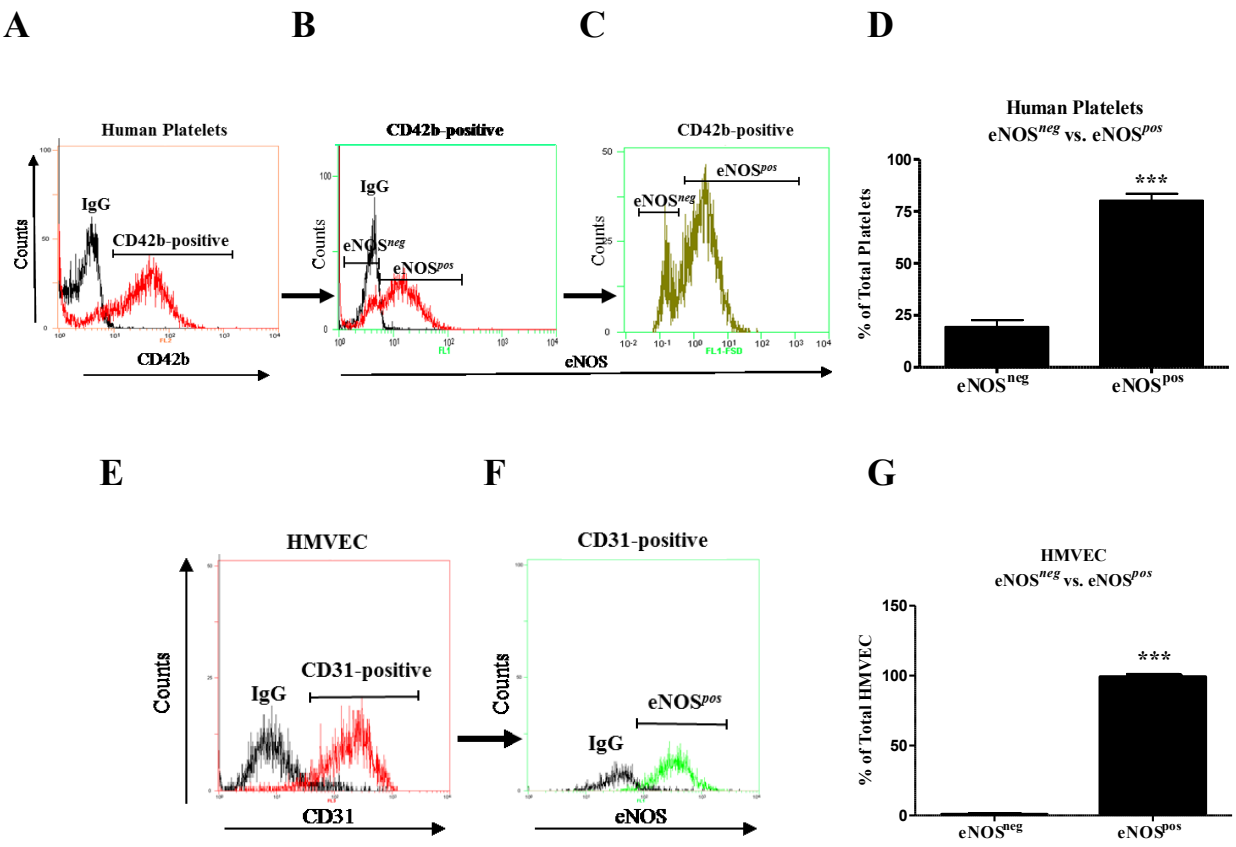

Figure 4.3. Identification of human eNOS-based platelet subpopulations

(A) Representative mean fluorescence intensity histogram overlay of IgG control (black) and CD42b-positive cells (red). **(B)** Representative mean fluorescence intensity histogram overlay of IgG control (black) and eNOS (red) for CD42b-positive cells. **(C)** Representative fluorescence surface density histogram of eNOS expression for CD42b-positive cells. **(D)** Summary bar graph of eNOS^{neg} to eNOS^{pos} human platelets. Statistics: paired, two-tailed Student's *t*-tests. $N = 10$. ***$P < 0.0001$. **(E)** Representative mean fluorescence intensity histogram overlay of IgG control (black) and CD31-positive cells (red). **(F)** Representative mean fluorescence intensity histogram overlay of IgG control (black) and eNOS (green) for CD31-positive cells. **(G)** Summary bar graph of eNOS^{neg} to eNOS^{pos} HMVEC. Statistics: paired, two-tailed Student's *t*-tests. $N = 3$. ***$P < 0.0001$.

4.3 Identification of NO-Producing and Low/Non-NO-Producing Platelet Subpopulations

After identifying eNOS^{neg} and eNOS^{pos} platelet subpopulations, next we decided to investigate the ability of human platelets to generate NO. We created NO-specific flow cytometry protocol using DAF-FM diacetate to detect NO-production by human platelets measured as DAF-FM fluorescence concentration instead of mean fluorescence intensity. This allowed us to account for differences in platelet volumes and exclude possibility that low/absent DAF-FM fluorescence resulted from measurement of smaller platelets. DAF-FM stained resting platelets preincubated with L-arginine (100 μM) showed NO-production identified on the histogram as two distinct overlapping fluorescence peaks, showed in Figure 4.4, Panel B. The smaller peak's fluorescence overlapped with that of the autofluorescence of unstained control platelets (Figure 4.4, Panel A); hence, these platelet were identified as low/non- NO producing platelets. The platelets found within the larger peak with greater DAF-FM fluorescence were identified as NO-producing (Figure 4.4, Panel B). Data analysis established that platelet subpopulation producing low-levels or no NO accounted for $17.9 \pm 2.4\%$ of total platelets, while the subpopulation that produced NO comprised of $82.1 \pm 2.4\%$ of total platelets (Figure 4.4, Panel C).

Further, we confirmed the presence of low/non-NO-producing and NO-producing platelets using fluorescence microscopy. Imaging of resting human platelets stained with DAF-FM diacetate and preincubated with L-arginine (100 μM) showed presence and absence of NO-production by an individual platelets, which is depicted in Figure 4.4, Panel D.

As a next step we decided to explore if low/non-NO-producing platelets are in fact eNOS^{neg} platelets. To test this we used DAF-FM staining and separated platelets based on their ability to generate NO by FACS-sorting (set to enrichment mode to gain on platelet yield), as showed in Figure 4.5, Panel A. Platelets gated within the bottom 20% of DAF-FM fluorescence histogram were defined as DAF-FM-negative and sorted into sterile tube. Evaluation of post-sort DAF-FM^{neg} platelet sample showed enrichment in DAF-FM^{neg} platelets seen as shift to the left of DAF-FM fluorescence histogram as depicted in Figure 4.5, Panel A. Next, we performed eNOS-staining on DAF-FM^{neg} platelet sample obtained by FACS and unsorted platelet sample, and evaluated the percentage of eNOS^{neg} platelets by flow cytometry (Figure 4.5, Panel B). As compared to unsorted platelet sample, FACS-sorted DAF-FM^{neg} platelets showed higher levels

of eNOS^{neg} platelets (Figure 4.5, Panel B-C). This confirms that majority of low/non-NO-producing platelets are in fact NOS^{neg} platelets.

In addition, we also performed pharmacological validation of NO production by human platelets using light transmission aggregometry. During platelet aggregation induced by high concentration of collagen (3 μg/ml) the NOS inhibitor L-NAME reversed inhibitory effect of L-arginine on platelet aggregation. (Figure 4.6, Panel A-B).

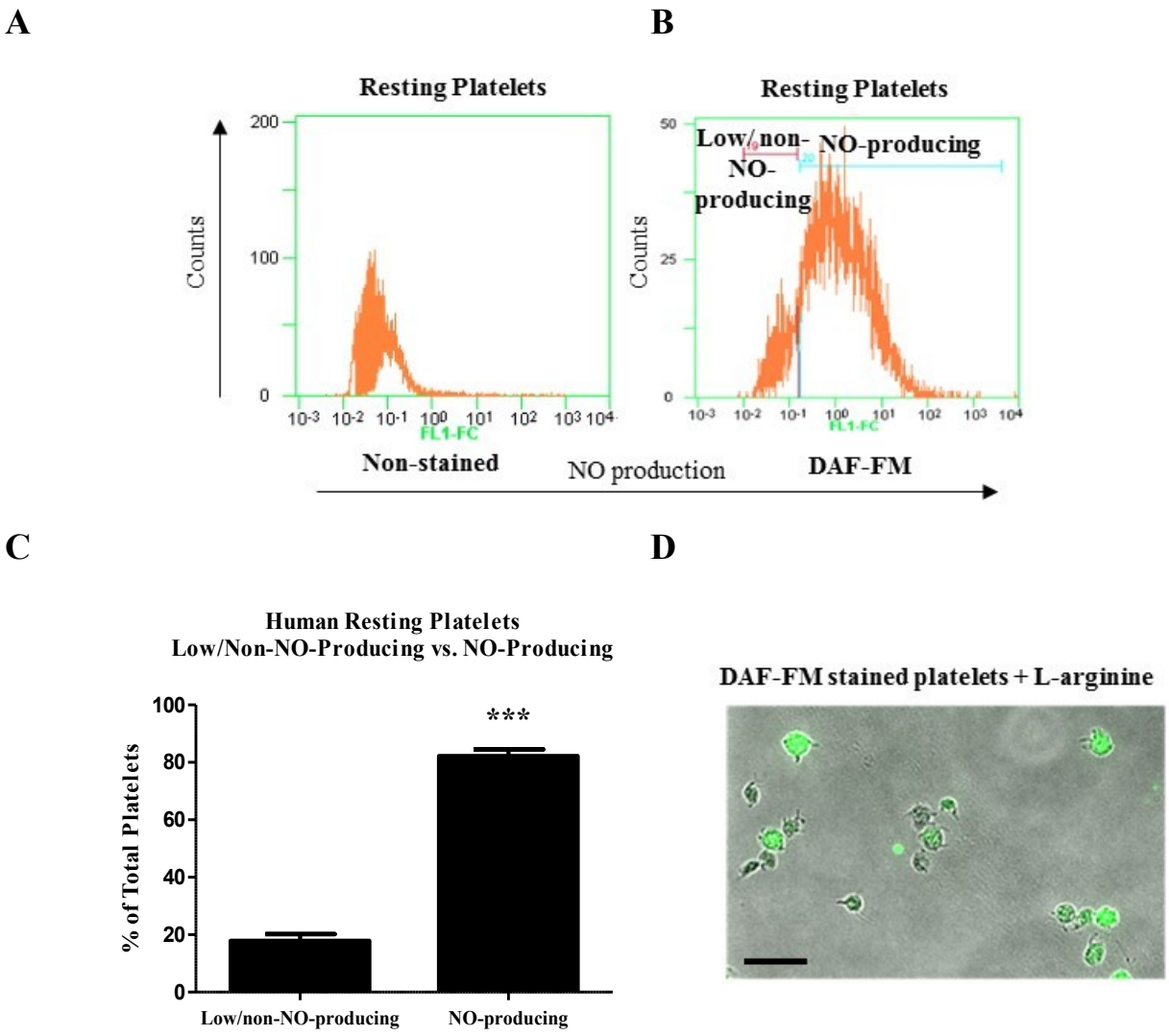

Figure 4.4. Identification of low/non-NO-producing and NO-producing platelet subpopulations

Representative fluorescence concentration histograms of **(A)** non-stained and **(B)** DAF-FM-stained platelets. **(C)** Summary bar graph of levels of low/non-NO producing and NO-producing human platelets. Statistics: paired, two-tailed Student's *t*-tests. $N = 4$. $^{***}P < 0.0001$. **(D)** Brightfield fluorescence microscopy showing NO-producing human platelets (green fluorescence) and low/non NO-producing platelets (no fluorescence). Scale bar = 10.0 μm. (Fluorescence microscopy was performed by Dr. Radziwon-Balicka).

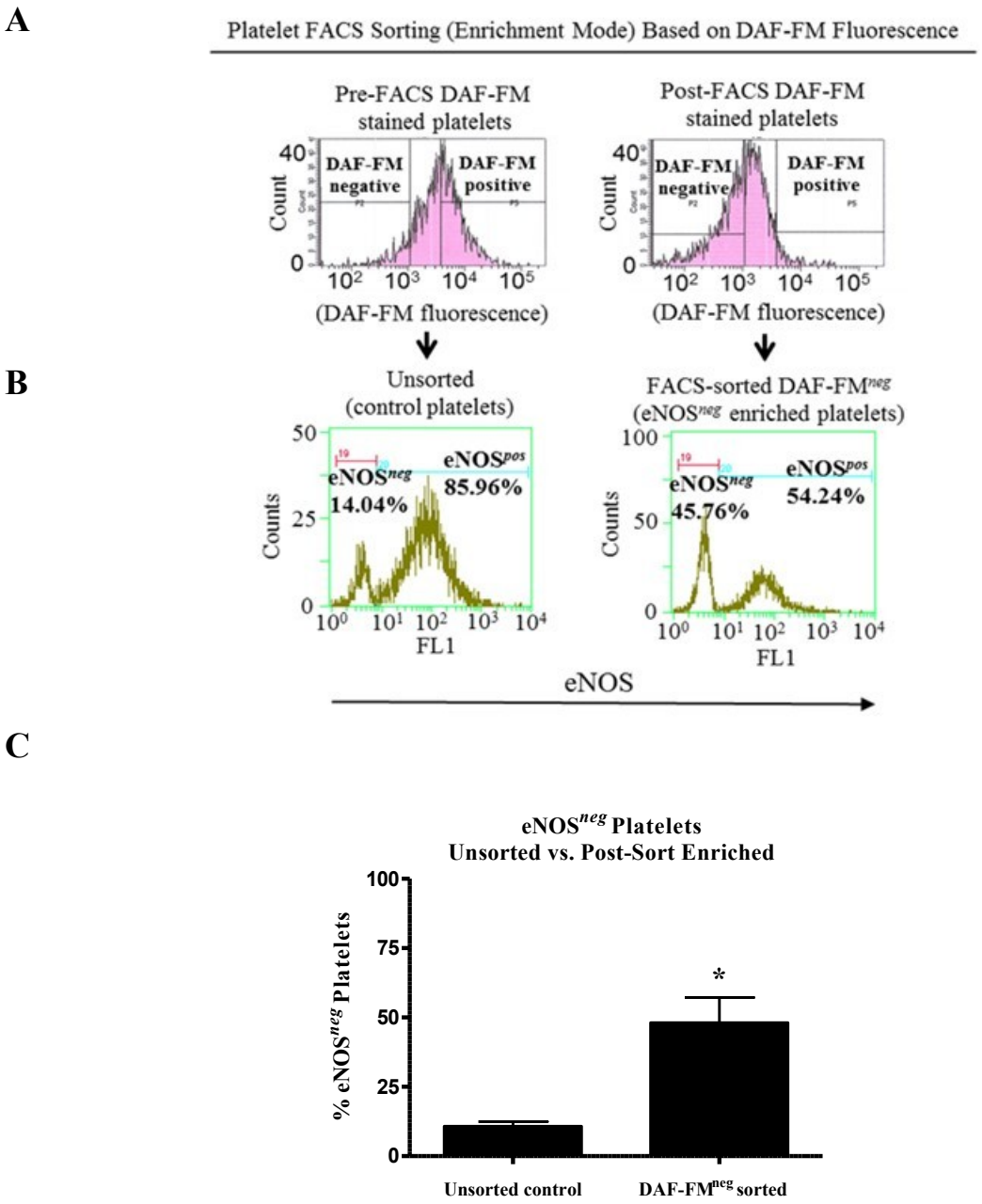

Figure 4.5. Platelet fluorescence-activated cell sorting based on DAF-FM staining

(A) Representative platelet DAF-FM fluorescence histograms and gating strategy defining DAF-FM-negative platelets (sample evaluation prior to and following FACS). **(B)** Representative eNOS fluorescence histograms of unsorted platelet sample and FACS-sorted DAF-FM^{neg} platelet sample. **(C)** Summary data of flow cytometry demonstrating that DAF-FM-based sorting enriched levels of eNOS^{neg} platelets. Statistics: paired, two-tailed Student's *t*-tests. $N = 3$. $^{*}P < 0.05$.

A

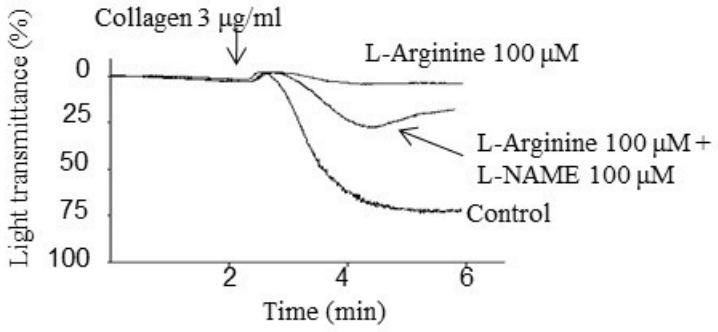

B

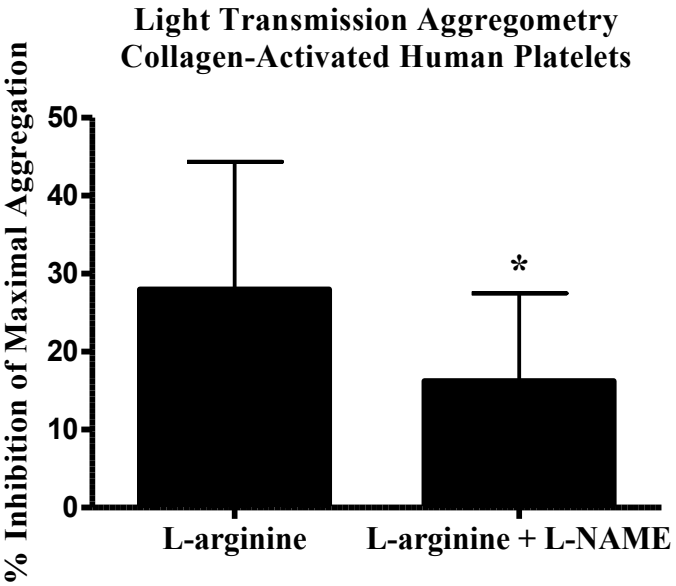

Figure 4.6. Platelet-derived NO limits platelet aggregation

(A) Representative platelet aggregometry trace demonstrating that the NOS inhibitor L-NAME reverses the inhibitory effect of L-arginine on platelet aggregation induced by a high concentration of collagen (3 µg/ml). **(B)** Summary bar graphs of platelet aggregometry. Statistics: paired, two-tailed Student's *t*-tests. $N = 5$. $^{*}P < 0.05$. (Platelet aggregometry performed by Dr. Radziwon Balicka).

4.4 Validation of DAF-FM Diacetate Specificity and Sensitivity for NO

Since some DAF-based NO indicators have been criticized as non-specific, we decided to validate DAF-FM diacetate specificity toward NO [580]. DAF-FM diacetate is a cell-permeable dye which is trapped within the platelets by action of intracellular esterases that cleave off the diacetate groups of DAF-FM diacetate. DAF-FM within the unbound form is weakly fluorescent but reaction with NO results in formation of its benzotriazole derivative which is highly fluorescent [575].

We performed mass spectrometry analysis on lysates of DAF-FM diacetate stained platelets to determine if we could detect its benzotriazole derivative (NO-bound form) (Figure 4.7, Panel A). The DAF-FM signal ($C_{21}H_{14}F_2N_2O_5$; *m/z* = 413.1) was detected in positive ionization mode [ES+] and the final metabolic product - benzotriazole derivate ($C_{21}H_{10}F_2N_3O_5$**)** was detected as the corresponding triple anion form (*m/z* = 421.1**)** in negative ionization mode [ES-] (Figure 4.7, Panel B).

Using flow cytometry we further confirmed DAF-FM specificity by stimulating HMVEC to generate NO with known eNOS activating agonist - VEGF. As depicted in Figure 4.8, Panel A, DAF-FM was able to detect changes in NO-production of maximally stimulated (50 ng/ml $VEGF_{165}$) HMVEC, as summarized in Figure 4.8, Panel B.

In addition, we also performed pharmacological validation of DAF-FM diacetate specificity for NO. Platelet NO-production was stimulated by collagen (5 μg/ml) in the presence of L-arginine (100 μM) using light transmission aggregometry. Subsequent flow cytometry analysis showed that the NOS inhibitor L-NAME reduced DAF-FM fluorescence, while SOD and a cell permeable SOD mimetic (TEMPOL) did not. This further confirmed the specificity of DAF-FM for NO detection (Figure 4.9, Panel A).

We also confirmed platelet NO-production with non-DAF-FM copper-based NO specific fluorescent probe - CuFL2E (20 μM). Platelet NO-production was stimulated by collagen (5 μg/ml) in the presence of L-arginine (100 μM) using light transmission aggregometry. Subsequent flow cytometry analysis showed that the NOS inhibitor L-NAME (100 μM) reduced CuFL2E-fluorescence but not superoxide dismutase (SOD) (100 U/ml), which further confirmed our findings of platelets ability to generate NO measured by DAF-FM diacetate (Figure 4.9, Panel B).

A

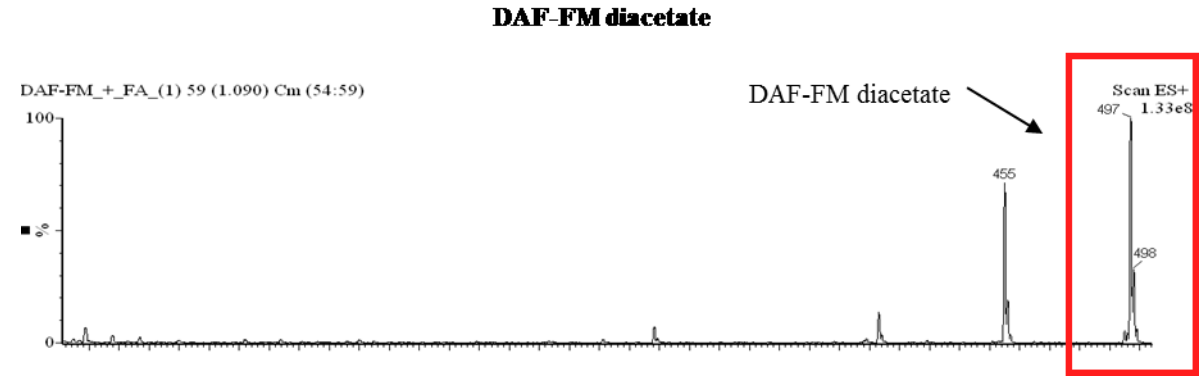

B

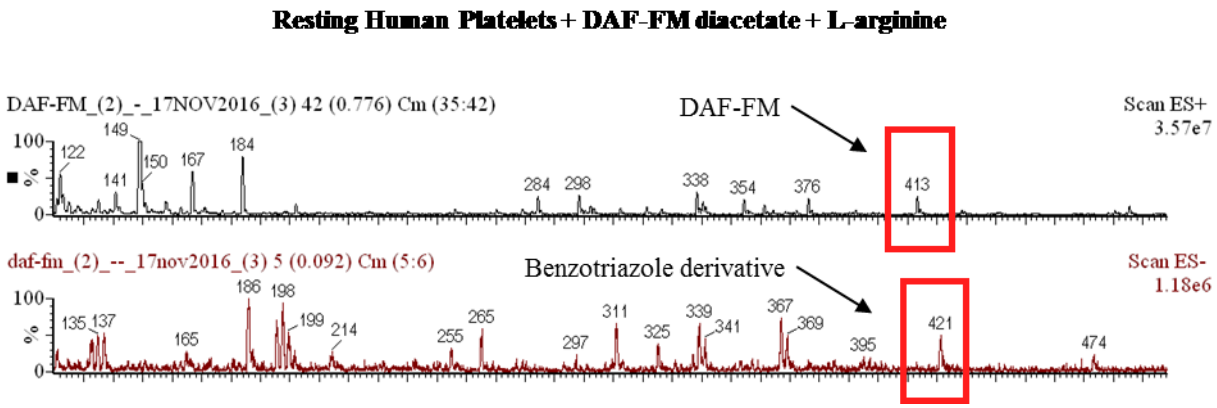

Figure 4.7. Mass spectrometry analysis of DAF-FM diacetate specificity toward NO

(A) Representative mass spectrum of DAF-FM diacetate. **(B)** Representative mass spectrum of DAF-FM ($C_{21}H_{14}F_2N_2O_5$; *m/z* = 413.1; ES+) and its benzotriazole derivative (NO-bound form) ($C_{21}H_{10}F_2N_3O_5$; *m/z* = 421.1; ES-**)** within resting platelets. *N* = 3. (Mass spectrometry analysis was performed by Dr. Carlos Velazquez-Martinez).

A

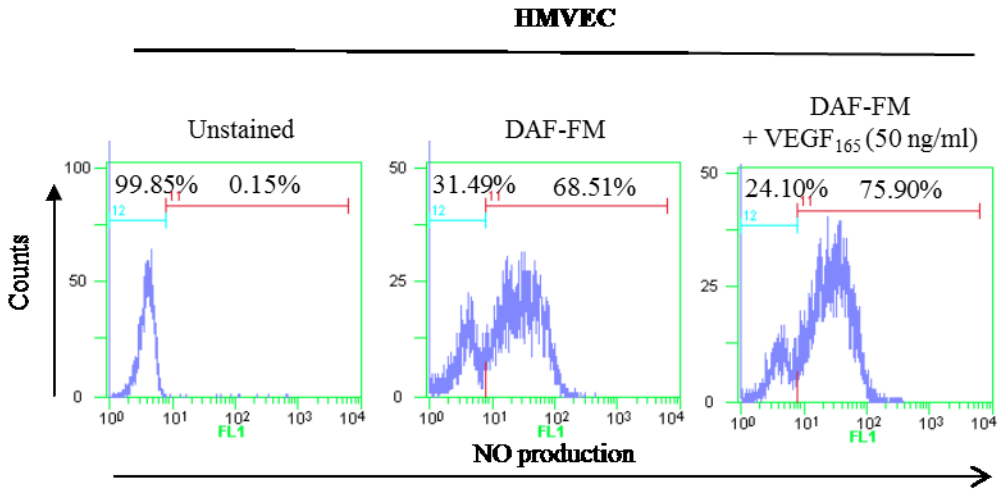

B

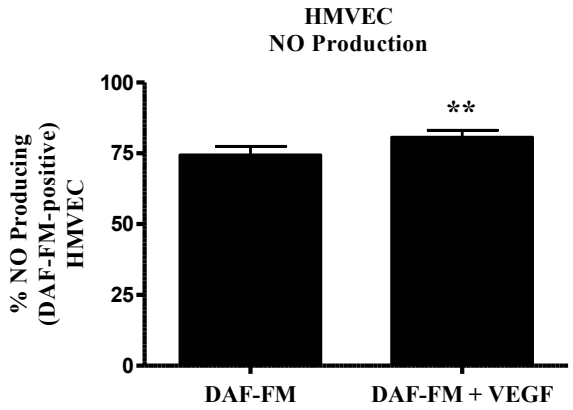

Figure 4.8. Flow cytometry analysis of DAF-FM diacetate specificity toward NO

(A) Representative flow cytometry histograms showing NO-production by HMVEC measured as mean fluorescence intensity. **(B)** Summary bar graph of DAF-FM diacetate specificity in detecting changes in NO-production. Statistics: paired, two-tailed Student's *t*-tests. $N = 3$. $^{**}P < 0.01$.

A

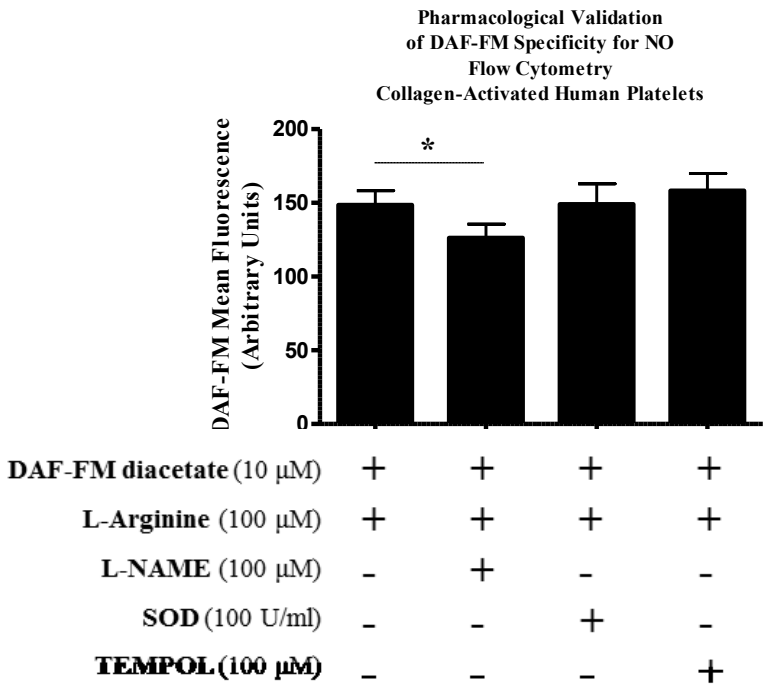

B

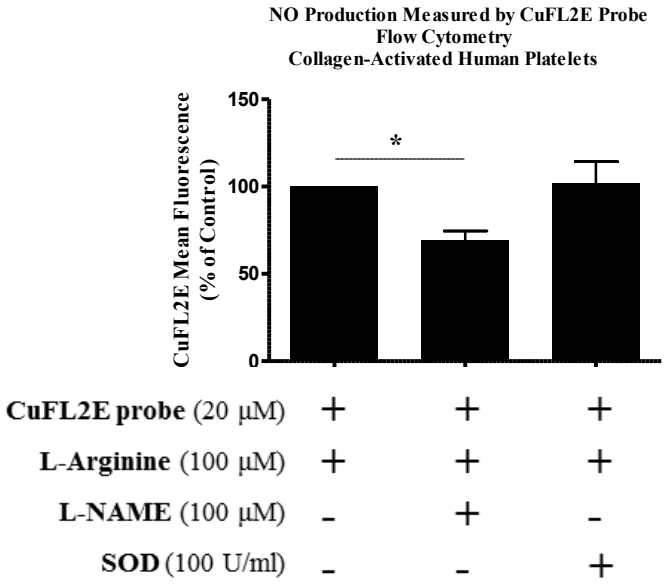

Figure 4.9. Pharmacological validation of platelet NO generation measured by DAF-FM diacetate and NO specific fluorescent probe (CuFL2E) (A) Summary data of platelet NO generation measured as mean fluorescence intensity of DAF-FM diacetate by flow cytometry. Statistics: One-way ANOVA with Dunnett post-hoc test. $N = 4$. $^*P < 0.05$. **(B)** Summary data of platelet NO generation measured as mean fluorescence intensity of CuFL2E probe by flow cytometry. Statistics: One-way ANOVA with Dunnett post-hoc test. $N = 4$. $^*P < 0.05$

4.5 eNOS-Negative Platelets Have a Downregulated sGC-PKG Signalling Pathway

To determine whether other biochemical differences exist between eNOS^{neg} and eNOS^{pos} platelets downstream of NO we investigated their sGC-PKG pathway.

First we looked at levels of platelet intracellular NO receptor - sGC in eNOS^{pos} and eNOS^{neg} platelets using flow cytometry. Based on eNOS-gating we determined that eNOS^{neg} platelets had significantly lower level of sGC comparing to eNOS^{pos} platelets measured as fluorescence concentration (1.18 ± 0.09 vs. 1.83 ± 0.22, arbitrary units of fluorescence, $P < 0.05$), which is showed and summarized in the Figure 4.10, Panel A-B.

Activation of sGC following NO binding catalyzes cGMP synthesis and because eNOS^{neg} platelets had less sGC, we hypothesized that as an effect they will generate less cGMP than eNOS^{pos} platelets. To preserve platelet functions and measure platelet cGMP synthesis we used DAF-FM staining and separated platelets based on their ability to generate NO by FACS-sorting as showed above in Figure 4.5, Panel A. FACS-sorted DAF-FM-negative (DAF-FM^{neg}) and DAF-FM-positive (DAF-FM^{pos}) platelets were stimulated with collagen (10 μg/mL) and cGMP was measured by ELISA. As compared to DAF-FM^{pos} platelets, DAF-FM^{neg} platelets generated significantly less cGMP upon activation with collagen (100.0% vs. 54.2 ± 11.9%, $P < 0.05$) (Figure 4.11, Panel A).

Next we compared levels of cGMP downstream target – PKG between eNOS^{neg} and eNOS^{pos} platelet subtypes using flow cytometry. Based on eNOS-gating we determined that eNOS^{neg} platelets had significantly lower level of PKG when compared to eNOS^{pos} platelets measured as fluorescence concentration (0.79 ± 0.21 vs. 5.76 ± 1.52, arbitrary units of fluorescence, $P < 0.05$) (Figure 4.12, Panel A-B).

Because eNOS^{neg} platelets had lower levels of PKG than eNOS^{pos} platelets we decided to compare levels of PKG downstream phosphorylation target - VASP between two eNOS-based platelet subtypes. Phosphorylation of VASP by PKG enables its binding to platelet cytoskeleton, which inhibits platelet integrin $\alpha_{IIb}\beta_3$ activation. Using flow cytometry and based on eNOS-gating we determined that eNOS^{neg} platelets had significantly lower level of VASP protein when compared to eNOS^{pos} platelets measured as fluorescence concentration (5.89 ± 1.80 vs. 12.75 ± 3.61, arbitrary units of fluorescence, $P < 0.05$) (Figure 4.13, Panel A-B).

Phosphorylated VASP localizes close to integrin $\alpha_{IIb}\beta_3$ focal adhesion sites and inhibits fibrinogen binding, which ultimately prevents formation of platelet aggregates. Since eNOS^{neg} platelets had lower levels of VASP than eNOS^{pos} platelets we decided to compare extent of $\alpha_{IIb}\beta_3$ activation between two eNOS-based platelet subtypes following collagen (3 μg/ml) stimulation. Based on eNOS-gating we determined that significantly greater percentage of eNOS^{neg} platelets showed activated integrin $\alpha_{IIb}\beta_3$ when compared to eNOS^{pos} platelets, measured as mean fluorescence intensity (87.9 ± 5.5% vs. 51.5 ± 8.2%, $P < 0.05$) (Figure 4.14, Panel A-B).

Taken together, above data show that eNOS^{neg} platelets have absent/down-regulated sGC-PKG signalling pathway which upon stimulation with platelet agonist results in enhanced $\alpha_{IIb}\beta_3$ activation by eNOS^{neg} platelets (Figure 4.15).

A

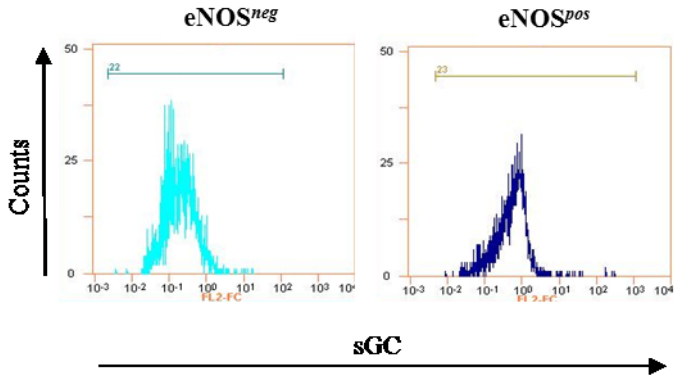

B

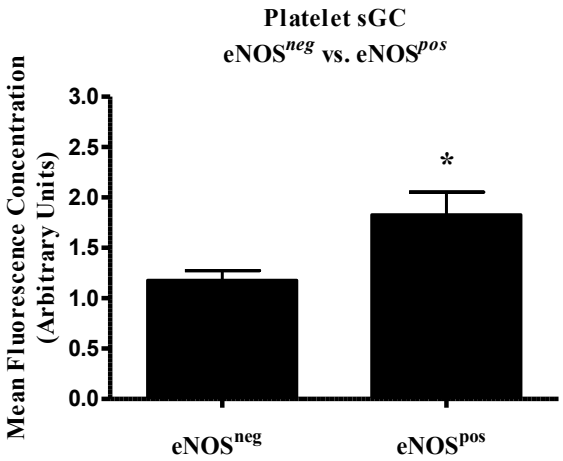

Figure 4.10. Flow cytometry analysis of sGC levels in eNOSneg and eNOSpos human platelets

(A) Representative flow cytometry histograms showing sGC levels in eNOS^{neg} and eNOS^{pos} platelets measured as fluorescence concentration. **(B)** Summary bar graph of sGC levels in eNOS^{neg} and eNOS^{pos} human platelets. Statistics: paired, two-tailed Student's *t*-tests. $N = 4$. $^{*}P < 0.05$. (Flow cytometry was performed by Dr. Radziwon-Balicka).

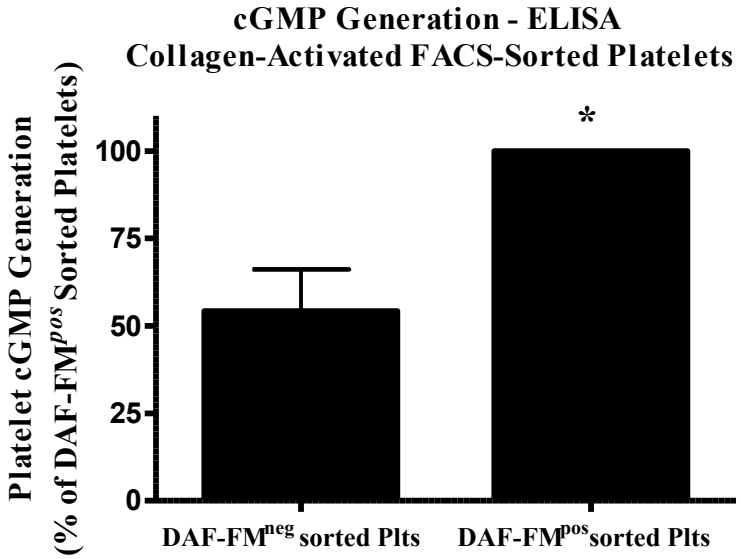

Figure 4.11. Generation of cGMP by DAF-FMneg and DAF-FMpos human platelets

Summary bar graph of cGMP generation by collagen (10 μg/ml) stimulated FACS-sorted DAF-FM^{neg} and DAF-FM^{pos} human platelets (Plts**)** measured by ELISA. Statistics: paired, two-tailed Student's *t*-tests. $N = 4$. *$P < 0.05$.

A

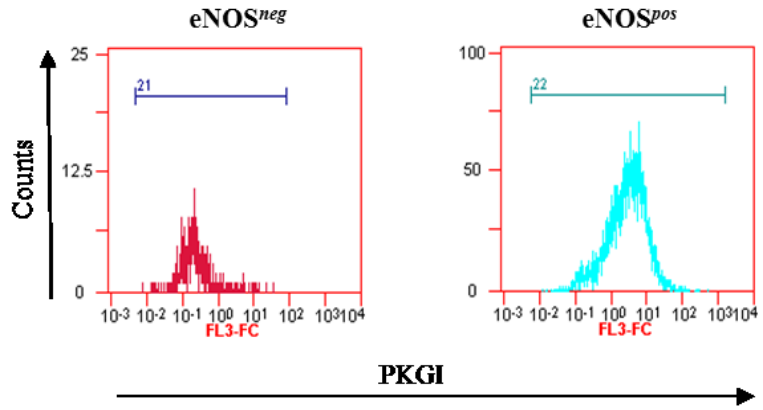

B

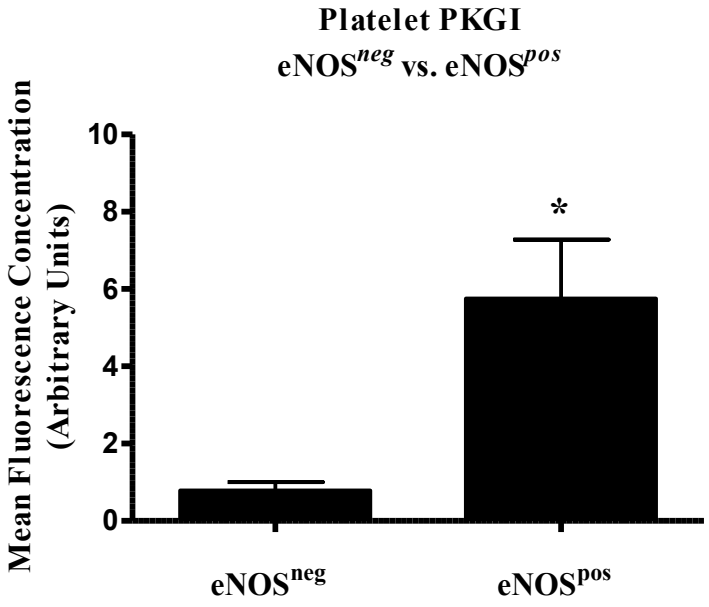

Figure 4.12. Flow cytometry analysis of PKGI levels in eNOSneg and eNOSpos human platelets

(A) Representative flow cytometry histograms showing PKGI levels in eNOS^{neg} and eNOS^{pos} platelets measured as fluorescence concentration. **(B)** Summary bar graph of PKGI levels in eNOS^{neg} and eNOS^{pos} human platelets. Statistics: paired, two-tailed Student's *t*-tests. $N = 5$. *$P < 0.05$. (Flow cytometry was performed by Dr. Radziwon-Balicka).

A

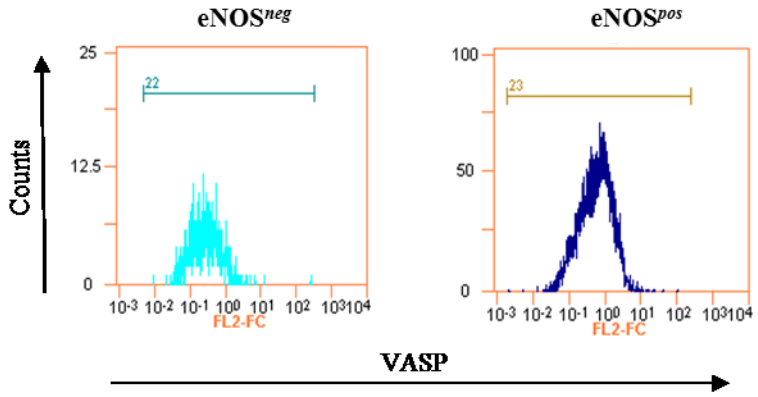

B

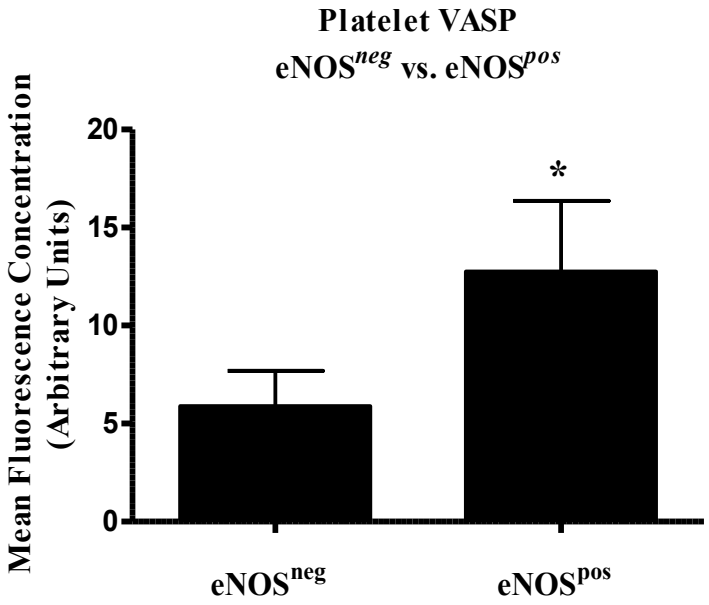

Figure 4.13. Flow cytometry analysis of VASP levels in eNOSneg and eNOSpos human platelets

(A) Representative flow cytometry histograms showing VASP levels in eNOS^{neg} and eNOS^{pos} platelets measured as fluorescence concentration. **(B)** Summary bar graph of VASP levels in eNOS^{neg} and eNOS^{pos} human platelets. Statistics: paired, two-tailed Student's *t*-tests. $N = 5$. $^{*}P < 0.05$. (Flow cytometry was performed by Dr. Radziwon-Balicka).

A

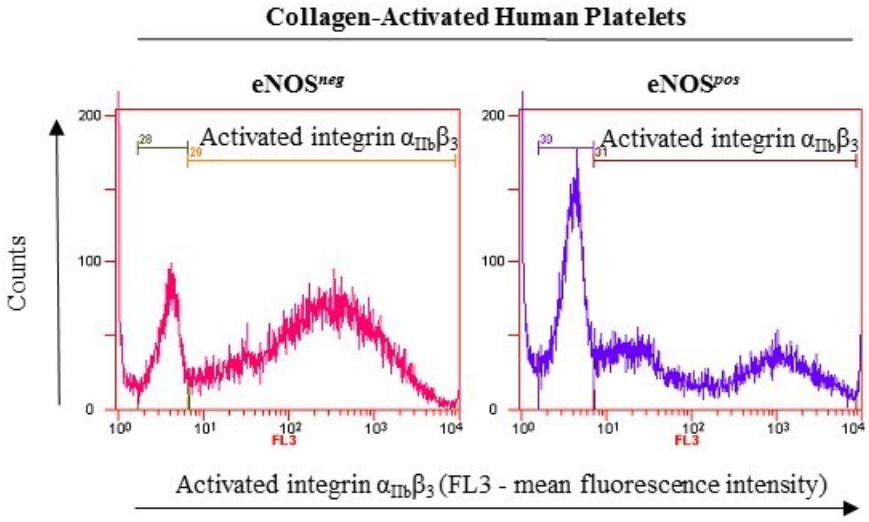

B

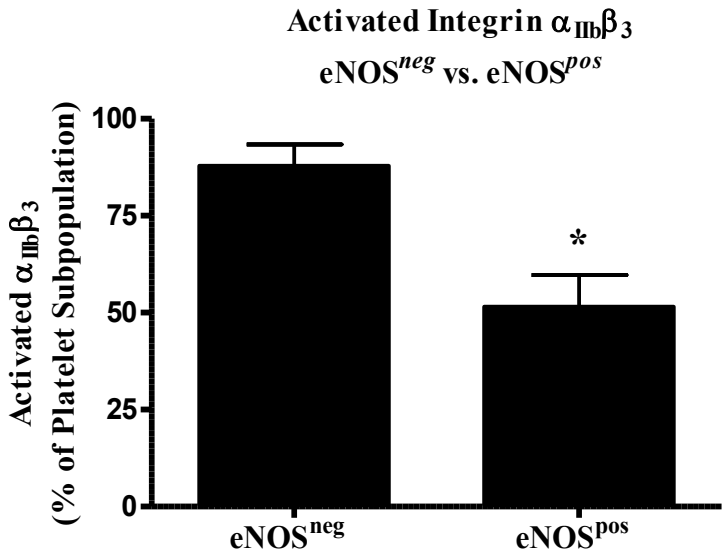

Figure 4.14. Flow cytometry analysis of activated integrin αIIbβ3 on eNOSneg and eNOSpos human platelets

(A) Representative mean fluorescence intensity histograms of activated $\alpha_{IIb}\beta_3$ (PAC-1 antibody) integrin on eNOS^{neg} and eNOS^{pos} human platelets stimulated with collagen (3 μg/ml)**. (B)** Summary data showing percent of eNOS^{neg} and eNOS^{pos} with activated $\alpha_{IIb}\beta_3$ integrin. Statistics: paired, two-tailed Student's *t*-tests. $N = 4$. $^*P < 0.05$.

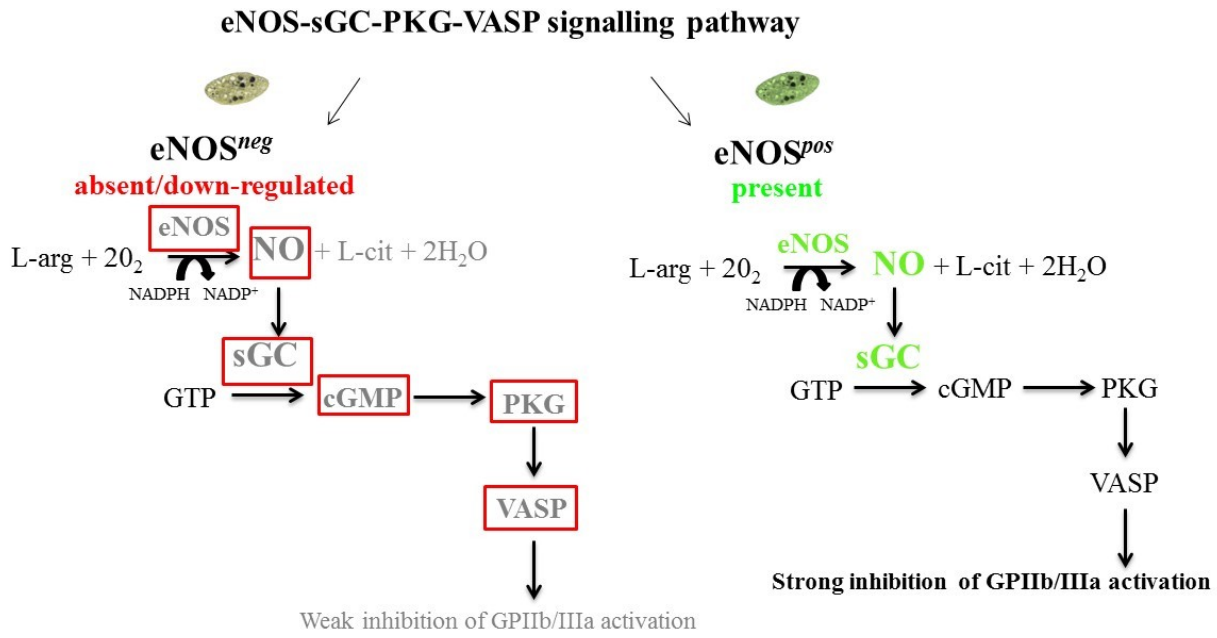

Figure 4.15. A cartoon summarizing biochemical differences of sGC-PKG signalling pathway between eNOS^{neg} and eNOS^{pos} platelets

Human eNOS^{neg} platelets have absent/down-regulated eNOS-sGC-PKG-VASP signalling pathway while eNOS^{pos} platelets have this pathway present. Absent/down-regulated eNOS-sGC-PKG-VASP signalling pathway of eNOS^{neg} results in weak inhibition of their integrin $\alpha_{IIb}\beta_3$ activation.

4.6 eNOS-Based Platelet Subpopulations Have Different Levels of Mediators that Regulate Platelet Aggregation

After indentifying that eNOS^{neg} platelets have a downregulated sGC-PKG signalling pathway and more readily activate their integrin $\alpha_{IIb}\beta_3$ in response to collagen, we decided to further investigate other biochemical differences between eNOS^{neg} and eNOS^{pos} platelets. In a growing platelet plug aggregation is amplified by secretion of endogenous platelet agonist such as TXA_2, ADP and MMP-2.

According to our studies secretion of latent form of MMP-2 called pro-MMP-2 occurs early on in the platelet aggregation process and reaches maximum at platelet shape change as depicted and summarized in the Figure 4.16, Panel A-C. This result is consistent with a previously described platelet aggregation priming effect of MMP-2 [164]. Therefore, we first decided to measure the MMP-2 pathway of aggregation in eNOS-based platelet subpopulations. To preserve platelet functions and measure platelet MMP-2 secretion we used DAF-FM staining and separated platelets based on their ability to generate NO by FACS-sorting. The DAF-FM^{neg} and DAF-FM^{pos} platelet samples obtained from FACS-sorting were lysed and gelatin zymography performed to determine intra-platelet MMP-2 levels. DAF-FM^{pos} platelets showed lower pro-MMP-2 levels when compared to DAF-FM^{neg} platelets (48.97 ± 20.57% vs.100%, $P < 0.05$), as presented and summarized in Figure 4.17, Panel A-B.

Next, we measured the amount of COX-1 in eNOS-based platelet subpopulations to establish whether they have similar enzymatic baseline for *de novo* synthesis of TXA_2. Using flow cytometry, we measured the level of COX-1 in eNOS^{pos} and eNOS^{neg} platelets. Based on eNOS-gating we determined that eNOS^{pos} platelets had higher level of COX-1 when compared to eNOS^{neg} platelets (4.50 ± 0.94 vs. 1.48 ± 0.43, arbitrary units of fluorescence, $P < 0.001$) (Figure 4.18, Panel A-B).

Consequently, we decided to delineate generation of TXA_2 in DAF-FM^{neg} and DAF-FM^{pos} FACS sorted platelets. Using LC-ESI-MS we assessed generation of TXA_2 by detecting its stable metabolite - TXB_2 in DAF-FM^{neg} and DAF-FM^{pos} FACS sorted platelets stimulated with collagen (10 μg/mL). Consistently with our findings showing that DAF-FM^{pos} platelets had higher levels of COX-1 they also generated significantly more TXA_2 than DAF-FM^{neg} platelets,

as determined by the measurement of the stable metabolite TXB_2 (DAF-FM^{pos} 43.2 ± 9.2 vs. DAF-FM^{neg} 25.4 ± 6.9 ng per 10^8 platelets, $P < 0.05$) (Figure 4.19).

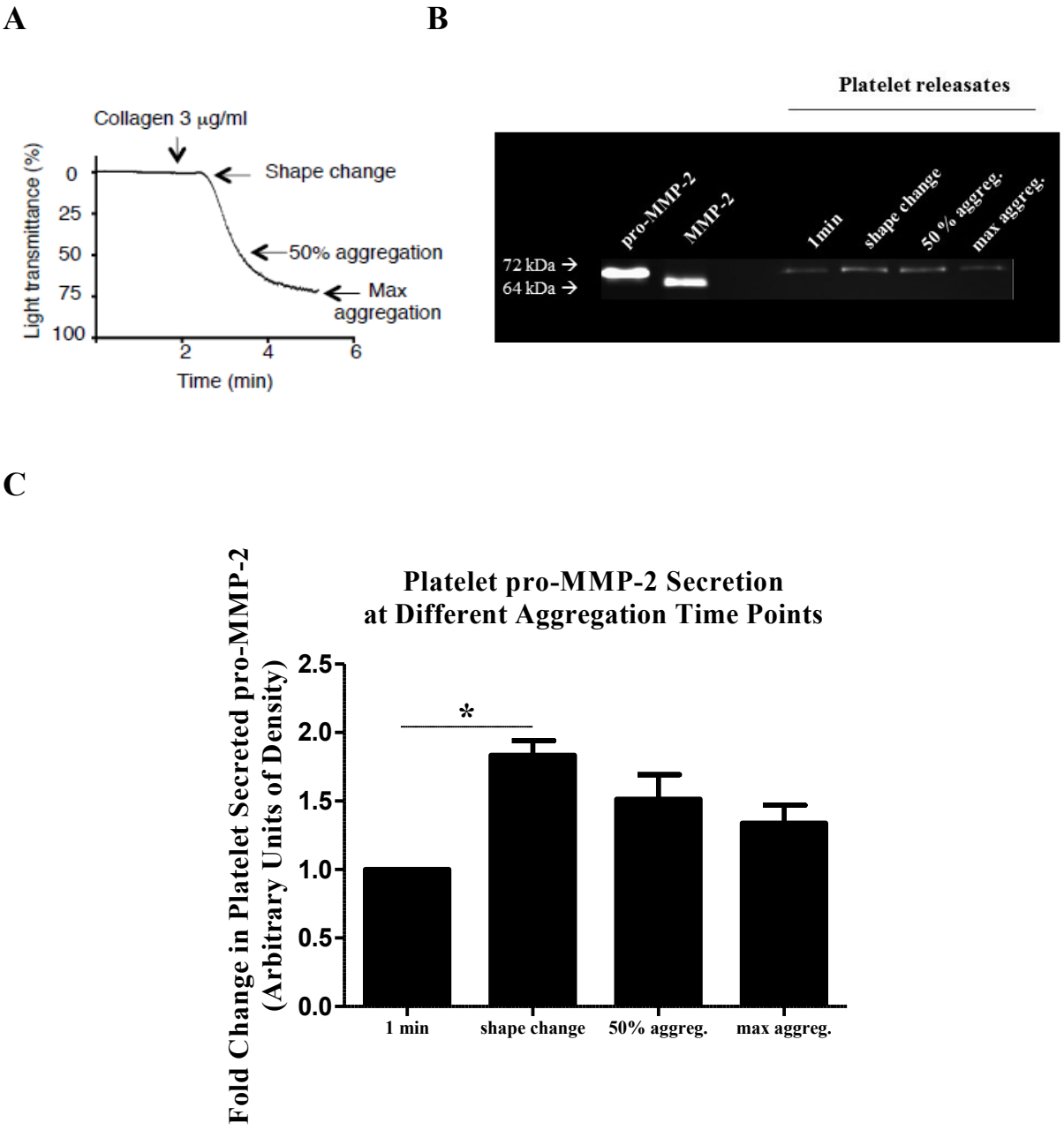

Figure 4.16. Platelet pro-MMP-2 secretion at different aggregation time points

(A) Representative platelet aggregometry trace indicating time points at which platelet releasates were taken for zymography analysis. **(B)** Representative zymogram of the platelet MMP-2 secretion time course. **(C)** Summary densitometry data of pro-MMP-2 secretion from platelets at different aggregation time points. Statistics: One-way ANOVA with Tukey post-hoc test. $N = 3$. $^{*}P < 0.05$.

A

B

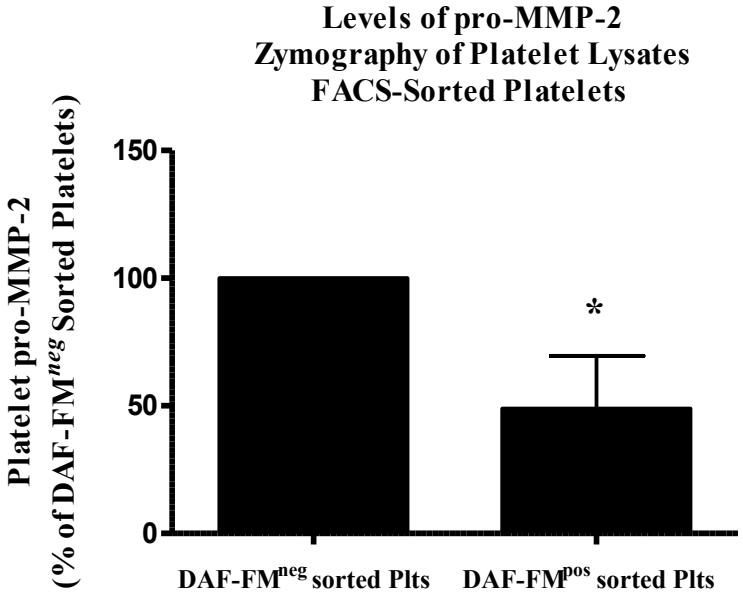

Figure 4.17. Levels of pro-MMP-2 in DAF^{neg} and DAF^{pos} FACS-sorted platelets

(A) Representative β-actin loading-controlled zymogram of platelet pro-MMP-2 in lysates from FACS-sorted DAF-FM^{neg} and DAF-FM^{pos} platelets. **(B)** Summary data of gelatin zymography showing levels of pro-MMP-2 in DAF^{neg} and DAF^{pos} FACS-sorted platelets (Plts). Statistics: paired, two-tailed Student's *t*-tests. $N = 4$. $^{*}P < 0.05$

A

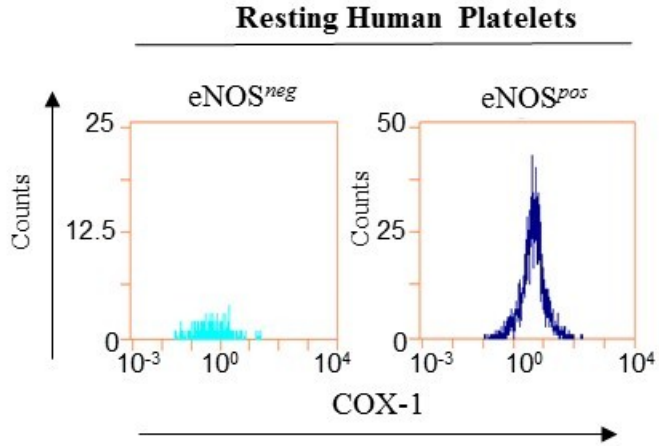

B

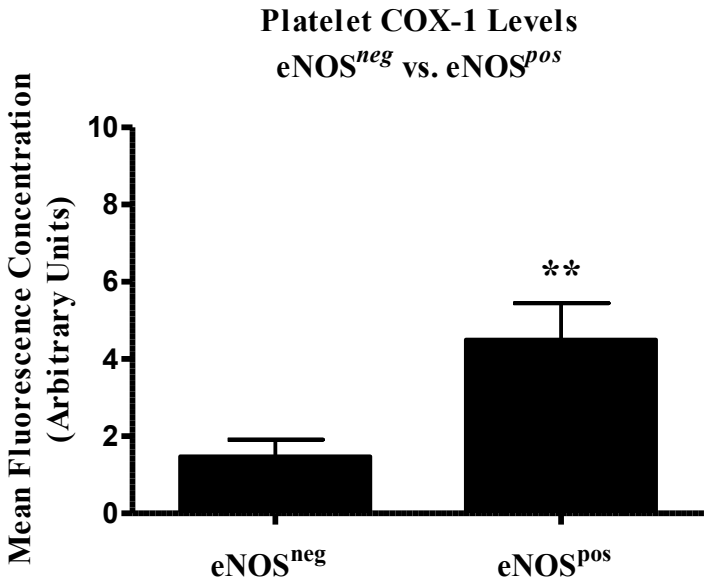

Figure 4.18. Flow cytometry analysis of COX-1 levels in eNOSneg and eNOSpos human platelets

(A) Representative flow cytometry histograms showing COX-1 levels in eNOS^{neg} and eNOS^{pos} platelets measured as fluorescence concentration. **(B)** Summary bar graph of COX-1 levels in eNOS^{neg} and eNOS^{pos} human platelets. Statistics: paired, two-tailed Student's *t*-tests. $N = 5$. $^{**}P < 0.001$. (Flow cytometry was performed by Dr. Radziwon-Balicka).

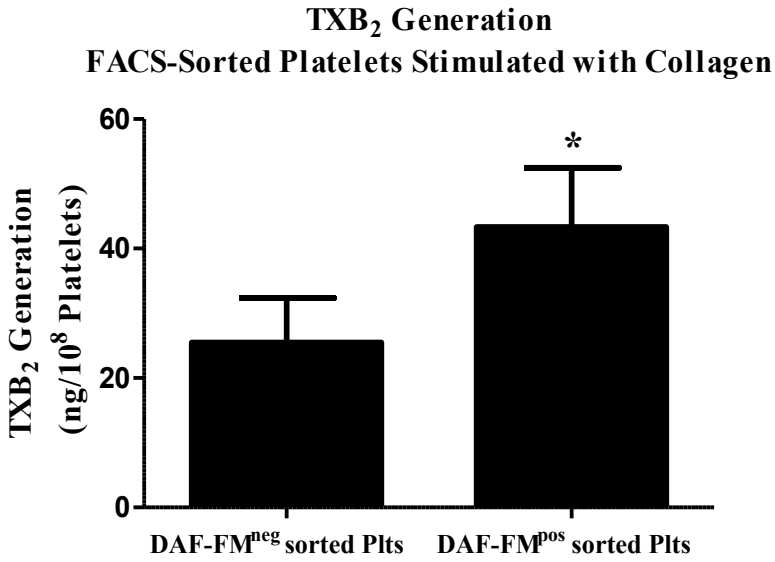

Figure 4.19. TXB_2 generation by DAF-FM^{neg} and DAF-FM^{pos} FACS-sorted platelets

Summary LC-ESI-MS data of TXB_2 generation by DAF-FM^{neg} and DAF-FM^{pos} FACS-sorted platelets in response to collagen (10 μg/mL). Statistics: paired, two-tailed Student's *t*-tests. $N = 4$. $^*P < 0.05$. (LC-ESI-MS was performed by Dr. Ahmed El-Sherbeni).

4.7 Low/Non-NO-Producing ($eNOS^{neg}$) Platelets Preferentially Adhere to Collagen and NO-Producing ($eNOS^{pos}$) Platelets Limit Size of an Aggregate via NO Generation

Based on these biochemical differences between $eNOS^{neg}$ and $eNOS^{pos}$ platelets, we further hypothesized that $eNOS^{neg}$ platelets are more reactive and hence would more readily initiate adhesion and aggregation reactions due to their down-regulated sGC-PKG signalling pathway, greater activation of integrin $\alpha_{IIb}\beta_3$ and higher levels of pro-MMP-2.

To test this hypothesis, we assessed the functional role of $eNOS^{neg}$ and $eNOS^{pos}$ platelets under flow conditions utilizing a flow chamber with collagen-coated (10 μg/ml) coverslips. Platelets were perfused (50 μl/min) over the coverslips in presence of L-arginine (100 μM) and non-adhered platelets that passed through the flow chamber were collected for further analysis to evaluate the ratio of $eNOS^{neg}$ to $eNOS^{pos}$ platelets by flow cytometry. Our data demonstrated a significant decrease in $eNOS^{neg}$ platelets in post-flow chamber sample compared to pre-flow chamber control sample, measured as % of total platelets ($22.2 \pm 3.4\%$ pre-flow control vs. $18.1 \pm 4.1\%$), confirming their preferential adhesion, as depicted and summarized in Figure 4.20, Panel A-B.

To further confirm our initial observation that $eNOS^{neg}$ platelets preferentially adhered to collagen, we performed light transmission aggregometry on DAF-FM-stained platelets stimulated with collagen (3 μg/ml) in the presence of L-arginine (100 μM) (Figure 4.21, Panel A). The qualitative fluorescence microscopy of DAF-FM-stained platelets revealed that at early stage of aggregation (shape change) low/non-NO-producing platelets were bound primarily to free strands of collagen as well to NO-producing platelets, while more abundant $eNOS^{pos}$ platelets were recruited to the growing aggregates and generated large amounts of NO seen as green fluorescence in Figure 4.21, Panel B.

Next, to better visualize and quantify preferential binding of low/non-NO-producing platelets to collagen we performed video confocal microscopy experiments of platelet adhesion to collagen under static conditions. The DAF-FM-stained platelets (pre-incubated with 100 μM L-arginine) adhered to collagen-coated (10 μg/ml) coverslips, as depicted in frames from time-lapse fluorescence microscopy in Figure 4.22, Panel A. The quantitative analysis of captured images demonstrated that, at early time points (0–5 min), significantly more low/non-NO-producing platelets adhered to collagen compared to NO-producers (Figure 4.22, Panel B). The

opposite was true at later time points (5–15 min) (Figure 4.22, Panel C). Subsequently, platelets were let to aggregate for further 45 min and the coverslips containing collagen-adhered and aggregated platelets were stained for eNOS and F-actin. Next, samples were imaged by confocal microscopy and obtained z-stacks of platelet aggregates were evaluated for eNOS-immunofluorescence (Figure 4.23, Panel A-B). The analysis of z-stacks showed low eNOS-immunofluorescence near the base (expressed as eNOS/F-actin immunofluorescence ratio) with increasing eNOS-immunofluorescence from the bottom to the top of the aggregates as summarized in Figure 4.23, Panel C-D.

Since low/non-NO-producing ($eNOS^{neg}$) platelets bound collagen at earlier time points we decided to further investigate whether NO-producing ($eNOS^{pos}$) platelets that bound at later time points limit aggregate formation by generation of NO. Hence, we decided to compare the aggregation ability of DAF-FM^{neg} and DAF-FM^{pos} FACS-sorted platelets ($eNOS^{neg}$ vs. $eNOS^{pos}$-enriched) in the presence of L-arginine (100 μM). Because the viability of platelets in vitro is limited to a few hours, FACS sorting was unable to yield enough platelets in a timely manner to compare the two subpopulations by classical light transmission aggregometry. Instead we used the aggregometer only to induce platelet aggregation in response to collagen (1 μg/ml) under stirring conditions. Subsequently, we evaluated area of the aggregates formed by DAF-FM^{neg} and DAF-FM^{pos} platelet samples using phase-contrast microscope and ImageJ analysis software. The results demonstrated that in response to collagen DAF-FM^{neg} platelets formed significantly larger aggregates than DAF-FM^{pos} platelets, measured as the mean aggregate area, which indicates that $eNOS^{pos}$ platelets limit aggregate size by generating NO (Figure 4.24, Panel A-C). This observation is supported by our experiment where inhibition of platelet NO production by L-NAME resulted in enhanced platelet aggregation in the presence of L-arginine (Figure 4.6).

A

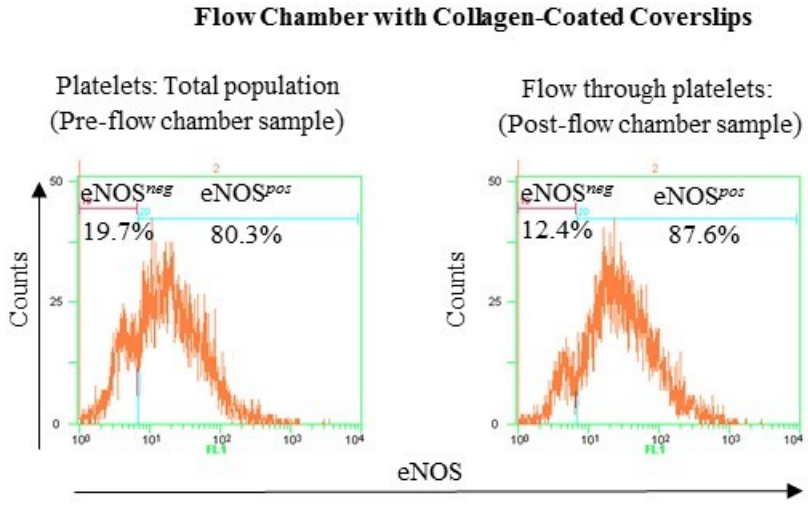

B

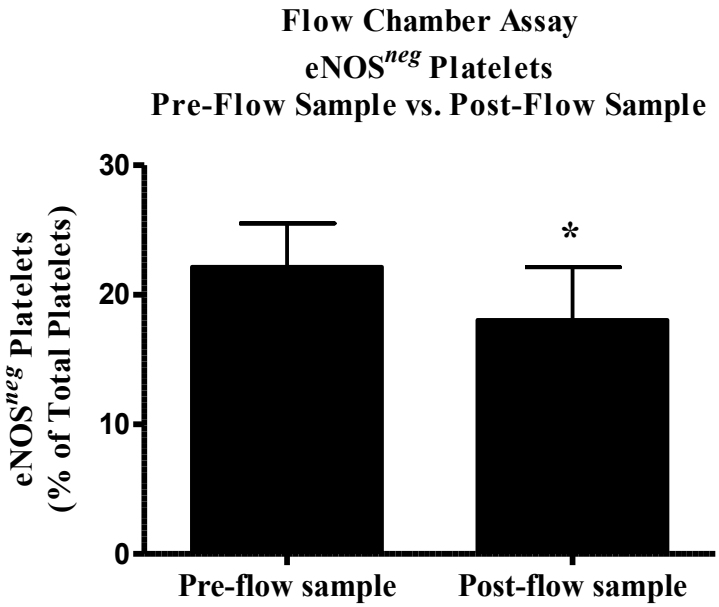

Figure 4.20. Preferential adhesion of eNOS^{neg} platelets to collagen under flow conditions

(A) Representative flow cytometry histograms of pre- and post-flow chamber samples showing % of eNOS^{neg} and eNOS^{pos} platelets. **(B)** Summary data of the percentage of eNOS^{neg} platelets in pre- vs. post-flow chamber samples. Statistics: paired, two-tailed Student's *t*-tests. $N = 4$. $^{*}P < 0.05$.

A

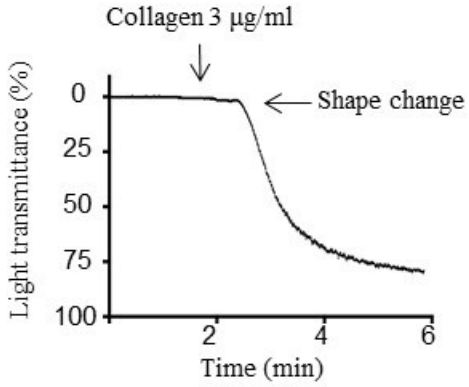

B

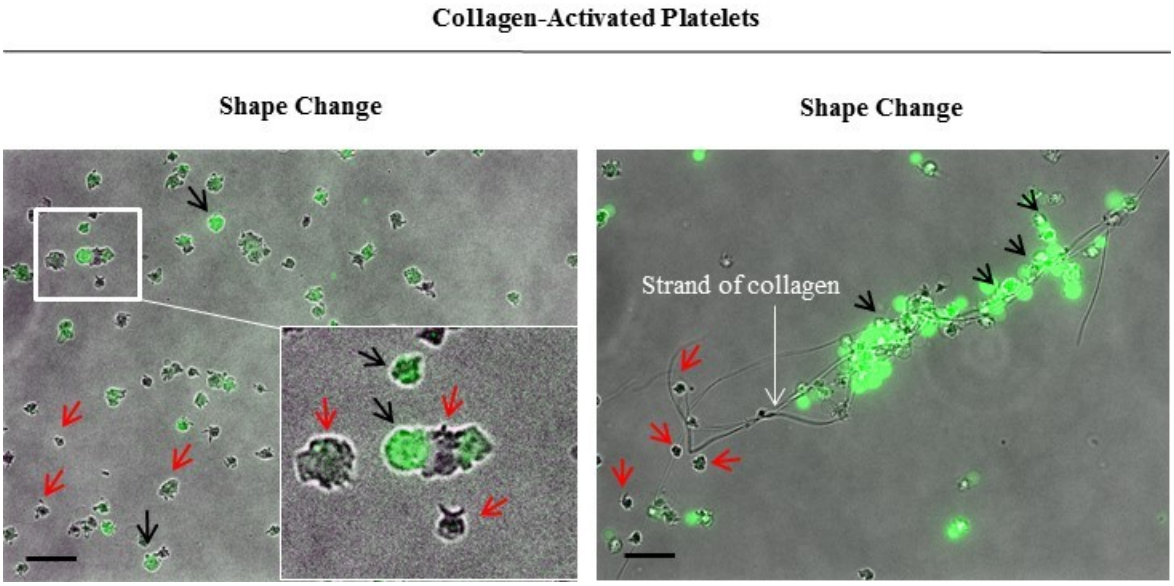

Figure 4.21. Preferential adhesion of eNOSneg platelets to collagen is followed by recruitment of eNOSpos platelets to the growing aggregates and generation of large amounts of NO (A) Representative platelet aggregometry trace indicating time point (shape change), at which DAF-FM-stained platelet samples were taken for fluorescence microscopy. **(B)** Merged brightfield-fluorescence microscopy images of low/non-NO-producing and NO-producing platelets binding to collagen strands (white arrow) and each other (inset). Black arrows indicate platelets producing large amounts of NO. Red arrows indicate platelets producing low or no NO. Representative images from $N = 3$. Scale bars = 10 µm. (Fluorescence microscopy was performed by Dr. Radziwon-Balicka).

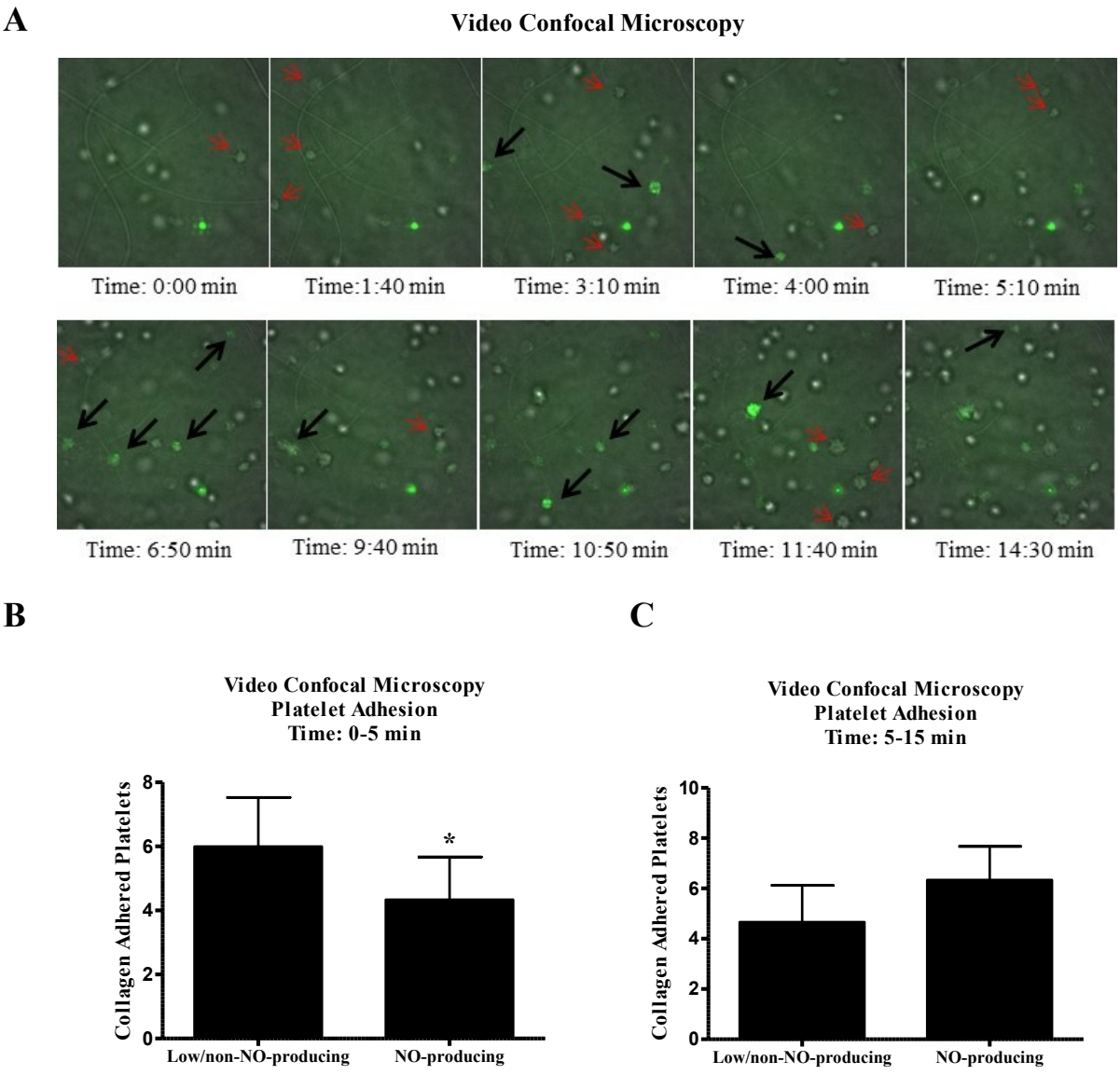

Figure 4.22. Low/non-NO-producing platelets initiate adhesion and aggregation reactions while NO-producing platelets adhere at later time points (A) Merged brightfield-fluorescence microscopy frames from confocal microscopy video of DAF-FM-stained human platelets adhering to collagen-coated coverslips under static conditions. Red arrows indicate low/no-NO-producing platelets and black arrows indicate NO-producing platelets. Bars indicate 10 μm. **(B)** Summary data of low/non-NO-producing and NO-producing platelets binding to collagen at early time points (0–5 min). Statistics: paired, two-tailed Student's *t*-tests. $N = 3$. $^*P < 0.05$. **(C)** Summary data of low/non-NO-producing and NO-producing platelets binding to collagen at later time points (5–15 min). Statistics: paired, two-tailed Student's *t*-tests. $N = 3$. Ns, $P > 0.05$. (Fluorescence microscopy was performed by Dr. Radziwon-Balicka).

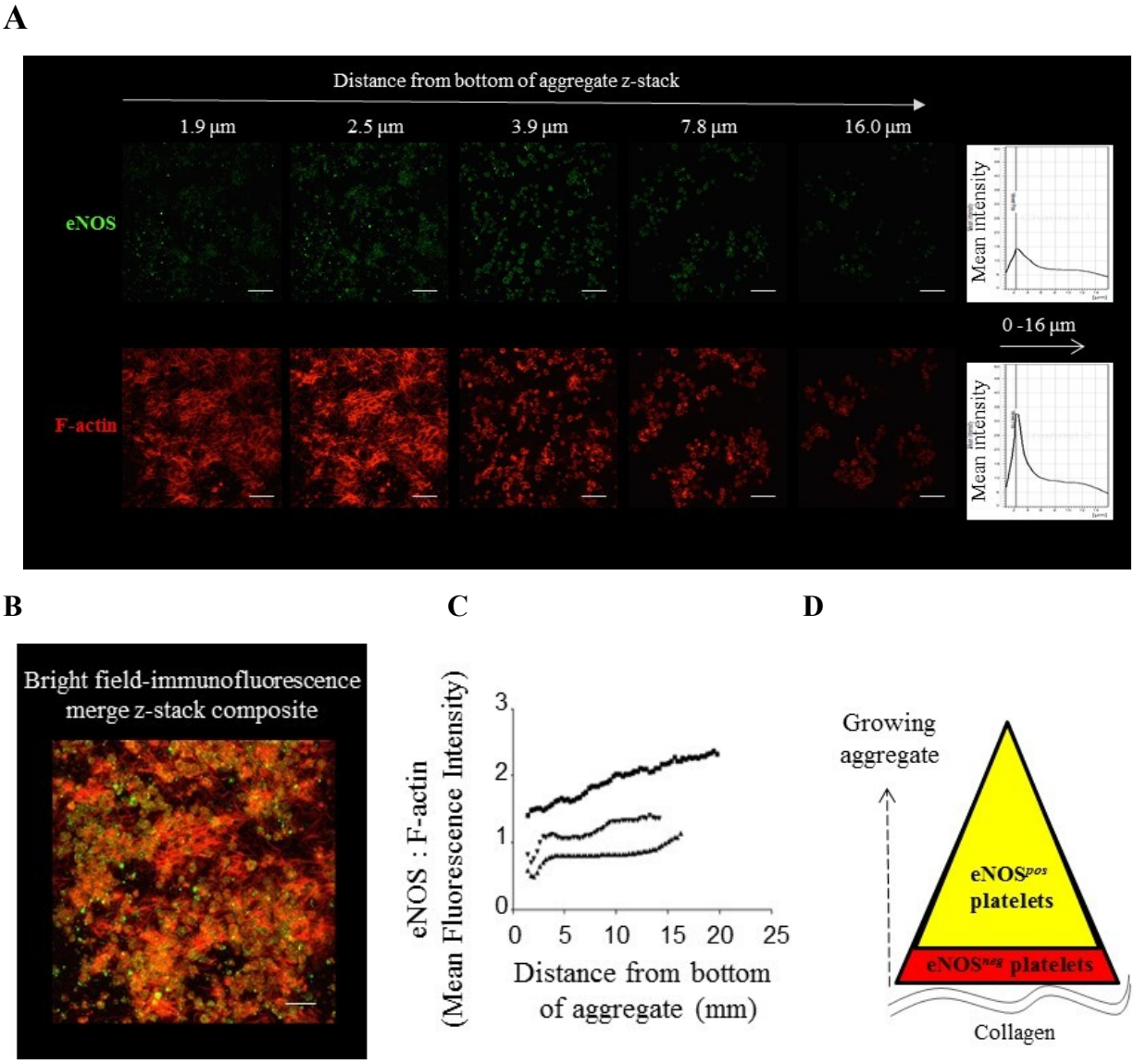

Figure 4.23. Localization of eNOS^{neg} and eNOS^{pos} platelets within 3-dimensional structure of an aggregate

(A) Representative immunofluorescence confocal microscopy z-stacks at different focal distances, and mean fluorescence intensity measurements demonstrating platelet eNOS (green) and F-actin (red) within the 3-dimensional structure of an aggregate. Scale bars = 10 µm. **(B)** Composite image of z-stacks from panel A. **(C)** A graph demonstrating the changes in the ratio of eNOS/F-actin fluorescence within the z-plane of aggregates from 3 independent experiments ($N = 3$). **(D)** A cartoon depicting conceptual model of the aggregate growth with less abundant eNOS^{neg} platelets initiating haemostatic reactions localized at the bottom of platelet aggregate and more abundant eNOS^{pos} platelets forming a bulk of an aggregate.

A

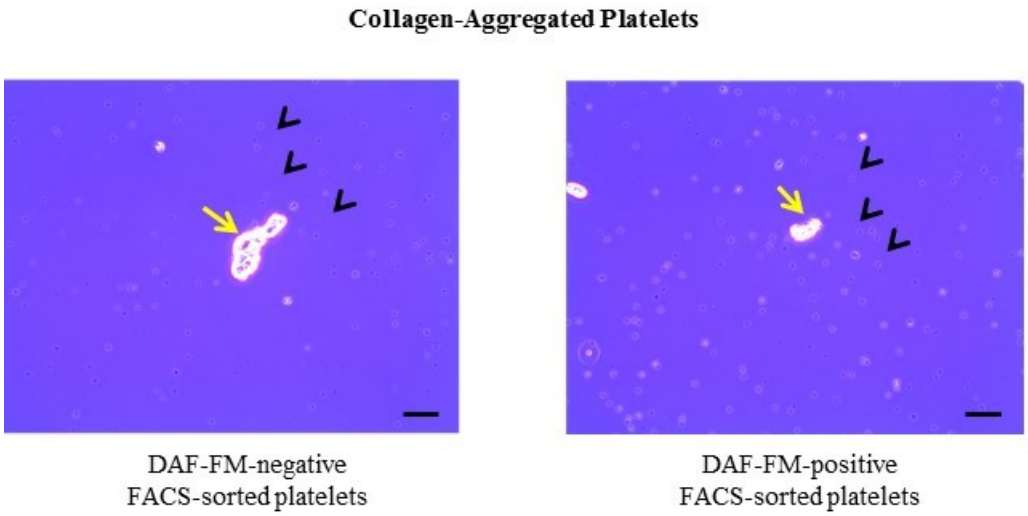

B

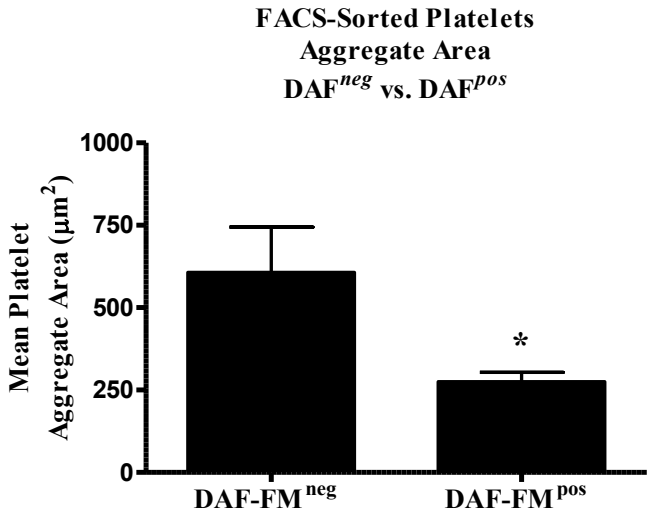

Figure 4.24. The eNOS^{pos} platelets limit aggregate formation via NO generation

(A) Representative phase-contrast microscopy of DAF-FM^{neg} and DAF-FM^{pos} platelet aggregates following aggregation with collagen. Yellow arrows indicate platelet aggregates and black arrows indicate individual platelets. Scale bars = 25 μm. **(B)** Summary data of aggregates size formed by DAF-FM^{neg} and DAF-FM^{pos} platelets. Statistics: paired, two-tailed Student's *t*-tests. $N = 4$. $*P < 0.05$. (Platelet aggregometry and microscopy were performed by Dr. Radziwon-Balicka).

4.8 The eNOS-Based Platelet Subpopulations Exist in eNOS-GFP Transgenic Mice but There are a Major Species Differences in eNOS-Signalling

To further study the role of eNOS-based platelet subpopulations in haemostatic reactions, we decided to utilize eNOS-GFP transgenic mice which in addition to mouse eNOS, express human eNOS fused to green fluorescent protein (GFP) driven by the human eNOS promoter. The mice were regenerated by breeding homozygous male eNOS-GFP transgenic mice with wild type (WT) female C57BL/6 mice. The eNOS-GFP-genotype zygosity of the offspring was determined by RT-qPCR followed by relative quantification standard curve method. WT mice obtained from non-transgenic littermates were used as negative controls.

Next, we decided to visualize the presence of eNOS-GFP fluorescence in eNOS-GFP homozygous mice using confocal microscopy. Gastrocnemius muscle tissue from homozygous eNOS-GFP mice exhibited a green fluorescence confirming presence of human eNOS expression which was not observed in WT mice tissue, as showed in the Figure 4.25, Panel A-B.

To establish whether eNOS-GFP-based platelet subpopulations exist in eNOS-GFP transgenic mice, we performed flow cytometry on platelet rich plasma (PRP) obtained from mouse blood samples. Based on GFP fluorescence of CD41-positive cells (platelet marker) we identified $eNOS^{neg}$ (GFP^{neg}) and $eNOS^{pos}$ (GFP^{pos}) platelet subpopulations in homozygous and hemizygous eNOS-GFP mice, as showed in the Figure 4.26, Panel A. Following subtraction of autofluorescence based on WT control, only $2.1 \pm 0.7\%$ of homozygous and $1.3 \pm 0.8\%$ of hemizygous eNOS-GFP mouse platelets expressed eNOS ($eNOS\text{-}GFP^{pos}$) (Figure 4.26, Panel B). These results revealed major differences between mouse and human platelet NO-signalling, as presented above data (Figure 4.3, Panel D) showed that 80.6 ± 3.3% of human platelets expressed eNOS ($eNOS^{pos}$).

To further delineate if low level of $eNOS\text{-}GFP^{pos}$ mouse platelets will result in low NO-production by mouse platelets, we performed flow cytometry on DAF-FM-stained platelets obtained from WT mice which were stimulated with collagen (0.6 μg/ml) in the presence of L-arginine (100 μM). Because eNOS-GFP transgenic mice overexpress eNOS we used platelets collected from WT mice and compared their NO-production to human platelets. Platelets collected from $eNOS^{-/-}$ mice were used as a negative control. Our results showed that only $5.4 \pm 2.1\%$ of platelets from WT mice generated NO, which greatly differed from $83.9 \pm 2.3\%$ of

NO-producing human platelets (Figure 4.27). This further confirmed differences in platelet NO-signalling between humans and mice. In addition, these interspecies differences also prevented us from utilizing eNOS-GFP transgenic mice as an *in vivo* model to further study the role of eNOS-based platelet subpopulations in haemostatic reactions.

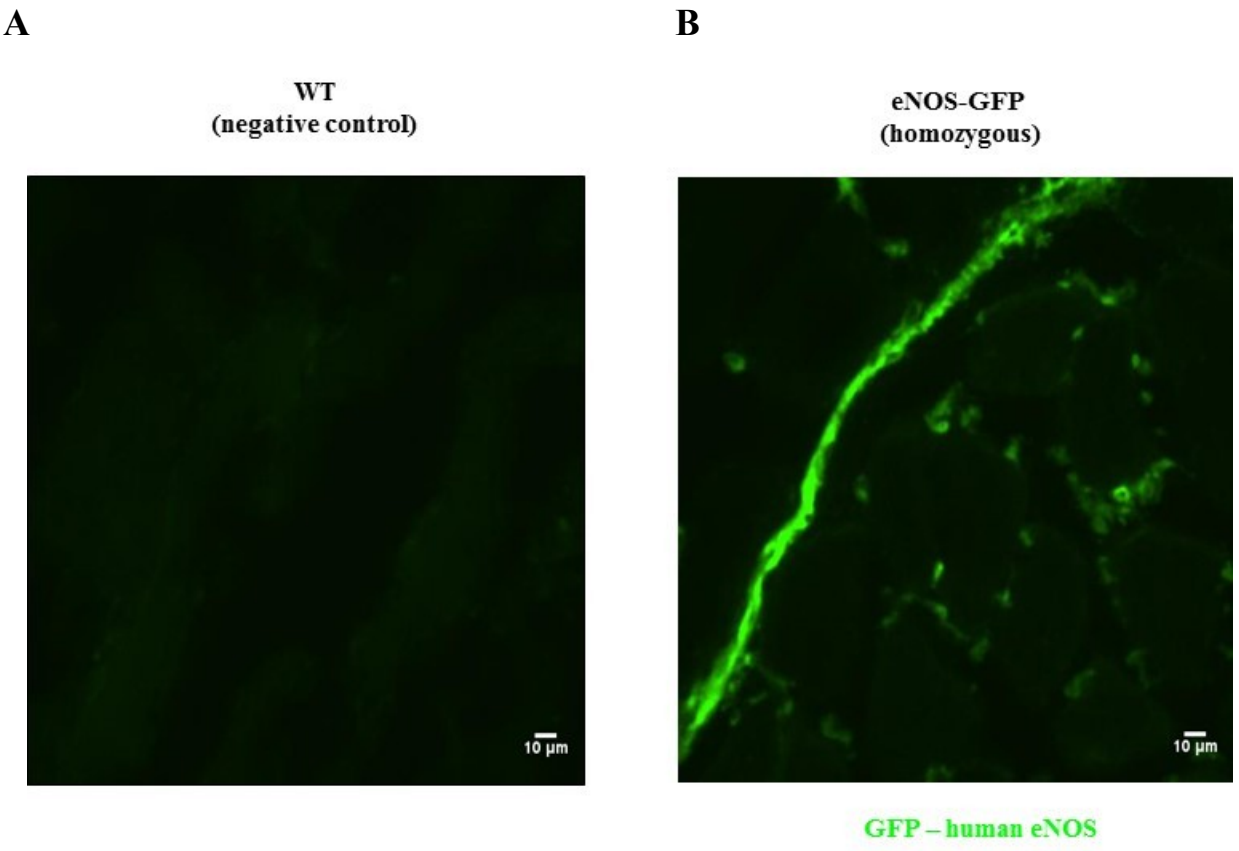

Figure 4.25. Detection of human eNOS-GFP expression in eNOS-GFP transgenic mice by confocal microscopy

(A) Representative image of gastrocnemius muscle tissue derived from control WT mice. **(B)** Representative image of gastrocnemius muscle tissue derived from homozygous eNOS-GFP mouse demonstrating expression of human eNOS detected as green fluorescence of GFP. Scale bars = 10 µm. Images of eNOS-GFP were obtained by exciting tissue with argon laser (488 nm). All images were taken with Leica TCS SP5 confocal microscope using the 20x/0.5 air lens.

A

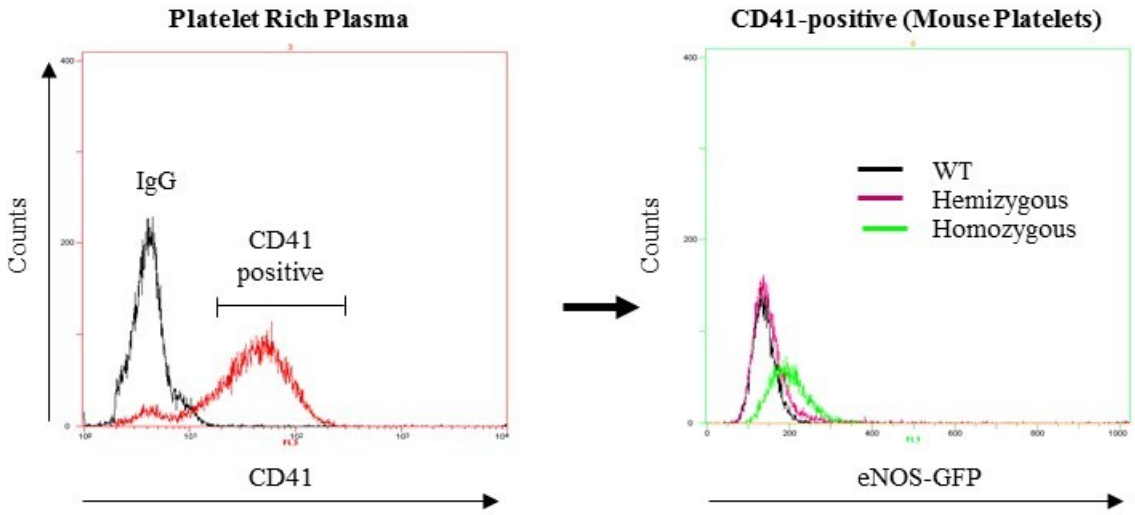

B

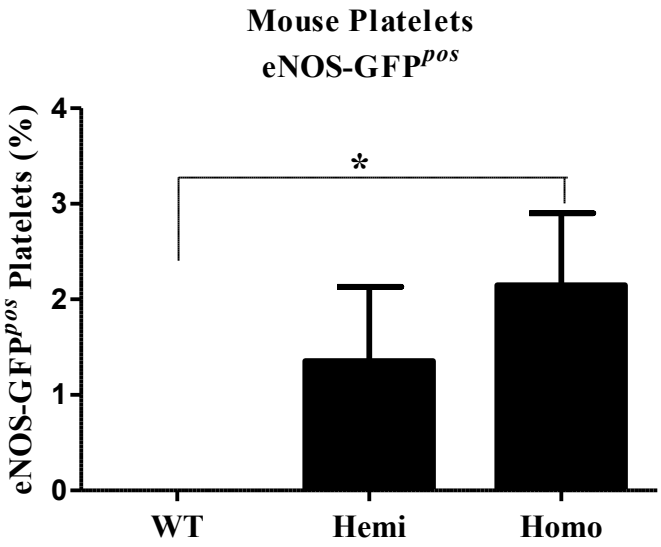

Figure 4.26. Identification of mouse eNOS-based platelet subpopulations

(A) Histogram overlay of CD41-positive cells and IgG isotype control. **(B)** Expression of eNOS-GFP in CD41-positive cells (mouse platelets) of WT, hemizygous and homozygous mice. **(C)** Summary data of flow cytometry comparing levels of eNOS-GFP^{pos} (eNOS^{pos}) platelets of WT, hemizygous and homozygous mice. Statistics: One-way ANOVA with Tukey post-hoc test. N = 4, *$P < 0.05$.

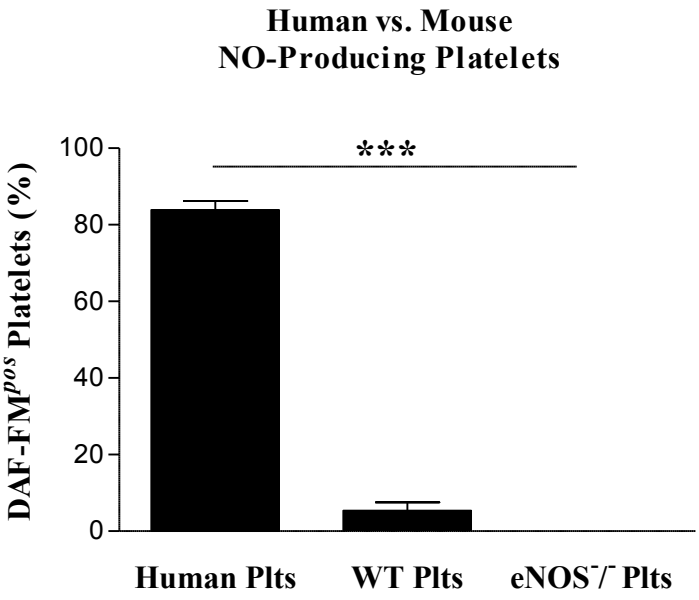

Figure 4.27. Levels of human and mouse NO-producing platelets

Summary data showing the amount of NO-producing platelets in samples collected from humans and WT mice. Platelets from eNOS$^{-/-}$ mice were used as a negative control. Statistics: One-way ANOVA with Tukey post-hoc test. $N = 4$. ***$P < 0.0001$.

4.9 Megakaryocyte Subpopulations Exist Within the Bone Marrow of eNOS-GFP Mice Based on the Presence or Absence of Functional eNOS and Their Ability to Produce NO

Since we identified that the majority of mouse platelets lack eNOS (eNOS-GFP^{neg}) and generate low or no NO (low/non-NO-producers), while small number generates NO (NO-producers) and has eNOS present (eNOS-GFP^{pos}), we decided to test the hypothesis that these platelets derive from respective eNOS^{pos} *and eNOS*^{neg} subpopulations of MKs found in the bone marrow of eNOS-GFP mice. Based on our results showing low level of eNOS^{pos} (eNOS-GFP^{pos}) platelets ($2.1 \pm 0.7\%$) in homozygous eNOS-GFP mice, we further hypothesized that homozygous eNOS-GFP mice have low level of eNOS^{pos} (eNOS-GFP^{pos}) MKs.

To test our hypothesis we collected bone marrow from homozygous eNOS-GFP transgenic mice. Following subtraction of autofluorescence based on WT control, flow cytometry data confirmed our hypothesis and similar to mouse platelets, the majority of mouse MKs were eNOS^{neg} (eNOS-GFP^{neg}) and only few MKs were eNOS^{pos} (eNOS-GFP^{pos}) (95.8 ± 0.7% vs. 4.2 ± 0.7%) (Figure 4.28, Panel A-E). Non-specific background signal of CD41 staining was controlled with respective IgG isotype control.

To further delineate the potential reason why there may be species differences in eNOS MK expression, we decided to investigate whether eNOS DNA methylation is responsible for low eNOS expression in mouse MKs. Importantly, eNOS gene methylation was previously described as a mechanism of negative epigenetic regulation of eNOS gene expression in cells with low eNOS expression [332, 581]. Therefore, we cultured MKs of homozygous eNOS-GFP transgenic mice with DNA methyltransferase inhibitor – 5-azacytidine and the flow cytometry analysis showed that 5-azacytidine increased the percentage of eNOS^{pos} mouse MKs by 2.5-fold (8.90 ± 2.2% untreated control vs. 20.99 ± 1.3%), as showed and summarized in Figure 4.29, Panel A and B. These results suggest that eNOS DNA methylation may in part be responsible for the differences in eNOS expression levels between mouse and human MKs and thus platelets.

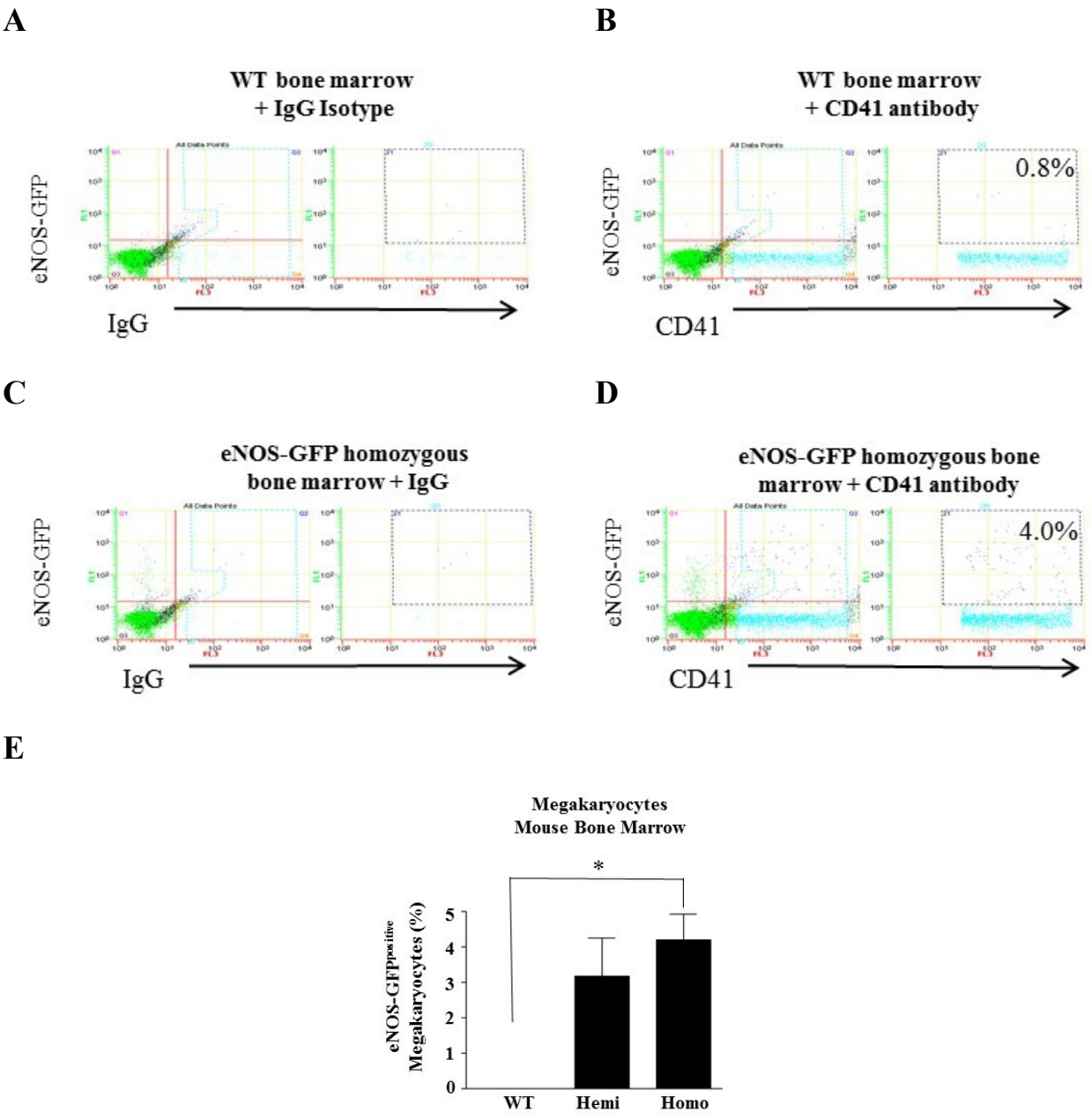

Figure 4.28. Identification of mouse eNOS-based megakaryocyte subpopulations

(A) Representative dot plot of bone marrow cells (WT mice) stained with IgG isotype control. **(B)** Representative dot plot indicating 0.8% of eNOS-GFP^{pos} MKs in the bone marrow of WT mice. **(C)** Representative dot plot of bone marrow cells (homozygous eNOS-GFP mice) stained with IgG isotype control. **(D)** Representative dot plot indicating 4.0% of eNOS-GFP^{pos} MKs in the bone marrow of homozygous eNOS-GFP mice. **(E)** Summary data comparing levels of eNOS-GFP^{pos} MKs in the bone marrow samples from WT, hemizygous and homozygous eNOS-GFP mice. Statistics: One-way ANOVA with Tukey post-hoc test. $N = 4$. *$P < 0.05$.

A

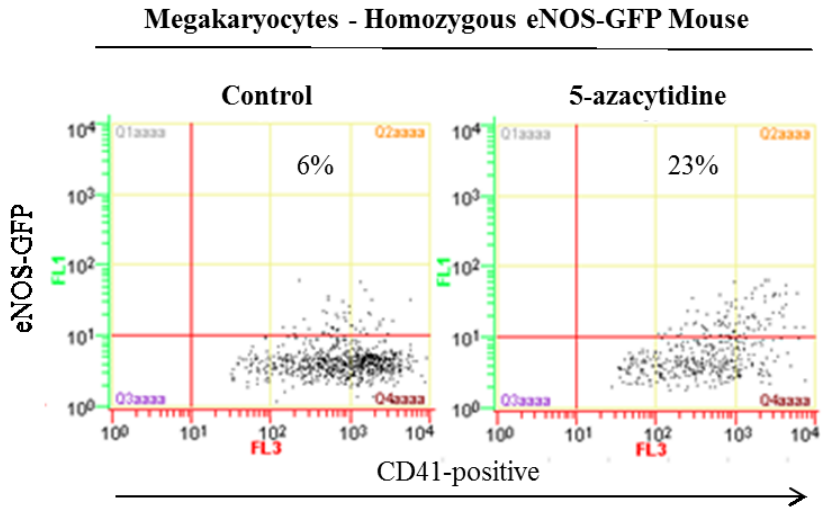

B

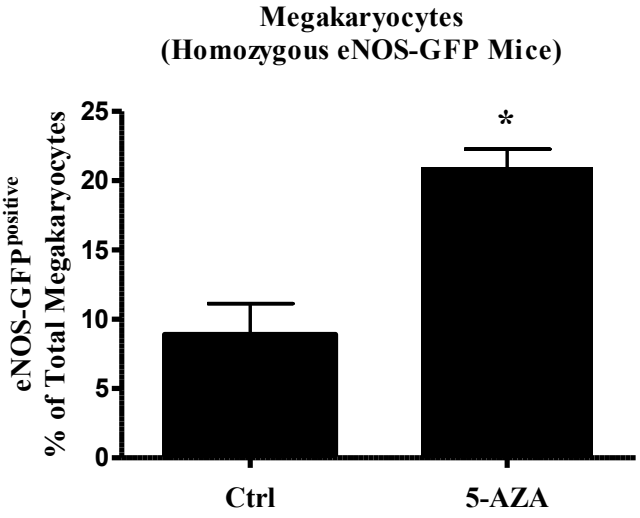

Figure 4.29. Epigenetic regulation of eNOS expression within mouse megakaryocytes

(A) Representative dot plots of MKs (CD41-positive cells) collected from homozygous eNOS-GFP mouse. The numbers indicate the percent of eNOS-GFP^{pos} MKs in untreated control sample and sample treated with 5-azacytidine. **(B)** Summary data comparing levels of eNOS-GFP^{pos} MKs in untreated control sample and sample treated with 5-azacytidine. Statistics: paired, two-tailed Student's *t*-tests. $N = 3$. $^{*}P < 0.05$. (Flow cytometry was performed by Dr. Paul Jurasz).

4.10 Megakaryocyte Subpopulations Exist Within Meg-01 Cell Line Based on the Presence or Absence of Functional eNOS and Their Ability to Produce NO

As we identified presence of two human platelet subpopulations based on the presence and absence of eNOS ($eNOS^{pos}$ and $eNOS^{neg}$) and the ability to generate NO (NO-producers and low/non-NO-producers), we decided to test the hypothesis that these platelets derive from respective $eNOS^{pos}$ and $eNOS^{neg}$ subpopulations of their parent cells – MKs. In our studies we utilized human megakaryoblastic cell line (Meg-01) in place of human bone marrow MKs. The reason why we used Meg-01 cell line instead human MKs is caused by the fact that obtaining human MKs would require bone marrow aspiration which is associated with significant stress and discomfort to the patient during this procedure. And this seemed unnecessary at the stage of optimizing experimental protocols and performing preliminary studies.

Human megakaryoblastic cell line Meg-01 has been shown previously to express eNOS [282]. However, we performed control experiments to validate eNOS expression in Meg-01 cells. RT-PCR followed by agarose gel electrophoresis showed presence of eNOS mRNA in Meg-01 cells, as depicted in Figure 4.30, Panel A. Semi-quantitative analysis demonstrated that in comparison to HUVEC Meg-01 cells expressed significantly less eNOS mRNA (100% vs. $32.0 \pm 1.1\%$), as summarized in Figure 4.30, Panel B. DNA sequencing further confirmed the specificity of the RT-PCR product detected on the agarose gel as eNOS cDNA (241 kb). The DNA sequencing showed two eNOS DNA matching nucleotide sequences both on positive (1^{st}-165 and 2^{nd} - 150 nucleotide long) and negative (1^{st}-164 and 2^{nd} - 72 nucleotide long) DNA strands between exons 25 and 26 of eNOS gene, as depicted in Figure 4.30, Panel C.

After confirming eNOS mRNA expression in Meg-01 cell, we performed eNOS-staining (using two different anti-eNOS antibodies: 6H2 and M221 clone) and utilized confocal microscopy to identify presence and localization of eNOS protein in Meg-01 cells. In addition to eNOS immunostaining (green fluorescence) we also stained cellular F-actin (red fluorescence) to outline the Meg-01 cells cytoskeleton. Confocal microscopy showed presence of eNOS protein in the megakaryoblasts. In addition to majority of Meg-01 cells that expressed eNOS (green fluorescence) (Figure 4.31, Panel A), we also identified rare individual Meg-01 cells that did not stain for eNOS protein ($eNOS^{neg}$), as depicted in Figure 4.31, Panel B.

Based on our confocal imaging data where few individual megakaryoblasts lacked eNOS protein, we decided to use flow cytometry to further investigate existence of megakaryoblast subpopulations based on the presence or absence of eNOS protein. To strengthen our data we performed two separate sets of experiments utilizing two different anti-eNOS antibodies: M221 clone and 6H2 clone. In both sets of experiments Meg-01 cells showed bimodal distribution of eNOS protein, as showed on the histogram Figure 4.32, Panel A and C. Based on the autofluorescence from unstained control we set the gate for the eNOS-negative Meg-01 cells. We defined Meg-01 cells found within the lower histogram peak as eNOS-negative ($eNOS^{neg}$) and Meg-01 cells found within the larger peak were defined as eNOS-positive ($eNOS^{pos}$). In the experiments with 6H2 clone of anti-eNOS antibodies the $eNOS^{neg}$ cells accounted for 8.5 ± 1.2 % and $eNOS^{pos}$ cells accounted for 91.5 ± 1.2 % of total Meg-01 cells (Figure 4.32, Panel B). In the experiments utilizing M221 clone of anti-eNOS antibodies the $eNOS^{neg}$ cells accounted for 12.4 ± 5.2% and $eNOS^{pos}$ cells accounted for 87.6 ± 5.2% of total Meg-01 cells (Figure 4.32, Panel D). Non-specific background signal of eNOS was controlled by IgG isotype control. We also controlled for Meg-01 cell viability using fixable viability dye (FVD) to verify if $eNOS^{neg}$ cell population is not an artifact caused by dead cells, as showed in Figure 4.33, Panel A and B.

Since we indentified two subpopulations of Meg-01 cells based on eNOS protein expression ($eNOS^{neg}$ and $eNOS^{pos}$), next we decided to evaluate the ability of Meg-01 cells to produce NO using DAF-FM diacetate staining. We performed flow cytometry on DAF-FM-stained Meg-01 cells preincubated with L-arginine (100 μM) and measured NO-production as DAF-FM mean fluorescence intensity. Flow cytometry histograms showed two distinct fluorescence peaks where one that overlapped with unstained control corresponded to Meg-01 cells that generated no or low-levels of NO and the larger peak represented Meg-01 cells that generated larger amount of NO (Figure 4.34, Panel A). Summary data showed that 8.0 ± 6.68% were low/non-NO producing Meg-01 cells and 92.0 ± 3.34% were NO-producing Meg-01 cells (Figure 4.34, Panel B), which is consistent with numbers obtained for $eNOS^{neg}$ and $eNOS^{pos}$ Meg-01 subpopulations, respectively (12.4 ± 5.2% vs. 87.6 ± 5.2%) (Figure 4.32, Panel D).

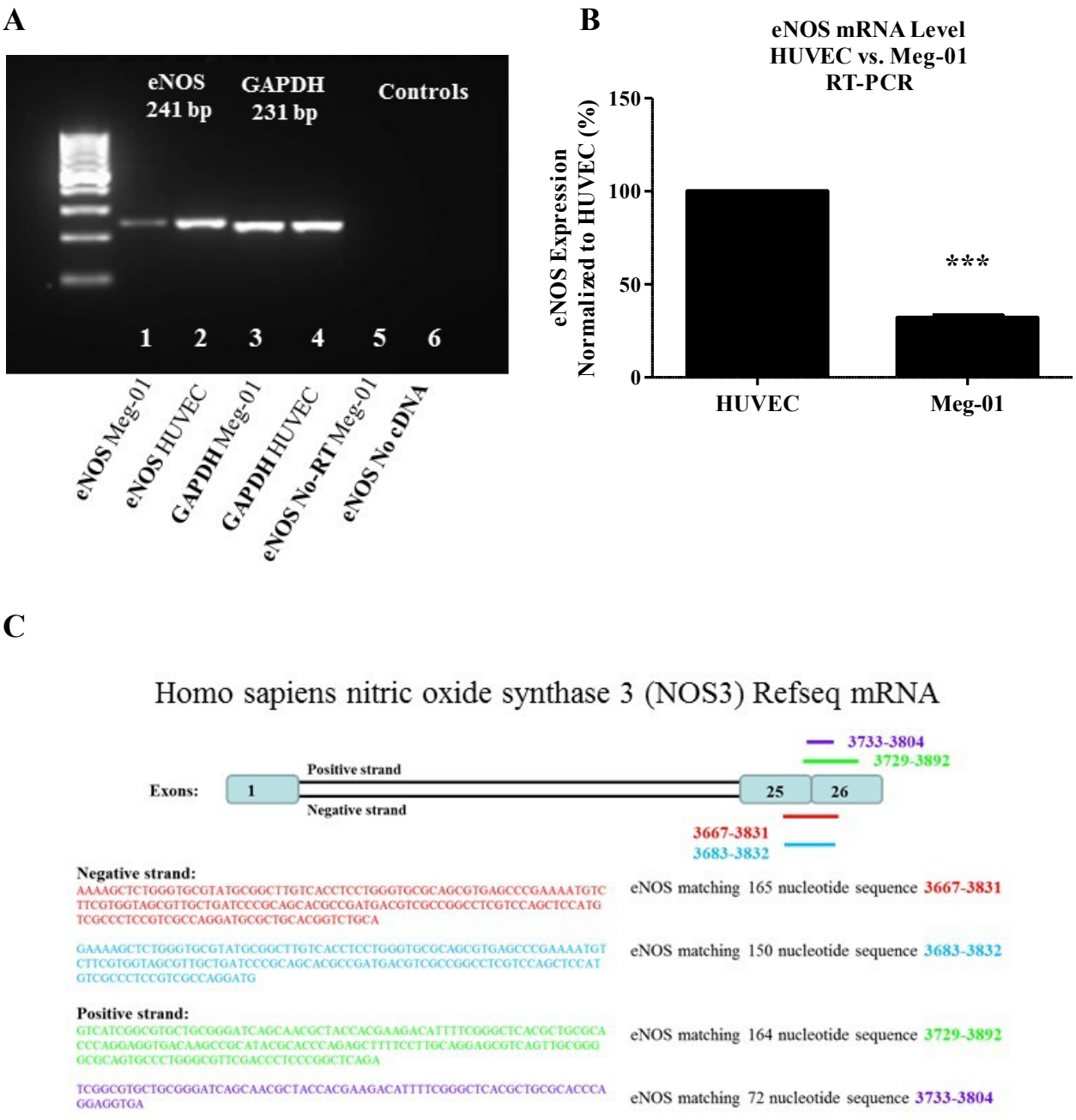

Figure 4.30. Identification of eNOS mRNA in Meg-01 cells by RT-PCR followed by Sanger sequencing

(A) Representative 2% agarose gel showing eNOS 241 bp cDNA band in Meg-01 cells (lane 1) and HUVEC cells (lane 2). **(B)** Summary data comparing eNOS expression in HUVEC vs. Meg-01 cells. **(C)** Summary of Sanger sequencing of Meg-01 cDNA samples from electrophoretic separation on 2% agarose. Statistics: paired, two-tailed Student's *t*-tests. $N = 3$. ***$P < 0.001$.

A

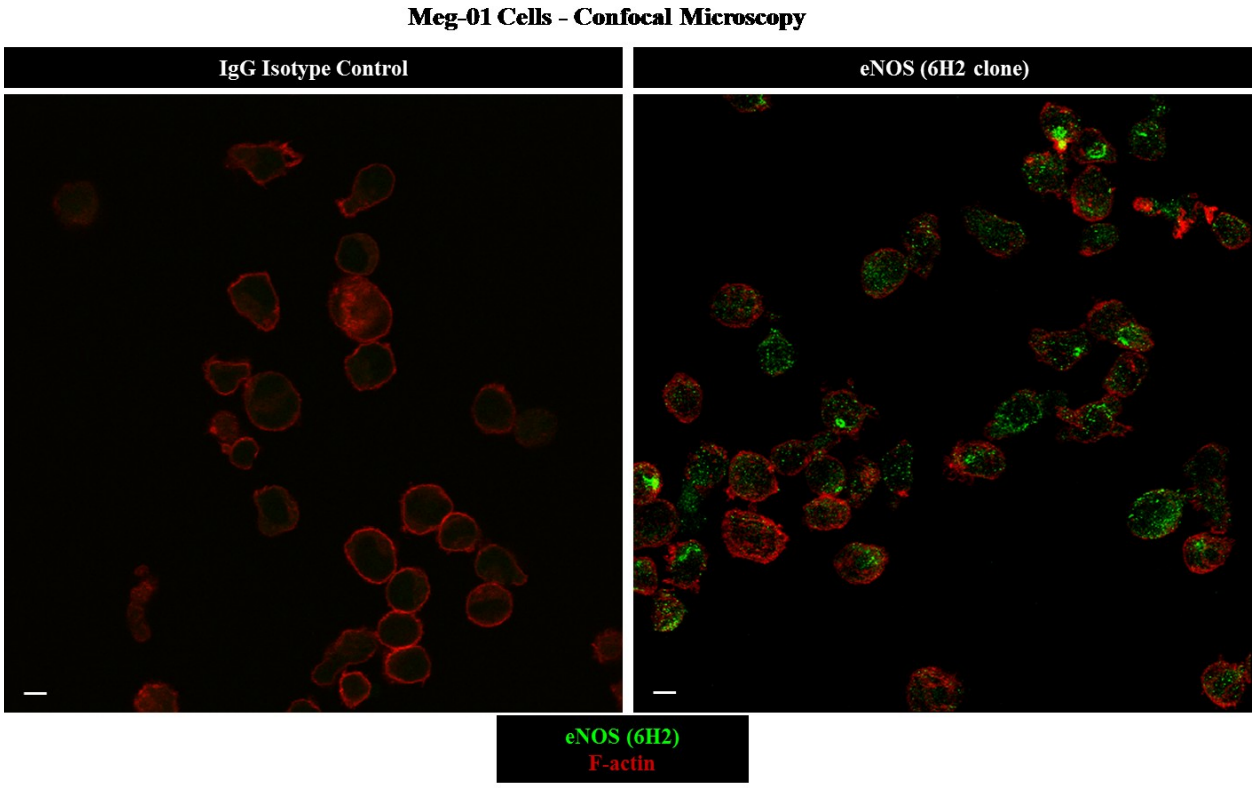

B

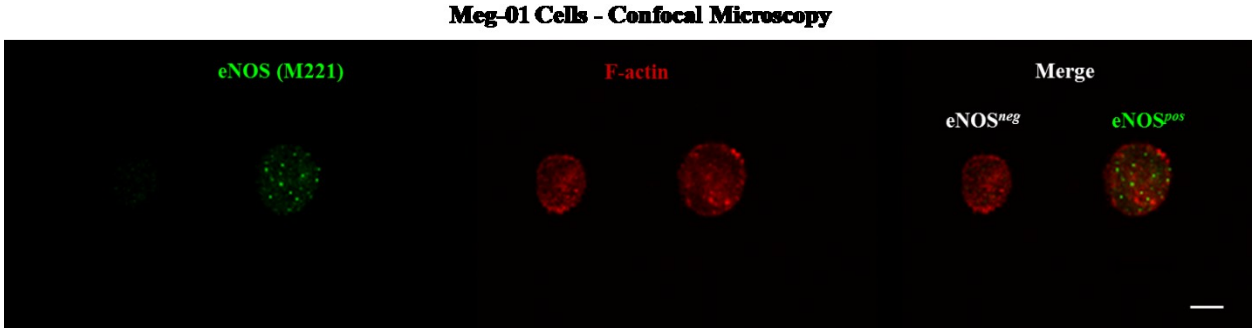

Figure 4.31. Identification of eNOS protein in Meg-01 cells by confocal microscopy

(A) Representative images of IgG isotype control and eNOS protein expression in Meg-01 cells. **(B)** Representative image of an individual $eNOS^{neg}$ and $eNOS^{pos}$ Meg-01 cells. Scale bars = 10 μm. Images of eNOS were obtained by exciting cells with argon laser (488 nm). Images of F-actin were obtained by exciting cells with the helium-neon laser (543 nm). All images were taken with Leica TCS SP5 confocal microscope using the 60x/1.2 water lens.

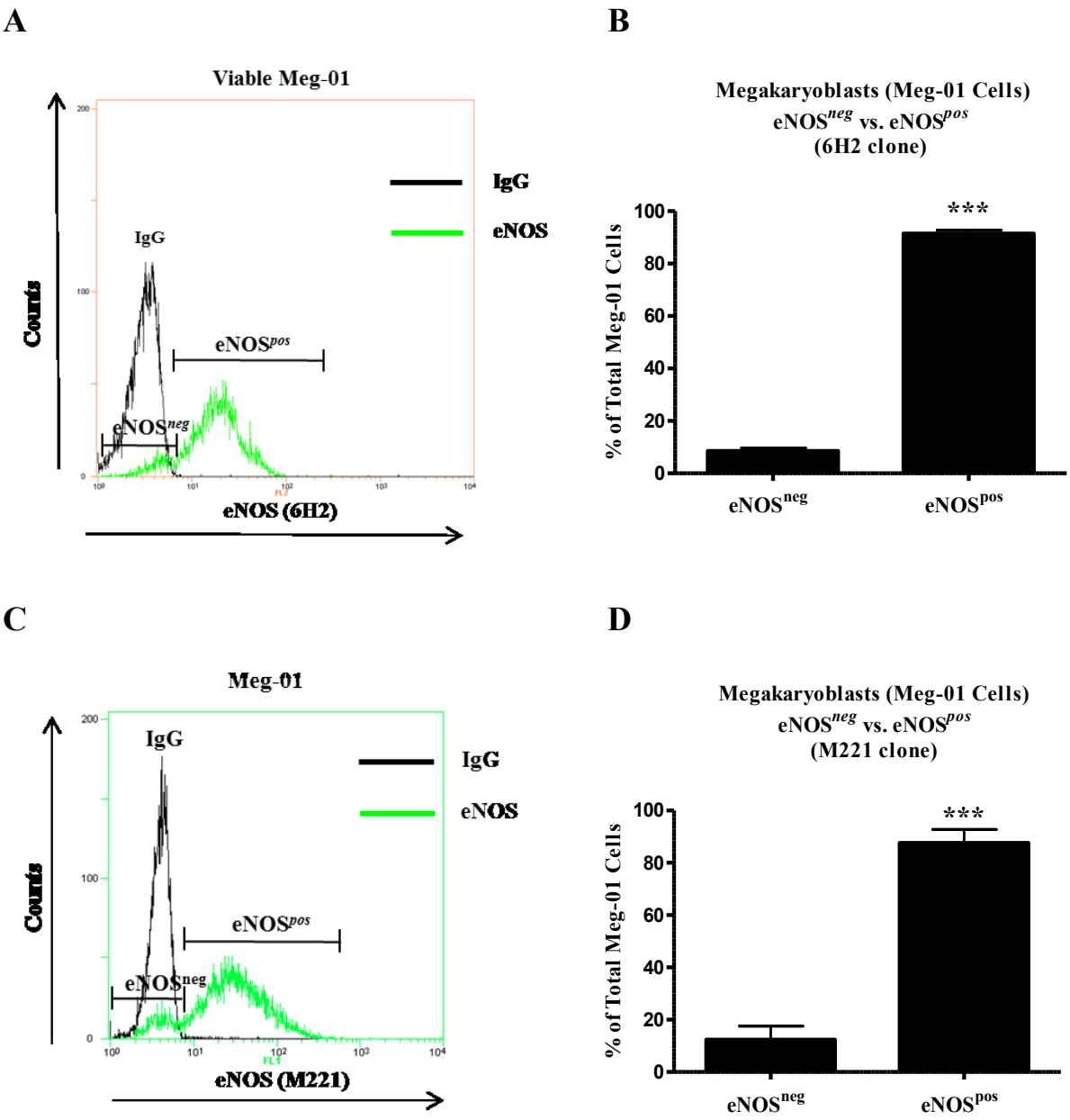

Figure 4.32. Flow cytometry data demonstrating eNOS-based Meg-01 cell subpopulations

(A) Representative overlay histograms of IgG isotype control and eNOS protein detected with anti-eNOS 6H2 clone antibody. **(B)** Summary data comparing percentage of eNOS^{neg} to eNOS^{pos} human Meg-01 cells using anti-eNOS 6H2 clone antibodies. Statistics: paired, two-tailed Student's *t*-tests. $N = 4$. ***$P < 0.001$. **(C)** Representative overlay histograms of IgG isotype control and eNOS protein detected with anti-eNOS M221 clone antibodies. **(D)** Summary data comparing percentage of eNOS^{neg} to eNOS^{pos} human Meg-01 cells using anti-eNOS M221 clone antibodies. Statistics: paired, two-tailed Student's *t*-tests. $N = 6$. ***$P < 0.001$.

A

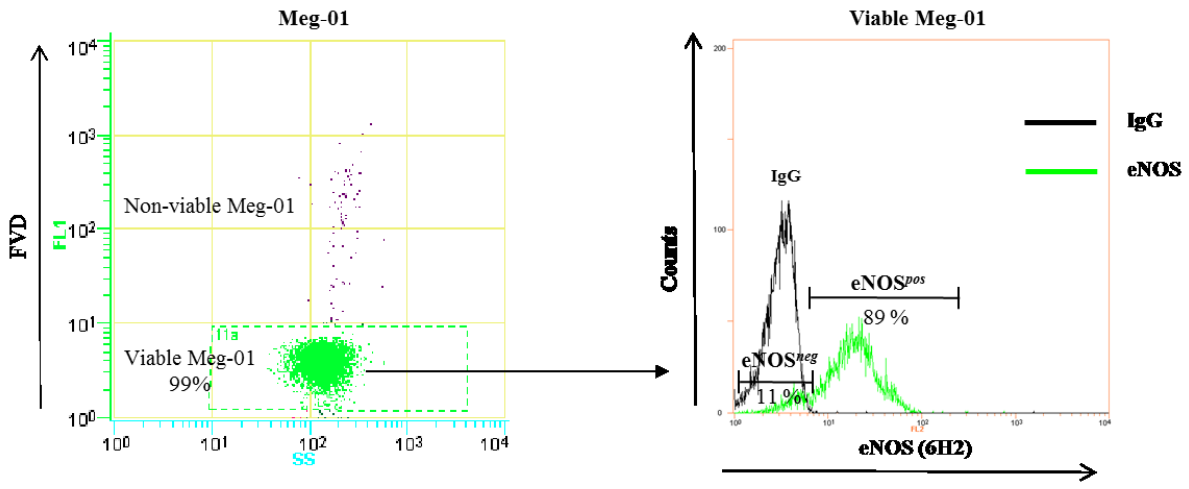

Figure 4.33. Flow cytometry results demonstrating gating strategy of viable Meg-01 cells and detection of eNOS-based Meg-01 cell subpopulations

Representative dot plot and gating strategy of viable Meg-01 cells based on FVD staining and representative IgG isotype control and eNOS histogram for viable Meg-01 cells showing percentage of $eNOS^{neg}$ and $eNOS^{pos}$. (Flow cytometry with anti-eNOS 6H2 clone antibodies and FVD was perfomed by Teresa Fong).

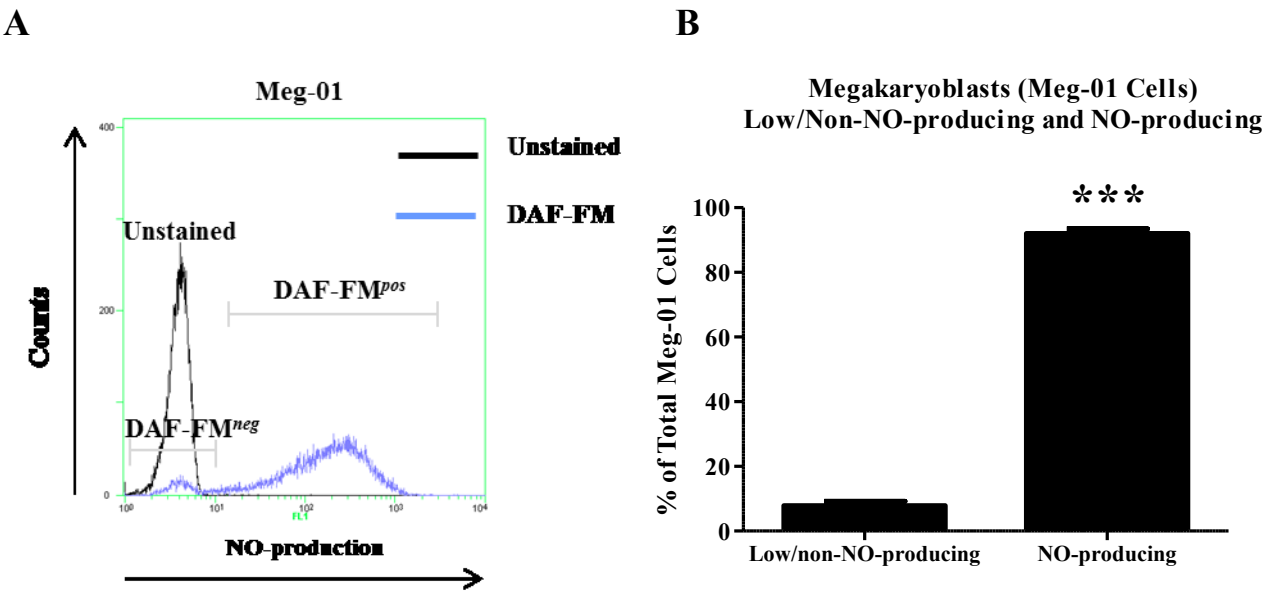

Figure 4.34. Identification of low/non-NO-producing and NO-producing Meg-01 cells

(A) Representative histogram overlay demonstrating unstained Meg-01 control and DAF-FM^{neg} (low/non NO-producers) and DAF-FM^{pos} (NO-producers) human Meg-01 cells. **(B)** Summary bar graph comparing level of low/non-NO-producing and NO-producing human Meg-01 cells. Statistics: paired, two-tailed Student's *t*-tests. $N = 8$. ***$P < 0.001$.

4.11 Characterization of eNOS-Based Meg-01 Cells

As a next step, after indentifying presence of eNOS-based megakaryocyte/blast subpopulations and their ability to generate NO, we decided to evaluate other characteristics of $eNOS^{neg}$ and $eNOS^{pos}$ Meg-01 cells. Previously it has been reported that human MKs are heterogenous based on their granularity and size therefore, we decided to investigate whether $eNOS^{neg}$ and $eNOS^{pos}$ Meg-01 cells have different granularity and size [544, 545].

Based on flow cytometry side scatter (SSC) we found no statistical difference in granularity between $eNOS^{neg}$ and $eNOS^{pos}$ Meg-01 cells (141.0 ± 4.3 vs.156.2 ± 12.6, arbitrary units of scattered light intesity, $P > 0.05$) (Figure 4.35, Panel A). However, $eNOS^{neg}$ Meg-01 cells were significantly smaller than $eNOS^{pos}$ Meg-01 cells measured as mean electronic volume (EV) (241.2 ± 11.7 vs. 421.6 ± 22.98, arbitrary units of volume, $P < 0.01$) (Figure 4.35, Panel B).

As our data indicated that $eNOS^{neg}$ Meg-01 subpopulation is smaller, we decided to investigate whether this is due to their earlier stage in maturation process. Meg-01 cells are primarily distributed across 3 ploidy classes 2n, 4n and 8n, and the higher ploidy the more mature are the cells [570]. We determined ploidy of eNOS-based Meg-01 cells using propidium iodine (PI) in addition to eNOS-staining (Figure 4.35, Panel C). Our two-colour flow cytometry showed that across three ploidy classes: 2n, 4n, and 8n the levels of both Meg-01 $eNOS^{neg}$ and $eNOS^{pos}$ cells have not significantly changed (Figure 4.35, Panel D). These results indicate that $eNOS^{neg}$ Meg-01 cells are not less differentiated than their $eNOS^{pos}$ counterparts and levels of these subpopulations do not shift as the Meg-01 cells maturate but rather remain fixed.

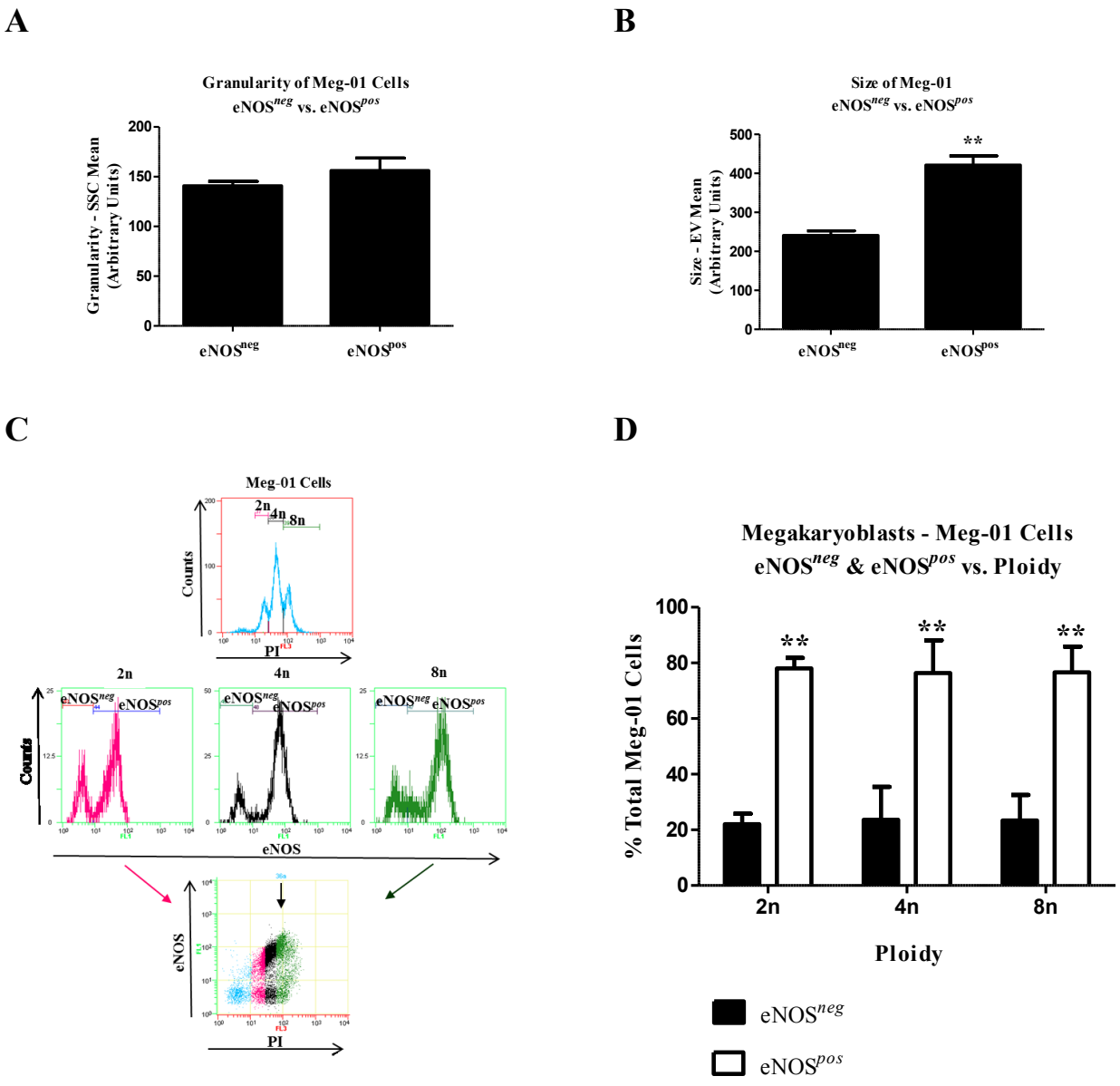

Figure 4.35. Characterization of eNOS-based Meg-01 cell subpopulations

(A) Summary bar graph comparing granularity of eNOS^{neg} and eNOS^{pos} Meg-01 cells. **(B)** Summary bar graph comparing size of eNOS^{neg} and eNOS^{pos} Meg-01 cells. **(C)** Representative gating strategy to determine the amount of eNOS^{neg} and eNOS^{pos} Meg-01 cells based on their three ploidy levels: 2n, 4n and 8n. **(D)** Summary bar graph comparing the amount of eNOS^{neg} and eNOS^{pos} Meg-01 cells between three ploidy levels: 2n, 4n and 8n. Statistics for **A** and **B**: paired, two-tailed Student's *t*-tests. $N = 5$. **A**: ns, $P > 0.05$, **B**: $^{**}P < 0.01$. Statistics for **C**: Two-way ANOVA, eNOS: $^{**}P < 0.01$, ploidy: ns $P > 0.05$.

4.12 Cytokines IFN-γ and IL-10 Counter-Regulate Formation of eNOS-Based Platelet Subpopulations via Their Effects on Megakaryocyte/blast eNOS Expression

Atherothrombotic disease is associated with inflammation, and thrombosis often complicates chronic inflammatory disorders. In addition, platelets from patients with CVD were reported have deficient NO-production and low expression of eNOS mRNA [315, 319, 582]. Importantly several pro- and anti-inflammatory cytokines regulate MK differentiation and eNOS expression in various cells [293, 470, 482-485, 496, 509]. However, the effects of pro-inflammatory IFN-γ and anti-inflammatory IL-10 on MK eNOS expression remain unknown. For our experiments we used a pro-inflammatory cytokine - IFN-γ because its excessive release has been associated with the pathogenesis of chronic inflammatory diseases like atherosclerosis [476]. Importantly, IFN-γ has been also reported to stimulate megakaryopoiesis but suppress expression of eNOS in various cells including ECs [482, 483, 488, 509, 510].

First, we tested the hypothesis that increasing concentrations of IFN-γ will increase level of $eNOS^{neg}$ Meg-01 cells as a consequence of suppression of total eNOS expression in megakaryoblasts. To test our hypothesis, we performed eNOS intracellular staining on Meg-01 cells cultured for 48h with increasing concentrations of IFN-γ (0.1-100 ng/ml). Flow cytometry analysis showed that IFN-γ in a concentration-dependent manner increased the number of $eNOS^{neg}$ Meg-01 cells. Moreover, IFN-γ (10 ng/ml) and IFN-γ (100 ng/ml) caused significant increase of $eNOS^{neg}$ Meg-01 cells when compared to untreated control (Figure 4.36, Panel A and B). Consequently, INF-γ at concentrations of 10 ng/ml and 100 ng/ml caused significant decrease of $eNOS^{pos}$ Meg-01 cells (Figure 4.36, Panel A and B).

Because IFN-γ (10 ng/ml) significantly increased level of $eNOS^{neg}$ Meg-01 cells without causing Meg-01 cells death (Figure 4.37, Panel A and B), we decided to utilize this concentration of IFN-γ for further experiments. As a next step we decided to test if anti-inflammatory cytokine IL-10 will counter-regulate IFN-γ-mediated suppression of megakaryoblast eNOS expression and increase the number of $eNOS^{pos}$ Meg-01. Importantly, IL-10 has been reported to antagonize IFN-γ-induced gene transcription and also to stimulate expression of eNOS in various cells including ECs [470, 495, 496, 514, 515]. Therefore, we performed RT-qPCR analysis on Meg-01 cells cultured for 48h with IFN-γ (10 ng/ml) and increasing concentrations of IL-10 (0.1-100 ng/ml). The RT-qPCR results demonstrated that increasing concentrations of IL-10 in

concentration-dependent manner partially reversed IFN-γ-mediated suppression of megakaryoblast eNOS mRNA expression. Moreover, IL-10 (100 ng/ml) significantly increased eNOS mRNA expression when compared to IFN-γ (10 ng/ml) (Figure 4.38).

Currently, it is unknown whether eNOS-based MK subpopulations give rise to their respective eNOS-based platelet subpopulations. As in our *in vitro* experiments pro-inflammatory IFN-γ increased the percentage of megakaryoblasts lacking eNOS, we hypothesized that this would contribute to generation of $eNOS^{neg}$ platelets by these megakaryocytes/blasts. Furthermore, our data showed that anti-inflammatory IL-10 partially reversed the lowering effect of IFN-γ on eNOS mRNA, hence we further hypothesized that IL-10 will promote formation of $eNOS^{pos}$ platelets.

To explore the effects of cytokines on generation of eNOS-based platelet subpopulations we used Meg-01 cell line that has been previously implemented in *in vitro* studies of platelet production [506, 571]. Meg-01 cells grown for 6 days in presence of TPO (100 ng/ml) generated platelets that were collected and stained for intercellular eNOS. Based on CD42b-positive staining we quantified the levels of Meg-01-derived $eNOS^{neg}$ and $eNOS^{pos}$ platelets. The results showed that compared to untreated control IFN-γ significantly enhanced *in vitro* generation of $eNOS^{neg}$ platelets (53.57 ± 5.22% untreated control vs. 68.92 ± 7.21%, $P < 0.001$) (Figure 4.39, Panel A and B). Furthermore, IL-10 in a concentration-dependent manner restored the levels of $eNOS^{neg}$ and $eNOS^{pos}$ platelets to the similar levels as eNOS-based platelets generated by untreated Meg-01 cells. This was exemplified by IL-10 at concentrations of 10 ng/ml and 100 ng/ml which significantly increased generation of $eNOS^{pos}$ platelets when compared to IFN-γ alone (19.80 ± 1.40% IFN-γ vs. 32.96 ± 2.27% IL-10 10 ng/ml vs. 37.65 ± 3.16% IL-10 100 ng/ml) (Figure 4.39, Panel A-C).

It has been shown that MKs from healthy humans also expresses iNOS mRNA and protein, in addition to eNOS [249]. Therefore we decided to investigate the effects of IFN-γ and IL-10 on iNOS expression of human megakaryoblasts. Based on reports that MKs form patients with severe coronary atherosclerosis had higher iNOS activity than eNOS [280], we hypothesized that pro-inflammatory IFN-γ will cause induction of iNOS expression in Meg-01 cells. In addition, anti-inflammatory IL-10 has been previously reported to act as a negative regulator of IFN-γ-mediated gene transcription, therefore we further hypothesized that IL-10 will

counter-regulate IFN-γ-mediated induction of iNOS expression in human megakaryoblasts [469, 583].

To test our hypothesis we performed 48h incubation of Meg-01 cells with IFN-γ (10 ng/ml) and increasing concentrations of IL-10 (0.1-100 ng/ml). Analysis of immunoblots revealed what appears to be biphasic effect of IL-10 on iNOS protein level of Meg-01 cells. While IL-10 at concentrations 0.1 ng/ml and 1.0 ng/ml further increased iNOS levels in the presence of IFN-γ, IL-10 at concentration of 100 ng/ml significantly decreased Meg-01 cells iNOS level when compared to IL-10 at concentration of 1.0 ng/ml (Figure 4.40, Panel A and B).

The RT-qPCR results similar to immunoblot data showed biphasic effect of IL-10 on iNOS mRNA levels of Meg-01 cells. While IL-10 at concentrations 0.1 ng/ml and 1.0 ng/ml further potentiated IFN-γ-mediated increase of iNOS mRNA levels, IL-10 (100.0 ng/ml) significantly decreased IFN-γ-mediated induction of iNOS mRNA levels within human megakaryoblasts (Figure 4.40, Panel C).

A

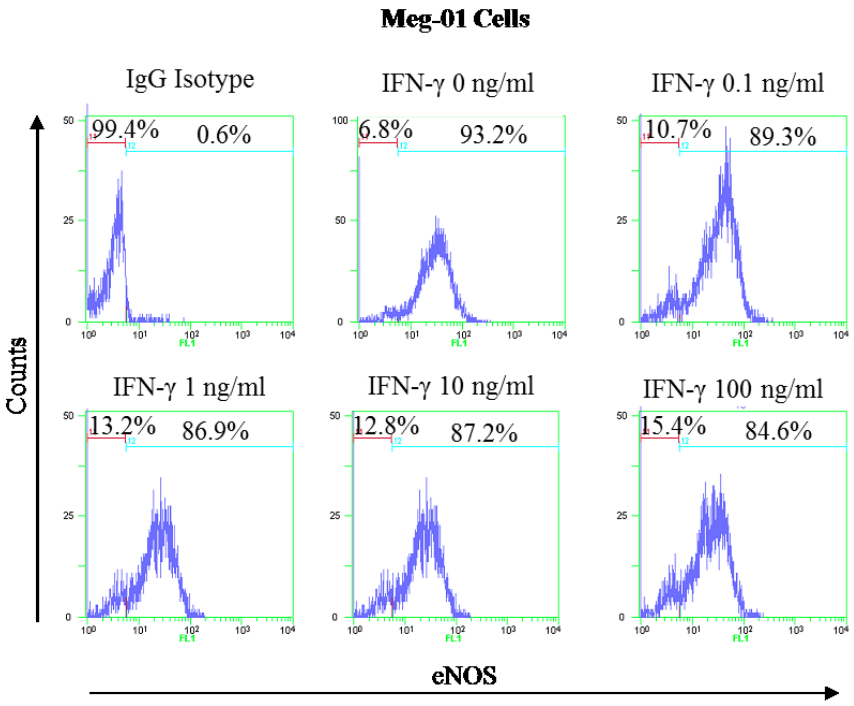

B

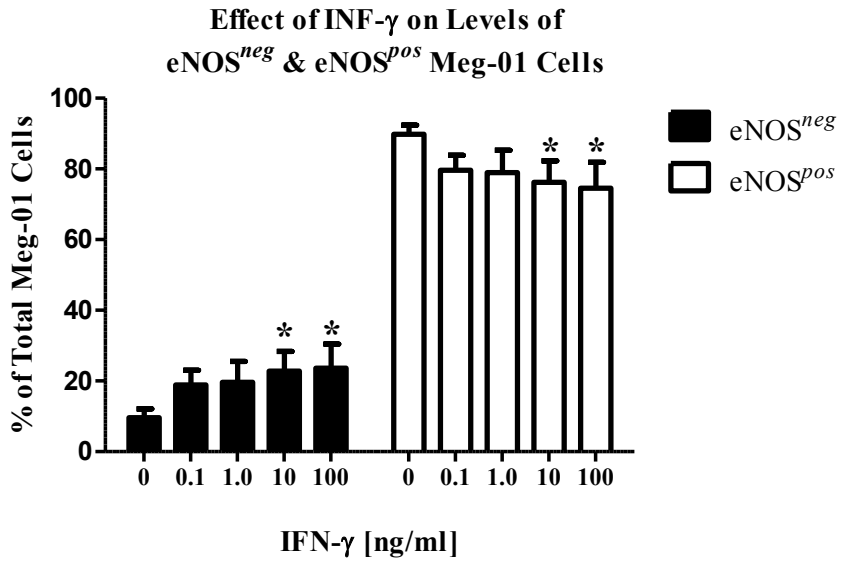

Figure 4.36. Pro-inflammatory IFN-γ promotes formation of eNOS^{neg} megakaryoblasts

(A) Representative histograms demonstrating percentage of eNOS^{neg} and eNOS^{pos} Meg-01 cells treated with increasing concentrations of IFN-γ (0.1–100 ng/ml). **(B)** Summary data of eNOS^{neg} and eNOS^{pos} Meg-01 cells after treatment with increasing concentrations of IFN-γ. Statistics: one-way ANOVA with Tukey post-hoc test. $N = 11$, $^*P < 0.05$ vs. untreated control. (Flow cytometry was performed by Dr. Radziwon-Balicka and Lisa Chan).

A

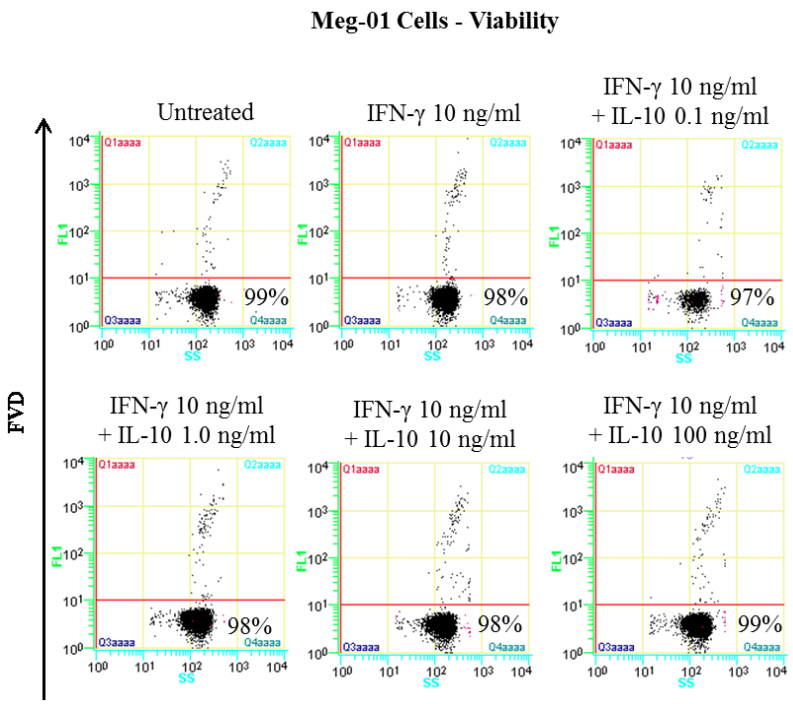

B

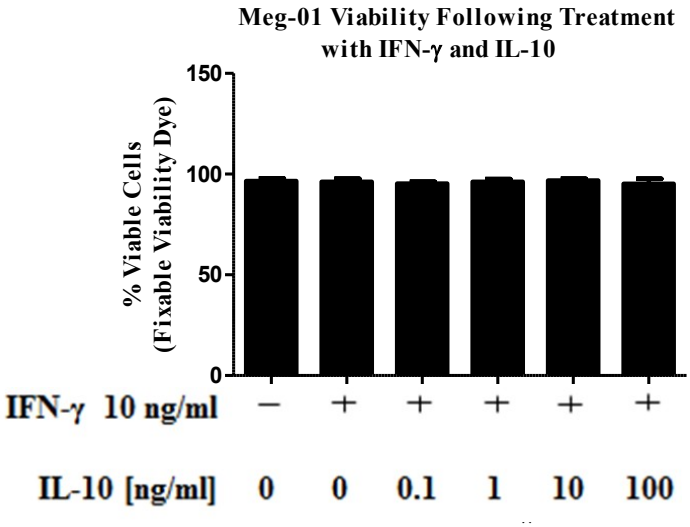

Figure 4.37. Viability of Meg-01 cells following treatment with IFN-γ and IL-10

(A) Representative flow cytometry dot plots showing percentage of viable Meg-01 cells (FVD-negative cells) following treatment with with IFN-γ (10 ng/ml) and IL-10 (0.1-100.0 ng/ml). **(B)** Flow cytometry summary data of percentage of viable Meg-01 cells following treatment with with IFN-γ (10 ng/ml) and IL-10 (0.1-100.0 ng/ml). Statistics: one-way ANOVA with Tukey post-hoc test. $N = 3$. Ns, $P > 0.05$.

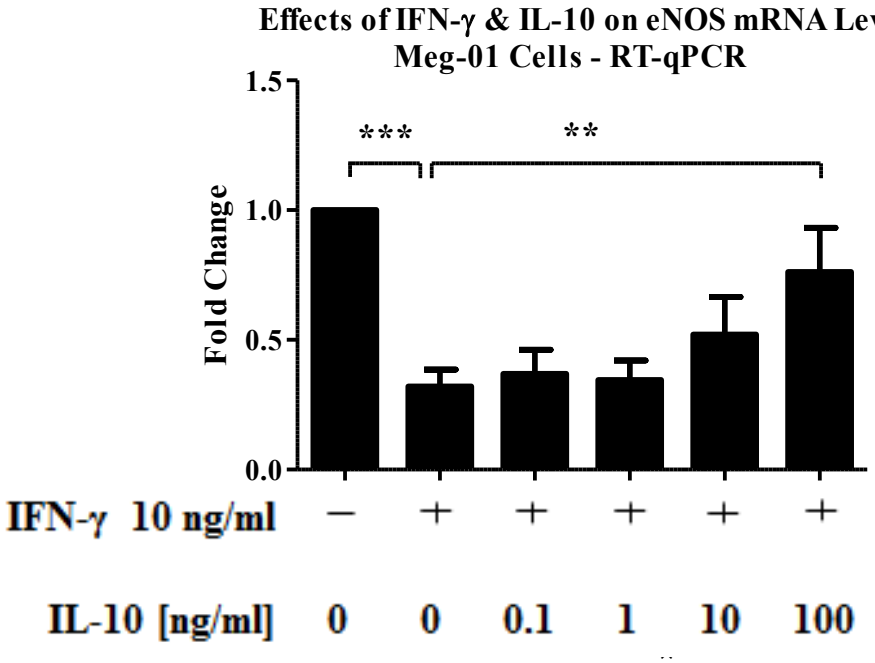

Figure 4.38. Effects of pro-inflammatory IFN-γ and anti-inflammatory IL-10 on eNOS mRNA level of megakaryoblasts

RT-qPCR summary data of eNOS mRNA level in Meg-01 cells, following the treatment with IFN-γ (10 ng/ml) and IL-10 (0.1-100.0 ng/ml). Statistics: one-way ANOVA with Tukey post-hoc test. $N = 5$, ***$P < 0.001$ and **$P < 0.01$.

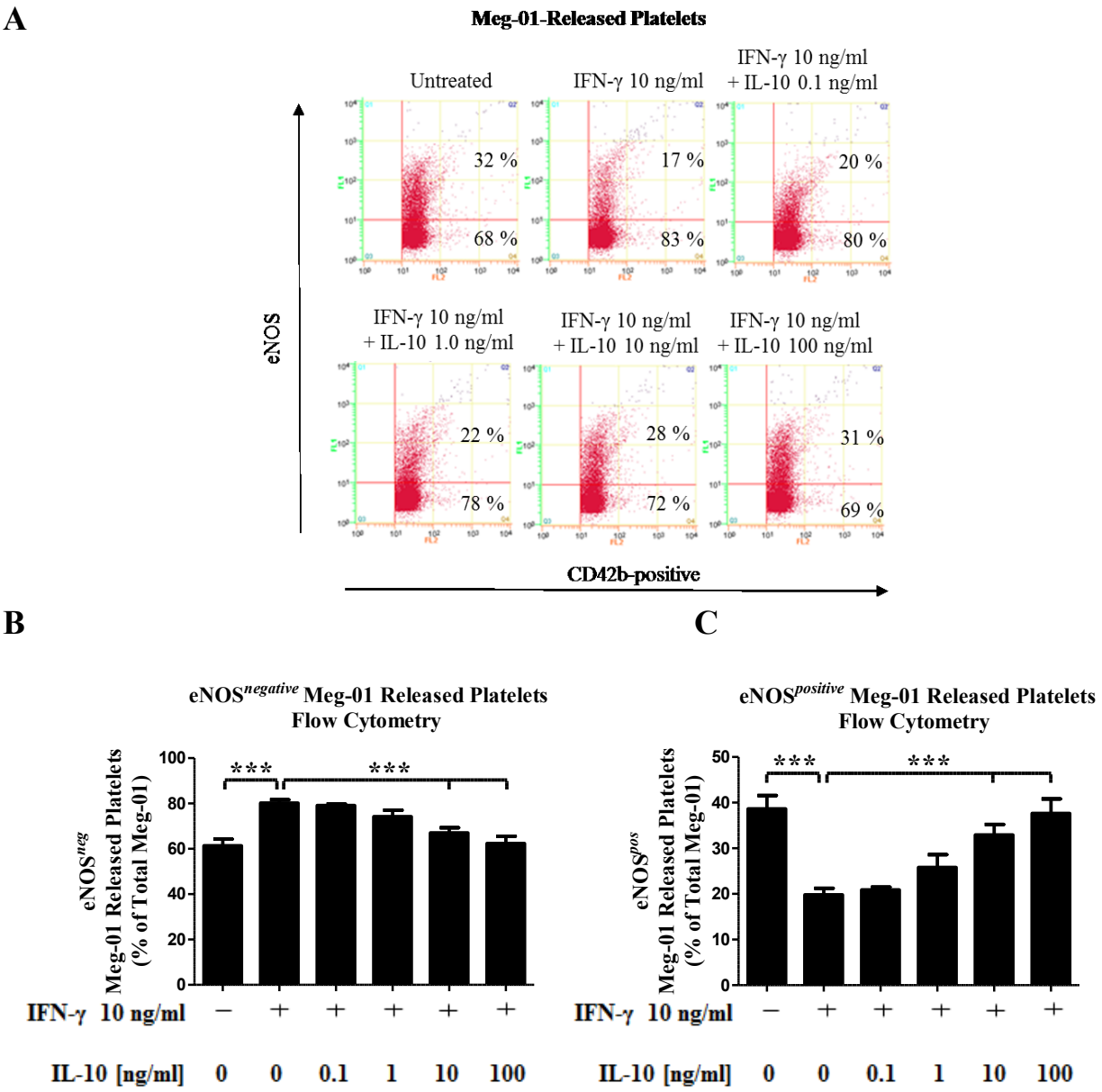

Figure 4.39. Cytokines IFN-γ and IL-10 counter-regulate formation of eNOS-based platelet subpopulations via their effects on megakaryoblast eNOS expression (A) Representative flow cytometry dot plots demonstrating eNOS^{neg} and eNOS^{pos} platelets (CD42b-positive) released from human Meg-01 cells. **(B)** Flow cytometry summary data indicating percentage of eNOS^{neg} platelets released from Meg-01 cells following treatment with IFNγ (10 ng/ml) and IL-10 (0.1-100.0 ng/ml). **(C)** Flow cytometry summary data indicating percentage of eNOS^{pos} platelets released from Meg-01 cells following treatment with IFNγ (10 ng/ml) and IL-10 (0.1-100.0 ng/ml). Statistics: one-way ANOVA with Tukey post-hoc test. $N = 3$. ***$P < 0.001$.

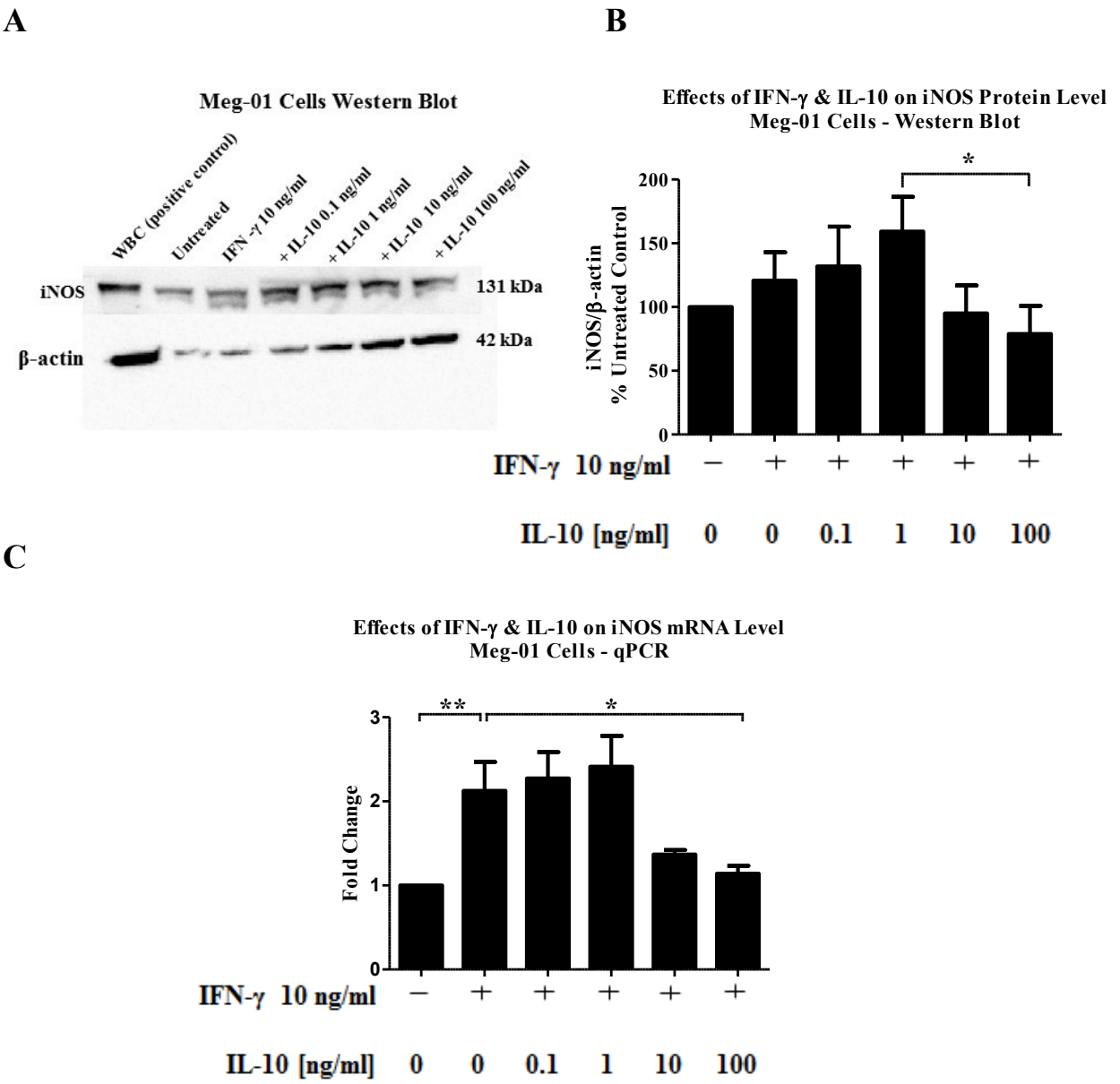

Figure 4.40. Effects of pro-inflammatory IFN-γ and anti-inflammatory IL-10 on iNOS levels by megakaryoblasts

(A) Representative immunoblot demonstrating presence of iNOS protein in human Meg-01 cells following treatment with IFN-γ (10 ng/ml) and IL-10 (0.1-100.0 ng/ml). **(B)** Immunoblot summary data. **(C)** Summary data of eNOS expression following the treatment of human Meg-01 cells with IFNγ (10 ng/ml) and IL-10 (0.1-100.0 ng/ml) by RT-qPCR. Statistics for **B** and **C**: one-way ANOVA with Tukey post-hoc test. $N = 5$, $^{**}P < 0.01$ and $^{*}P < 0.05$.

5. DISCUSSION

The main role of platelets is to maintain haemostasis by forming a blood clot, which stops bleeding upon vascular injury. However, the pathological extension of haemostasis – thrombosis – can lead to uncontrolled thrombus formation, which in some cases obstructs the blood flow to the vital organs like brain and heart. Thrombosis is often associated with atherosclerosis caused by plaque buildup inside arteries and in some cases plaque rupture. Atherosclerosis is also the leading cause of CVD as a result of chronic vascular inflammation mediated by inflammatory cytokines. CVD of brain and heart vessels can sometimes result in thrombosis causing ischemic stroke and MI. Importantly, CVD is the prevalent cause of death worldwide and it has been estimated that the annual number of CVD deaths will continue to rise [1]. CVD is also the second leading cause of death in Canada and almost half of all CV deaths are caused by ischemic events such as ischemic stroke or MI [584]. Platelets being the main cellular culprit of arterial thrombosis are also the main target for the pharmacological prevention and/or therapy of thrombotic events associated with CVD.

Currently, anti-platelet therapies are used for primary and secondary prevention of thrombotic events. Low dose of aspirin, which inhibits platelet COX-1 and thus prevents platelet aggregation is widely used in primary prevention of MI and stoke. On the other hand, the secondary prevention of thrombotic events mainly involves use of ADP receptor (P2Y12) blockers such as ticagrelor and clopidogrel or inhibitors of platelet GPIIb/IIIa (integrin $\alpha_{IIb}\beta_3$) such as eptifibatide. More recently also dual antiplatelet therapy (concomitant use of aspirin and P2Y12 blocker) gained more interest in an effort to reduce the risk of CV events [585]. Although these anti-platelet strategies are well established and relatively well tolerated, in some cases they cause life-threatening bleeding. This major side-effect of anti-platelet therapy is caused by inhibition of platelet haemostatic function which occurs along with inhibiting thrombosis. It has been estimated that individual variability in response to aspirin and other antiplatelet drugs with both hyper- and hyporesponsiveness occurs in 5 to 25% of patients [562-564, 586]. Moreover, randomised trials present quite modest overall effectiveness of antiplatelet therapy in reduction the likelihood of suffering from an ischemic event only by 25%. In addition, aspirin long-term secondary prevention of ischemic events reports only a 13% relative reduction in risk of recurrent ischemic stroke [26, 27]. However, most antiplatelet strategies in high-risk patients

have been applied for secondary prevention at a rather advanced atherosclerotic disease state [587]. Since anti-platelet therapy is burdened by side-effects such as bleeding or in some instances is ineffective, there is a need to better understand platelet biology to enable design of safer and more effective drugs. The ideal drug candidate would an agent that could effectively inhibit or limit thrombus formation with minimal inhibition of haemostasis, thus maintaining the ability to stop instances of bleeding.

Because anucleate platelets have long been considered simple cell fragments there was little investigations into existence of biochemically distinct subpopulations with differential roles in haemostasis and thrombosis. This fairly unknown aspect of platelet biology and function can potentially explain why in some individuals anti-platelet therapy fails to prevent from ischemic events or causes serious adverse effects such as bleeding. Current anti-platelet therapies target different aspects of the platelet system, such as the enzyme and surface receptors. However, there are currently no drugs that target platelet-specific subpopulation with pro-thrombotic/more reactive phenotype and/or function. Hence, our discovery of biochemically distinct eNOS^{neg} and eNOS^{pos} platelets with differential functions has potential important implications for haemostasis and thrombosis.

Synthesis of NO by eNOS in vascular tissues plays an important role as a protective mediator in the CV system, which includes regulation of vascular tone. Importantly, in the late 1980's, Radomski and Moncada proposed that endothelium-derived NO inhibits platelet aggregation which prevents circulating platelets from spontaneous activation and provides support to other inhibitory mechanism mediated by endothelium-derived PGI_2. Subsequently, the same group showed existence of NOS-signaling pathway within human platelets as an endogenous negative-feedback mechanism that prevents platelet adhesion and aggregation [153, 200, 245, 246]. Since then platelet NOS activity has been attributed primarily to the eNOS isoform, although the ability of platelets to produce NO has been questioned in recent years [201, 249, 252, 262, 588].

Currently, there are three prevailing theories arguing that platelet eNOS-signalling pathway (NO-sGC-cGMP-PKG) plays: (i) an inhibitory, (ii) a stimulatory or (iii) not significant role for platelet activation. Our data similar to earlier studies support inhibitory role of platelet eNOS-signalling pathway on their aggregation via NO generation from L-arginine, regardless of the platelet-activating stimulus [200, 247, 253]. In contrast studies advanced by one group [258,

259, 589] propose that the platelet sGC-PKG pathway is involved in biphasic role based on extent of platelet activation. A stimulatory role at low NO concentrations (in response to stimulation with low agonist concentrations) and an inhibitory role at high NO concentrations activation (in response to stimulation with high agonist concentrations), however, these observations could not be confirmed by others [200, 590-592]. In addition, whether NO or $ONOO^-$ was actually generated was not investigated in a study arguing NO biphasic role. NO may react with $O_2^{\bullet -}$ that may be generated when eNOS is uncoupled to form $ONOO^-$, and $ONOO^-$ has been demonstrated to potentiate aggregation. Hence, we argue that NO, unless it reacts with $O_2^{\bullet -}$, only serves as a platelet negative-feedback regulator. Finally, some reports argue that platelet eNOS-signalling pathway (NO-sGC-PKG) plays a minor role in inhibition of platelet activation [260]. This study draws conclusions based on mouse experiments, however, our data provide evidence that let us question utility of mouse platelets to study eNOS-signalling which will be further discussed in this chapter.

To explain some of these discrepancies in findings, we proposed that differences in platelet eNOS levels might account for a part of the divergent results. More importantly, we further hypothesized that if two platelet subpopulations exist based on differential NO-signalling, they may represent functionally distinct platelet subpopulations with differential roles in adhesion and aggregation.

The main objective of our initial experiments was to detect eNOS expression in human platelets. Using confocal microscopy and western blot we showed that human platelets express eNOS protein which is consistent with earlier reports [200, 201, 249, 252, 319]. However, the total amount of eNOS in platelets was 5-fold lower than that of ECs (HMVEC). We further established that eNOS is localized in the platelet plasma membrane which is concordant with the previous reports that eNOS localizes to the plasma membrane lipid raft - caveolae [361, 593]. Our data suggest that identification of such small amount of eNOS protein in human platelets requires optimized eNOS-staining protocol and sensitive methods of detection. And if these standards are not met this may contribute to false negative data and could explain why some studies failed to detect eNOS in human platelets [262, 588]. Finally, confocal microscopy also revealed that some platelets lacked eNOS staining. To further investigate this observation, we decided to use high throughput method – flow cytometry that allows studying cell subsets within total cell population.

In the following flow cytometry experiments we identified platelet subpopulations based on presence or absence of eNOS protein expression ($eNOS^{pos}$ and $eNOS^{neg}$) and the ability to produce NO (low/non NO-producers and NO-producers). This finding is consistent with previously published reports showing presence of NOS/eNOS within human platelets [200, 201, 249]. In our experiments utilizing fluorescent NO indicators we identified that majority of human platelets generated NO (NO-producers), although small subset of human platelets showed no NO production (low/non NO-producers). This observation also corroborates previous reports but most importantly recent study by Cozzi and colleagues where authors visualized the NO production by an individual platelet using DAF-FM diacetate staining [154, 257]. However, that study did not investigate or speculate on whether platelet subpopulations exist with a differential ability to generate NO. While others have previously demonstrated eNOS expression in human platelets and their ability to generate NO, we for the first time indentified a small subset of $eNOS^{neg}$ platelets that generated no or low levels of NO. However, the possibility exists that eNOS levels within $eNOS^{neg}$ (low/no NO-producers) platelets may be below detection limits and that these subpopulations may represent distinct $eNOS^{low}$ or $eNOS^{high}$ platelets. Importantly, we also identified $eNOS^{neg}$ and $eNOS^{pos}$ platelet subpopulations in eNOS-GFP transgenic mice, but unlike in humans the vast majority of mouse platelets were $eNOS^{neg}$ signifying that perhaps major differences in platelet eNOS-signalling exist between the two species. In addition, low eNOS expression in mouse platelets may explain why Ozuyaman *et al.* found eNOS-deficiency to not affect mouse platelet aggregation or bleeding time, although Freedman *et al.* found eNOS-deficient mice to have shorter bleeding times and enhanced platelet recruitment [260, 594]. These disparate findings may also be influenced by factors such as mouse age and/or strain of eNOS-deficient mice. Importantly, to date, eNOS has not been identified in mouse or human platelets by mass spectrometry (MS), although most platelet MS studies have utilized shotgun MS approaches and have not targeted eNOS identification directly, thereby potentially missing this relatively low abundance but important protein [595-598].

To explore potential biochemical differences of $eNOS^{neg}$ and $eNOS^{pos}$ platelets downstream of NO we compared their sGC-PKG-VASP signalling pathways. Our results showed that $eNOS^{neg}$ platelets have down-regulated sGC-PKG signalling pathway, which results in weaker inhibition of fibrinogen receptor - integrin $\alpha_{IIb}\beta_3$ (GPIIb/IIIa). Therefore, we propose that absence of endogenous NO generation coupled with refractoriness to NO due to down-

regulated sGC-PKG-signalling within eNOS^{neg} platelets would result in their preferential binding to exposed collagen and/or vWF in response to vascular injury. Importantly, inactive (but present) platelet sGC-PKG pathway observed in patients with CVD or diabetes has been linked to platelet hyperreactive response to common agonists and refractoriness to NO-donors [24, 315, 319, 322]. Moreover, attenuated platelet NO production in patients with CAD is an independent predictor of ACS [582]. Other study showed that platelets from patients with AMI have increased levels of fibrinogen receptor - integrin $\alpha_{IIb}\beta_3$ in the total platelet population; however, this study failed to test the levels of activated $\alpha_{IIb}\beta_3$ [599]. In our experiments we showed that subpopulation of eNOS^{neg} platelets more readily activates $\alpha_{IIb}\beta_3$, which stabilizes initial rolling and adhesion [600]. Further characterization of eNOS-based platelet subpopulations demonstrated that less abundant eNOS^{neg} platelets secrete higher levels of pro-MMP-2. Secretion of platelet MMP-2 during activation aids recruitment of other platelets to the forming aggregate and potentiates platelet adhesion and aggregation. Importantly, MMP-2 derived from pre-activated platelets was shown to promote intracoronary platelet activation when released in the coronary circulation of ACS patients [160, 164, 601]. On the other hand, more abundant eNOS^{pos} platelets have higher levels of COX-1 and TXB_2 (stable metabolite of TXA_2), which mediate platelet secondary aggregation. Finally, we showed that eNOS^{neg} platelets are more reactive and initiate aggregate formation, while more abundant eNOS^{pos} platelets adhere to collagen at later time points and form bulk an aggregate. In addition, eNOS^{pos} platelets generate NO, which inhibits further platelet recruitment and ultimately limits aggregate size (Figure 5.1). In addition, our experiments showed that increasing the ratio of eNOS^{neg} to eNOS^{pos} platelets or pharmacological inhibition of eNOS results in enhanced platelet aggregation. Our findings suggest that biochemical differences of eNOS^{neg} and eNOS^{pos} platelets may predetermine their haemostatic functions. Similar to our findings, others have demonstrated that platelet-derived NO provides endogenous negative-feedback mechanism, which regulates thrombus formation *in vitro* by inhibiting platelet recruitment to a growing aggregate; however, these studies did not provide evidence of population of low/no NO-producting platelets [253, 602]. Different *in vivo* study highlights the importance of platelet eNOS where intravenous administration of the NOS inhibitor L-N^G-monomethylarginine citrate (L-NMMA) in healthy volunteers results in enhanced platelet aggregation (isolated from the whole blood) in response to agonists [603]. Similar observation was also made by Zhou et al. where addition of NOS inhibitor (L-NAME) to human

resting platelets inhibits their NO generation [604]. Therefore, in light of these reports potential alterations in the ratios of eNOS-based platelet subpopulations may predispose individuals to thrombotic or haemorrhagic events.

Our findings reveal previously unrecognized characteristics and complexity of platelets and their regulation of adhesion/aggregation. This also raises the question whether there is predetermined biochemical diversity and functional heterogeneity among platelets. The identification of platelet subpopulations also has potentially important consequences to human health and disease as impaired platelet NO-signalling has been identified in patients with coronary artery disease [316, 319].

Since our studies were in part driven by discrepant findings that raised concerns to presence of eNOS within human platelets, we carefully designed experiments and validated our methods. The first major concern raised by some authors in the platelet NO-field is that detection of eNOS within human platelets is most likely caused by utilizing non-specific reagents (e.g. anti-eNOS antibodies and NO-indicators) or contamination of platelet samples with other cell types. To address these concerns we performed a series of validation experiments [262, 588]. Based on reports that some commercial antibodies that detect phosphorylated-eNOS non-specifically recognize a protein of similar size, we utilized two different monoclonal anti-eNOS antibodies that do not target phosphorylated-eNOS but amino acid sequence in C-terminus (anti-eNOS M221 clone) and N-terminus (anti-eNOS 6H2 clone) of eNOS protein [262]. Another concern was related to false positive platelet NO production due to contamination by iNOS-expressing leucocytes. Therefore we established sensitive and NO-specific flow cytometry and fluorescence microscopy protocols based on DAF-FM diacetate staining to detect platelet NO production [588]. Due to that specificity of DAF-based compounds as NO-indicators have been questioned as well, we also confirmed DAF-FM specificity toward NO in a series of control experiments [580, 605]. The mass spectrometry of DAF-FM diacetate stained platelets confirmed its conversion to DAF-FM and further reaction with NO resulting in formation of highly fluorescent product– benzotriazole derivative. In addition we were able to detect changes in NO production by VEGF (eNOS agonist) stimulated ECs (HMVEC) measured by DAF-FM. Finally, we also validated NO production within platelets by non-DAF-FM copper-based NO specific fluorescent dye - CuFL2E. It is also noteworthy that criticism related to DAF-FM specificity as NO-indicator is based on studies that measured NO-non-specific fluorescent DAF-

derivatives generated in presence of large amount of H_2O_2 in tobacco plants treated with a fungal elicitor [605]. Using DAF-FM diacetate has another advantage as it provides direct measure of NO synthesis in contrast to cGMP, which is often used as a surrogate of NOS activity but its formation may also result from other mechanism that stimulate activation of sGC such as phosphorylation or protein-protein interactions [606-608].

To explore the genesis of eNOS-based platelet subpopulations, we investigated the presence of eNOS^{neg} and eNOS^{pos} MKs using human megakaryoblastic cell line (Meg-01) and bone marrow of eNOS-GFP mice. As platelets derive from their parent cells MKs, we hypothesized that eNOS^{neg} and eNOS^{pos} subpopulations of MKs exist and give rise to their respective eNOS-based platelet subpopulations. Our experiments identified eNOS-based megakaryocyte/blast subpopulations in Meg-01 cell line and bone marrow of eNOS-GFP mice, although our results showed that major species differences exist in their ratios likely due to negative epigenetic regulation of eNOS gene transcription in mouse MKs. Importantly, while majority of human megakaryoblasts expressed eNOS, we identified only small number of GFP^{pos} (eNOS^{pos}) mouse MKs. Moreover, our flow cytometry experiments demonstrated presence of small subset of Meg-01 cells lacking eNOS protein (eNOS^{neg}). In line with our findings are also studies by Lelchuk et al. and de Belder et al. demonstrating presence of eNOS within Meg-01 cells. However, in contrast to our experiments both authors did not use techniques that allow for identification of cellular subsets based on eNOS-staining, hence they unable to identify eNOS^{neg} Meg-01 cells [280, 282]. Furthermore, our experiments with bone marrow obtained from homozygous eNOS-GFP mice identified that majority of mouse MKs are eNOS^{neg} (GFP^{neg}), which was in agreement with our results showing greater number eNOS^{neg} (GFP^{neg}) platelets in mouse blood samples. This suggests that high level of eNOS^{neg} MKs in the mouse bone marrow may reflect high level of eNOS^{neg} platelets in the mouse circulation. Study by Freedman et al. also demonstrated presence of eNOS mRNA in mouse MKs but in a different mouse strain [254]. In contrast to our study, they measured eNOS mRNA level in total MK population whereas our flow cytometry experiments allowed us to identify presence of eNOS protein that was found only in a small subset of mouse MKs.

To delineate the cause of such high number of eNOS^{neg} MKs in eNOS-GFP mice we decided to investigate DNA methylation that is a natural epigenetic mechanism, which negatively regulates gene expression including eNOS gene in various tissues and cells [332,

609]. We hypothesized that DNA methylation of eNOS gene in mouse MKs is responsible for the low eNOS expression in these cells. Mouse bone marrow samples exposed to 5-azacytosine (DNA methyltransferase inhibitor) showed increased number of $eNOS^{pos}$ (GFP^{pos}) MKs. It has been previously reported that DNA methylation of eNOS gene promoter is responsible for total repression of eNOS in mouse VSMs thereby regulates cell-specific gene transcription [609]. This suggests that DNA-methylation may in part explain the differences of $eNOS^{pos}$ megakaryocytes/blasts between humans and mice. However, 5-azacytinine did not restore the levels of $eNOS^{pos}$ mouse MKs to that observed in human megakaryoblasts which again points out the potential species difference.

Since pro- and anti-inflammatory cytokines are known to have opposing effects on MK differentiation and eNOS expression, we investigated whether pro-inflammatory IFN-γ and anti-inflammatory IL-10 counter-regulate MK eNOS expression and formation of eNOS-based MK subpopulations. Our data revealed that exposure of Meg-01 cells to increasing concentrations of IFN-γ alone decreased number of $eNOS^{pos}$ megakaryoblasts in a concentration-depended manner. In a subsequent experiment, we showed that the reduction of Meg-01 eNOS caused by IFN-γ also occurs at the total population level. These observations suggest that IFN-γ promotes differentiation of megakaryoblasts lacking eNOS by reducing overall eNOS expression in total megakaryoblast population. Currently there are no other studies indicating the effects of pro-inflammatory IFN-γ on eNOS levels in MKs. However, in ECs, which derive from the same common precursor cell as MKs and thus share many developmental regulators, IFN-γ suppresses eNOS expression [508, 509]. Moreover, study by Lelchuk et.al demonstrated reduction of eNOS activity in Meg-01 cells stimulated with pro-inflammatory IL-1β [282]. Overall this novel observation highlights the potential role of pro-inflammatory cytokines in regulating eNOS levels of the bone marrow MKs. However, whether chronic inflammatory state promotes differentiation of $eNOS^{neg}$ MKs *in vivo* is yet to be established. Nonetheless, it is tempting to speculate that chronic inflammatory state such as atherosclerosis would enhance differentiation of $eNOS^{neg}$ MKs. Especially that in a study by de Belder and colleagues the bone marrow MKs from patients with severe coronary atherosclerosis showed very low or no eNOS activity when compared to age-matched control group. This study however has not investigated whether decreased eNOS activity in MKs from patients with atherosclerosis is accompanied by attenuation of MK eNOS protein level. In addition, authors also demonstrate that MKs from

atherosclerotic patients have increased iNOS protein level and activity when compared to MKs from patients with normal coronary arteries [280]. This is concordant with our experiment showing increase of iNOS mRNA level in Meg-01 cells upon stimulation with IFN-γ. Furthermore, in a study by Lelchuk et al. pro-inflammatory cytokines IL-1β and TNF-α caused induction of iNOS in Meg-01 cells and when added together IL-1β and TNF-α showed synergistic effect on iNOS activity. Interestingly, the same study also showed that simultaneous incubation of Meg-01 cells with IL-1β and dexamethasone prevented induction of iNOS activity and preserved eNOS activity. And addition of dexamethasone 24h after stimulation with IL-1β caused time-dependent decrease in iNOS activity and partially restored eNOS activity [282]. Described effects of pro-inflammatory cytokines on eNOS activity are consistent with those observed in endothelial dysfunction in response to chronic inflammation. Enhanced oxidative stress during inflammation results in increased production of free radicals such as $O_2^{\bullet -}$ which is known for its deleterious effects on endothelial eNOS homodimer causing its uncoupling and thus enzymatic inactivation. Another harmful mechanism of inflammation on eNOS is associated with induction of iNOS protein which in long term depletes BH_4 which is necessary for eNOS enzyme coupling. Enzymatic production of NO by iNOS is far greater than by eNOS and local release of a large amount of NO results in its reaction with $O_2^{\bullet -}$ and formation of eNOS and cell-damaging oxidative products such as $ONOO^-$. Therefore both of these mechanisms by depleting eNOS protein contribute to the development of endothelial dysfunction and in consequence CVD. There is a possibility that these mechanisms have negative effect on MK overall eNOS levels which results in enhanced formation of $eNOS^{neg}$ megakaryoblasts during their differentiation in the bone marrow.

In addition, high amount of NO production associated with induction of iNOS in Meg-01 cells has been linked to their enhanced platelet production [283, 506]. In addition, high amount of NO (from exogenous and endogenous sources) has been linked with suppressed growth of bone marrow MKs and apoptosis [505, 506]. Since high level of NO (generated by iNOS) was linked to enhanced platelet production it could also contribute to thrombocytosis that often accompanies inflammatory conditions. Our data however indicate that the change in eNOS level occurs also at the mRNA level, which suggests that pro-inflammatory cytokines may regulate eNOS gene expression. For example one mechanism in which pro-inflammatory TNF-α

decreases the eNOS protein expression is through destabilization of eNOS mRNA by cytosolic proteins, which bind to the 3'-UTR of eNOS mRNA [293, 610, 611].

In a study by Zhang et al. pro-inflammatory cytokines (IFN-γ, TNF-α, IL-1β) caused loss of eNOS activity in membrane fraction of pulmonary ECs combined with significant reduction of eNOS mRNA and protein content. These results suggest that cytokine-induced loss of eNOS catalytic activity and protein is associated with a reduction in eNOS mRNA and protein mass, and that cytokines alter eNOS mRNA stability [502].

Reported by Lelchuk et al. effect of corticosteroid-dexamethasone on activity of both NOS enzymes suggests that immunosuppression plays supportive role in preserving or restoring MK eNOS activity while mitigating iNOS activity during inflammation. Moreover, in our previous experiment IFN-γ suppressed Meg-01 eNOS levels, hence we decided to investigate the ability of anti-inflammatory (immunosuppressive) cytokine IL-10 to counter-regulate negative effects of IFN-γ on eNOS levels in Meg-01 cells. Our results showed that IL-10 in a concentration-dependent manner partially restored megakaryoblast eNOS mRNA levels while decreasing iNOS in Meg-01 cells. There is no literature available describing the effects of reciprocal interaction of IFN-γ and IL-10 on MK eNOS levels. However, in ECs and other cell types IL-10 counteracts the effects of IFN-γ by inhibiting induction of iNOS and enhancing eNOS expression and activity [288, 469, 470, 513]. Studies by Cattaruzza et al. and more recent by Hutchins et al. report that in ECs IL-10 promotes eNOS expression by binding to IL-10 receptor (IL-10R), which activates JAK-STAT3 pathway, and phosphorylated STAT3 translocates to the nucleus where it binds to eNOS gene promoter [470, 514]. In monocytes for example IL-10 suppresses IFN-induced tyrosine phosphorylation of STAT1 and thus prevents STAT1-assebley to its specific promoter motifs on IFN-γ-inducible genes [515, 516]. This mechanism of IL-10 is mediated by upregulation of suppressor of cytokine signalling 3 (SOCS3) gene which is a negative regulator of cytokine signalling. Taken together, our data suggest that within humans the balance between IFN-γ and IL-10 may counter regulates megakaryocyte/blast eNOS levels. However, the exact mechanism by which IL-10 mitigates IFN-γ-mediated induction of iNOS while promoting eNOS expression in Meg-01 cells requires further investigation.

Since IFN-γ and IL-10 counter-regulated MK eNOS levels, and IFN-γ promoted formation of $eNOS^{neg}$ megakaryoblasts, we decided to investigate whether this would contribute

to generation of higher levels of eNOS^{neg} platelets, which we have shown are more reactive than their eNOS^{pos} counterparts. In our experiments Meg-01 cells treated with IFN-γ alone, generated higher percentage of eNOS^{neg} platelets (or platelet-like particles) compared to untreated control sample. Interestingly, addition of increasing concentrations of anti-inflammatory IL-10 restored the ratio of eNOS^{neg} to eNOS^{pos} Meg-01-derived platelets to that observed in untreated control sample. This suggests that modulatory effects of cytokines on eNOS levels and the ratio of eNOS^{neg} to eNOS^{pos} MKs observed in our earlier experiments also influence generation of respective platelet subpopulations. Moreover, it appears that IL-10 counter-regulates IFN-γ-induced effect, which promotes generation of eNOS^{neg} Meg-01-derived platelets. Based on our data it seems possible that inflammatory conditions impair the delicate balance of the bone marrow microenvironment and therefore megakaryopoiesis. As a result, inflammatory bone marrow milieu may promote differentiation of eNOS^{neg} MKs that generate more reactive/pro-thrombotic eNOS^{neg} platelets. Further studies should elucidate the inflammation-mediated mechanisms that suppress eNOS expression/levels in MKs. It is also possible that inflammatory cytokines modulate other aspects of platelet biology and thus enhance their pro-thrombotic phenotype. This type of regulatory system may have evolved to simultaneously enhance haemostasis and combat infection upon injury. If so, the evolution of megakaryocyte and platelet subpopulations based on eNOS signalling in response to IL-10/IFN-γ may also help explain why thrombosis often complicates inflammatory disorders [460]. In contrast to their precursor cells, platelets are anucleate and thus have only a limited residual capacity for protein synthesis. Since platelets inherit most of their content from MKs they may also derive eNOS from their parent cells [523, 524]. Therefore, in a disease state factors that modulate the ratio of eNOS^{neg} to eNOS^{pos} precursor cells (MKs) would probably change the ratio of eNOS^{neg} to eNOS^{pos} platelets and promote generation of more reactive/pro-thrombotic platelets increasing risk of thrombosis.

Impaired platelet NO responsiveness was showed to be an independent predictor of increased CV morbidity and mortality in patients with high-risk ACS [316]. Platelet insensitivity to NO-donors is also accompanied by impaired platelet NO production observed in patients with high-risk ACS, which correlates negatively with increasing numbers of coronary risk factors [314, 315]. It was postulated that chronic inflammation, which often accompanies CVD, suppresses platelet sGC-cGMP signaling pathway which leads not only to platelet pre-activation and reduced endogenous NO production but also to unresponsiveness to exogenous NO-donors

[322]. The platelet NO resistance observed in patients with CVD has been linked with partial inactivation of sGC which suppresses cGMP generation and/or scavenging of NO by increased concentrations of $O_2^{\bullet -}$ [322-325]. Chronic inflammation accompanied by reactive oxygen species production can cause the oxidation or loss of the heme moiety of sGC, which results in enzyme insensitivity to NO [326]. Emami and colleagues showed reduced platelet eNOS mRNA level and activity in patients with CVD [319].

Overall or data introduce novel characteristics and complexity of platelets and their regulation of adhesion and aggregation. The concept of platelet heterogeneity and existence of platelets with different reactivity is not novel. Initially platelet subpopulations were characterized by size and density [541, 542]. Later Patel et al. proposed that "vanguard platelets" are a population of platelets that first adhere to collagen, and are followed by second population of "follower platelets" that adhere over the top of "vanguards". Another platelet subpopulation described in the literature are "COAT" platelets identified based on their differential procoagulant ability and enhanced retention of procoagulant proteins on their surface [13, 17, 555]. Moreover, "COAT" platelets were identified at higher levels in some of stroke patients than healthy controls, which is not surprising considering the prothrombotic nature of this platelet subpopulation [18]. However, in our studies we have not investigated the roles of eNOS-based platelet subpopulations in coagulation hence we cannot speculate whether more reactive $eNOS^{neg}$ platelets are in fact "COAT" platelets.

With current anti-platelet therapies causing bleeding as an undesired adverse effect or in other instances being ineffective and thus contributing to higher mortality among patients with CVD, novel therapies can be more beneficial if directed against specific platelet priming conditions or subpopulations. The discovery of eNOS-based platelet subpopulations with different haemostatic functions not only provides the new insight into platelet biology but also presents more reactive $eNOS^{neg}$ platelets as a novel potential drug target. We also hope that these studies identifying and characterizing platelet subpopulations based on the presence or absence of eNOS-signaling pathway will lead to future prognostic tests that better identify patients at risk of ischemic stroke or MI.

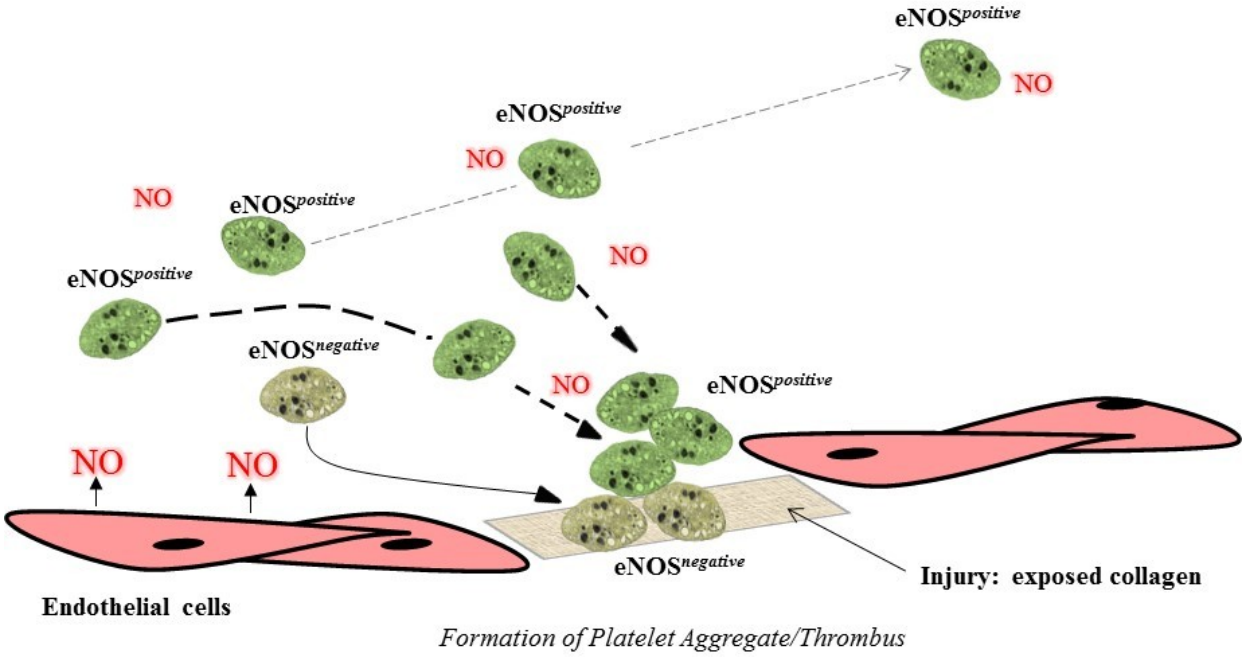

Figure 5.1. A conceptual model of eNOS-based platelet subpopulations in thrombosis and haemostasis

5.1 Limitations of the Study

One of our initial objectives was to perform functional *in vivo* studies to establish different roles of platelet subpopulations in haemostatic reactions and in mouse model of arterial thrombosis. In attempt to perform such experiments, we received eNOS-GFP mice as a gift from Dr. Robert Krams (Imperial College London, UK). The major advantage of using these mice is that they express human eNOS fused to GFP, which eliminates the need for intracellular eNOS staining. Unfortunately, our initial characterization of mouse platelets revealed that unlike in humans the vast majority of mouse platelets are $eNOS^{neg}$ signifying that perhaps major differences in platelet eNOS-signalling exist between the two species. In addition, we also performed intracellular eNOS-staining on platelets from C57BL/6 mice (not presented in this thesis) but again these experiments confirmed our previous findings obtained with eNOS-GFP mice. For this reason, we decided not to peruse further mouse *in vivo* experiments. A potential solution to this problem although technically more challenging, could be utilizing pigs as they are evolutionary more advanced than mice and share more similarities with humans, maybe even similar ratio of $eNOS^{neg}$ to $eNOS^{pos}$ platelets. Another potential solution could be staining human atherosclerotic plaques following rupture to verify the preferential location of $eNOS^{neg}$ and $eNOS^{pos}$ platelets within human thrombus.

Another limitation of our study was utilizing human megakaryoblastic cell line (Meg-01) as a surrogate of human bone marrow MKs. This cell line was derived from the bone marrow of patient with megakaryoblastic crisis of chronic myelogenous leukemia, and cell lines do not always accurately replicate the primary cells [569]. However, due to ethical concerns we decided to utilize Meg-01 cells in our initial experiments, mainly because procedure of bone marrow biopsy is associated with significant stress and discomfort to the patient. In addition, our intention was to perform preliminary studies and optimize protocols for MK flow cytometry eNOS-staining prior utilizing human MKs. Moreover, Meg-01 cells had another advantage as they were previously used and validated as efficient *in vitro* model of platelet generation, and we intended to perform initial mechanistic studies of platelet generation in presence of cytokines before attempting studies with human bone marrow MKs [506].

In this study, we also performed *in vitro* experiments using high concentrations of pro-inflammatory cytokine IFN-γ and anti-inflammatory IL-10. The concentrations of both cytokines

used in experiments match those found in human septic condition. Therefore, this model was purely to establish the proof of concept that requires further diligent studies. Such studies would require utilizing MKs exposed to conditions that better mimic chronic inflammation where numerous pro- and anti-inflammatory factors are present at the same time, as it occurs within human body.

6. CONCLUDING REMARKS

The over-arching goal of this study was to explore whether two platelet subpopulations exist based on the presence or absence of endogenous eNOS-signalling, and thereby represent functionally distinct platelet subpopulations with differential roles in adhesion and aggregation. Importantly, inflammation is associated with atherosclerosis and thrombosis, and presence of hyperreactive platelets has been reported in CVD. For this reason, we studied if pro- and anti-inflammatory cytokines modulate the ratio of $eNOS^{neg}$ to $eNOS^{pos}$ megakaryocytes/blast and consequently the ratio of $eNOS^{neg}$ to $eNOS^{pos}$ platelets. Based on our results we propose:

1) *Human and mouse platelet subpopulations exist based on the presence ($eNOS^{pos}$) and absence ($eNOS^{neg}$) of eNOS-signalling, however in contrast to humans, majority of mouse platelets lack eNOS, in part due to negative epigenetic regulation of eNOS expression within mouse megakaryocytes.*

2) *Biochemical differences exist between human $eNOS^{neg}$ and $eNOS^{pos}$ platelet subpopulations. Less abundant $eNOS^{neg}$ platelets contain higher levels of pro-MMP-2, have downregulated sGC-cGMP-PKG-VASP signalling pathway and more readily activate integrin $\alpha_{IIb}\beta_3$ compared to more abundant $eNOS^{pos}$ platelets that have higher levels of COX-1 and TXB_2.*

3) *Biochemical differences of $eNOS^{neg}$ and $eNOS^{pos}$ platelets contribute to their differential roles during adhesion and aggregation. While $eNOS^{neg}$ platelets are more reactive and initiate aggregate formation, $eNOS^{pos}$ platelets limit the size of an aggregate by generation of NO.*

4) *Human and mouse subpopulations of $eNOS^{neg}$ and $eNOS^{pos}$ megakaryocytes/blasts exist but similar to platelets majority of mouse megakaryocytes lack eNOS. Moreover, it appears that DNA methylation of mouse megakaryocyte eNOS gene is partially responsible for this interspecies variability.*

5) *Pro-inflammatory cytokine IFN-γ attenuates megakaryocyte/blast eNOS levels and promotes formation of megakaryocytes/blasts lacking eNOS that give rise to more reactive eNOS^{neg} platelets.*

6) *Anti-inflammatory cytokine IL-10 counter-regulates IFN-γ inhibitory effect on megakaryocytes/blasts eNOS levels and promotes generation of eNOS^{pos} platelets.*

Taken together our findings suggest that alterations in the ratio of *eNOS^{neg}*/*eNOS^{pos}* platelets may predispose individuals to thrombotic or haemorrhagic events. Furthermore, inflammation may promote differentiation of *eNOS^{neg}* megakaryocytes that give rise to more reactive *eNOS^{neg}* platelets with enhanced aggregation thus increasing the risk of acute ischemic events. Previous studies have reported that platelets from ACS patients have impaired NO production, and that platelet NO production correlates negatively with increasing number of coronary artery disease risk factors [315, 319, 582]. Moreover, platelet refractoriness to the NO-donor sodium nitroprusside was found to be predictive of increased morbidity and mortality in patients with high-risk ACS [316, 466]. These previous clinical studies describe platelet responses that would be characteristic of eNOS^{neg} platelets (absence of eNOS and down-regulation of sGC). Hence, an elevated ratio of eNOS^{neg}/eNOS^{pos} platelets may contribute to ACS etiology and other adverse cardiovascular events such as ischaemic stroke. If so, this raises the prospect that the ratio of eNOS^{neg}/eNOS^{pos} platelets may serve as an effective prognostic biomarker of these adverse cardiovascular events. Finally, further characterization of eNOS^{neg} and eNOS^{pos} platelets may offer the opportunity for early targeting of occlusive thrombus formation, drug development and improved anti-thrombotic therapy.

7. FUTURE DIRECTIONS

The data presented in this thesis provide a basis for many potential avenues for further research.

Our experiments have demonstrated major biochemical differences between eNOS^{neg} and eNOS^{pos} platelets and their differential haemostatic functions. We also showed that eNOS^{neg} platelets more readily activate fibrinogen receptor (integrin $\alpha_{IIb}\beta_3$) compared to eNOS^{pos} platelets. Future studies should further characterize eNOS-based platelet subpopulations based on the activation status of their major surface receptors (e.g. collagen receptor integrin $\alpha_2\beta_1$) in response to agonists. Should such studies identify greater extent of $\alpha_2\beta_1$ receptor activation by eNOS^{neg} platelets, then integrin $\alpha_2\beta_1$ could serve as a novel platelet drug target whose inhibition would preferentially suppress thrombi-initiating eNOS^{neg} platelets.

Another important aspect of potential future studies is evaluation whether currently used anti-platelet agents inhibit eNOS^{neg} and eNOS^{pos} platelets equally or not. These studies could provide the rationale and scientific basis for future development of novel small molecule inhibitors that target eNOS^{neg} platelets. In addition, these experiments may provide insight into whether alterations in eNOS^{neg} to eNOS^{pos} ratios contribute to the observed variability in platelet responses to anti-platelet therapy [563, 612-614].

In our experiments, we have also investigated the differential roles of eNOS^{neg} and eNOS^{pos} platelets during adhesion and aggregation. Future studies should elucidate whether eNOS-based platelet subpopulations also maintain differential functions in platelet-based coagulation. Such studies should include evaluation of platelet differential PS-selectin exposure following activation and platelet surface binding of coagulation factors: IX or IXa, which contribute to the acceleration of coagulation at the wound site. This aspect of eNOS-based platelet subpopulations is especially interesting, as previous studies have shown presence of distinct procoagulant platelet subpopulation – COAT platelets - with phenotype that supports their function in platelet-based coagulation. However, whether eNOS^{neg} platelets are COAT platelets is yet to be established.

Furthermore, our results have demonstrated that in healthy humans majority of platelets are eNOS^{pos} platelets that generate NO due to presence of endogenous eNOS signalling. In contrast, their less abundant eNOS^{neg} counterparts have enhanced adhesiveness and reactivity

due to an absence of endogenous NO generation. In addition, decreased sGC-PKG-VASP signaling within eNOS^{neg} platelets also facilitates refractoriness to endothelial-derived NO and increases integrin $\alpha_{IIb}\beta_3$ activation. These findings may have significant clinical implications as a number of clinical studies have reported that platelets from patients with CVD are refractory to NO-donors and hyperreactive in response to stimulation with agonists [316, 325, 466, 582]. Therefore further studies should measure the ratio of eNOS^{neg} to eNOS^{pos} platelets among these patients as described in the literature platelet responses are characteristic of eNOS^{neg} platelets. In addition, altered ratio of eNOS^{neg} to eNOS^{pos} platelets could serve as an independent prognostic factor of future thrombotic stroke or MI.

Finally, in our studies, we have also identified presence of eNOS-based megakaryoblast subpopulations within human megakaryoblastic cell line Meg-01. Further characterization has demonstrated that majority of human megakaryoblasts are eNOS^{pos} and only few are eNOS^{neg}. Moreover, our experiments showed that pro-inflammatory IFN-γ promotes formation of eNOS^{neg} megakaryoblasts and consequently generation of eNOS^{neg} platelets. However, as mentioned earlier despite some advantages Meg-01 cell line is not ideal to study physiology of human MKs, as it derives from patient with leukemia. Therefore, future studies should evaluate presence and the ratio of eNOS^{neg} to eNOS^{pos} MKs in the bone marrow of healthy humans and patients with various inflammatory disorders, including atherosclerosis – the major culprit of CVD. I hope that such studies would fully elucidate whether inflammation alters the ratio of eNOS^{neg} to eNOS^{pos} MKs within human bone marrow, in a way that promotes formation of eNOS^{neg} MKs that generate more reactive eNOS^{neg} platelets. Importantly, presence of such pathophysiological mechanism would link thrombosis and inflammation and shed light on the cause of increased incidence of arterial thrombosis among patients with CVD.

REFERENCES

1. Organization, W.H., *Technical package for cardiovascular disease management in primary health care*, in https://www.who.int/cardiovascular_diseases/publications/en/. 2016, © World Health Organization 2016: Geneva, Switzerland. p. 11-15.
2. Lusis, A.J., *Atherosclerosis.* Nature, 2000. **407**(6801): p. 233-41.
3. Stary, H.C., *The sequence of cell and matrix changes in atherosclerotic lesions of coronary arteries in the first forty years of life.* Eur Heart J, 1990. **11 Suppl E**: p. 3-19.
4. Insull, W., Jr., *The pathology of atherosclerosis: plaque development and plaque responses to medical treatment.* Am J Med, 2009. **122**(1 Suppl): p. S3-s14.
5. Armstrong, D.A., *Oxidized LDL, ceroid, and prostaglandin metabolism in human atherosclerosis.* Medical Hypotheses, 1992. **38**(3): p. 244-248.
6. Zhao, B., et al., *Endothelial cells injured by oxidized low density lipoprotein.* 1995. **49**(3): p. 250-252.
7. Jackson, C.L. and M.A. Reidy, *Basic fibroblast growth factor: its role in the control of smooth muscle cell migration.* Am J Pathol, 1993. **143**(4): p. 1024-31.
8. Kohno, M., et al., *Induction by Lysophosphatidylcholine, a Major Phospholipid Component of Atherogenic Lipoproteins, of Human Coronary Artery Smooth Muscle Cell Migration.* 1998. **98**(4): p. 353-359.
9. LINDEMANN, S., et al., *Platelets, inflammation and atherosclerosis.* 2007. **5**(s1): p. 203-211.
10. Davies, P.F., et al., *The atherosusceptible endothelium: endothelial phenotypes in complex haemodynamic shear stress regions in vivo.* Cardiovasc Res, 2013. **99**(2): p. 315-27.
11. Hahn, C. and M.A. Schwartz, *Mechanotransduction in vascular physiology and atherogenesis.* Nat Rev Mol Cell Biol, 2009. **10**(1): p. 53-62.
12. Sakariassen, K.S. and R.M. Barstad, *Mechanisms of thromboembolism at arterial plaques.* Blood Coagul Fibrinolysis, 1993. **4**(4): p. 615-25.
13. London, F.S., M. Marcinkiewicz, and P.N. Walsh, *A subpopulation of platelets responds to thrombin- or SFLLRN-stimulation with binding sites for factor IXa.* J Biol Chem, 2004. **279**(19): p. 19854-9.

14. Alberio, L.J. and K.J. Clemetson, *All platelets are not equal: COAT platelets.* Current hematology reports, 2004. **3**(5): p. 338-343.
15. Batar, P. and G.L. Dale, *Simultaneous engagement of thrombin and Fc gamma RIIA receptors results in platelets expressing high levels of procoagulant proteins.* J Lab Clin Med, 2001. **138**(6): p. 393-402.
16. Kempton, C.L., et al., *Platelet heterogeneity: variation in coagulation complexes on platelet subpopulations.* Arterioscler Thromb Vasc Biol, 2005. **25**(4): p. 861-6.
17. Dale, G.L., et al., *Stimulated platelets use serotonin to enhance their retention of procoagulant proteins on the cell surface.* Nature, 2002. **415**(6868): p. 175-9.
18. Prodan, C.I. and G.L. Dale, *Coated-Platelets in Ischemic Stroke – Potential Insight into the Etiology of Stroke Subtypes.* International Journal of Stroke, 2008. **3**(4): p. 249-250.
19. Carvalho, A.C.A., R.W. Colman, and R.S. Lees, *Platelet Function in Hyperlipoproteinemia.* 1974. **290**(8): p. 434-438.
20. Aoki, I., et al., *Platelet-Dependent Thrombin Generation in Patients With Hyperlipidemia.* Journal of the American College of Cardiology, 1997. **30**(1): p. 91-96.
21. Razmara, M., et al., *Platelet hyperprocoagulant activity in Type 2 diabetes mellitus: attenuation by glycoprotein IIb/IIIa inhibition.* J Thromb Haemost, 2008. **6**(12): p. 2186-92.
22. Siess, W., et al., *Lysophosphatidic acid mediates the rapid activation of platelets and endothelial cells by mildly oxidized low density lipoprotein and accumulates in human atherosclerotic lesions.* 1999. **96**(12): p. 6931-6936.
23. Aviram, M., *Modified forms of low density lipoprotein affect platelet aggregation in vitro.* Thrombosis Research, 1989. **53**(6): p. 561-567.
24. Schaeffer, G., et al., *Alterations in platelet Ca2+ signalling in diabetic patients is due to increased formation of superoxide anions and reduced nitric oxide production.* Diabetologia, 1999. **42**(2): p. 167-76.
25. McNicol, A. and S.J. Israels, *Beyond hemostasis: the role of platelets in inflammation, malignancy and infection.* Cardiovasc Hematol Disord Drug Targets, 2008. **8**(2): p. 99-117.
26. *Collaborative meta-analysis of randomised trials of antiplatelet therapy for prevention of death, myocardial infarction, and stroke in high risk patients.* 2002. **324**(7329): p. 71-86.

27. Baigent, C., et al., *Aspirin in the primary and secondary prevention of vascular disease: collaborative meta-analysis of individual participant data from randomised trials.* Lancet, 2009. **373**(9678): p. 1849-60.
28. Palta, S., R. Saroa, and A. Palta, *Overview of the coagulation system.* Indian journal of anaesthesia, 2014. **58**(5): p. 515-523.
29. Celi, A., et al., *Thrombus formation: direct real-time observation and digital analysis of thrombus assembly in a living mouse by confocal and widefield intravital microscopy.* J Thromb Haemost, 2003. **1**(1): p. 60-8.
30. Gale, A.J., *Continuing education course #2: current understanding of hemostasis.* Toxicologic pathology, 2011. **39**(1): p. 273-280.
31. Nilsson, I.M., *Coagulation and fibrinolysis.* Scand J Gastroenterol Suppl, 1987. **137**: p. 11-8.
32. Pallister, C.J. and M.S. Watson, *Haematology.* Scion Publishing, 2010: p. pp. 336–347.
33. Smith, S.A., R.J. Travers, and J.H. Morrissey, *How it all starts: Initiation of the clotting cascade.* Critical reviews in biochemistry and molecular biology, 2015. **50**(4): p. 326-336.
34. Brummel-Ziedins, K. and K.G. Mann, *Chapter 126 - Molecular Basis of Blood Coagulation*, in *Hematology (Seventh Edition)*, R. Hoffman, et al., Editors. 2018, Elsevier. p. 1885-1905.e8.
35. Kalluri, R., *Basement membranes: structure, assembly and role in tumour angiogenesis.* Nature Reviews Cancer, 2003. **3**: p. 422.
36. Yurdagul, A., Jr. and A.W. Orr, *Blood Brothers: Hemodynamics and Cell-Matrix Interactions in Endothelial Function.* Antioxidants & redox signaling, 2016. **25**(7): p. 415-434.
37. Majesky Mark, W., et al., *The Adventitia.* Arteriosclerosis, Thrombosis, and Vascular Biology, 2011. **31**(7): p. 1530-1539.
38. Wagner, D.D. and P.S. Frenette, *The vessel wall and its interactions.* Blood, 2008. **111**(11): p. 5271-5281.
39. Loscalzo, J., P. Libby, and J.A. Epstein, *Basic Biology of the Cardiovascular System*, in *Harrison's Principles of Internal Medicine, 19e*, D. Kasper, et al., Editors. 2014, McGraw-Hill Education: New York, NY.

40. Pappano, A.J., *Cardiovascular physiology*, W.G. Wier, Editor. 2019, PA: Elsevier: Philadelphia.
41. Bluestein, D., et al., *Fluid mechanics of arterial stenosis: relationship to the development of mural thrombus.* Ann Biomed Eng, 1997. **25**(2): p. 344-56.
42. Ruggeri, Z.M., et al., *Activation-independent platelet adhesion and aggregation under elevated shear stress.* 2006. **108**(6): p. 1903-1910.
43. Kerr, P., R. Tam, and F. Plane, *Endothelium*, in *Mechanisms of Vascular Disease: A Reference Book for Vascular Specialists*, R. Fitridge and M. Thompson, Editors. 2011, University of Adelaide Press: Adelaide (AU).
44. McIntyre, T.M., et al., *Cultured endothelial cells synthesize both platelet-activating factor and prostacyclin in response to histamine, bradykinin, and adenosine triphosphate.* J Clin Invest, 1985. **76**(1): p. 271-80.
45. Furchgott, R.F. and J.V. Zawadzki, *The obligatory role of endothelial cells in the relaxation of arterial smooth muscle by acetylcholine.* Nature, 1980. **288**(5789): p. 373-376.
46. Moncada, S., et al., *An enzyme isolated from arteries transforms prostaglandin endoperoxides to an unstable substance that inhibits platelet aggregation.* Nature, 1976. **263**(5579): p. 663-665.
47. Rubanyi, G.M., J.C. Romero, and P.M. Vanhoutte, *Flow-induced release of endothelium-derived relaxing factor.* 1986. **250**(6): p. H1145-H1149.
48. Brozovich, F.V., et al., *Mechanisms of Vascular Smooth Muscle Contraction and the Basis for Pharmacologic Treatment of Smooth Muscle Disorders.* Pharmacological reviews, 2016. **68**(2): p. 476-532.
49. Groves, P., et al., *Role of endogenous bradykinin in human coronary vasomotor control.* Circulation, 1995. **92**(12): p. 3424-30.
50. Miranda, C.H., et al., *Evaluation of the endothelial glycocalyx damage in patients with acute coronary syndrome.* Atherosclerosis, 2016. **247**: p. 184-188.
51. Reitsma, S., et al., *The endothelial glycocalyx: composition, functions, and visualization.* Pflugers Archiv : European journal of physiology, 2007. **454**(3): p. 345-359.
52. Olesen, S.P., D.E. Clapham, and P.F. Davies, *Haemodynamic shear stress activates a K+ current in vascular endothelial cells.* Nature, 1988. **331**(6152): p. 168-70.

53. Yamamoto, K., et al., *Fluid shear stress activates Ca(2+) influx into human endothelial cells via P2X4 purinoceptors.* Circ Res, 2000. **87**(5): p. 385-91.
54. Nauli, S.M., et al., *Endothelial cilia are fluid shear sensors that regulate calcium signaling and nitric oxide production through polycystin-1.* Circulation, 2008. **117**(9): p. 1161-71.
55. Hsieh, H.J., et al., *Increase of reactive oxygen species (ROS) in endothelial cells by shear flow and involvement of ROS in shear-induced c-fos expression.* J Cell Physiol, 1998. **175**(2): p. 156-62.
56. Givens, C. and E. Tzima, *Endothelial Mechanosignaling: Does One Sensor Fit All?* Antioxidants & redox signaling, 2016. **25**(7): p. 373-388.
57. Collins, C., et al., *Haemodynamic and extracellular matrix cues regulate the mechanical phenotype and stiffness of aortic endothelial cells.* Nat Commun, 2014. **5**: p. 3984.
58. Cicmil, M., et al., *Platelet endothelial cell adhesion molecule-1 signaling inhibits the activation of human platelets.* Blood, 2002. **99**(1): p. 137-44.
59. Jones, K.L., et al., *Platelet endothelial cell adhesion molecule-1 is a negative regulator of platelet-collagen interactions.* Blood, 2001. **98**(5): p. 1456-63.
60. Falati, S., et al., *Platelet PECAM-1 inhibits thrombus formation in vivo.* Blood, 2006. **107**(2): p. 535-541.
61. Chen, L., et al., *Inflammatory responses and inflammation-associated diseases in organs.* Oncotarget, 2017. **9**(6): p. 7204-7218.
62. André, P., et al., *Platelets adhere to and translocate on von Willebrand factor presented by endothelium in stimulated veins.* 2000. **96**(10): p. 3322-3328.
63. Massberg, S., et al., *Fibrinogen deposition at the postischemic vessel wall promotes platelet adhesion during ischemia-reperfusion in vivo.* Blood, 1999. **94**(11): p. 3829-38.
64. Khandoga, A., et al., *Platelet adhesion mediated by fibrinogen-intercelllular adhesion molecule-1 binding induces tissue injury in the postischemic liver in vivo.* Transplantation, 2002. **74**(5): p. 681-8.
65. Bombeli, T., B.R. Schwartz, and J.M. Harlan, *Adhesion of activated platelets to endothelial cells: evidence for a GPIIbIIIa-dependent bridging mechanism and novel roles for endothelial intercellular adhesion molecule 1 (ICAM-1), alphavbeta3 integrin, and GPIbalpha.* J Exp Med, 1998. **187**(3): p. 329-39.

66. Lagadec, P., et al., *Involvement of a CD47-dependent pathway in platelet adhesion on inflamed vascular endothelium under flow.* Blood, 2003. **101**(12): p. 4836-43.
67. Bonnefoy, A., et al., *Thrombospondin-1 controls vascular platelet recruitment and thrombus adherence in mice by protecting (sub)endothelial VWF from cleavage by ADAMTS13.* Blood, 2006. **107**(3): p. 955-964.
68. Jurk, K., et al., *Thrombospondin-1 mediates platelet adhesion at high shear via glycoprotein Ib (GPIb): an alternative/backup mechanism to von Willebrand factor.* Faseb j, 2003. **17**(11): p. 1490-2.
69. Wittchen, E.S., *Endothelial signaling in paracellular and transcellular leukocyte transmigration.* Front Biosci (Landmark Ed), 2009. **14**: p. 2522-45.
70. McEver, R.P. and C. Zhu, *Rolling cell adhesion.* Annual review of cell and developmental biology, 2010. **26**: p. 363-396.
71. da Costa Martins, P., et al., *P-selectin glycoprotein ligand-1 is expressed on endothelial cells and mediates monocyte adhesion to activated endothelium.* Arterioscler Thromb Vasc Biol, 2007. **27**(5): p. 1023-9.
72. Tailor, A., D. Cooper, and D.N. Granger, *Platelet-vessel wall interactions in the microcirculation.* Microcirculation, 2005. **12**(3): p. 275-85.
73. Koupenova, M., et al., *Thrombosis and platelets: an update.* European Heart Journal, 2017. **38**(11): p. 785-791.
74. *Thrombosis: a major contributor to the global disease burden.* J Thromb Haemost, 2014. **12**(10): p. 1580-90.
75. Mackman, N., *Triggers, targets and treatments for thrombosis.* Nature, 2008. **451**(7181): p. 914-918.
76. Sleiman, K., et al., *Acute cerebrovascular incident in a young woman: Venous or arterial stroke? - Comparative analysis based on two case reports.* Polish journal of radiology, 2013. **78**(4): p. 70-78.
77. Semenov, S., et al., *How to Distinguish between Venous and Arterial Strokes and Why?* Neuroradiol J, 2011. **24**(2): p. 289-99.
78. Shibata, T., et al., *Prevalence, Clinical Features, and Prognosis of Acute Myocardial Infarction Attributable to Coronary Artery Embolism.* Circulation, 2015. **132**(4): p. 241-50.

79. Raphael, C.E., et al., *Coronary Embolus.* An Underappreciated Cause of Acute Coronary Syndromes, 2018. **11**(2): p. 172-180.
80. Esmon, C.T., *Basic mechanisms and pathogenesis of venous thrombosis.* Blood reviews, 2009. **23**(5): p. 225-229.
81. Previtali, E., et al., *Risk factors for venous and arterial thrombosis.* Blood transfusion = Trasfusione del sangue, 2011. **9**(2): p. 120-138.
82. Szotowski, B., et al., *Procoagulant soluble tissue factor is released from endothelial cells in response to inflammatory cytokines.* Circ Res, 2005. **96**(12): p. 1233-9.
83. Hankey, G.J., *Stroke.* Lancet, 2017. **389**(10069): p. 641-654.
84. Kamel, H. and J.S. Healey, *Cardioembolic Stroke.* Circ Res, 2017. **120**(3): p. 514-526.
85. Eberth, J. and C. Schimmelbusch, *Experimentelle Untersuchungen uber Thrombose Die Anfange der Thrombenbildung.* Fortschr Med, 1885. **3**: p. 379-389.
86. Hayem, G., *Recherches sur l'evolution des hematies dans le sang de l'homme et des vertebres.* Arch Physiol Norm Pathol II, 1878. **5**: p. 692-734.
87. Osler, W., *On certain problems in the physiology of the blood corpuscles.* . The Medical News, 1886. **48**: p. 421-425.
88. Zahn, F., *Untersuchungen uber thrombose.* . Centrralbl Med Wissensch, 1872. **10**: p. 129-130.
89. Bizzozero, G., *Bizzozero's new corpuscle.* . Lancet, 1882. **1**: p. 446.
90. Bizzozero, G., *Su di un nuovo elemento morfologico del sangue dei mammiferi e della sua importanza nella trombosi e nella coagulazione.* L'Osservatore, 1881. **17**: p. 785-787.
91. Bizzozero, G., *On a new blood particle and its role in thrombosis and blood coagulation.* Virchows Arch Pathol Anat Physiol Klin Med, 1882. **90**: p. 261-332.
92. Harker, L.A. and C.A. Finch, *Thrombokinetics in man.* J Clin Invest, 1969. **48**(6): p. 963-74.
93. Aster, R.H., *Studies of the mechanism of "hypersplenic" thrombocytopenia in rats.* J Lab Clin Med, 1967. **70**(5): p. 736-51.
94. Kaushansky, K., *Determinants of platelet number and regulation of thrombopoiesis.* Hematology Am Soc Hematol Educ Program, 2009: p. 147-52.
95. Tavassoli, M. and M. Aoki, *Localization of megakaryocytes in the bone marrow.* Blood Cells, 1989. **15**(1): p. 3-14.

96. Fritsma, G.A., *Platelet Structure and Function.* 2015. **28**(2): p. 125-131.
97. Okumura, T. and G.A. Jamieson, *Platelet glycocalicin. I. Orientation of glycoproteins of the human platelet surface.* J Biol Chem, 1976. **251**(19): p. 5944-9.
98. Harrison, P., et al., *Uptake of plasma fibrinogen into the alpha granules of human megakaryocytes and platelets.* The Journal of Clinical Investigation, 1989. **84**(4): p. 1320-1324.
99. Coller, B.S., *BIOCHEMICAL AND ELECTROSTATIC CONSIDERATIONS IN PRIMARY PLATELET AGGREGATIONa.* 1983. **416**(1): p. 693-708.
100. Grozovsky, R., et al., *The Ashwell-Morell receptor regulates hepatic thrombopoietin production via JAK2-STAT3 signaling.* Nat Med, 2015. **21**(1): p. 47-54.
101. Heemskerk, J.W., E.M. Bevers, and T. Lindhout, *Platelet activation and blood coagulation.* Thromb Haemost, 2002. **88**(2): p. 186-93.
102. Simons, K. and E. Ikonen, *Functional rafts in cell membranes.* Nature, 1997. **387**(6633): p. 569-72.
103. Stan, R.V., *Structure of caveolae.* Biochim Biophys Acta, 2005. **1746**(3): p. 334-48.
104. Rendu, F. and B. Brohard-Bohn, *The platelet release reaction: granules' constituents, secretion and functions.* Platelets, 2001. **12**(5): p. 261-73.
105. Cimmino, G. and P. Golino, *Platelet biology and receptor pathways.* J Cardiovasc Transl Res, 2013. **6**(3): p. 299-309.
106. Rumbaut, R.E. and P. Thiagarajan, *Platelet-Vessel Wall Interactions in Hemostasis and Thrombosis.* 2010, San Rafael (CA): Morgan & Claypool Life Sciences.
107. Behnke, O., *Electron microscopic observations on the membrane systems of the rat blood platelet.* 1967. **158**(2): p. 121-137.
108. Escolar, G., E. Leistikow, and J.G. White, *The fate of the open canalicular system in surface and suspension-activated platelets.* Blood, 1989. **74**(6): p. 1983-8.
109. Gerrard, J.M., J.G. White, and D.A. Peterson, *The platelet dense tubular system: its relationship to prostaglandin synthesis and calcium flux.* Thromb Haemost, 1978. **40**(2): p. 224-31.
110. Ebbeling, L., et al., *Rapid ultrastructural changes in the dense tubular system following platelet activation.* Blood, 1992. **80**(3): p. 718-23.

111. Keularts, I.M., et al., *alpha(2A)-adrenergic receptor stimulation potentiates calcium release in platelets by modulating cAMP levels.* J Biol Chem, 2000. **275**(3): p. 1763-72.
112. Kovacsovics, T.J. and J.H. Hartwig, *Thrombin-induced GPIb-IX centralization on the platelet surface requires actin assembly and myosin II activation.* Blood, 1996. **87**(2): p. 618-29.
113. Bogusławska, D.M., et al., *Spectrin and phospholipids — the current picture of their fascinating interplay.* Cellular & Molecular Biology Letters, 2014. **19**(1): p. 158-179.
114. Thon, J.N., et al., *Microtubule and cortical forces determine platelet size during vascular platelet production.* Nature Communications, 2012. **3**: p. 852.
115. Steiner, M. and Y. Ikeda, *Quantitative Assessment of Polymerized and Depolymerized Platelet Microtubules: CHANGES CAUSED BY AGGREGATING AGENTS.* The Journal of Clinical Investigation, 1979. **63**(3): p. 443-448.
116. White, J.G. and G.H. Rao, *Microtubule coils versus the surface membrane cytoskeleton in maintenance and restoration of platelet discoid shape.* The American journal of pathology, 1998. **152**(2): p. 597-609.
117. Patel, S.R., et al., *Differential roles of microtubule assembly and sliding in proplatelet formation by megakaryocytes.* Blood, 2005. **106**(13): p. 4076-4085.
118. Maxwell, M.J., et al., *Shear Induces a Unique Series of Morphological Changes in Translocating Platelets.* 2006. **26**(3): p. 663-669.
119. Hamilton, J.R., *Structure and function of the open canalicular system – the platelet's specialized internal membrane network AU - Selvadurai, Maria V.* Platelets, 2018. **29**(4): p. 319-325.
120. Frojmovic, M.M. and J.G. Milton, *Human platelet size, shape, and related functions in health and disease.* Physiol Rev, 1982. **62**(1): p. 185-261.
121. MAYNARD, D.M., et al., *Proteomic analysis of platelet α-granules using mass spectrometry.* 2007. **5**(9): p. 1945-1955.
122. Youssefian, T., et al., *Platelet and Megakaryocyte Dense Granules Contain Glycoproteins Ib and IIb-IIIa.* 1997. **89**(11): p. 4047-4057.
123. McNicol, A. and S.J. Israels, *Platelet dense granules: structure, function and implications for haemostasis.* Thromb Res, 1999. **95**(1): p. 1-18.

124. Guppy, M., et al., *Fuel Choices by Human Platelets in Human Plasma.* 1997. **244**(1): p. 161-167.

125. Reuter, H. and R. Gross, *Platelet metabolism.* Suppl Thromb Haemost, 1978. **63**: p. 87-95.

126. Chacko, B.K., et al., *Methods for defining distinct bioenergetic profiles in platelets, lymphocytes, monocytes, and neutrophils, and the oxidative burst from human blood.* Lab Invest, 2013. **93**(6): p. 690-700.

127. Akahori, M., et al., *Hypoxia alters the energy metabolism and aggregation of washed human platelets.* Haematologia (Budap), 1995. **26**(4): p. 191-8.

128. Choo, H.-J., et al., *Mitochondrial Calcium and Reactive Oxygen Species Regulate Agonist-Initiated Platelet Phosphatidylserine Exposure.* Arteriosclerosis, Thrombosis, and Vascular Biology, 2012. **32**(12): p. 2946-2955.

129. Obydennyy, S.I., et al., *Dynamics of calcium spiking, mitochondrial collapse and phosphatidylserine exposure in platelet subpopulations during activation.* 2016. **14**(9): p. 1867-1881.

130. Mason, K.D., et al., *Programmed anuclear cell death delimits platelet life span.* Cell, 2007. **128**(6): p. 1173-86.

131. Kodama, T., et al., *BH3-only activator proteins Bid and Bim are dispensable for Bak/Bax-dependent thrombocyte apoptosis induced by Bcl-xL deficiency: molecular requisites for the mitochondrial pathway to apoptosis in platelets.* J Biol Chem, 2011. **286**(16): p. 13905-13.

132. Mutlu, A., et al., *Activation of caspases-9, -3 and -8 in human platelets triggered by BH3-only mimetic ABT-737 and calcium ionophore A23187: caspase-8 is activated via bypass of the death receptors.* Br J Haematol, 2012. **159**(5): p. 565-71.

133. Josefsson, E.C., et al., *Platelet production proceeds independently of the intrinsic and extrinsic apoptosis pathways.* Nat Commun, 2014. **5**: p. 3455.

134. Lebois, M. and E.C. Josefsson, *Regulation of platelet lifespan by apoptosis.* Platelets, 2016. **27**(6): p. 497-504.

135. Sørensen, A.L., et al., *Role of sialic acid for platelet life span: exposure of β-galactose results in the rapid clearance of platelets from the circulation by asialoglycoprotein receptor–expressing liver macrophages and hepatocytes.* 2009. **114**(8): p. 1645-1654.

136. Rumjantseva, V., et al., *Dual roles for hepatic lectin receptors in the clearance of chilled platelets.* Nat Med, 2009. **15**(11): p. 1273-80.
137. Chen, W., et al., *Inhibiting GPIbα Shedding Preserves Post-Transfusion Recovery and Hemostatic Function of Platelets After Prolonged Storage.* Arteriosclerosis, thrombosis, and vascular biology, 2016. **36**(9): p. 1821-1828.
138. GARDINER, E.E., et al., *Controlled shedding of platelet glycoprotein (GP)VI and GPIb–IX–V by ADAM family metalloproteinases.* 2007. **5**(7): p. 1530-1537.
139. Soslau, G. and J. Giles, *The loss of sialic acid and its prevention in stored human platelets.* Thromb Res, 1982. **26**(6): p. 443-55.
140. Deng, W., et al., *Platelet clearance via shear-induced unfolding of a membrane mechanoreceptor.* Nature Communications, 2016. **7**: p. 12863.
141. Lillicrap, D., *von Willebrand disease: advances in pathogenetic understanding, diagnosis, and therapy.* Blood, 2013. **122**(23): p. 3735-3740.
142. Harrington, W.J., et al., *Demonstration of a thrombocytopenic factor in the blood of patients with thrombocytopenic purpura.* J Lab Clin Med, 1951. **38**(1): p. 1-10.
143. McKenzie, S.E., et al., *The Role of the Human Fc Receptor FcγRIIA in the Immune Clearance of Platelets: A Transgenic Mouse Model.* 1999. **162**(7): p. 4311-4318.
144. Rubinstein, E., et al., *Anti-platelet antibody interactions with Fc gamma receptor.* Semin Thromb Hemost, 1995. **21**(1): p. 10-22.
145. Anderson, G.P., J.G. van de Winkel, and C.L. Anderson, *Anti-GPIIb/IIIa (CD41) monoclonal antibody-induced platelet activation requires Fc receptor-dependent cell-cell interaction.* Br J Haematol, 1991. **79**(1): p. 75-83.
146. Shattil, S.J. and P.J. Newman, *Integrins: dynamic scaffolds for adhesion and signaling in platelets.* Blood, 2004. **104**(6): p. 1606-15.
147. Savage, B., E. Saldivar, and Z.M. Ruggeri, *Initiation of platelet adhesion by arrest onto fibrinogen or translocation on von Willebrand factor.* Cell, 1996. **84**(2): p. 289-97.
148. Henrita van Zanten, G., et al., *Platelet adhesion to collagen type IV under flow conditions.* Blood, 1996. **88**(10): p. 3862-71.
149. Moser, M., et al., *Kindlin-3 is essential for integrin activation and platelet aggregation.* Nat Med, 2008. **14**(3): p. 325-30.

150. Varga-Szabo, D., I. Pleines, and B. Nieswandt, *Cell adhesion mechanisms in platelets.* Arterioscler Thromb Vasc Biol, 2008. **28**(3): p. 403-12.

151. Szalai, G., A.C. LaRue, and D.K. Watson, *Molecular mechanisms of megakaryopoiesis.* Cell Mol Life Sci, 2006. **63**(21): p. 2460-76.

152. Moncada, S. and J.R. Vane, *The role of prostacyclin in vascular tissue.* Fed Proc, 1979. **38**(1): p. 66-71.

153. Radomski, M.W., R.M. Palmer, and S. Moncada, *The anti-aggregating properties of vascular endothelium: interactions between prostacyclin and nitric oxide.* Br J Pharmacol, 1987. **92**(3): p. 639-46.

154. Malinski, T., et al., *Direct electrochemical measurement of nitric oxide released from human platelets.* Biochem Biophys Res Commun, 1993. **194**(2): p. 960-5.

155. Radomski, A., et al., *Identification, regulation and role of tissue inhibitor of metalloproteinases-4 (TIMP-4) in human platelets.* Br J Pharmacol, 2002. **137**(8): p. 1330-8.

156. Santos-Martinez, M.J., et al., *Role of metalloproteinases in platelet function.* Thromb Res, 2008. **121**(4): p. 535-42.

157. Sheu, J.R., et al., *Expression of matrix metalloproteinase-9 in human platelets: regulation of platelet activation in in vitro and in vivo studies.* Br J Pharmacol, 2004. **143**(1): p. 193-201.

158. Lee, Y.M., et al., *Inhibitory mechanisms of activated matrix metalloproteinase-9 on platelet activation.* Eur J Pharmacol, 2006. **537**(1-3): p. 52-8.

159. Sawicki, G., et al., *Localization and translocation of MMP-2 during aggregation of human platelets.* Thromb Haemost, 1998. **80**(5): p. 836-9.

160. Sawicki, G., et al., *Release of gelatinase A during platelet activation mediates aggregation.* Nature, 1997. **386**(6625): p. 616-9.

161. CHOI, W.-S., et al., *MMP-2 regulates human platelet activation by interacting with integrin αIIbβ3.* 2008. **6**(3): p. 517-523.

162. Radomski, A., et al., *Pharmacological characteristics of solid-phase von Willebrand factor in human platelets.* Br J Pharmacol, 2001. **134**(5): p. 1013-20.

163. Martinez, A., et al., *Matrix metalloproteinase-2 in platelet adhesion to fibrinogen: interactions with nitric oxide.* Med Sci Monit, 2001. **7**(4): p. 646-51.

164. FALCINELLI, E., et al., *Intraplatelet signaling mechanisms of the priming effect of matrix metalloproteinase-2 on platelet aggregation.* 2005. **3**(11): p. 2526-2535.

165. Sebastiano, M., et al., *A novel mechanism regulating human platelet activation by MMP-2-mediated PAR1 biased signaling.* Blood, 2017. **129**(7): p. 883-895.

166. Soslau, G., et al., *Intracellular matrix metalloproteinase-2 (MMP-2) regulates human platelet activation via hydrolysis of talin.* Thromb Haemost, 2014. **111**(1): p. 140-53.

167. Lenti, M., et al., *Matrix metalloproteinase-2 of human carotid atherosclerotic plaques promotes platelet activation. Correlation with ischaemic events.* Thromb Haemost, 2014. **111**(6): p. 1089-101.

168. Momi, S., et al., *Loss of matrix metalloproteinase 2 in platelets reduces arterial thrombosis in vivo.* J Exp Med, 2009. **206**(11): p. 2365-79.

169. Galt Spencer, W., et al., *Outside-In Signals Delivered by Matrix Metalloproteinase-1 Regulate Platelet Function.* Circulation Research, 2002. **90**(10): p. 1093-1099.

170. Daniel, J.L., et al., *Molecular basis for ADP-induced platelet activation. I. Evidence for three distinct ADP receptors on human platelets.* J Biol Chem, 1998. **273**(4): p. 2024-9.

171. Neer, E.J., *Heterotrimeric G proteins: organizers of transmembrane signals.* Cell, 1995. **80**(2): p. 249-57.

172. Woulfe, D., et al., *Activation of Rap1B by G(i) family members in platelets.* J Biol Chem, 2002. **277**(26): p. 23382-90.

173. Fabre, J.E., et al., *Decreased platelet aggregation, increased bleeding time and resistance to thromboembolism in P2Y1-deficient mice.* Nat Med, 1999. **5**(10): p. 1199-202.

174. Jones, S., R.J. Evans, and M.P. Mahaut-Smith, *Ca²⁺ Influx through P2X1 Receptors Amplifies P2Y1 Receptor-Evoked Ca²⁺ Signaling and ADP-Evoked Platelet Aggregation.* 2014. **86**(3): p. 243-251.

175. Knezevic, I., C. Borg, and G.C. Le Breton, *Identification of Gq as one of the G-proteins which copurify with human platelet thromboxane A2/prostaglandin H2 receptors.* J Biol Chem, 1993. **268**(34): p. 26011-7.

176. Offermanns, S., et al., *G proteins of the G12 family are activated via thromboxane A2 and thrombin receptors in human platelets.* Proceedings of the National Academy of Sciences of the United States of America, 1994. **91**(2): p. 504-508.

177. Ushikubi, F., K. Nakamura, and S. Narumiya, *Functional reconstitution of platelet thromboxane A2 receptors with Gq and Gi2 in phospholipid vesicles.* Mol Pharmacol, 1994. **46**(5): p. 808-16.

178. Dorsam, R.T., et al., *Coordinated signaling through both G12/13 and G(i) pathways is sufficient to activate GPIIb/IIIa in human platelets.* J Biol Chem, 2002. **277**(49): p. 47588-95.

179. Radomski, A., et al., *Identification, regulation and role of tissue inhibitor of metalloproteinases-4 (TIMP-4) in human platelets.* British journal of pharmacology, 2002. **137**(8): p. 1330-1338.

180. Hernandez-Barrantes, S., et al., *Differential roles of TIMP-4 and TIMP-2 in pro-MMP-2 activation by MT1-MMP.* Biochem Biophys Res Commun, 2001. **281**(1): p. 126-30.

181. Fernandez-Patron, C., et al., *Differential regulation of platelet aggregation by matrix metalloproteinases-9 and -2.* Thromb Haemost, 1999. **82**(6): p. 1730-5.

182. Larkin, C.M., et al., *Role of matrix metalloproteinases 2 and 9, toll-like receptor 4 and platelet-leukocyte aggregate formation in sepsis-associated thrombocytopenia.* PLoS One, 2018. **13**(5): p. e0196478.

183. Cecchetti, L., et al., *Megakaryocytes differentially sort mRNAs for matrix metalloproteinases and their inhibitors into platelets: a mechanism for regulating synthetic events.* 2011. **118**(7): p. 1903-1911.

184. Falcinelli, E., et al., *Response: MMP-9 in platelets: maybe, maybe not.* 2011. **118**(24): p. 6471-6473.

185. Mastenbroek Tom, G., et al., *Platelet-Associated Matrix Metalloproteinases Regulate Thrombus Formation and Exert Local Collagenolytic Activity.* Arteriosclerosis, Thrombosis, and Vascular Biology, 2015. **35**(12): p. 2554-2561.

186. Baramova, E.N., et al., *Involvement of PA/plasmin system in the processing of pro-MMP-9 and in the second step of pro-MMP-2 activation.* FEBS Lett, 1997. **405**(2): p. 157-62.

187. Desrivieres, S., et al., *Activation of the 92 kDa type IV collagenase by tissue kallikrein.* J Cell Physiol, 1993. **157**(3): p. 587-93.

188. Vissers, M.C. and C.C. Winterbourn, *Activation of human neutrophil gelatinase by endogenous serine proteinases.* Biochem J, 1988. **249**(2): p. 327-31.

189. Kurzepa, J., et al., *The significance of matrix metalloproteinase (MMP)-2 and MMP-9 in the ischemic stroke.* International Journal of Neuroscience, 2014. **124**(10): p. 707-716.

190. Best, L.C., et al., *Prostacyclin increases cyclic AMP levels and adenylate cyclase activity in platelets.* Nature, 1977. **267**(5614): p. 850-2.

191. Beck, F., et al., *Time-resolved characterization of cAMP/PKA-dependent signaling reveals that platelet inhibition is a concerted process involving multiple signaling pathways.* 2014. **123**(5): p. e1-e10.

192. Hathaway, D.R., C.R. Eaton, and R.S. Adelstein, *Regulation of human platelet myosin light chain kinase by the catalytic subunit of cyclic AMP-dependent protein kinase.* Nature, 1981. **291**(5812): p. 252-6.

193. Aburima, A., et al., *cAMP signaling regulates platelet myosin light chain (MLC) phosphorylation and shape change through targeting the RhoA-Rho kinase-MLC phosphatase signaling pathway.* 2013. **122**(20): p. 3533-3545.

194. Yusuf, M.Z., et al., *Prostacyclin reverses platelet stress fibre formation causing platelet aggregate instability.* Scientific Reports, 2017. **7**(1): p. 5582.

195. Harbeck, B., et al., *Phosphorylation of the vasodilator-stimulated phosphoprotein regulates its interaction with actin.* J Biol Chem, 2000. **275**(40): p. 30817-25.

196. Bodnar, R.J., et al., *Regulation of glycoprotein Ib-IX-von Willebrand factor interaction by cAMP-dependent protein kinase-mediated phosphorylation at Ser 166 of glycoprotein Ib(beta).* J Biol Chem, 2002. **277**(49): p. 47080-7.

197. Horstrup, K., et al., *Phosphorylation of focal adhesion vasodilator-stimulated phosphoprotein at Ser157 in intact human platelets correlates with fibrinogen receptor inhibition.* Eur J Biochem, 1994. **225**(1): p. 21-7.

198. Stamler, J.S., et al., *Nitric oxide circulates in mammalian plasma primarily as an S-nitroso adduct of serum albumin.* Proc Natl Acad Sci U S A, 1992. **89**(16): p. 7674-7.

199. Ignarro, L.J., et al., *Oxidation of nitric oxide in aqueous solution to nitrite but not nitrate: comparison with enzymatically formed nitric oxide from L-arginine.* 1993. **90**(17): p. 8103-8107.

200. Radomski, M.W., R.M. Palmer, and S. Moncada, *An L-arginine/nitric oxide pathway present in human platelets regulates aggregation.* Proc Natl Acad Sci U S A, 1990. **87**(13): p. 5193-7.

201. Sase, K. and T. Michel, *Expression of constitutive endothelial nitric oxide synthase in human blood platelets.* Life Sci, 1995. **57**(22): p. 2049-55.

202. Mergia, E., et al., *Spare guanylyl cyclase NO receptors ensure high NO sensitivity in the vascular system.* The Journal of clinical investigation, 2006. **116**(6): p. 1731-1737.

203. Ignarro, L.J., *Signal transduction mechanisms involving nitric oxide.* Biochemical Pharmacology, 1991. **41**(4): p. 485-490.

204. Smolenski, A., et al., *Analysis and regulation of vasodilator-stimulated phosphoprotein serine 239 phosphorylation in vitro and in intact cells using a phosphospecific monoclonal antibody.* J Biol Chem, 1998. **273**(32): p. 20029-35.

205. Antl, M., et al., *IRAG mediates NO/cGMP-dependent inhibition of platelet aggregation and thrombus formation.* 2007. **109**(2): p. 552-559.

206. Schinner, E., K. Salb, and J. Schlossmann, *Signaling via IRAG is essential for NO/cGMP-dependent inhibition of platelet activation.* Platelets, 2011. **22**(3): p. 217-27.

207. Wang, G.R., et al., *Mechanism of platelet inhibition by nitric oxide: in vivo phosphorylation of thromboxane receptor by cyclic GMP-dependent protein kinase.* Proc Natl Acad Sci U S A, 1998. **95**(9): p. 4888-93.

208. Marcondes, S., et al., *Cyclic GMP-independent mechanisms contribute to the inhibition of platelet adhesion by nitric oxide donor: a role for alpha-actinin nitration.* Proc Natl Acad Sci U S A, 2006. **103**(9): p. 3434-9.

209. Irwin, C., W. Roberts, and K.M. Naseem, *Nitric oxide inhibits platelet adhesion to collagen through cGMP-dependent and independent mechanisms: the potential role for S-nitrosylation.* Platelets, 2009. **20**(7): p. 478-86.

210. Moro, M.A., et al., *cGMP mediates the vascular and platelet actions of nitric oxide: confirmation using an inhibitor of the soluble guanylyl cyclase.* Proc Natl Acad Sci U S A, 1996. **93**(4): p. 1480-5.

211. Friebe, A., et al., *Fatal gastrointestinal obstruction and hypertension in mice lacking nitric oxide-sensitive guanylyl cyclase.* 2007. **104**(18): p. 7699-7704.

212. Ito, M., et al., *Characterization of the Isoenzymes of cyclic nucleotide phosphodiesterase in human platelets and the effects of E4021.* Cellular Signalling, 1996. **8**(8): p. 575-581.

213. Kotera, J., et al., *Allosteric sites of phosphodiesterase-5 sequester cyclic GMP.* Front Biosci, 2004. **9**: p. 378-86.

214. Gopal, V.K., S.H. Francis, and J.D. Corbin, *Allosteric sites of phosphodiesterase-5 (PDE5). A potential role in negative feedback regulation of cGMP signaling in corpus cavernosum.* Eur J Biochem, 2001. **268**(11): p. 3304-12.

215. Haslam, R.J., N.T. Dickinson, and E.K. Jang, *Cyclic nucleotides and phosphodiesterases in platelets.* Thromb Haemost, 1999. **82**(2): p. 412-23.

216. DICKINSON, N.T., E.K. JANG, and R.J. HASLAM, *Activation of cGMP-stimulated phosphodiesterase by nitroprusside limits cAMP accumulation in human platelets: effects on platelet aggregation.* 1997. **323**(2): p. 371-377.

217. Dunkern, T.R. and A. Hatzelmann, *The effect of Sildenafil on human platelet secretory function is controlled by a complex interplay between phosphodiesterases 2, 3 and 5.* Cell Signal, 2005. **17**(3): p. 331-9.

218. Huang, S.A. and J.D. Lie, *Phosphodiesterase-5 (PDE5) Inhibitors In the Management of Erectile Dysfunction.* P & T : a peer-reviewed journal for formulary management, 2013. **38**(7): p. 407-419.

219. Honour, A.J., et al., *Platelet Behaviour and Drugs Used in Cardiovascular Disease.* Cardiovascular Research, 1967. **1**(2): p. 101-107.

220. Arnold, W.P., et al., *Nitric oxide activates guanylate cyclase and increases guanosine 3':5'-cyclic monophosphate levels in various tissue preparations.* 1977. **74**(8): p. 3203-3207.

221. Murad, F., *Guanylate cyclase : Activation by azide, nitro compounds, nitric oxide, and hydroxyl radical and inhibition by hemoglobin and myoglobin.* Adv Cyclic Nucleotide Res, 1978. **9**: p. 145-158.

222. Loscalzo, J., *N-Acetylcysteine potentiates inhibition of platelet aggregation by nitroglycerin.* J Clin Invest, 1985. **76**(2): p. 703-8.

223. Mellion, B., et al., *Evidence for the inhibitory role of guanosine 3', 5'-monophosphate in ADP-induced human platelet aggregation in the presence of nitric oxide and related vasodilators.* 1981. **57**(5): p. 946-955.

224. Ignarro, L.J., et al., *Association between cyclic GMP accumulation and acetylcholine-elicited relaxation of bovine intrapulmonary artery.* J Pharmacol Exp Ther, 1984. **228**(3): p. 682-90.

225. Rapoport, R.M. and F. Murad, *Agonist-induced endothelium-dependent relaxation in rat thoracic aorta may be mediated through cGMP.* Circ Res, 1983. **52**(3): p. 352-7.

226. Furchgott, R.F., et al., *Endothelial cells as mediators of vasodilation of arteries.* J Cardiovasc Pharmacol, 1984. **6 Suppl 2**: p. S336-43.

227. Ignarro, L.J., B. R.E., and K.S. Wood, *Biochemical and pharmacological properties of endothelium-derived relaxing factor and its similarity to nitric oxide radical Vasodilatation: Vascular Smooth Muscle, Peptide, Autonomic Nerves and Endotheliumed. Vanhoutte, P.M.* New York: Raven Press, 1988: p. 427–436.

228. Furchgott, R.F., *Studies on relaxation of rabbit aorta by sodium nitrite: the basis for the proposal that the acid-activable inhibitory factor from bovine retractor penis is inorganic nitrite and the endothelium-derived relaxing factor is nitric oxide. In P.M. Vanhoutte ed. Mechanism of Vasodilatation.* Raven Press, New York, 1988: p. 401–414.

229. Ignarro, L.J., R.E. Byrns, and W.K. S., *Biochemical and pharmacological properties of EDRF and its similarity to nitric oxide radical In P.M. Vanhoutte (ed.) Mechanism of Vasodilatation.* Raven Press, New York, 1988: p. 427–35.

230. Palmer, R.M.J., A.G. Ferrige, and S. Moncada, *Nitric oxide release accounts for the biological activity of endothelium-derived relaxing factor.* Nature, 1987. **327**(6122): p. 524-526.

231. Palmer, R.M.J., D.S. Ashton, and S. Moncada, *Vascular endothelial cells synthesize nitric oxide from L-arginine.* Nature, 1988. **333**(6174): p. 664-666.

232. Rees, D.D., et al., *A specific inhibitor of nitric oxide formation from L-arginine attenuates endothelium-dependent relaxation.* Br J Pharmacol, 1989. **96**(2): p. 418-24.

233. Moncada, S., R.M.J. Palmer, and E.A. Higgs, *Biosynthesis of nitric oxide from l-arginine: A pathway for the regulation of cell function and communication.* Biochemical Pharmacology, 1989. **38**(11): p. 1709-1715.

234. Vallance, P., et al., *Accumulation of an endogenous inhibitor of nitric oxide synthesis in chronic renal failure.* Lancet, 1992. **339**(8793): p. 572-5.

235. Hibbs, J.B., Jr., R.R. Taintor, and Z. Vavrin, *Macrophage cytotoxicity: role for L-arginine deiminase and imino nitrogen oxidation to nitrite.* Science, 1987. **235**(4787): p. 473-6.

236. Iyengar, R., D.J. Stuehr, and M.A. Marletta, *Macrophage synthesis of nitrite, nitrate, and N-nitrosamines: precursors and role of the respiratory burst.* Proc Natl Acad Sci U S A, 1987. **84**(18): p. 6369-73.

237. Garthwaite, J., S.L. Charles, and R. Chess-Williams, *Endothelium-derived relaxing factor release on activation of NMDA receptors suggests role as intercellular messenger in the brain.* Nature, 1988. **336**(6197): p. 385-388.

238. Bredt, D.S. and S.H. Snyder, *Isolation of nitric oxide synthetase, a calmodulin-requiring enzyme.* 1990. **87**(2): p. 682-685.

239. Bredt, D.S., et al., *Cloned and expressed nitric oxide synthase structurally resembles cytochrome P-450 reductase.* Nature, 1991. **351**(6329): p. 714-718.

240. Yui, Y., et al., *Purification of nitric oxide synthase from rat macrophages.* J Biol Chem, 1991. **266**(19): p. 12544-7.

241. Lyons, C.R., G.J. Orloff, and J.M. Cunningham, *Molecular cloning and functional expression of an inducible nitric oxide synthase from a murine macrophage cell line.* J Biol Chem, 1992. **267**(9): p. 6370-4.

242. Pollock, J.S., et al., *Purification and characterization of particulate endothelium-derived relaxing factor synthase from cultured and native bovine aortic endothelial cells.* 1991. **88**(23): p. 10480-10484.

243. Sessa, W.C., et al., *Molecular cloning and expression of a cDNA encoding endothelial cell nitric oxide synthase.* J Biol Chem, 1992. **267**(22): p. 15274-6.

244. Azuma, H., M. Ishikawa, and S. Sekizaki, *Endothelium-dependent inhibition of platelet aggregation.* 1986. **88**(2): p. 411-415.

245. Radomski, M.W., R.M. Palmer, and S. Moncada, *The role of nitric oxide and cGMP in platelet adhesion to vascular endothelium.* Biochem Biophys Res Commun, 1987. **148**(3): p. 1482-9.

246. PRÓNAI, L., et al., *Investigation of the existence and biological role of l-arginine/nitric oxide pathway in human platelets by spin-trapping/EPR studies.* 1991. **202**(3): p. 923-930.

247. Nguyen, B.L., M. Saitoh, and J.A. Ware, *Interaction of nitric oxide and cGMP with signal transduction in activated platelets.* Am J Physiol, 1991. **261**(4 Pt 2): p. H1043-52.

248. Muruganandam, A. and B. Mutus, *Isolation of nitric oxide synthase from human platelets.* Biochimica et Biophysica Acta (BBA) - General Subjects, 1994. **1200**(1): p. 1-6.

249. Wallerath, T., et al., *Identification of the NO synthase isoforms expressed in human neutrophil granulocytes, megakaryocytes and platelets.* Thromb Haemost, 1997. **77**(1): p. 163-7.

250. Mehta, J.L., et al., *Identification of constitutive and inducible forms of nitric oxide synthase in human platelets.* J Lab Clin Med, 1995. **125**(3): p. 370-7.

251. Chen, L.Y. and J.L. Mehta, *Further evidence of the presence of constitutive and inducible nitric oxide synthase isoforms in human platelets.* J Cardiovasc Pharmacol, 1996. **27**(1): p. 154-8.

252. Ji, Y., et al., *β-Actin regulates platelet nitric oxide synthase 3 activity through interaction with heat shock protein 90.* Proc Natl Acad Sci U S A, 2007. **104**(21): p. 8839-8844.

253. Freedman, J.E., et al., *Nitric oxide released from activated platelets inhibits platelet recruitment.* J Clin Invest, 1997. **100**(2): p. 350-6.

254. Freedman, J.E., et al., *Deficient platelet-derived nitric oxide and enhanced hemostasis in mice lacking the NOSIII gene.* Circ Res, 1999. **84**(12): p. 1416-21.

255. Kobzik, L., et al., *Nitric oxide in skeletal muscle.* Nature, 1994. **372**(6506): p. 546-8.

256. Blatter, L.A., et al., *Simultaneous measurements of Ca2+ and nitric oxide in bradykinin-stimulated vascular endothelial cells.* Circ Res, 1995. **76**(5): p. 922-4.

257. Cozzi, M.R., et al., *Visualization of nitric oxide production by individual platelets during adhesion in flowing blood.* Blood, 2015. **125**(4): p. 697-705.

258. Li, Z., et al., *A stimulatory role for cGMP-dependent protein kinase in platelet activation.* Cell, 2003. **112**(1): p. 77-86.

259. Marjanovic, J.A., et al., *Stimulatory roles of nitric-oxide synthase 3 and guanylyl cyclase in platelet activation.* J Biol Chem, 2005. **280**(45): p. 37430-8.

260. Ozuyaman, B., et al., *Endothelial nitric oxide synthase plays a minor role in inhibition of arterial thrombus formation.* Thromb Haemost, 2005. **93**(6): p. 1161-7.

261. Iafrati, M.D., et al., *Compensatory mechanisms influence hemostasis in setting of eNOS deficiency.* 2005. **288**(4): p. H1627-H1632.

262. GAMBARYAN, S., et al., *NO-synthase-/NO-independent regulation of human and murine platelet soluble guanylyl cyclase activity.* 2008. **6**(8): p. 1376-1384.
263. Tymvios, C., et al., *Platelet aggregation responses are critically regulated in vivo by endogenous nitric oxide but not by endothelial nitric oxide synthase.* Br J Pharmacol, 2009. **158**(7): p. 1735-42.
264. Chen, P.F. and K.K. Wu, *Structural elements contribute to the calcium/calmodulin dependence on enzyme activation in human endothelial nitric-oxide synthase.* J Biol Chem, 2003. **278**(52): p. 52392-400.
265. Hemmens, B. and B. Mayer, *Enzymology of nitric oxide synthases.* Methods Mol Biol, 1998. **100**: p. 1-32.
266. Ortiz de Montellano, P.R., et al., *Nitric oxide synthase structure and electron transfer.* Drug Metab Dispos, 1998. **26**(12): p. 1185-9.
267. Stuehr, D.J., *Enzymes of the L-Arginine to Nitric Oxide Pathway.* The Journal of Nutrition, 2004. **134**(10): p. 2748S-2751S.
268. Dudzinski, D.M., et al., *The regulation and pharmacology of endothelial nitric oxide synthase.* Annu Rev Pharmacol Toxicol, 2006. **46**: p. 235-76.
269. Fulton, D.J.R., *Chapter Two - Transcriptional and Posttranslational Regulation of eNOS in the Endothelium*, in *Advances in Pharmacology*, R.A. Khalil, Editor. 2016, Academic Press. p. 29-64.
270. Stuehr, D.J., *Structure-function aspects in the nitric oxide synthases.* Annu Rev Pharmacol Toxicol, 1997. **37**: p. 339-59.
271. Vasquez-Vivar, J., et al., *Superoxide generation by endothelial nitric oxide synthase: the influence of cofactors.* Proc Natl Acad Sci U S A, 1998. **95**(16): p. 9220-5.
272. Wever, R.M., et al., *Tetrahydrobiopterin regulates superoxide and nitric oxide generation by recombinant endothelial nitric oxide synthase.* Biochem Biophys Res Commun, 1997. **237**(2): p. 340-4.
273. Zou, M.H., C. Shi, and R.A. Cohen, *Oxidation of the zinc-thiolate complex and uncoupling of endothelial nitric oxide synthase by peroxynitrite.* J Clin Invest, 2002. **109**(6): p. 817-26.

274. Greenacre, S.A. and H. Ischiropoulos, *Tyrosine nitration: localisation, quantification, consequences for protein function and signal transduction.* Free Radic Res, 2001. **34**(6): p. 541-81.

275. Lu, T.M., et al., *Plasma levels of asymmetrical dimethylarginine and adverse cardiovascular events after percutaneous coronary intervention.* Eur Heart J, 2003. **24**(21): p. 1912-9.

276. Meinitzer, A., et al., *Asymmetrical dimethylarginine independently predicts total and cardiovascular mortality in individuals with angiographic coronary artery disease (the Ludwigshafen Risk and Cardiovascular Health study).* Clin Chem, 2007. **53**(2): p. 273-83.

277. Forstermann, U., et al., *Isoforms of nitric oxide synthase. Characterization and purification from different cell types.* Biochem Pharmacol, 1991. **42**(10): p. 1849-57.

278. Berkels, R., et al., *Evidence for a NO synthase in porcine platelets which is stimulated during activation/aggregation.* Eur J Haematol, 1997. **58**(5): p. 307-13.

279. Tannous, M., et al., *Evidence for iNOS-dependent peroxynitrite production in diabetic platelets.* Diabetologia, 1999. **42**(5): p. 539-44.

280. de Belder, A., et al., *Megakaryocytes from patients with coronary atherosclerosis express the inducible nitric oxide synthase.* Arterioscler Thromb Vasc Biol, 1995. **15**(5): p. 637-41.

281. Gambaryan, S. and D.J.A.A. Tsikas, *A review and discussion of platelet nitric oxide and nitric oxide synthase: do blood platelets produce nitric oxide from l-arginine or nitrite?* 2015. **47**(9): p. 1779-1793.

282. Lelchuk, R., et al., *Constitutive and inducible nitric oxide synthases in human megakaryoblastic cells.* J Pharmacol Exp Ther, 1992. **262**(3): p. 1220-4.

283. Battinelli, E. and J. Loscalzo, *Nitric oxide induces apoptosis in megakaryocytic cell lines.* 2000. **95**(11): p. 3451-3459.

284. Dusting, G.J., S. Selemidis, and F. Jiang, *Mechanisms for suppressing NADPH oxidase in the vascular wall.* Mem Inst Oswaldo Cruz, 2005. **100 Suppl 1**: p. 97-103.

285. Gunnett, C.A., et al., *Mechanisms of inducible nitric oxide synthase-mediated vascular dysfunction.* Arterioscler Thromb Vasc Biol, 2005. **25**(8): p. 1617-22.

286. Hibbs, J.B., et al., *Nitric oxide: A cytotoxic activated macrophage effector molecule.* Biochemical and Biophysical Research Communications, 1988. **157**(1): p. 87-94.
287. Lowenstein, C.J. and E. Padalko, *iNOS (NOS2) at a glance.* 2004. **117**(14): p. 2865-2867.
288. Arimoto, T., et al., *Interleukin-10 protects against inflammation-mediated degeneration of dopaminergic neurons in substantia nigra.* Neurobiology of Aging, 2007. **28**(6): p. 894-906.
289. Ferlazzo, V., et al., *Anti-inflammatory effects of annexin-1: stimulation of IL-10 release and inhibition of nitric oxide synthesis.* Int Immunopharmacol, 2003. **3**(10-11): p. 1363-9.
290. Gunnett, C.A., et al., *Vascular interleukin-10 protects against LPS-induced vasomotor dysfunction.* Am J Physiol Heart Circ Physiol, 2005. **289**(2): p. H624-30.
291. Tai, S.C., G.B. Robb, and P.A. Marsden, *Endothelial nitric oxide synthase: a new paradigm for gene regulation in the injured blood vessel.* Arterioscler Thromb Vasc Biol, 2004. **24**(3): p. 405-12.
292. Marsden, P.A., et al., *Structure and chromosomal localization of the human constitutive endothelial nitric oxide synthase gene.* J Biol Chem, 1993. **268**(23): p. 17478-88.
293. Yoshizumi, M., et al., *Tumor necrosis factor downregulates an endothelial nitric oxide synthase mRNA by shortening its half-life.* Circ Res, 1993. **73**(1): p. 205-9.
294. Ludmer, P.L., et al., *Paradoxical vasoconstriction induced by acetylcholine in atherosclerotic coronary arteries.* N Engl J Med, 1986. **315**(17): p. 1046-51.
295. Angus, J.A., et al., *THE ACETYLCHOLINE PARADOX: A CONSTRICTOR OF HUMAN SMALL CORONARY ARTERIES EVEN IN THE PRESENCE OF ENDOTHELIUM.* 1991. **18**(1): p. 33-36.
296. Gokce, N., et al., *Predictive value of noninvasively determined endothelial dysfunction for long-term cardiovascular events in patients with peripheral vascular disease.* J Am Coll Cardiol, 2003. **41**(10): p. 1769-75.
297. Schachinger, V., M.B. Britten, and A.M. Zeiher, *Prognostic impact of coronary vasodilator dysfunction on adverse long-term outcome of coronary heart disease.* Circulation, 2000. **101**(16): p. 1899-906.
298. Wilcox, J.N., et al., *Expression of multiple isoforms of nitric oxide synthase in normal and atherosclerotic vessels.* Arterioscler Thromb Vasc Biol, 1997. **17**(11): p. 2479-88.

299. Fukuchi, M. and A. Giaid, *Endothelial expression of endothelial nitric oxide synthase and endothelin-1 in human coronary artery disease. Specific reference to underlying lesion.* Laboratory investigation; a journal of technical methods and pathology, 1999. **79**(6): p. 659-670.

300. *GISSI-3: effects of lisinopril and transdermal glyceryl trinitrate singly and together on 6-week mortality and ventricular function after acute myocardial infarction. Gruppo Italiano per lo Studio della Sopravvivenza nell'infarto Miocardico.* Lancet, 1994. **343**(8906): p. 1115-22.

301. Brunton, T.L., *On the use of nitrite of amyl in angina pectoris.* Lancet, 1867(2): p. 97-98.

302. Nesto, R.W. and G.J. Kowalchuk, *The ischemic cascade: temporal sequence of hemodynamic, electrocardiographic and symptomatic expressions of ischemia.* Am J Cardiol, 1987. **59**(7): p. 23c-30c.

303. Kelly, R.P., et al., *Nitroglycerin has more favourable effects on left ventricular afterload than apparent from measurement of pressure in a peripheral artery.* Eur Heart J, 1990. **11**(2): p. 138-44.

304. Abrams, J., *How to use nitrates.* Cardiovasc Drugs Ther, 2002. **16**(6): p. 511-4.

305. Bogaert, M.G., *Clinical pharmacokinetics of nitrates.* Cardiovasc Drugs Ther, 1994. **8**(5): p. 693-9.

306. Chintala, M.S., V. Bernardino, and P.J. Chiu, *Cyclic GMP but not cyclic AMP prevents renal platelet accumulation after ischemia-reperfusion in anesthetized rats.* 1994. **271**(3): p. 1203-1208.

307. Wu, C.-C., F.-N. Ko, and C.-M. Teng, *Inhibition of Platelet Adhesion to Collagen by cGMP-Elevating Agents.* Biochemical and Biophysical Research Communications, 1997. **231**(2): p. 412-416.

308. de Belder, A.J., et al., *Effects of S-nitroso-glutathione in the human forearm circulation: evidence for selective inhibition of platelet activation.* Cardiovasc Res, 1994. **28**(5): p. 691-4.

309. Chirkov, Y.Y., et al., *Antiplatelet effects of nitroglycerin in healthy subjects and in patients with stable angina pectoris.* Journal of cardiovascular pharmacology, 1993. **21**(3): p. 384-389.

310. Katz, S.D., et al., *Impaired endothelium-mediated vasodilation in the peripheral vasculature of patients with congestive heart failure.* Journal of the American College of Cardiology, 1992. **19**(5): p. 918-925.
311. Schachinger, V. and A.M. Zeiher, *Quantitative assessment of coronary vasoreactivity in humans in vivo. Importance of baseline vasomotor tone in atherosclerosis.* Circulation, 1995. **92**(8): p. 2087-94.
312. Parker, J.D., *Therapy with nitrates: increasing evidence of vascular toxicity.* J Am Coll Cardiol, 2003. **42**(10): p. 1835-7.
313. Thomas, G.R., et al., *Once daily therapy with isosorbide-5-mononitrate causes endothelial dysfunction in humans: evidence of a free-radical-mediated mechanism.* J Am Coll Cardiol, 2007. **49**(12): p. 1289-95.
314. Freedman, J.E., et al., *Impaired Platelet Production of Nitric Oxide Predicts Presence of Acute Coronary Syndromes.* 1998. **98**(15): p. 1481-1486.
315. Ikeda, H., et al., *Platelet-derived nitric oxide and coronary risk factors.* Hypertension, 2000. **35**(4): p. 904-7.
316. Willoughby, S.R., et al., *Platelet Nitric Oxide Responsiveness.* 2005. **25**(12): p. 2661-2666.
317. Woods, J.D., J.S. Edwards, and J.M. Ritter, *Inhibition by nitroprusside of platelet calcium mobilization: evidence for reduced sensitivity to nitric oxide in essential hypertension.* J Hypertens, 1993. **11**(12): p. 1369-73.
318. Anfossi, G., et al., *Platelet resistance to nitrates in obesity and obese NIDDM, and normal platelet sensitivity to both insulin and nitrates in lean NIDDM.* Diabetes Care, 1998. **21**(1): p. 121-6.
319. Emami, Z., et al., *Expression and Activity of Platelet Endothelial Nitric Oxide Synthase Are Decreased in Patients with Coronary Thrombosis and Stenosis.* Avicenna journal of medical biotechnology, 2019. **11**(1): p. 88-93.
320. Chrapko, W.E., et al., *Decreased platelet nitric oxide synthase activity and plasma nitric oxide metabolites in major depressive disorder.* Biol Psychiatry, 2004. **56**(2): p. 129-34.
321. Chrapko, W., et al., *Alteration of decreased plasma NO metabolites and platelet NO synthase activity by paroxetine in depressed patients.* Neuropsychopharmacology, 2006. **31**(6): p. 1286-93.

322. Bergandi, L., et al., *Altered nitric oxide/cGMP platelet signaling pathway in platelets from patients with acute coronary syndromes.* Clin Res Cardiol, 2010. **99**(9): p. 557-64.
323. Chirkov, Y.Y., et al., *Nitrate resistance in platelets from patients with stable angina pectoris.* Circulation, 1999. **100**(2): p. 129-34.
324. Belch, J.J., et al., *Oxygen free radicals and congestive heart failure.* Br Heart J, 1991. **65**(5): p. 245-8.
325. Anderson, R.A., et al., *Determinants of platelet responsiveness to nitric oxide in patients with chronic heart failure.* 2004. **6**(1): p. 47-54.
326. Stasch, J.P., et al., *Targeting the heme-oxidized nitric oxide receptor for selective vasodilatation of diseased blood vessels.* J Clin Invest, 2006. **116**(9): p. 2552-61.
327. Karantzoulis-Fegaras, F., et al., *Characterization of the human endothelial nitric-oxide synthase promoter.* J Biol Chem, 1999. **274**(5): p. 3076-93.
328. Lister, R., et al., *Human DNA methylomes at base resolution show widespread epigenomic differences.* Nature, 2009. **462**(7271): p. 315-322.
329. Robinson, L.J. and T. Michel, *Mutagenesis of palmitoylation sites in endothelial nitric oxide synthase identifies a novel motif for dual acylation and subcellular targeting.* 1995. **92**(25): p. 11776-11780.
330. Zhang, R., W. Min, and W.C. Sessa, *Functional analysis of the human endothelial nitric oxide synthase promoter. Sp1 and GATA factors are necessary for basal transcription in endothelial cells.* J Biol Chem, 1995. **270**(25): p. 15320-6.
331. Fleming, I. and R. Busse, *Molecular mechanisms involved in the regulation of the endothelial nitric oxide synthase.* Am J Physiol Regul Integr Comp Physiol, 2003. **284**(1): p. R1-12.
332. Chan, Y., et al., *The cell-specific expression of endothelial nitric-oxide synthase: a role for DNA methylation.* J Biol Chem, 2004. **279**(33): p. 35087-100.
333. Lund, G., et al., *DNA methylation polymorphisms precede any histological sign of atherosclerosis in mice lacking apolipoprotein E.* J Biol Chem, 2004. **279**(28): p. 29147-54.
334. Radziwon-Balicka, A., et al., *Differential eNOS-signalling by platelet subpopulations regulates adhesion and aggregation.* Cardiovascular research, 2017. **113**(14): p. 1719-1731.

335. Garcia-Cardena, G., et al., *Dissecting the interaction between nitric oxide synthase (NOS) and caveolin. Functional significance of the nos caveolin binding domain in vivo.* J Biol Chem, 1997. **272**(41): p. 25437-40.

336. Shaul, P.W., et al., *Acylation targets emdothelial nitric-oxide synthase to plasmalemmal caveolae.* J Biol Chem, 1996. **271**(11): p. 6518-22.

337. Blair, A., et al., *Oxidized low density lipoprotein displaces endothelial nitric-oxide synthase (eNOS) from plasmalemmal caveolae and impairs eNOS activation.* J Biol Chem, 1999. **274**(45): p. 32512-9.

338. Gratton, J.P., et al., *Reconstitution of an endothelial nitric-oxide synthase (eNOS), hsp90, and caveolin-1 complex in vitro. Evidence that hsp90 facilitates calmodulin stimulated displacement of eNOS from caveolin-1.* J Biol Chem, 2000. **275**(29): p. 22268-72.

339. Pollock, J.S., et al., *Purification and characterization of particulate endothelium-derived relaxing factor synthase from cultured and native bovine aortic endothelial cells.* Proceedings of the National Academy of Sciences of the United States of America, 1991. **88**(23): p. 10480-10484.

340. Nishida, C.R. and P.R. Ortiz de Montellano, *Autoinhibition of endothelial nitric-oxide synthase. Identification of an electron transfer control element.* J Biol Chem, 1999. **274**(21): p. 14692-8.

341. Bucci, M., et al., *In vivo delivery of the caveolin-1 scaffolding domain inhibits nitric oxide synthesis and reduces inflammation.* Nature Medicine, 2000. **6**: p. 1362.

342. Fernández-Hernando, C., et al., *Endothelial-Specific Overexpression of Caveolin-1 Accelerates Atherosclerosis in Apolipoprotein E-Deficient Mice.* The American Journal of Pathology, 2010. **177**(2): p. 998-1003.

343. Robinson, L., et al., *Mutagenesis of palmitoylation sites in endothelial nitric oxide synthase identifies a novel motif for dual acylation and subcellular targeting.* 1995. **92**: p. 11776-11780.

344. Michel, T., et al., *Phosphorylation and subcellular translocation of endothelial nitric oxide synthase.* 1993. **90**: p. 6252-6256.

345. Lisanti, M.P., et al., *Caveolae, transmembrane signalling and cellular transformation.* Mol Membr Biol, 1995. **12**(1): p. 121-4.

346. Parton, R.G. and K. Simons, *The multiple faces of caveolae.* Nat Rev Mol Cell Biol, 2007. **8**(3): p. 185-94.

347. Radel, C. and V. Rizzo, *Integrin mechanotransduction stimulates caveolin-1 phosphorylation and recruitment of Csk to mediate actin reorganization.* Am J Physiol Heart Circ Physiol, 2005. **288**(2): p. H936-45.

348. Gratton, J., et al., *Reconstitution of an endothelial nitric-oxide synthase (eNOS), hsp90, and caveolin-1 complex in vitro. Evidence that hsp90 facilitates calmodulin stimulated displacement of eNOS from caveolin-1.* 2000. **275**: p. 22268-22272.

349. Garcia-Cardena, G., et al., *Dynamic activation of endothelial nitric oxide synthase by Hsp90.* 1998. **392**: p. 821-824.

350. Papapetropoulos, A., et al., *Interaction between the 90-kDa Heat Shock Protein and Soluble Guanylyl Cyclase: Physiological Significance and Mapping of the Domains Mediating Binding<sup/>.* 2005. **68**(4): p. 1133-1141.

351. Jiang, J., et al., *Chaperone-dependent regulation of endothelial nitric-oxide synthase intracellular trafficking by the co-chaperone/ubiquitin ligase CHIP.* J Biol Chem, 2003. **278**(49): p. 49332-41.

352. DEDIO, J., et al., *NOSIP, a novel modulator of endothelial nitric oxide synthase activity.* 2001. **15**(1): p. 79-89.

353. Uittenbogaard, A., et al., *High density lipoprotein prevents oxidized low density lipoprotein-induced inhibition of endothelial nitric-oxide synthase localization and activation in caveolae.* J Biol Chem, 2000. **275**(15): p. 11278-83.

354. Zimmermann, K., et al., *NOSTRIN: A protein modulating nitric oxide release and subcellular distribution of endothelial nitric oxide synthase.* 2002. **99**(26): p. 17167-17172.

355. Feron, O., et al., *Dynamic Regulation of Endothelial Nitric Oxide Synthase: Complementary Roles of Dual Acylation and Caveolin Interactions.* Biochemistry, 1998. **37**(1): p. 193-200.

356. Fernandez-Hernando, C., et al., *Identification of Golgi-localized acyl transferases that palmitoylate and regulate endothelial nitric oxide synthase.* 2006. **174**: p. 369-377.

357. Prabhakar, P., V. Cheng, and T. Michel, *A chimeric transmembrane domain directs endothelial nitric-oxide synthase palmitoylation and targeting to plasmalemmal caveolae.* J Biol Chem, 2000. **275**(25): p. 19416-21.

358. Fernandez-Hernando, C., et al., *Identification of Golgi-localized acyl transferases that palmitoylate and regulate endothelial nitric oxide synthase.* J Cell Biol, 2006. **174**(3): p. 369-77.

359. Liu, J., T.E. Hughes, and W.C. Sessa, *The first 35 amino acids and fatty acylation sites determine the molecular targeting of endothelial nitric oxide synthase into the Golgi region of cells: a green fluorescent protein study.* J Cell Biol, 1997. **137**(7): p. 1525-35.

360. Liu, J., G. Garcia-Cardena, and W.C. Sessa, *Biosynthesis and Palmitoylation of Endothelial Nitric Oxide Synthase: Mutagenesis of Palmitoylation Sites, Cysteines-15 and/or -26, Argues against Depalmitoylation-Induced Translocation of the Enzyme.* Biochemistry, 1995. **34**(38): p. 12333-12340.

361. Garcia-Cardena, G., et al., *Targeting of nitric oxide synthase to endothelial cell caveolae via palmitoylation: implications for nitric oxide signaling.* Proc Natl Acad Sci U S A, 1996. **93**(13): p. 6448-53.

362. Fulton, D., et al., *Localization of endothelial nitric-oxide synthase phosphorylated on serine 1179 and nitric oxide in Golgi and plasma membrane defines the existence of two pools of active enzyme.* J Biol Chem, 2002. **277**(6): p. 4277-84.

363. Boo, Y.C., et al., *Shear stress stimulates phosphorylation of endothelial nitric-oxide synthase at Ser1179 by Akt-independent mechanisms: role of protein kinase A.* J Biol Chem, 2002. **277**(5): p. 3388-96.

364. Butt, E., et al., *Endothelial nitric-oxide synthase (type III) is activated and becomes calcium independent upon phosphorylation by cyclic nucleotide-dependent protein kinases.* J Biol Chem, 2000. **275**(7): p. 5179-87.

365. Chen, Z.-P., et al., *AMP-activated protein kinase phosphorylation of endothelial NO synthase.* 1999. **443**(3): p. 285-289.

366. Fleming, I., et al., *Phosphorylation of Thr(495) regulates Ca(2+)/calmodulin-dependent endothelial nitric oxide synthase activity.* Circ Res, 2001. **88**(11): p. E68-75.

367. Gonzalez, E., et al., *Subcellular targeting and agonist-induced site-specific phosphorylation of endothelial nitric-oxide synthase.* J Biol Chem, 2002. **277**(42): p. 39554-60.

368. Bauer, P.M., et al., *Compensatory phosphorylation and protein-protein interactions revealed by loss of function and gain of function mutants of multiple serine phosphorylation sites in endothelial nitric-oxide synthase.* J Biol Chem, 2003. **278**(17): p. 14841-9.

369. Michell, B.J., et al., *Identification of regulatory sites of phosphorylation of the bovine endothelial nitric-oxide synthase at serine 617 and serine 635.* J Biol Chem, 2002. **277**(44): p. 42344-51.

370. Boo, Y.C., et al., *Shear stress stimulates phosphorylation of eNOS at Ser(635) by a protein kinase A-dependent mechanism.* Am J Physiol Heart Circ Physiol, 2002. **283**(5): p. H1819-28.

371. Kou, R., D. Greif, and T. Michel, *Dephosphorylation of endothelial nitric-oxide synthase by vascular endothelial growth factor. Implications for the vascular responses to cyclosporin A.* J Biol Chem, 2002. **277**(33): p. 29669-73.

372. Li, C., et al., *Role of eNOS phosphorylation at Ser-116 in regulation of eNOS activity in endothelial cells.* Vascular Pharmacology, 2007. **47**(5): p. 257-264.

373. Ruan, L., et al., *Pin1 Prolyl Isomerase Regulates Endothelial Nitric Oxide Synthase.* 2011. **31**(2): p. 392-398.

374. Fulton, D., et al., *Src kinase activates endothelial nitric-oxide synthase by phosphorylating Tyr-83.* J Biol Chem, 2005. **280**(43): p. 35943-52.

375. Fulton, D., et al., *Agonist-Stimulated Endothelial Nitric Oxide Synthase Activation and Vascular Relaxation.* 2008. **102**(4): p. 497-504.

376. Fisslthaler, B., et al., *Inhibition of endothelial nitric oxide synthase activity by proline-rich tyrosine kinase 2 in response to fluid shear stress and insulin.* Circ Res, 2008. **102**(12): p. 1520-8.

377. Loot, A.E., et al., *Angiotensin II impairs endothelial function via tyrosine phosphorylation of the endothelial nitric oxide synthase.* J Exp Med, 2009. **206**(13): p. 2889-96.

378. Wright, J.H., *A Rapid Method for the Differential Staining of Blood Films and Malarial Parasites.* The Journal of medical research, 1902. **7**(1): p. 138-144.
379. WRIGHT, J.H., *The Origin and Nature of the Blood Plates.* 1906. **154**(23): p. 643-645.
380. Wright, J.C., *The histogenesis of the blood platelets.* The Journal of Experimental Medicine, 1910. **21**(21): p. 263–278.
381. Larson, M.K. and S.P. Watson, *A product of their environment: do megakaryocytes rely on extracellular cues for proplatelet formation?* Platelets, 2006. **17**(7): p. 435-40.
382. Lefrançais, E., et al., *The lung is a site of platelet biogenesis and a reservoir for haematopoietic progenitors.* Nature, 2017. **544**: p. 105.
383. Sharma, G.K. and I.C. Talbot, *Pulmonary megakaryocytes: "missing link" between cardiovascular and respiratory disease?* 1986. **39**(9): p. 969-976.
384. Machlus, K.R. and J.E. Italiano, *The incredible journey: From megakaryocyte development to platelet formation.* J Cell Biol Jun, 2013. **201**(6): p. 785-796.
385. Italiano, J.E., Jr., et al., *Blood platelets are assembled principally at the ends of proplatelet processes produced by differentiated megakaryocytes.* J Cell Biol, 1999. **147**(6): p. 1299-312.
386. Zimmet, J. and K. Ravid, *Polyploidy: Occurrence in nature, mechanisms, and significance for the megakaryocyte-platelet system.* Experimental Hematology, 2000. **28**(1): p. 3-16.
387. Wang, Z., et al., *Cyclin D3 is essential for megakaryocytopoiesis.* 1995. **86**(10): p. 3783-3788.
388. Geng, Y., et al., *Cyclin E Ablation in the Mouse.* Cell, 2003. **114**(4): p. 431-443.
389. Behnke, O., *An electron microscope study of the megacaryocyte of the rat bone marrow. I. The development of the demarcation membrane system and the platelet surface coat.* J Ultrastruct Res, 1968. **24**(5): p. 412-33.
390. Radley, J.M. and C.J. Haller, *The demarcation membrane system of the megakaryocyte: a misnomer?* Blood, 1982. **60**(1): p. 213-9.
391. Zucker-Franklin, D. and C.S. Philipp, *Platelet production in the pulmonary capillary bed: new ultrastructural evidence for an old concept.* Am J Pathol, 2000. **157**(1): p. 69-74.

392. Lepage, A., et al., *The alpha(IIb)beta(3) integrin and GPIb-V-IX complex identify distinct stages in the maturation of CD34(+) cord blood cells to megakaryocytes.* Blood, 2000. **96**(13): p. 4169-77.
393. *Williams hematology*, K. Kaushansky, et al., Editors.
394. Junt, T., et al., *Dynamic visualization of thrombopoiesis within bone marrow.* Science, 2007. **317**(5845): p. 1767-70.
395. Patel, S.R., J.H. Hartwig, and J.E. Italiano, Jr., *The biogenesis of platelets from megakaryocyte proplatelets.* J Clin Invest, 2005. **115**(12): p. 3348-54.
396. Mattia, G., et al., *Different ploidy levels of megakaryocytes generated from peripheral or cord blood CD34⁺ cells are correlated with different levels of platelet release.* 2002. **99**(3): p. 888-897.
397. Mazzi, S., et al., *Megakaryocyte and polyploidization.* Exp Hematol, 2018. **57**: p. 1-13.
398. Richardson, J.L., et al., *Mechanisms of organelle transport and capture along proplatelets during platelet production.* 2005. **106**(13): p. 4066-4075.
399. Ebbe, S. and F. Stohlman, Jr., *MEGAKARYOCYTOPOIESIS IN THE RAT.* Blood, 1965. **26**: p. 20-35.
400. Bianchi, E., et al., *Genomic landscape of megakaryopoiesis and platelet function defects.* 2016. **127**(10): p. 1249-1259.
401. Visvader, J.E., et al., *GATA-1 but not SCL induces megakaryocytic differentiation in an early myeloid line.* Embo j, 1992. **11**(12): p. 4557-64.
402. Stachura, D.L., S.T. Chou, and M.J. Weiss, *Early block to erythromegakaryocytic development conferred by loss of transcription factor GATA-1.* 2006. **107**(1): p. 87-97.
403. Vyas, P., et al., *Consequences of GATA-1 Deficiency in Megakaryocytes and Platelets.* 1999. **93**(9): p. 2867-2875.
404. Whyatt, D.J., et al., *The level of the tissue-specific factor GATA-1 affects the cell-cycle machinery.* Genes Funct, 1997. **1**(1): p. 11-24.
405. Dore, L.C. and J.D. Crispino, *Transcription factor networks in erythroid cell and megakaryocyte development.* Blood, 2011. **118**(2): p. 231-9.
406. Amigo, J.D., et al., *The role and regulation of friend of GATA-1 (FOG-1) during blood development in the zebrafish.* 2009. **114**(21): p. 4654-4663.

407. Jackers, P., et al., *Ets-dependent regulation of target gene expression during megakaryopoiesis.* J Biol Chem, 2004. **279**(50): p. 52183-90.

408. Shivdasani, R.A., et al., *Transcription factor NF-E2 is required for platelet formation independent of the actions of thrombopoietin/MGDF in megakaryocyte development.* Cell, 1995. **81**(5): p. 695-704.

409. Shivdasani, R.A., *The role of transcription factor NF-E2 in megakaryocyte maturation and platelet production.* Stem Cells, 1996. **14 Suppl 1**: p. 112-5.

410. Schwer, H.D., et al., *A lineage-restricted and divergent beta-tubulin isoform is essential for the biogenesis, structure and function of blood platelets.* Curr Biol, 2001. **11**(8): p. 579-86.

411. Kunishima, S., et al., *Mutation of the beta1-tubulin gene associated with congenital macrothrombocytopenia affecting microtubule assembly.* Blood, 2009. **113**(2): p. 458-61.

412. Lecine, P., et al., *Hematopoietic-specific β1 tubulin participates in a pathway of platelet biogenesis dependent on the transcription factor NF-E2.* 2000. **96**(4): p. 1366-1373.

413. Deveaux, S., et al., *p45 NF-E2 regulates expression of thromboxane synthase in megakaryocytes.* The EMBO journal, 1997. **16**(18): p. 5654-5661.

414. Shiraga, M., et al., *Primary Megakaryocytes Reveal a Role for Transcription Factor Nf-E2 in Integrin αiibβ3 Signaling.* 1999. **147**(7): p. 1419-1430.

415. Eto, K., et al., *Megakaryocytes derived from embryonic stem cells implicate CalDAG-GEFI in integrin signaling.* 2002. **99**(20): p. 12819-12824.

416. Reagan, M.R. and C.J. Rosen, *Navigating the bone marrow niche: translational insights and cancer-driven dysfunction.* Nature reviews. Rheumatology, 2016. **12**(3): p. 154-168.

417. Wang, J.-Y., S. Ye, and H. Zhong, *The role of bone marrow microenvironment in platelet production and their implications for the treatment of thrombocytopenic diseases.* Hematology, 2017. **22**(10): p. 630-639.

418. Kaushansky, K., *Hematopoietic growth factors, signaling and the chronic myeloproliferative disorders.* Cytokine & Growth Factor Reviews, 2006. **17**(6): p. 423-430.

419. Makar, R.S., et al., *Thrombopoietin levels in patients with disorders of platelet production: diagnostic potential and utility in predicting response to TPO receptor agonists.* Am J Hematol, 2013. **88**(12): p. 1041-4.

420. Debili, N., et al., *The Mpl receptor is expressed in the megakaryocytic lineage from late progenitors to platelets.* Blood, 1995. **85**(2): p. 391-401.
421. Forsberg, E.C., et al., *Differential expression of novel potential regulators in hematopoietic stem cells.* PLoS Genet, 2005. **1**(3): p. e28.
422. Kaushansky, K., et al., *Thrombopoietin, the Mp1 ligand, is essential for full megakaryocyte development.* Proc Natl Acad Sci U S A, 1995. **92**(8): p. 3234-8.
423. Kobayashi, M., et al., *Thrombopoietin supports proliferation of human primitive hematopoietic cells in synergy with steel factor and/or interleukin-3.* 1996. **88**(2): p. 429-436.
424. Kaushansky, K., et al., *Promotion of megakaryocyte progenitor expansion and differentiation by the c-Mpl ligand thrombopoietin.* Nature, 1994. **369**(6481): p. 568-71.
425. Choi, E.S., et al., *Platelets generated in vitro from proplatelet-displaying human megakaryocytes are functional.* Blood, 1995. **85**(2): p. 402-13.
426. de Sauvage, F.J., et al., *Physiological regulation of early and late stages of megakaryocytopoiesis by thrombopoietin.* 1996. **183**(2): p. 651-656.
427. Vijey, P., B. Posorske, and K.R. Machlus, *In vitro culture of murine megakaryocytes from fetal liver-derived hematopoietic stem cells.* Platelets, 2018. **29**(6): p. 583-588.
428. Ezumi, Y., H. Takayama, and M. Okuma, *Thrombopoietin, c-Mpl ligand, induces tyrosine phosphorylation of Tyk2, JAK2, and STAT3, and enhances agonists-induced aggregation in platelets in vitro.* FEBS Lett, 1995. **374**(1): p. 48-52.
429. Morita, H., et al., *Functional analysis of the cytoplasmic domain of the human Mpl receptor for tyrosine-phosphorylation of the signaling molecules, proliferation and differentiation.* FEBS Lett, 1996. **395**(2-3): p. 228-34.
430. Drachman, J.G., K.M. Millett, and K. Kaushansky, *Thrombopoietin signal transduction requires functional JAK2, not TYK2.* J Biol Chem, 1999. **274**(19): p. 13480-4.
431. Varghese, L.N., et al., *The Thrombopoietin Receptor: Structural Basis of Traffic and Activation by Ligand, Mutations, Agonists, and Mutated Calreticulin.* Frontiers in endocrinology, 2017. **8**: p. 59-59.
432. Rojnuckarin, P., J.G. Drachman, and K. Kaushansky, *Thrombopoietin-induced activation of the mitogen-activated protein kinase (MAPK) pathway in normal megakaryocytes: role in endomitosis.* Blood, 1999. **94**(4): p. 1273-82.

433. Rawlings, J.S., K.M. Rosler, and D.A. Harrison, *The JAK/STAT signaling pathway.* 2004. **117**(8): p. 1281-1283.

434. Geddis, A.E., N.E. Fox, and K. Kaushansky, *Phosphatidylinositol 3-kinase is necessary but not sufficient for thrombopoietin-induced proliferation in engineered Mpl-bearing cell lines as well as in primary megakaryocytic progenitors.* J Biol Chem, 2001. **276**(37): p. 34473-9.

435. Kaushansky, K., *The molecular mechanisms that control thrombopoiesis.* The Journal of Clinical Investigation, 2005. **115**(12): p. 3339-3347.

436. Barroga, C.F., H. Pham, and K. Kaushansky, *Thrombopoietin regulates c-Myb expression by modulating micro RNA 150 expression.* Exp Hematol, 2008. **36**(12): p. 1585-92.

437. Malara, A., et al., *The secret life of a megakaryocyte: emerging roles in bone marrow homeostasis control.* Cell Mol Life Sci, 2015. **72**(8): p. 1517-36.

438. Stoffel, R., A. Wiestner, and R.C. Skoda, *Thrombopoietin in thrombocytopenic mice: evidence against regulation at the mRNA level and for a direct regulatory role of platelets.* Blood, 1996. **87**(2): p. 567-73.

439. Fielder, P.J., et al., *Regulation of thrombopoietin levels by c-mpl-mediated binding to platelets.* Blood, 1996. **87**(6): p. 2154-61.

440. Gurney, A.L., et al., *Thrombocytopenia in c-mpl-deficient mice.* Science, 1994. **265**(5177): p. 1445-7.

441. Alexander, W.S., et al., *Deficiencies in progenitor cells of multiple hematopoietic lineages and defective megakaryocytopoiesis in mice lacking the thrombopoietic receptor c-Mpl.* Blood, 1996. **87**(6): p. 2162-70.

442. Ng, A.P., et al., *Mpl expression on megakaryocytes and platelets is dispensable for thrombopoiesis but essential to prevent myeloproliferation.* 2014. **111**(16): p. 5884-5889.

443. Nishimura, S., et al., *IL-1α induces thrombopoiesis through megakaryocyte rupture in response to acute platelet needs.* 2015. **209**(3): p. 453-466.

444. Italiano, J.E. and J.H. Hartwig, *Chapter 124 - Megakaryocyte and Platelet Structure*, in *Hematology (Seventh Edition)*, R. Hoffman, et al., Editors. 2018, Elsevier. p. 1857-1869.

445. Cheng, L., et al., *Human mesenchymal stem cells support megakaryocyte and pro-platelet formation from CD34(+) hematopoietic progenitor cells.* J Cell Physiol, 2000. **184**(1): p. 58-69.

446. Ishibashi, T., et al., *Human interleukin 6 is a direct promoter of maturation of megakaryocytes in vitro.* Proceedings of the National Academy of Sciences of the United States of America, 1989. **86**(15): p. 5953-5957.

447. Hodohara, K., et al., *Stromal cell-derived factor-1 (SDF-1) acts together with thrombopoietin to enhance the development of megakaryocytic progenitor cells (CFU-MK).* 2000. **95**(3): p. 769-775.

448. Hamada, T., et al., *Transendothelial migration of megakaryocytes in response to stromal cell-derived factor 1 (SDF-1) enhances platelet formation.* J Exp Med, 1998. **188**(3): p. 539-48.

449. Wang, J.F., Z.Y. Liu, and J.E. Groopman, *The alpha-chemokine receptor CXCR4 is expressed on the megakaryocytic lineage from progenitor to platelets and modulates migration and adhesion.* Blood, 1998. **92**(3): p. 756-64.

450. Majka, M., et al., *Stromal-derived factor 1 and thrombopoietin regulate distinct aspects of human megakaryopoiesis.* 2000. **96**(13): p. 4142-4151.

451. Schweitzer, K.M., et al., *Constitutive expression of E-selectin and vascular cell adhesion molecule-1 on endothelial cells of hematopoietic tissues.* Am J Pathol, 1996. **148**(1): p. 165-75.

452. Jiang, S., et al., *Cytokine production by primary bone marrow megakaryocytes.* Blood, 1994. **84**(12): p. 4151-6.

453. Zhao, M., et al., *Megakaryocytes maintain homeostatic quiescence and promote post-injury regeneration of hematopoietic stem cells.* Nat Med, 2014. **20**(11): p. 1321-6.

454. Kaser, A., et al., *Interleukin-6 stimulates thrombopoiesis through thrombopoietin: role in inflammatory thrombocytosis.* Blood, 2001. **98**(9): p. 2720-5.

455. Kaser, A., et al., *Interleukin-6 stimulates thrombopoiesis through thrombopoietin: role in inflammatory thrombocytosis.* 2001. **98**(9): p. 2720-2725.

456. Alonzi, T., et al., *Essential Role of STAT3 in the Control of the Acute-Phase Response as Revealed by Inducible Gene Activation in the Liver.* 2001. **21**(5): p. 1621-1632.

457. Muraoka, K., et al., *Thrombopoietin-independent effect of interferon-gamma on the proliferation of human megakaryocyte progenitors.* Br J Haematol, 1997. **98**(2): p. 265-73.

458. Masamoto, Y. and M. Kurokawa, *Inflammation-induced emergency megakaryopoiesis: inflammation paves the way for platelets.* Stem cell investigation, 2016. **3**: p. 16-16.

459. Kaptoge, S., et al., *Inflammatory cytokines and risk of coronary heart disease: new prospective study and updated meta-analysis.* European heart journal, 2014. **35**(9): p. 578-589.

460. SMYTH, S.S., et al., *Platelet functions beyond hemostasis.* J Thromb Haemost, 2009. **7**(11): p. 1759-1766.

461. Vinholt, P.J., et al., *Platelet count is associated with cardiovascular disease, cancer and mortality: A population-based cohort study.* Thrombosis Research, 2016. **148**: p. 136-142.

462. Griesshammer, M., et al., *Aetiology and clinical significance of thrombocytosis: analysis of 732 patients with an elevated platelet count.* J Intern Med, 1999. **245**(3): p. 295-300.

463. Thaulow, E., et al., *Blood platelet count and function are related to total and cardiovascular death in apparently healthy men.* Circulation, 1991. **84**(2): p. 613-7.

464. Langford, E.J., R.J. Wainwright, and J.F. Martin, *Platelet activation in acute myocardial infarction and unstable angina is inhibited by nitric oxide donors.* Arterioscler Thromb Vasc Biol, 1996. **16**(1): p. 51-5.

465. Hamm, C.W., et al., *Biochemical evidence of platelet activation in patients with persistent unstable angina.* 1987. **10**(5): p. 998-1004.

466. Chirkov, Y.Y., et al., *Stable angina and acute coronary syndromes are associated with nitric oxide resistance in platelets.* 2001. **37**(7): p. 1851-1857.

467. Willoughby, S., A. Holmes, and J. Loscalzo, *Platelets and cardiovascular disease.* Eur J Cardiovasc Nurs, 2002. **1**(4): p. 273-88.

468. Ferroni, P., et al., *Low-density lipoprotein-lowering medication and platelet function.* Pathophysiol Haemost Thromb, 2006. **35**(3-4): p. 346-54.

469. Roach, T.I., et al., *Opposing effects of interferon-gamma on iNOS and interleukin-10 expression in lipopolysaccharide- and mycobacterial lipoarabinomannan-stimulated macrophages.* Immunology, 1995. **85**(1): p. 106-13.

470. Cattaruzza, M., et al., *Interleukin-10 induction of nitric-oxide synthase expression attenuates CD40-mediated interleukin-12 synthesis in human endothelial cells.* J Biol Chem, 2003. **278**(39): p. 37874-80.

471. Niedzielska, I. and S. Cierpka, *Interferon gamma in the etiology of atherosclerosis and periodontitis.* Thromb Res, 2010. **126**(4): p. 324-7.
472. Min, X., et al., *Serum Cytokine Profile in Relation to the Severity of Coronary Artery Disease.* BioMed research international, 2017. **2017**: p. 4013685-4013685.
473. Heinisch, R.H., et al., *Serial changes in plasma levels of cytokines in patients with coronary artery disease.* Vascular health and risk management, 2005. **1**(3): p. 245-250.
474. Lauw, F.N., et al., *Elevated Plasma Concentrations of Interferon (IFN)-γ and the IFN-γ—Inducing Cytokines Interleukin (IL)-18, IL-12, and IL-15 in Severe Melioidosis.* The Journal of Infectious Diseases, 1999. **180**(6): p. 1878-1885.
475. Pinsky, M.R., et al., *Serum Cytokine Levels in Human Septic Shock: Relation to Multiple-System Organ Failure and Mortality.* Chest, 1993. **103**(2): p. 565-575.
476. Voloshyna, I., M.J. Littlefield, and A.B. Reiss, *Atherosclerosis and interferon-γ: new insights and therapeutic targets.* Trends in cardiovascular medicine, 2014. **24**(1): p. 45-51.
477. Liang, K., S.R. Dong, and H. Peng, *Serum levels and clinical significance of IFN-gamma and IL-10 in patients with coronary heart disease.* Eur Rev Med Pharmacol Sci, 2016. **20**(7): p. 1339-43.
478. Fiorentino, D.F., et al., *IL-10 inhibits cytokine production by activated macrophages.* J Immunol, 1991. **147**(11): p. 3815-22.
479. Marchant, A., et al., *Interleukin-10 controls interferon-gamma and tumor necrosis factor production during experimental endotoxemia.* Eur J Immunol, 1994. **24**(5): p. 1167-71.
480. Mallat, Z., et al., *Protective role of interleukin-10 in atherosclerosis.* Circ Res, 1999. **85**(8): p. e17-24.
481. Gogos, C.A., et al., *Pro- versus Anti-inflammatory Cytokine Profile in Patients with Severe Sepsis: A Marker for Prognosis and Future Therapeutic Options.* The Journal of Infectious Diseases, 2000. **181**(1): p. 176-180.
482. Masumi, A., et al., *Interferon regulatory factor-2 induces megakaryopoiesis in mouse bone marrow hematopoietic cells.* 2009. **583**(21): p. 3493-3500.
483. Griffin, C.G. and B.W. Grant, *Effects of recombinant interferons on human megakaryocyte growth.* Experimental hematology, 1990. **18**(9): p. 1013-1018.

484. Key, L.L., et al., *Long-Term Treatment of Osteopetrosis with Recombinant Human Interferon Gamma.* 1995. **332**(24): p. 1594-1599.

485. Tsuji-Takayama, K., et al., *IFN-gamma in combination with IL-3 accelerates platelet recovery in mice with 5-fluorouracil-induced marrow aplasia.* J Interferon Cytokine Res, 1996. **16**(6): p. 447-51.

486. Zoumbos, N.C., et al., *Interferon is a mediator of hematopoietic suppression in aplastic anemia in vitro and possibly in vivo.* Proc Natl Acad Sci U S A, 1985. **82**(1): p. 188-92.

487. Schulze, H. and R.A. Shivdasani, *Mechanisms of thrombopoiesis.* J Thromb Haemost, 2005. **3**(8): p. 1717-24.

488. Tsuji-Takayama, K., et al., *Interferon-gamma enhances megakaryocyte colony-stimulating activity in murine bone marrow cells.* J Interferon Cytokine Res, 1996. **16**(9): p. 701-8.

489. Tsuji, K., K. Muraoka, and T. Nakahata, *Interferon-γ and Human Megakaryopoiesis.* Leukemia & Lymphoma, 1998. **31**(1-2): p. 107-113.

490. Li, J., et al., *Megakaryocytic differentiation of HIMeg-1 cells induced by interferon gamma and tumour necrosis factor alpha but not by thrombopoietin.* Cytokine, 1998. **10**(11): p. 880-9.

491. Huang, Z., et al., *STAT1 promotes megakaryopoiesis downstream of GATA-1 in mice.* The Journal of Clinical Investigation, 2007. **117**(12): p. 3890-3899.

492. Shiohara, M., K. Koike, and T. Nakahata, *Synergism of interferon-gamma and stem cell factor on the development of murine hematopoietic progenitors in serum-free culture.* Blood, 1993. **81**(6): p. 1435-41.

493. KAZUE TSUJI-TAKAYAMA, et al., *Interferon-γ Enhances Megakaryocyte Colony-Stimulating Activity in Murine Bone Marrow Cells.* 1996. **16**(9): p. 701-708.

494. Kang, Y.J., et al., *A novel function of interleukin-10 promoting self-renewal of hematopoietic stem cells.* Stem Cells, 2007. **25**(7): p. 1814-22.

495. Asano, Y., et al., *Effect of Interleukin 10 on the Hematopoietic Progenitor Cells from Patients with Aplastic Anemia.* 1999. **17**(3): p. 147-151.

496. Rennick, D., et al., *Interleukin-10 promotes the growth of megakaryocyte, mast cell, and multilineage colonies: analysis with committed progenitors and Thy1loSca1+ stem cells.* Exp Hematol, 1994. **22**(2): p. 136-41.

497. Westermann, F., et al., *Interleukin 10 inhibits cytokine production of human AML cells.* Ann Oncol, 1996. **7**(4): p. 397-404.

498. Sosman, J.A., et al., *Interleukin 10-induced thrombocytopenia in normal healthy adult volunteers: evidence for decreased platelet production.* 2000. **111**(1): p. 104-111.

499. Huhn, R.D., et al., *Pharmacodynamics of subcutaneous recombinant human interleukin-10 in healthy volunteers.* Clin Pharmacol Ther, 1997. **62**(2): p. 171-80.

500. Del Vecchio, G.C., et al., *Clinical significance of serum cytokine levels and thrombopoietic markers in childhood idiopathic thrombocytopenic purpura.* Blood Transfus, 2012. **10**(2): p. 194-9.

501. Chen, L.Y. and J.L. Mehta, *Variable effects of L-arginine analogs on L-arginine-nitric oxide pathway in human neutrophils and platelets may relate to different nitric oxide synthase isoforms.* J Pharmacol Exp Ther, 1996. **276**(1): p. 253-7.

502. Zhang, J., et al., *Proinflammatory cytokines downregulate gene expression and activity of constitutive nitric oxide synthase in porcine pulmonary artery endothelial cells.* Res Commun Mol Pathol Pharmacol, 1997. **96**(1): p. 71-87.

503. Shami, P. and J. Weinberg, *Differential effects of nitric oxide on erythroid and myeloid colony growth from CD34+ human bone marrow cells.* 1996. **87**(3): p. 977-982.

504. Maciejewski, J.P., et al., *Nitric oxide suppression of human hematopoiesis in vitro. Contribution to inhibitory action of interferon-gamma and tumor necrosis factor-alpha.* The Journal of Clinical Investigation, 1995. **96**(2): p. 1085-1092.

505. Schattner, M., et al., *Effect of nitric oxide on megakaryocyte growth induced by thrombopoietin.* J Lab Clin Med, 2001. **137**(4): p. 261-9.

506. Battinelli, E., et al., *Induction of platelet formation from megakaryocytoid cells by nitric oxide.* 2001. **98**(25): p. 14458-14463.

507. Han, Z.C. and J.P. Caen, *Are megakaryocytes and endothelial cells sisters?* J Lab Clin Med, 1993. **121**(6): p. 821-5.

508. Choi, K., et al., *A common precursor for hematopoietic and endothelial cells.* 1998. **125**(4): p. 725-732.

509. Koh, K.P., et al., *T cell-mediated vascular dysfunction of human allografts results from IFN-gamma dysregulation of NO synthase.* The Journal of clinical investigation, 2004. **114**(6): p. 846-856.

510. Morikawa, A., et al., *Augmentation of nitric oxide production by gamma interferon in a mouse vascular endothelial cell line and its modulation by tumor necrosis factor alpha and lipopolysaccharide.* Infection and immunity, 2000. **68**(11): p. 6209-6214.
511. Kamijo, R., et al., *Requirement for transcription factor IRF-1 in NO synthase induction in macrophages.* 1994. **263**(5153): p. 1612-1615.
512. Darnell, J.E., Jr., I.M. Kerr, and G.R. Stark, *Jak-STAT pathways and transcriptional activation in response to IFNs and other extracellular signaling proteins.* Science, 1994. **264**(5164): p. 1415-21.
513. Cunha, F.Q., S. Mohcada, and F.Y. Liew, *Interleukin-10 (IL-10) inhibits the induction of nitric oxide synthase by interferon-γ in murine macrophages.* Biochemical and Biophysical Research Communications, 1992. **182**(3): p. 1155-1159.
514. Hutchins, A.P., D. Diez, and D. Miranda-Saavedra, *The IL-10/STAT3-mediated anti-inflammatory response: recent developments and future challenges.* Briefings in functional genomics, 2013. **12**(6): p. 489-498.
515. Ito, S., et al., *Interleukin-10 Inhibits Expression of Both Interferon □– and Interferon γ–Induced Genes by Suppressing Tyrosine Phosphorylation of STAT1.* 1999. **93**(5): p. 1456-1463.
516. Wenta, N., et al., *Tyrosine phosphorylation regulates the partitioning of STAT1 between different dimer conformations.* 2008. **105**(27): p. 9238-9243.
517. Starr, R. and D.J. Hilton, *Negative regulation of the JAK/STAT pathway.* Bioessays, 1999. **21**(1): p. 47-52.
518. van der Meijden, P.E.J. and J.W.M. Heemskerk, *Platelet biology and functions: new concepts and clinical perspectives.* Nat Rev Cardiol, 2019. **16**(3): p. 166-179.
519. Heemskerk, J.W., N.J. Mattheij, and J.M. Cosemans, *Platelet-based coagulation: different populations, different functions.* J Thromb Haemost, 2013. **11**(1): p. 2-16.
520. Sodergren, A.L. and S. Ramstrom, *Platelet subpopulations remain despite strong dual agonist stimulation and can be characterised using a novel six-colour flow cytometry protocol.* Sci Rep, 2018. **8**(1): p. 1441.
521. van der Meijden, P.E.J. and J.W.M. Heemskerk, *Platelet biology and functions: new concepts and clinical perspectives.* Nat Rev Cardiol, 2018.

522. Agbani, E.O. and A.W. Poole, *Procoagulant platelets: generation, function, and therapeutic targeting in thrombosis.* Blood, 2017. **130**(20): p. 2171-2179.
523. Moreau, T., et al., *Large-scale production of megakaryocytes from human pluripotent stem cells by chemically defined forward programming.* Nature Communications, 2016. **7**: p. 11208.
524. Gladwin, A.M., et al., *Identification of mRNA for PDGF B-chain in human megakaryocytes isolated using a novel immunomagnetic separation method.* 1990. **76**(3): p. 333-339.
525. Clancy, L., et al., *The role of RNA uptake in platelet heterogeneity.* Thromb Haemost, 2017. **117**(5): p. 948-961.
526. McManus, D.D. and J.E. Freedman, *MicroRNAs in platelet function and cardiovascular disease.* Nature Reviews Cardiology, 2015. **12**: p. 711.
527. Lindsay, C.R. and L.C. Edelstein, *MicroRNAs in Platelet Physiology and Function.* Semin Thromb Hemost, 2016. **42**(3): p. 215-22.
528. KONDKAR, A.A., et al., *VAMP8/endobrevin is overexpressed in hyperreactive human platelets: suggested role for platelet microRNA.* 2010. **8**(2): p. 369-378.
529. Landry, P., et al., *Existence of a microRNA pathway in anucleate platelets.* Nature Structural &Amp; Molecular Biology, 2009. **16**: p. 961.
530. Wang, H., et al., *Hematopoietic Deficiency of miR-223 Attenuates Thrombosis in Response to Photochemical Injury in Mice.* Scientific Reports, 2017. **7**(1): p. 1606.
531. Shi, R., et al., *Decreased platelet miR-223 expression is associated with high on-clopidogrel platelet reactivity.* Thromb Res, 2013. **131**(6): p. 508-13.
532. Pan, Y., et al., *Platelet-Secreted MicroRNA-223 Promotes Endothelial Cell Apoptosis Induced by Advanced Glycation End Products via Targeting the Insulin-like Growth Factor 1 Receptor.* 2014. **192**(1): p. 437-446.
533. Willeit, P., et al., *Circulating microRNAs as novel biomarkers for platelet activation.* Circ Res, 2013. **112**(4): p. 595-600.
534. Zampetaki, A., et al., *Prospective Study on Circulating MicroRNAs and Risk of Myocardial Infarction.* Journal of the American College of Cardiology, 2012. **60**(4): p. 290-299.

535. Yu, X.Y., et al., *Plasma miR-126 as a potential marker predicting major adverse cardiac events in dual antiplatelet-treated patients after percutaneous coronary intervention.* EuroIntervention, 2013. **9**(5): p. 546-54.

536. Baaten, C.C.F.M.J., et al., *Platelet populations and priming in hematological diseases.* Blood Reviews, 2017. **31**(6): p. 389-399.

537. Prodan, C.I., A.S. Vincent, and G.L. Dale, *Coated-platelet levels are elevated in patients with transient ischemic attack.* Transl Res, 2011. **158**(1): p. 71-5.

538. Kirkpatrick, A.C., et al., *Coated-platelets improve prediction of stroke and transient ischemic attack in asymptomatic internal carotid artery stenosis.* Stroke, 2014. **45**(10): p. 2995-3001.

539. Schneider David, J. and S. Taatjes-Sommer Heidi, *Augmentation of Megakaryocyte Expression of FcγRIIa by Interferon γ.* Arteriosclerosis, Thrombosis, and Vascular Biology, 2009. **29**(7): p. 1138-1143.

540. Lood, C., et al., *Platelet transcriptional profile and protein expression in patients with systemic lupus erythematosus: up-regulation of the type I interferon system is strongly associated with vascular disease.* 2010. **116**(11): p. 1951-1957.

541. Karpatkin, S., *Heterogeneity of human platelets. I. Metabolic and kinetic evidence suggestive of young and old platelets.* J Clin Invest, 1969. **48**(6): p. 1073-82.

542. Karpatkin, S., *Heterogeneity of human platelets. II. Functional evidence suggestive of young and old platelets.* J Clin Invest, 1969. **48**(6): p. 1083-7.

543. Savage, B., et al., *The relation of platelet density to platelet age: survival of low- and high-density 111indium-labeled platelets in baboons.* Blood, 1986. **68**(2): p. 386-93.

544. Penington, D.G., K. Streatfield, and A.E. Roxburgh, *Megakaryocytes and the heterogeneity of circulating platelets.* Br J Haematol, 1976. **34**(4): p. 639-53.

545. Bessman, J.D., *The relation of megakaryocyte ploidy to platelet volume.* Am J Hematol, 1984. **16**(2): p. 161-70.

546. Healy, A.M., et al., *Platelet expression profiling and clinical validation of myeloid-related protein-14 as a novel determinant of cardiovascular events.* Circulation, 2006. **113**(19): p. 2278-84.

547. Petersen, R., et al., *Platelet function is modified by common sequence variation in megakaryocyte super enhancers.* Nature Communications, 2017. **8**: p. 16058.

548. Deppermann, C., et al., *Gray platelet syndrome and defective thrombo-inflammation in Nbeal2-deficient mice.* J Clin Invest, 2013.

549. Kahr, W.H., et al., *Mutations in NBEAL2, encoding a BEACH protein, cause gray platelet syndrome.* Nat Genet, 2011. **43**(8): p. 738-40.

550. Jackson, C.W. and L.K. Jennings, *Heterogeneity of fibrinogen receptor expression on platelets activated in normal plasma with ADP: analysis by flow cytometry.* 1989. **72**(3): p. 407-414.

551. Munnix, I.C., et al., *Segregation of platelet aggregatory and procoagulant microdomains in thrombus formation: regulation by transient integrin activation.* Arterioscler Thromb Vasc Biol, 2007. **27**(11): p. 2484-90.

552. Södergren, A.L. and S. Ramström, *Platelet subpopulations remain despite strong dual agonist stimulation and can be characterised using a novel six-colour flow cytometry protocol.* Scientific Reports, 2018. **8**(1): p. 1441.

553. López, J.A., *The platelet Fc receptor: a new role for an old actor.* 2013. **121**(10): p. 1674-1675.

554. Mammadova-Bach, E., et al., *Platelet glycoprotein VI binds to polymerized fibrin and promotes thrombin generation.* Blood, 2015. **126**(5): p. 683-91.

555. Dale, G.L., *Coated-platelets: an emerging component of the procoagulant response.* J Thromb Haemost, 2005. **3**(10): p. 2185-92.

556. Heemskerk, J.W., et al., *Collagen but not fibrinogen surfaces induce bleb formation, exposure of phosphatidylserine, and procoagulant activity of adherent platelets: evidence for regulation by protein tyrosine kinase-dependent Ca2+ responses.* Blood, 1997. **90**(7): p. 2615-25.

557. Agbani, E.O., et al., *Membrane Ballooning in Aggregated Platelets is Synchronised and Mediates a Surge in Microvesiculation.* Scientific Reports, 2017. **7**(1): p. 2770.

558. Prodan, C.I., J.A. Stoner, and G.L. Dale, *Lower Coated-Platelet Levels Are Associated With Increased Mortality After Spontaneous Intracerebral Hemorrhage.* 2015. **46**(7): p. 1819-1825.

559. Prodan, C.I., et al., *Coated-platelet levels are low in patients with spontaneous intracerebral hemorrhage.* Stroke, 2009. **40**(7): p. 2578-80.

560. Prodan, C.I., A.S. Vincent, and G.L. Dale, *Coated platelet levels correlate with bleed volume in patients with spontaneous intracerebral hemorrhage.* Stroke, 2010. **41**(6): p. 1301-3.

561. Patel, D., et al., *Dynamics of GPIIb/IIIa-mediated platelet-platelet interactions in platelet adhesion/thrombus formation on collagen in vitro as revealed by videomicroscopy.* 2003. **101**(3): p. 929-936.

562. Michelson, A.D., *Antiplatelet therapies for the treatment of cardiovascular disease.* Nat Rev Drug Discov, 2010. **9**(2): p. 154-69.

563. Gum, P.A., et al., *A prospective, blinded determination of the natural history of aspirin resistance among stable patients with cardiovascular disease.* J Am Coll Cardiol, 2003. **41**(6): p. 961-5.

564. Ferraris, V.A., S.P. Ferraris, and S.P. Saha, *Antiplatelet drugs: mechanisms and risks of bleeding following cardiac operations.* The International journal of angiology : official publication of the International College of Angiology, Inc, 2011. **20**(1): p. 1-18.

565. Radomski, M.W., R.M. Palmer, and S. Moncada, *Endogenous nitric oxide inhibits human platelet adhesion to vascular endothelium.* Lancet, 1987. **2**(8567): p. 1057-8.

566. Pitchford, S.C., *Novel uses for anti-platelet agents as anti-inflammatory drugs.* Br J Pharmacol, 2007. **152**(7): p. 987-1002.

567. Cardaropoli, S., et al., *Infectious and inflammatory stimuli decrease endothelial nitric oxide synthase activity in vitro.* J Hypertens, 2003. **21**(11): p. 2103-10.

568. Hein, T.W., et al., *Human C-reactive protein induces endothelial dysfunction and uncoupling of eNOS in vivo.* Atherosclerosis, 2009. **206**(1): p. 61-8.

569. Ogura, M., et al., *Establishment of a novel human megakaryoblastic leukemia cell line, MEG-01, with positive Philadelphia chromosome.* Blood, 1985. **66**(6): p. 1384-92.

570. Schweinfurth, N., et al., *Valproic acid and all trans retinoic acid differentially induce megakaryopoiesis and platelet-like particle formation from the megakaryoblastic cell line MEG-01.* Platelets, 2010. **21**(8): p. 648-57.

571. Takeuchi, K., et al., *Platelet-like particle formation in the human megakaryoblastic leukaemia cell lines, MEG-01 and MEG-01s.* 1998. **100**(2): p. 436-444.

572. Radomski, M. and S. Moncada, *An improved method for washing of human platelets with prostacyclin.* Thromb Res, 1983. **30**(4): p. 383-9.

573. Shesely, E.G., et al., *Elevated blood pressures in mice lacking endothelial nitric oxide synthase.* Proc Natl Acad Sci U S A, 1996. **93**(23): p. 13176-81.
574. van Haperen, R., et al., *Functional expression of endothelial nitric oxide synthase fused to green fluorescent protein in transgenic mice.* Am J Pathol, 2003. **163**(4): p. 1677-86.
575. Kojima, H., et al., *Fluorescent Indicators for Imaging Nitric Oxide Production.* Angew Chem Int Ed Engl, 1999. **38**(21): p. 3209-3212.
576. Kleiner, D.E. and W.G. Stetler-Stevenson, *Quantitative zymography: detection of picogram quantities of gelatinases.* Anal Biochem, 1994. **218**(2): p. 325-9.
577. Jurasz, P., et al., *Matrix metalloproteinase 2 in tumor cell-induced platelet aggregation: regulation by nitric oxide.* Cancer Res, 2001. **61**(1): p. 376-82.
578. Govindasamy, N., M. Yan, and P. Jurasz, *Incorporation of β-actin loading control into zymography.* Journal of biological methods, 2016. **3**(4): p. e61.
579. Bohmer, A., S. Gambaryan, and D. Tsikas, *Human blood platelets lack nitric oxide synthase activity.* Platelets, 2015. **26**(6): p. 583-8.
580. Gambaryan, S. and D. Tsikas, *A review and discussion of platelet nitric oxide and nitric oxide synthase: do blood platelets produce nitric oxide from L-arginine or nitrite?* Amino Acids, 2015. **47**(9): p. 1779-93.
581. Fish, J.E., et al., *The expression of endothelial nitric-oxide synthase is controlled by a cell-specific histone code.* J Biol Chem, 2005. **280**(26): p. 24824-38.
582. Freedman, J.E., et al., *Impaired platelet production of nitric oxide predicts presence of acute coronary syndromes.* Circulation, 1998. **98**(15): p. 1481-6.
583. Saura, M., et al., *Interaction of interferon regulatory factor-1 and nuclear factor κB during activation of inducible nitric oxide synthase transcription11Edited by M. Yaniv.* Journal of Molecular Biology, 1999. **289**(3): p. 459-471.
584. Canada, S., *Table 13-10-0147-01 Deaths, by cause, Chapter IX: Diseases of the circulatory system (I00 to I99).* 2018.
585. Mehta, S.R., et al., *2018 Canadian Cardiovascular Society/Canadian Association of Interventional Cardiology Focused Update of the Guidelines for the Use of Antiplatelet Therapy.* Can J Cardiol, 2018. **34**(3): p. 214-233.
586. Quinn, M.J. and E.J. Topol, *Common variations in platelet glycoproteins: pharmacogenomic implications.* Pharmacogenomics, 2001. **2**(4): p. 341-52.

587. Gawaz, M., H. Langer, and A.E. May, *Platelets in inflammation and atherogenesis.* The Journal of Clinical Investigation, 2005. **115**(12): p. 3378-3384.

588. Böhmer, A., S. Gambaryan, and D. Tsikas, *Human blood platelets lack nitric oxide synthase activity.* Platelets, 2015. **26**(6): p. 583-588.

589. Li, Z., et al., *Sequential activation of p38 and ERK pathways by cGMP-dependent protein kinase leading to activation of the platelet integrin alphaIIb beta3.* Blood, 2006. **107**(3): p. 965-72.

590. Begonja, A.J., et al., *Thrombin stimulation of p38 MAP kinase in human platelets is mediated by ADP and thromboxane A2 and inhibited by cGMP/cGMP-dependent protein kinase.* Blood, 2007. **109**(2): p. 616-8.

591. Walter, U. and S. Gambaryan, *Roles of cGMP/cGMP-dependent protein kinase in platelet activation.* Blood, 2004. **104**(8): p. 2609.

592. Gambaryan, S., et al., *Potent inhibition of human platelets by cGMP analogs independent of cGMP-dependent protein kinase.* 2004. **103**(7): p. 2593-2600.

593. Rizzo, V., et al., *In situ flow activates endothelial nitric oxide synthase in luminal caveolae of endothelium with rapid caveolin dissociation and calmodulin association.* J Biol Chem, 1998. **273**(52): p. 34724-9.

594. Freedman, J.E. and J. Loscalzo, *Arterial and Venous Thrombosis*, in *Harrison's Principles of Internal Medicine, 19e*, D. Kasper, et al., Editors. 2014, McGraw-Hill Education: New York, NY.

595. Zeiler, M., M. Moser, and M. Mann, *Copy number analysis of the murine platelet proteome spanning the complete abundance range.* Mol Cell Proteomics, 2014. **13**(12): p. 3435-45.

596. Senis, Y.A., et al., *A comprehensive proteomics and genomics analysis reveals novel transmembrane proteins in human platelets and mouse megakaryocytes including G6b-B, a novel immunoreceptor tyrosine-based inhibitory motif protein.* Mol Cell Proteomics, 2007. **6**(3): p. 548-64.

597. Lewandrowski, U., et al., *Platelet membrane proteomics: a novel repository for functional research.* Blood, 2009. **114**(1): p. e10-9.

598. Burkhart, J.M., et al., *The first comprehensive and quantitative analysis of human platelet protein composition allows the comparative analysis of structural and functional pathways.* Blood, 2012. **120**(15): p. e73-82.

599. Giles, H., R.E. Smith, and J.F. Martin, *Platelet glycoprotein IIb-IIIa and size are increased in acute myocardial infarction.* Eur J Clin Invest, 1994. **24**(1): p. 69-72.

600. Roberts, W., et al., *Nitric oxide inhibits von Willebrand factor-mediated platelet adhesion and spreading through regulation of integrin alpha(IIb)beta(3) and myosin light chain.* J Thromb Haemost, 2009. **7**(12): p. 2106-15.

601. Gresele, P., et al., *Platelets release matrix metalloproteinase-2 in the coronary circulation of patients with acute coronary syndromes: possible role in sustained platelet activation.* European Heart Journal, 2010. **32**(3): p. 316-325.

602. Williams, R.H. and M.U.J.T.J. Nollert, *Platelet-derived NO slows thrombus growth on a collagen type III surface.* 2004. **2**(1): p. 11.

603. Bodzenta-Lukaszyk, A., et al., *Nitric oxide synthase inhibition and platelet function.* Thromb Res, 1994. **75**(6): p. 667-72.

604. Zhou, Q., G.R. Hellermann, and L.P. Solomonson, *Nitric oxide release from resting human platelets.* Thromb Res, 1995. **77**(1): p. 87-96.

605. Rumer, S., et al., *DAF-fluorescence without NO: elicitor treated tobacco cells produce fluorescing DAF-derivatives not related to DAF-2 triazol.* Nitric Oxide, 2012. **27**(2): p. 123-35.

606. Balashova, N., et al., *Characterization of a novel type of endogenous activator of soluble guanylyl cyclase.* J Biol Chem, 2005. **280**(3): p. 2186-96.

607. Venema, R.C., et al., *Novel complexes of guanylate cyclase with heat shock protein 90 and nitric oxide synthase.* Am J Physiol Heart Circ Physiol, 2003. **285**(2): p. H669-78.

608. Meurer, S., et al., *Reactive oxygen species induce tyrosine phosphorylation of and Src kinase recruitment to NO-sensitive guanylyl cyclase.* J Biol Chem, 2005. **280**(39): p. 33149-56.

609. Shirodkar, A.V., et al., *A mechanistic role for DNA methylation in endothelial cell (EC)-enriched gene expression: relationship with DNA replication timing.* 2013. **121**(17): p. 3531-3540.

610. Sanchez de Miguel, L., et al., *Evidence that an endothelial cytosolic protein binds to the 3'-untranslated region of endothelial nitric oxide synthase mRNA.* J Vasc Res, 1999. **36**(3): p. 201-8.

611. Yan, G., et al., *Tumor necrosis factor-alpha downregulates endothelial nitric oxide synthase mRNA stability via translation elongation factor 1-alpha 1.* Circulation research, 2008. **103**(6): p. 591-597.

612. Ben-Dor, I., N.S. Kleiman, and E. Lev, *Assessment, mechanisms, and clinical implication of variability in platelet response to aspirin and clopidogrel therapy.* Am J Cardiol, 2009. **104**(2): p. 227-33.

613. Sweeny, J.M., D.A. Gorog, and V. Fuster, *Antiplatelet drug 'resistance'. Part 1: mechanisms and clinical measurements.* Nat Rev Cardiol, 2009. **6**(4): p. 273-82.

614. Gorog, D.A., J.M. Sweeny, and V. Fuster, *Antiplatelet drug 'resistance'. Part 2: laboratory resistance to antiplatelet drugs-fact or artifact?* Nat Rev Cardiol, 2009. **6**(5): p. 365-73.